Tropospheric Ozone as a Tracer to Investigate Deep Convection and its Influence on the Humidity in the Marine Tropics
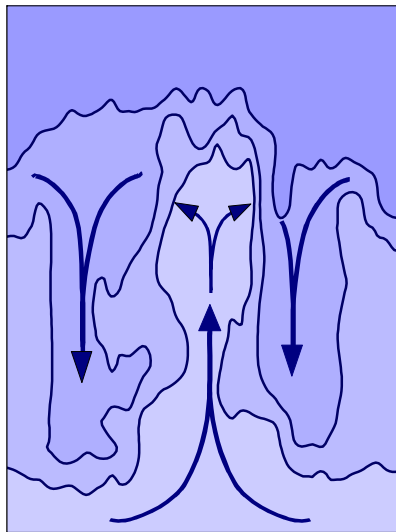
von
Herman G.J. Smit

Aachen 2004

„Alle goede dingen duren lang"

Met dank aan mijn ouders
en mijn zuster Dity

Angefertigt mit Genehmigung vom Fachbereich C – Mathematik und Naturwissenschaften der Bergischen Universität Wuppertal

1. Referent: Prof. em. Dr. Dieter Kley

               Fachbereich 9 - Physikalische Chemie der Bergischen Universität Wuppertal und

               Institut für Chemie und Dynamik der Geosphäre: Troposphäre, Forschungszentrum Jülich

2. Referent: Prof. em. Dr. Karl-Heinz Becker

               Fachbereich 9 - Physikalische Chemie der Bergischen Universität Wuppertal

Tag der mündlichen Prüfung: 3. September 2004

Abstract

In this thesis the chemical and dynamical aspects governing the tropospheric ozone distribution in the marine tropics are investigated and characterized in order to use ozone as a quantitative proxy to study deep convection in relation to the vertical distribution of humidity. The investigations make use of combined vertical ozone and humidity balloon soundings made from board of the research vessel RV "Polarstern" during two cruises on the Central Atlantic Ocean between 36°S and 52°N, mostly along the 30°W meridian in March/April 1987 and September/October 1988.. In order to achieve the high accuracy required for ozone and humidity measurements in the middle and upper troposphere, special correctional methods for data processing are developed.

To understand whether the observed features in the meridional ozone distributions are caused by photochemistry or dynamics local photochemical changes of ozone are estimated as a function of latitude and altitude through the use of a photochemical box model and compared with the characteristic time scales of horizontal and vertical transport of the tropical Hadley circulation. In the tropical marine boundary layer (MBL), high water vapor content, high UV-flux and low (<10 pptv) mixing ratios of NO_X act together to cause significant photochemical ozone destruction. A net chemical ozone life times of less than 5-7 days provides an effective ozone loss mechanism thus causing low ozone values in the MBL. In the free troposphere, due to a low water vapor concentrations, low temperature and the absence of significant sources of NO, the in-situ photochemistry in the free troposphere is too slow compared to tropical motion systems involving deep convection and large scale subsidence. Therefore, the morphology of ozone as observed during both cruises was governed by dynamics. As a consequence ozone can be used a quasi-conservative tracer for the description of transport in the context of deep convection and large scale subsidence.

Active or recent deep convection marks its appearance in the upper tropical troposphere by relatively low ozone mixing ratios whereby inside of cumulonimbus convective clouds, so called "hot towers", ozone deficient surface air is lifted to the upper troposphere where it detrains and displaces air with higher mixing ratios. The ozone distribution observed in the equatorial trough region during the 1988 cruise maps the morphology of the deep convective middle/upper troposphere such that approximately the 40 ppbv ozone mixing ratio contour line, which envelopes the spatial extension of a mesoscale convective cell (MCC) and consisting of a cluster of individual deep convective cells, can be used to define the convective cell. The MCC consists of three compartments: (i) The lower convergence zone (0 < Z < 3 km) comprises the regime of convergence of the trade wind inflow with low MBL ozone (≈20-25 ppbv) and high humidities (ii) An upper convergence zone (3 < Z < 7 km) describing the entrainment (confluence) of dry mid tropospheric air with enhanced ozone mixing ratios (≈60-70 ppbv) into the deep convective cell. The enhanced ozone values show that the fast vertical transport from the lower convergence zone virtually bypasses this middle part of the troposphere. (iii) The divergence zone (7 < Z < 14 km), also referred to as the detrainment part. The ozone mixing ratios in that part (≈30-40 ppbv) are low, but significantly higher compared to the respective values in the low level convergence part, which implies the strength of entrainment.

From the air and ozone mass balances over the three compartments inside the MCC the turn over time of an air parcel in the lower convergence part is estimated to be about 2-3 days. The entrainment flow of mid-troshperic air is large compared to the upward flow from the low

level convergence in the trade wind regime. As a consequence, this implies a substantial large scale inflow from regions with enhanced ozone mixing ratios and low moist static energy content, presumably from the subtropics. Entrainment of these amounts of dry, low moist static energy air in the updrafts of the mesocale cluster of deep convective cells will substantially decrease the moist static energy and, and thus buoyancy, of the lifted air thus producing a significant influence on the rising and penetrating power of the deep convection.

An intriguing aspect is given by the existence of dry air tongues with enhanced ozone mixing ratios and low moist static energy in the lower/middle troposphere between 2 and 6 km altitude, most pronounced at the edge of the MCC. These filaments of dry, ozone rich air are radiatively stable and can be transported over long distance. They presumably have their origin at higher latitudes in the subtropics or even in the midlatitudes. This could occur through a coupling of the meridional circulation in the tropics with intrusions of dry and ozone rich air originating from breaking Rossby waves associated with the life cycle of baroclinic waves at mid latitudes. The results presented in this work suggest that deep convection "pumps" mid-/upper- tropospheric air from the subtropics and thus indicate a linkage between tropical and extra-tropical dynamics. If this is so, then, a negative feedback to deep convection seems to operate in the sense that advection and entrainment of dry air with low moist static energy acts like a controlling valve which regulates the deep convection.

Zusammenfassung

In dieser Arbeit werden die chemischen und dynamischen Beiträge zur Ozonverteilung in der Troposphäre über dem tropischen Ozean untersucht mit dem Ziel, Ozon als quantitativen Tracer für den Einfluss von hochreichender Konvektion (Cumulonimbus Konvektion) auf die Vertikalverteilung der Feuchte zu verwenden. Grundlage der Untersuchung bilden Vertikalsondierungen von Ozon und relativer Feuchte die während zwei Fahrten des Forschungsschiffes "Polarstern" im März/April 1987 und im September/Oktober 1988 auf dem Atlantik zwischen 36°S and 52°N, entlang des 30°W Meridian durchgeführt wurden. Zur Vebesserung der Genauigkeit der Ozon- und Feuchtedaten, insbesondere in der mittleren und oberen Troposphäre, werden Korrekturverfahren für die Auswertung der Sondierungsdaten entwickelt.

Um den Einfluss von Photochemie und Dynamik auf die beobachteten Raum-Zeit Strukturen in der Meridionalverteilung von Ozon abzuschätzen, wurden zunächst die chemischen Tendenzen in den verschiedenen Höhenbereichen und bei verschiedenen geographischen Breiten mit einem photochemisches Boxmodell berechnet. Diese wurden dann mit den charakteristischen Zeitskalen für die Advektion und den Vertikaltransport im tropischen Ast der Hadley Zirkulation verglichen. Wegen der hohen Wasserdampfkonzentrationen, der hohen UV-Flussdichte und der niedrigen Stickoxidkonzentrationen (< 10ppt) ist die tropische marine Grenzschicht (MBL=Marine Boundary Layer) eine starke Senke für Ozon mit Lebensdauern von 5-7 Tagen. Das erklärt die beobachteten, sehr niedrigen Ozonmischungsverhältnisse in der tropischen MBL. Wegen der sehr viel niedrigeren Wasserdampfkonzentrationen, der niedrigeren Temperaturen und der Abwesenheit signifikanter NO-Quellen ist die chemische Tendenz von Ozon in der freien Troposphäre über den Ozeanen klein im Vergleich zu Änderungen durch Vertikalaustausch (Konvektion und großräumiges Absinken). Die während beider Kampagnen beobachtete Morphologie von Ozon ist deshalb weitgehend durch dynamische Prozesse bestimmt und Ozone kann in guter Näherung als quasi passiver Tracer verwendet werden, um die Wirkung von Transportprozessen auf die Verteilung von Wasserdampf zu beschreiben.

Das Vorhandensein hochreichender Konvektion in der oberen tropischen Troposphäre manifestiert sich durch niedrige Ozonmischungsverhältnisse. Ozon abgereicherte Luft aus der MBL wird in Cumulonimben (sogenannten „hot towers") in die obere Troposphäre verfrachtet und verdrängt dort Luft mit höheren Ozonmischungsverhältnissen. Die während der 1988 Fahrt im äquatorialen Trog beobachtete Ozonverteilung zeigt die Morphologie der konvektiven mittleren und oberen Troposphäre. Die 40 ppb Isoplete umgrenzt die Struktur einer mesoskaligen Konvektionszelle (MCC), welche aus einem Cluster individueller konvektiver Zellen besteht. Die MCC lässt sich grob in drei Zonen unterteilen: (i) die untere Konvergenzzone (0 < z < 3 km), in der niedriges Ozon (≈20-25 ppbv) und hohe Feuchte durch den Passatwind einfließt, (ii) die obere Konvergenzzone (3 < z < 7 km), in der trockene Luft mit höheren Ozonmischungsverhältnissen (≈60-70 ppbv) in die konvektive Zelle eingemischt wird. Die erhöhten Ozonwerte zeigen, daß der schnelle vertikale Transport aus der unteren Konvergenzzone praktisch diesen mittlern Teil der Troposphäre überbrückt. (iii) die Divergenzzone (7 < z < 14 km). Die Ozonmischungsverhältnisse in diesem Teil sind niedriger (≈30-40 ppbv) als in der nicht durch Konvektion beinflussten oberen Troposphäre, jedoch signifikant höher als die Werte in der unteren Konvergenzzone, woraus sich auf den Eintrag von Luft aus der mittleren Troposphäre schliessen läßt.

Die Austauschzeit eines Luftpakets in der unteren Konvergenzzone wurde aus den Massenbilanzen für Luft und Ozon in den drei Zonen zu 2-3 Tagen abgeschätzt. Der Eintrag von Luft aus der mittleren Troposphäre ist vergleichbar zum vertikalen Fluss aus der unteren Konvergenzzone. Dies impliziert einen substantiellen mesoskaligen Eintrag von trockener, ozonreicher Luft mit niedriger feucht-statischer Energie, höchstwahrscheinlich aus den Subtropen. Der Eintrag dieser Luftmassen in die konvektiven Zellen führt zu einer signifikanten Erniedrigung des Auftriebs und hat damit einen erheblichen Einfluss auf die Höhe der Konvektion.

Interessant sind weiterhin trockene Filamente mit hohen Ozonwerten und niedriger feucht-statischer Energie in der mittleren und unteren Troposphäre zwischen 2 und 6 km Höhe. Diese Filamente befinden sich im Strahlungsgleichgewicht und können über weite Strecken transportiert werden. Sie stammen wahrscheinlich aus den Subtropen oder sogar aus mittleren Breiten. Dieses könnte durch eine Kopplung der meridionalen tropischen Zirkulation mit Eindringen der trockener und ozonreichen Luft auftreten, verursacht durch dem Brechen von Rossby Wellen als Teil der Lebenszyklus von barokliner Wellen in mittleren Breiten. Die Ergebnisse dieser Arbeit legen nahe, dass die hochreichende Konvektion in den Tropen Luft aus der mittleren Troposphäre von mittleren Breiten in die obere Troposphäre pumpt. Diese Advektion von Luft mit niedriger feucht-statischer Energie wirkt als negative Rückkopplung und reguliert somit die hochreichende Konvektion in den Tropen.

List of Abbreviations

ADC	Analog Digital Converter
asl	above sea level
Cb	Cumulonimbus
CEPEX	Central Equatorial Pacific Experiment
CFC	Chlorofluorocarbons
DU	Dobson Unit
ECC	Electrochemical Concentration Cell
ECHAM	European Center Hamburg Model
ECMWF	European Centre for Medium Range Weather Forecasts
ESC	Environmental Simulation Chamber
ESF	Environmental Simulation Facility
FPH	Frost Point Hygrometer
FSK	Frequency Shifted Key
FZJ	Forschungszentrum Jülich
GAW	Global Atmosphere Watch
GCM	General Circulation Model
IGAC	International Global Atmospheric Chemistry
INDAS	Integrating Data System
IOC	International Ozone Commission
IPCC	Intergovernmental Panel on Climate Change
IR	Infrared
ITCZ	Inter Tropical Convergence Zone
JOSIE	Jülich Ozone Sonde Intercomparison Experiment
LS	Lower Stratosphere
MBL	Maritime Boundary Layer
MCC	Mesoscale Convective Cell
MCS	Mesoscale Convective System
MCU	Micro Computer Unit
MJO	Madden Julian Oscillation
MOZAIC	Measurement of Ozone and Water Vapor by Airbus In-Service Aircraft
NMHC	Non Methane Hydrocarbons
NH	Northern Hemisphere
OLR	Outgoing Longwave Radiation
PBL	Planetary Boundary Layer
QA	Quality Assurance
RH	Relative Humidity
RHI	Relative Humidity with respect to Ice at temperatures below $0^{o}C$

RHL	Relative Humidity with respect to Liquid water
RV	Research Vessel
SAFARI/ TRACE A	Southern African Fire Atmospheric Research Initiative/ Transport and Atmospheric Chemistry near the Equator Atlantic
SH	Southern Hemisphere
SHADOZ	Southern Hemisphere Additional Ozonesondes
SPARC	Stratospheric Processes And their Role in Climate
SST	Sea Surface Temperature
STE	Stratosphere Troposphere Exchange
STRATOZ	Stratoz Ozone Experiment
TOGA-COARE	Tropical Ocean and Global Atmosphere- Coupled Ocean Atmosphere Response Experiment
TOMS	Total Ozone Mapping Spectrometer
TP	Tropopause
TROPOZ	Tropospheric Ozone Experiment
TTL	Tropical Transition Layer
TWS	Twin Sounding
UT	Upper Troposphere
UTH	Upper Tropospheric Humidity
UTC	Universal Time Coordination
UV	Ultraviolet
VOC	Volatile Organic Carbons
WMO	World Meteorological Organization

Table of Contents

x

Chapter 1

Introduction

The climate of the Earth is governed by a delicate balancing system of physical and chemical processes in the atmosphere, the oceans, and land surfaces [e.g. *Junge,* 1963, *Warneck,* 1988, *Graedel and Crutzen,* 1993, *IGAC*, 2003]. Within the atmosphere, ozone and water vapor, two extraordinary intriguing species in atmospheric science, play a crucial role in the interaction between climate and chemistry of the atmosphere [e.g. *Ramanathan et al.,* 1987]. There is mounting evidence that long-term changes of carbon dioxide, water vapor and ozone, which have been observed over the last decades, are linked to human activities and that such changes influence our natural climate system [e.g. *World Meteorological Organization: Scientific Assessment of Ozone Depletion,* 1995, 1999, 2003, *Intergovernmental Panel on Climate Change (IPPC),* 1996, 2001].

In a chemical sense, ozone and water vapor are strongly involved in the oxidation capacity i.e. "self cleansing" effect of the atmosphere [e.g. *Crutzen,* 1988, *Thompson,* 1992]. Although, water vapor is a photochemically non-reactive compound in all but the highest parts of the Earth's atmosphere its presence is of crucial importance for the photochemistry of ozone. Water vapor reacts with $O(^1D)$, a product of UV-B ozone photolysis, to form hydroxyl (OH) radicals [*Levy,* 1971].

$$O_3 \quad + \quad h\nu(\lambda < 320nm) \quad \rightarrow \quad O(^1D) \quad + \quad O_2 \quad (R1)$$

$$O(^1D) \quad + \quad H_2O \quad \rightarrow \quad 2\,OH \quad (R2)$$
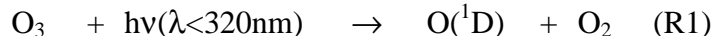
The above reaction sequence is the major mechanism to initiate the oxidative removal processes of reduced atmospheric compounds [*Levy,* 1973, *Crutzen,* 1973] and plays a dominant role for the photochemical fate of ozone. Through the reactions R1, 2 water vapor is a major supplier of odd-hydrogen ($HO_X = OH + HO_2$) radicals to the atmosphere. OH is the principal radical to oxidize CO, CH_4 and volatile organic compounds (VOC) which, in the presence of nitrogen oxides ($NO_X=NO+NO_2$), leads to photochemical ozone formation [*Crutzen,* 1973, 1974, *Chameides and Walker,* 1973, *Fishman and Crutzen*, 1978]. Furthermore, water vapor is strongly involved in heterogeneous chemistry at the surfaces of aerosols or cloud droplets, which can be important for the removal of trace gases like sulfur dioxide, nitrogen oxides or organic compounds [e.g. *Ravishankara*, 1997].

A considerable number of global studies, reported over the last two decades, have shown that much of the ozone in the troposphere is of photochemical origin [e.g. *Fishman et al.*, 1979, *Liu et al.,* 1980, *Jacob et al., 1993, Müller and Brasseur,* 1995, *Roelofs et al.*, 1997-a, *Levy et al.,* 1997, *Wang et al.,* 1998, *Lelieveld and Dentener*, 2000]. These studies suggested that the amount of ozone that is photochemically produced (3500-4500 Tg/yr) largely balance the chemical loss (3400-4100 Tg/yr). Transport into and out of the troposphere caused by stratospheric input (400-800 Tg/yr) and dry deposition (500-1200 Tg/yr), respectively, are of comparable magnitude. There is a controversy to the relative importance of tropospheric ozone production versus stratospheric influx in controlling tropospheric ozone concentrations, including the tropics [e.g. Liu et al., 1980, Levy et al., 1985, Krisnamurti, 1993]. Considerable uncertainty thereby is the origin and magnitude of NO_X, the limiting precursor for ozone

production in the troposphere [e.g. *Crutzen* 1988, *Horowitz and Jacob*, 1999]. In the remote marine region over the oceans the NO_X levels [e.g. *Drummond et al*., 1988, *Rohrer et al.,* 1997] can be very low such that in-situ photochemical formation of ozone is low and photochemical destruction can even dominate [e.g. Liu et al., 1980, Crutzen, 1988], which may particularly be the case in the remote areas over the tropical oceans. In the tropics an important contributor to the regional but also large scale ozone budget is related to biomass burning activities, particularly during the wet season [e.g. *Crutzen and Andreae*, 1990, *Jacob et al*. 1996]. In combination with convective transport and fast zonal winds in the upper troposphere can extend photochemically produced ozone and its precursors over large areas of the tropical oceans [*Krisnamurti et al*., 1993, *Pickering et al.*, 1996]. In these convective processes water vapor acts as an engine for atmospheric dynamics [e.g. *Ludlum*, 1980, *Curry and Webster,* 1999] and is thus strongly involved in transport, mixing and redistribution of atmospheric trace gases [e.g. *Gidel,* 1983, *Chatfield and Crutzen*, 1984].

The natural greenhouse effect, due to the infra-red absorption of atmospheric trace gases, is responsible for a radiative forcing which raises the Earth surface temperature by about 33 K to an average level of 288 K [e.g. *Hartmann,* 1994]. Besides the radiative forcing by ozone, which is comparable to that by carbon dioxide, water vapor is far out the predominant greenhouse gas. In a cloudless atmosphere, radiative forcing by water vapor contributes more than 60% to the (cloud free) greenhouse effect [*Harries et al.,* 1996]. To assess the impact of increasing greenhouse gases such as carbon dioxide (CO_2), chlorofluorocarbons (CFCs), ozone (O_3) etc. on climate changes it is absolutely necessary to address the radiative feedback of water vapor and particularly that of clouds [e.g. *Held and Soden*, 2000]. For example, conventional climate models show for a doubling of the CO_2 concentration a temperature increase of 2-5°C whereby only 1/3 is direct via CO_2, but 2/3 part is caused by a positive feedback of water vapor. This means that an increase of the atmosphere's temperature enables the atmosphere to increase its water vapor content and causing an additional temperature increase, provided that the relative humidity remains nearly constant [*Manabe and Wetherald*, 1967].

However, the atmospheric increase of water vapor in response to climate warming is not well understood. Particularly the underlying processes controlling the water vapor content in the middle/upper troposphere in the tropics are poorly understood [e.g. *SPARC,* 2000]. At present a controversy exist whether an increase of the sea surface temperature will also cause an enhancement of water vapor in the upper troposphere [e.g. *Ramanathan and Collins,* 1989, *Inamdar et al*, 1994] or will have a drying effect [e.g. *Lindzen,* 1990]. An increased sea surface temperature might produce deeper convection with higher, colder cloud tops, such that relatively dry air will be detrained in the upper troposphere. The processes controlling the vertical mass flux in deep convection are not well known for tropical mesoscale convective systems [e.g. *Webster,* 1994]. The magnitude and sign of the local tropical water vapor feedback remains controversial. Additional difficulty arises from the fact that the local tropical moisture budget in mesoscale convective systems in the upper troposphere is strongly influenced by large scale horizontal advection [e.g. *Newell et al.*, 1992, *Pierrehumbert and Yang,* 1993], particularly the inflow of dry air from the subtropics [*Pierrehumbert, 1995, Waugh and Polvani,* 2000].

Large uncertainties exist, particularly about the impact of clouds to any temperature change.. These are so large that it is not possible to predict whether the climate system will tend to amplify or reduce the climatic change [*IPCC,* 2001]. Clouds can have a positive as well as a negative contribution to the greenhouse effect [*Ramanathan et al.,* 1989]. A positive

contribution is due to absorption of infrared radiation emanating from the Earth surface but also through a recently discovered phenomenon, namely direct absorption of short wave solar radiation [*Cess et al.*, 1995, *Ramanathan et al.*, 1995]. A negative contribution is caused by the fact that clouds reflect a part of the direct solar radiation back into space. The intricate processes controlling the formation of clouds, cloudiness and their net radiative effect on the climate system is quantitatively still poorly understood [*IPCC*, 2001].

In order to make reliable predictions of the potential climate change caused by changes of ozone and water vapor, there is a need for a better understanding of the processes that control the large scale distributions of ozone and water vapor. In this regard, the vast regions of the tropics and sub-tropics between 30°S and 30°N are of crucial importance because they not only cover more than 50 % of the Earth's surface but they are also marked by providing the most pronounced impact on climate and chemistry of the Earth's atmosphere [*IPCC,* 2001]. In the tropics, due to highest solar UV-radiative flux, in conjunction with the largest atmospheric water vapor concentration, hydroxyl (OH) production is higher than elsewhere [e.g. *Liu et al.,* 1983]. This causes the photochemical oxidation processes in the tropics to be faster and thus the oxidation capacity of the tropical atmosphere higher compared to higher latitudes [e.g. *Crutzen,* 1988]. Fast deep (cumulonimbus) convection can transport surface air in less than one hour to the upper troposphere or even to the stratosphere [e.g. *Riehl,* 1979, *Holton,* 1979, *Newell et al.,* 1981]. This constitutes an efficient mechanism to redistribute atmospheric constituents from the surface into upper air levels and can have a large influence on tropospheric chemistry [e.g. *Gidel,* 1983, *Lelieveld and Crutzen,* 1991, *Kley et al.,* 1996]. The large scale distribution of water vapor in the tropics is dependent on the properties of deep convection [*Betts*, 1990]. However, an adequate understanding of the anatomy of moist convection and how it interacts with the large scale flow is still missing.

The objective of this thesis is to characterize the chemical and dynamical aspects governing the ozone distribution in the tropics over remote „warm" oceans and to investigate the influence of deep convection in conjunction with large scale subsidence on the water vapor distribution in the troposphere. An important aspect thereby is to investigate in how far ozone can be used as a quantitative proxy to describe vertical transport processes such as deep convection and subsidence, and permits to map the morphology of the corresponding water vapor distribution. The investigations were performed following an experimental approach to analyse the cross sections of latitudinal/altitude distribution of ozone and water vapor which were simultaneously measured over the Central Atlantic ocean between 36°S and 52°N, mostly along the 30°W meridian. The cross-sections were obtained from vertical ozone/humidity balloon soundings made from board the research vessel „Polarstern" during two cruises in March/April 1987 (ANT-V/5) and September/October 1988 (ANT-VII/1). Although, these conventional ozone and humidity sonde types have been flown worldwide since many years, little is known about the performance of the sensors in the middle and upper troposphere and particularly at the extremely low temperatures and low ozone concentrations of the upper tropical troposphere [*SPARC-IOC-GAW*, 1998]. To assess the precision and accuracy of the measured sounding data a number of laboratory and field studies were conducted to investigate the instrumental performance of the used ozone-radiosonde combination.

Chapter 2

Some Aspects of Ozone and Water Vapor in the Marine Tropics

An important mechanism for the large scale transport of momentum, energy and trace gases in the tropics and exchange with the extra-tropics is the tropical Hadley-circulation [e.g. *Riehl*, 1979, *Newell et al,* 1974]. Near the surface trade winds that originate in the sub-tropics in SH and NH blowing in the lower troposphere towards the ITCZ (Inter Tropical Convergence Zone) characterize this circulation. In the ITCZ, this causes strong convergence and vertical transport by deep convection up to the tropopause region followed by long-range latitudinal transport in combination with subsidence, and finally return to the trade wind regions of the sub-tropics [Figure 2.1]. This chapter will give a brief overview of the dynamical and photochemical processes governing the water vapor and ozone content in the remote troposphere over tropical oceans. The first part deals with the tropical dynamics and particularly the underlying processes of deep convection and large scale subsidence. The second part gives an overview about the photochemistry of tropospheric ozone under remote maritime conditions in the tropics.
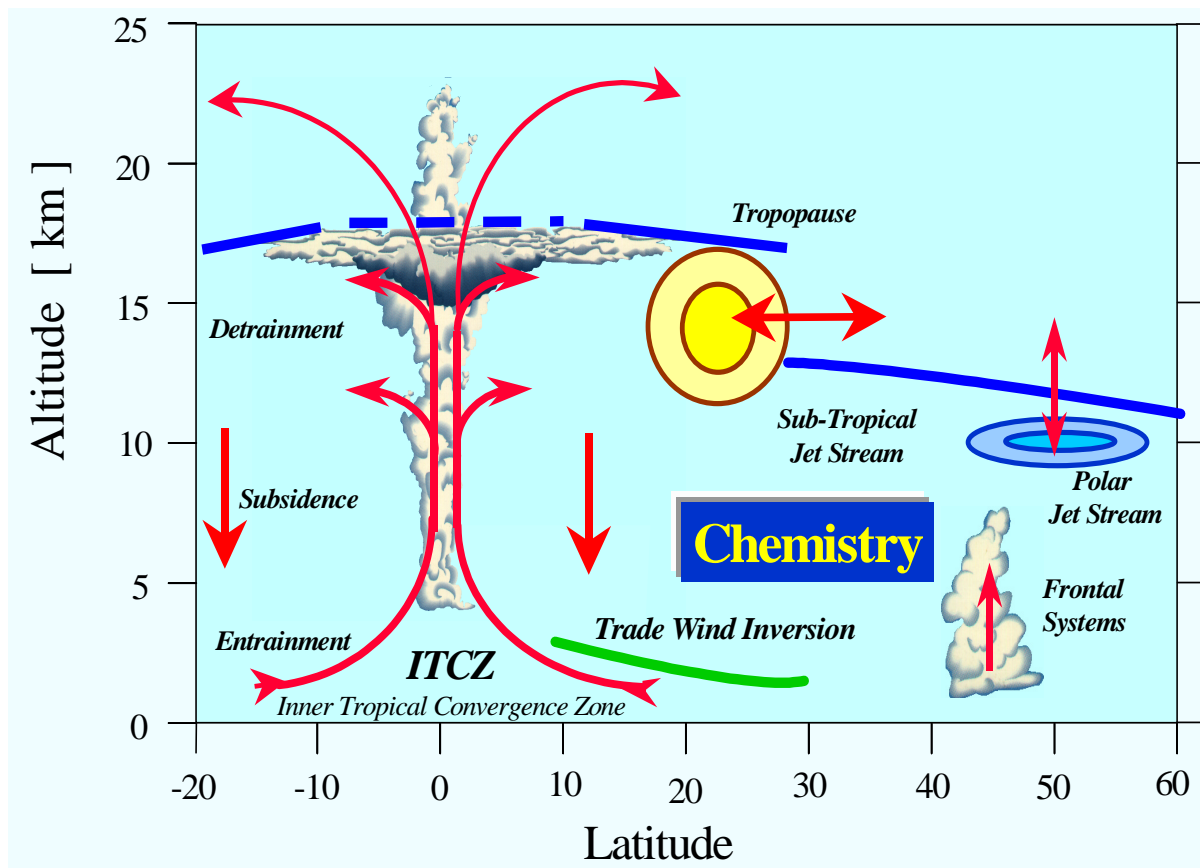
Figure 2.1: *Large scale latitudinal circulation patterns in tropics and extra-tropics*

2.1 Tropical Dynamics

2.1.1 Introduction

The ultimate energy source for all weather and climate is radiation from the sun, which enters the Earth system (global annual mean 342 Wm^{-2}), is absorbed, reflected, stored, transformed, put to work, and released back into outer space [see Figure 2.2]. About a third of incoming solar (short wave) radiation is reflected back to space (107 Wm^{-2}), while most is absorbed by the Earth's surface (land, ocean and ice) and a minor part by the Earth's atmosphere. The solar radiation absorbed by the Earth's surface (168 Wm^{-2}) and atmosphere (67 Wm^{-2}) is re-emitted as infrared radiation (235 Wm^{-2}) and is balanced at the top of the atmosphere. Naturally occurring infrared radiation absorbing species in the atmosphere (principally water vapor, but also carbon dioxide, ozone, methane, nitrogen oxide, aerosols and clouds) absorb and re-radiate at lower than surface temperatures of the atmosphere in all directions the outgoing infrared radiation originating from Earth's surface and atmosphere which keeps the surface and troposphere about 33°C warmer than it would be otherwise (natural greenhouse effect). A concentration increase of greenhouse gases compared to the natural (pre-industrialized) situation enhances this infrared absorption and causes an additional heating effect of Earth's surface and troposphere (enhanced greenhouse effect)
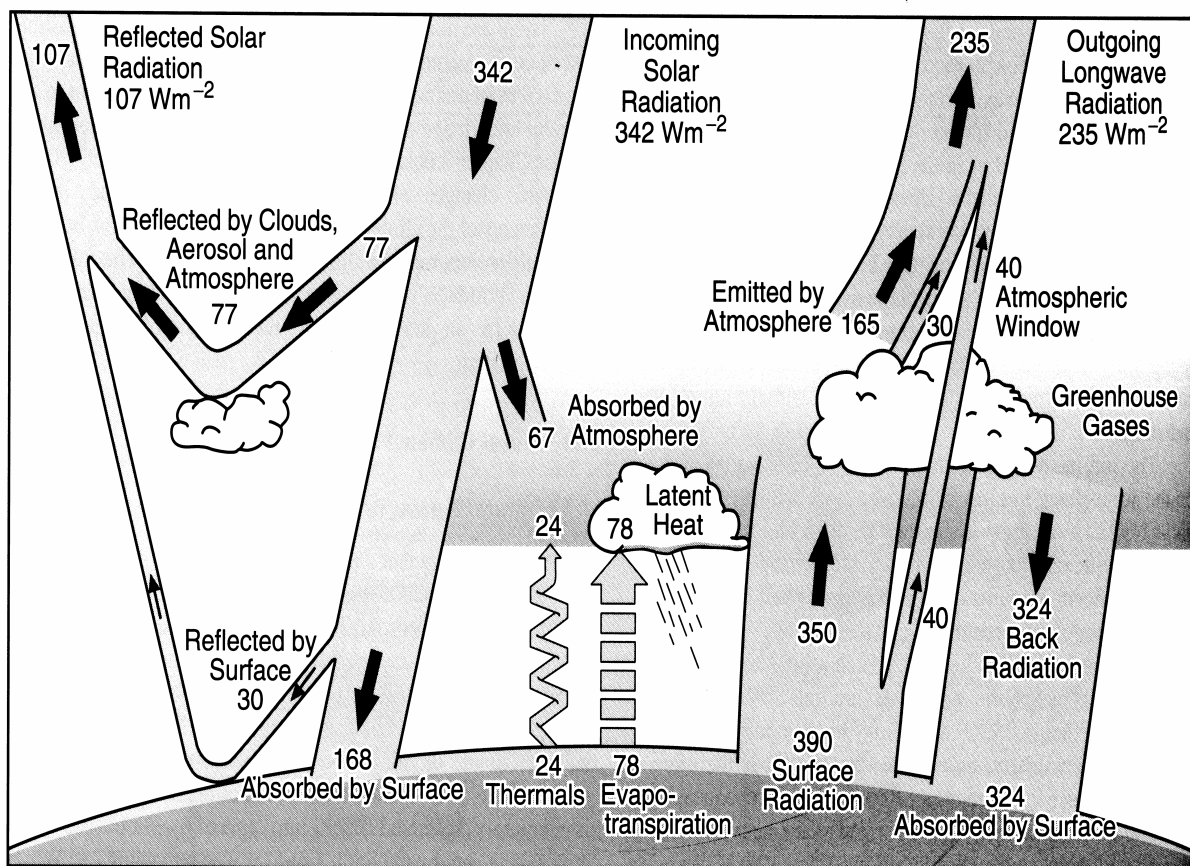
Figure 2.2: *The Earth's annual and global mean energy balance. Source: Kiehl and Trenberth, 1997.*

The latitudinal variation of the net short wave and long wave irrradiance at the top of the atmosphere is shown in the left panel of Figure 2.3. On an annual basis, the mean net (difference between incoming solar and outgoing IR) radiative budget is positive equator wards of 40° latitude and negative at higher latitudes, which means that a transport of heat from equatorial to polar regions will occur. This transport occurs via fluid motions in the atmosphere and ocean which are driven by horizontal pressure gradients generated by the uneven heating.
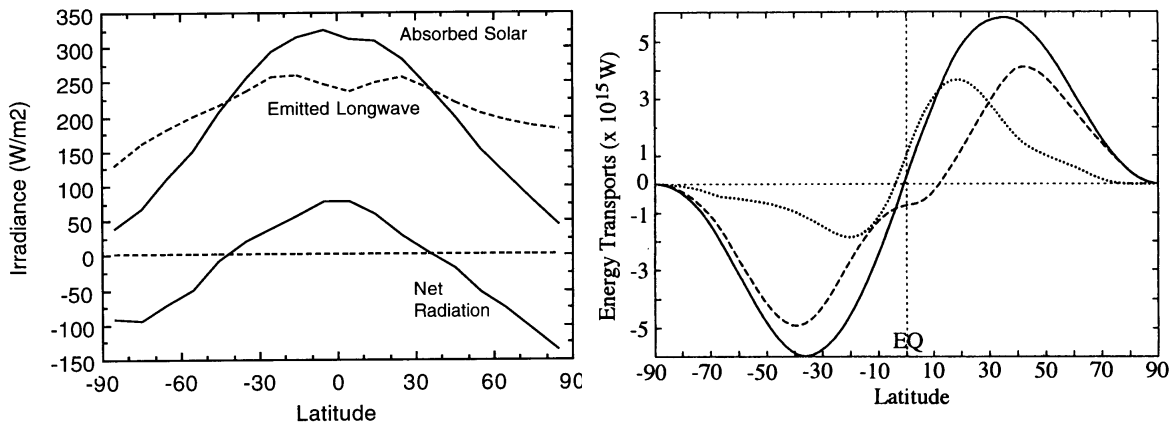
Figure 2.3: *Left panel: Annual mean absorbed short wave, outgoing long wave, and net radiation averaged around latitude circles [From Hartmann, 1994]. Right panel: Annual mean lateral energy transports required to equalize the pole-equator radiative imbalance. The solid line represents the top of the atmosphere radiation budget, the dashed line represents the atmosphere, and the dotted line represents the ocean [From Zhang and Rossow, 1997]*

The right panel of Figure 2.3 shows an estimate of the total annual mean latitudinal energy transport required to equalize the pole-equator radiative imbalance. More detailed, the partitioning between atmosphere and ocean is not well known. The actual mean equator to pole heat transport is considerably complicated by the Earth rotation, angular momentum and subsequent hydrodynamical instabilities, especially polewards of the subtropics where large scale eddies (e.g. storms), produced in mid-latitudes, rapidly transfer heat poleward to equalize the meridional energy inbalance. This is also implied by the fact that the tropical Hadley circulation cell virtually extends from the equator towards about 30° latitude [See also Figure 2.1].

In the tropics, in response to turbulent heat fluxes into the atmosphere, caused by surface temperature gradients arising from the geographical distribution of continents, a zonally directed circulation pattern occurs, the Walker circulation [See Figure 2.4].

This circulation is generally symmetric about the equator with ascending motion over South America, Africa, and over the warm pool region of the Pacific Oceans including the Indonesian Archipelago, and descent over the western Indian Ocean and the Eastern Pacific Ocean. Weakening or reversal of the Walker circulation, whith a rising motion in the eastern Pacific and sinking motion in the western Pacific, occurs several times in a decade and is referred to as El Nino [*Philander,* 1990].

The rising motions, caused by the convergence of low level winds, are associated with the convergence of moisture leading to the condensation of water vapor and the release of large amounts of latent heat also drive cumulonimbus (Cb) convection. This is very pronounced in the equatorial region where the low level trade winds from both hemispheres converge in the Inter Tropical Convergence Zone (ITCZ), which, in turn, gives rise to a narrow zonal band of vigorous Cb convection associated with heavy cloudiness with low level cumulus clouds and high level anvil clouds.
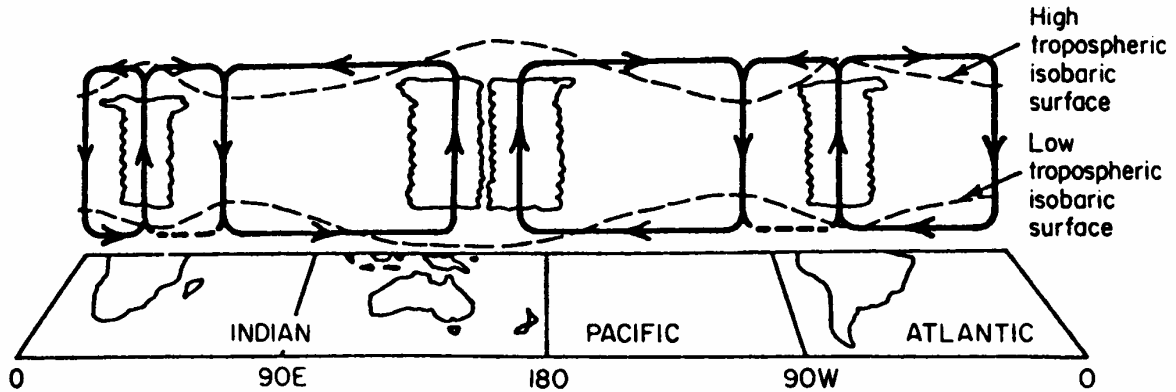
Figure 2.4: *Schematic view of the east-west Walker circulation along the equator. [From Webster, 1987]*

2.1.2 The Inter Tropical Convergence Zone and Cumulonimbus Convection

In a climatological sense, the equatorial region is characterized by a low pressure anomaly (trough) near the surface together with a high pressure anomaly in the upper troposphere, and the reverse in the outskirts. With such a climatological distribution, one expects low level convergence of air from both hemispheres toward the trough in the intertropical convergence zone (ITCZ) where by reasons of continuity the fluid is forced to rise and, subsequently, to produce high level divergence. Finally, the circulation is closed by large-scale subsidence in the subtropics thus constituting a circulation cell at all heights. However, this traditional view of large scale overturning is not consistent with the observed vertical profile of moist static energy (Q_{MS})[1] [See left panel of Figure 2.5], which shows a mid-tropospheric minimum.

The latitude/altitude cross section of Q_{MS} across the tropics [See right panel of Figure 2.5], composed from a large set of radiosoundings [*Riehl and Simpson*, 1979], shows that this mid-tropospheric layer of minimum Q_{MS} with higher values above and below is a persistent feature of the tropical atmosphere. Together with the existence of an apparently stable Q_{MS} gradient in the middle/upper troposphere, it is clear that a simple large scale upward mass flux would be controverse to the gradient of Q_{MS} and lower the energy content in the upper troposphere instead of generating potential energy to satisfy the heat balance in the equatorial zone. It is clear that such large scale upward mass flux as part of a steady state circulation as suggested before cannot exist.

---

[1] Moist static energy (Q_{MS}) is the total energy of a unit mass of air, when kinetic energy is omitted as a small contributor, and expressed as: $Q_{MS} = g{\cdot}Z + c_p{\cdot}T + L{\cdot}q$, where $g{\cdot}Z$ is potential energy (g acceleration of gravity, Z height); $c_p{\cdot}T$ is specific enthalpy (c_p specific heat at constant pressure, T temperature) and $L{\cdot}q$ (L latent heat of condensation, q specific humidity).

Riehl and Simpson [1979] solved the enigma of the vertical energy and mass transfer problem in the equatorial trough zone by introducing the concept of undiluted cumulonimbus convection, which penetrates the middle troposphere in narrow chimneys.
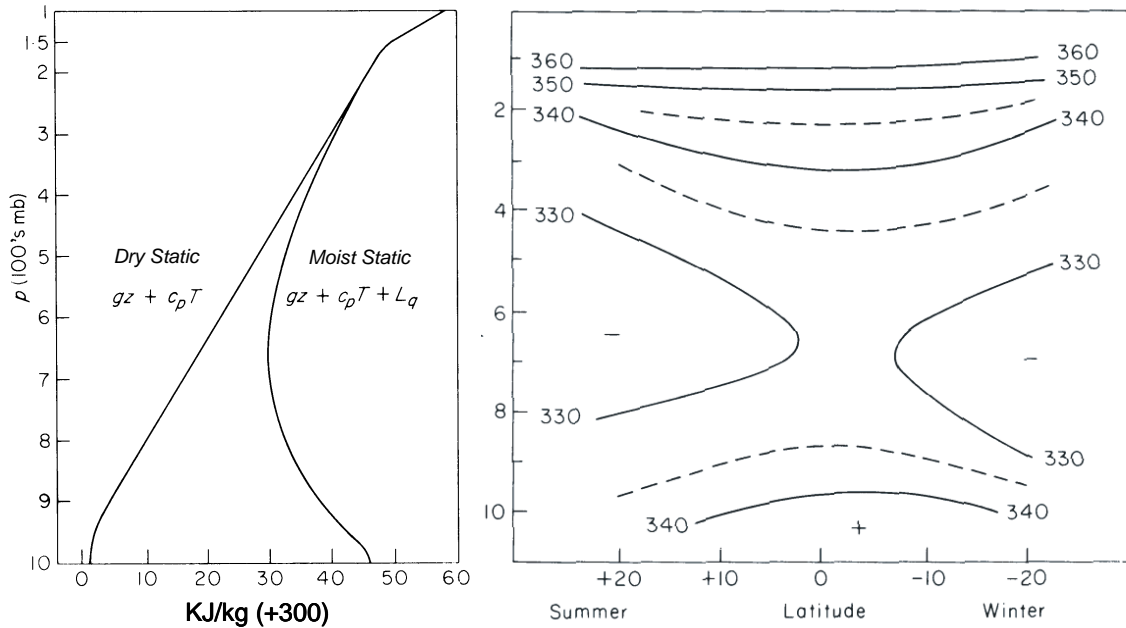
Figure 2.5: *Left panel: Vertical profile of dry static energy and moist static energy in the ITCZ. The abscissa indicates the excess over 300 KJ/kg. Right panel: Latitude/altitude cross-section of moist static energy (in KJ/kg) across the tropics [From Riehl and Simpson, 1979]*

In fact it appears that the only way in which heat can be effectively be brought from the surface to the upper-troposphere in the ITCZ is through pseudo-adiabatic ascent in the cores of cumulonimbus clouds (so-called "hot towers"). For such motions, the air parcels approximately conserve their surface values of moist static energy and can therefore arrive in the upper troposphere where they start to move outward in the cumulonimbus anvil where they reach their level of static equilibrium with the surroundings. Not considering the possibility of overshooting the neutral buoyancy level, the equilibrium height of the ascending parcel can be obtained by considering its surface values, $Q_{MS, surf} \approx 345$ kJ kg^{-1}, against Q_{MS} of the upper troposphere at a given altitude.

Thus, the heat balance of the ITCZ can be accounted for, at least qualitatively, provided that the vertical motion in the ITCZ is confined primarily to the updrafts of individual convective cells [*Riehl and Simpson*, 1979]. Only a small number (1500-2500) of individual undiluted hot towers are required to be active at one time if their average area is 25 km^2 and ascent speed is 2-3 m/s [*Riehl,* 1979]. The hot towers act as an atmospheric heat engine by converting latent heat into potential energy through raising high enthalpy air from the surface layer to the upper troposphere.

The ITCZ is a narrow zonal band of vigorous cumulus convection where precipitation greatly exceeds the moisture supplied by evaporation from the ocean surface below. Thus, much of the vapor necessary to maintain the convection in the ITCZ must be supplied by the converging trade wind flow in the lower troposphere. In this manner, the large scale flow provides the latent heat supply for the convection and the convective heating in turn produces the large scale pressure field, which maintains the low level inflow.

However, this description of ITCZ is oversimplified. In reality, over the oceans the ITCZ appears normally as a number of clusters of heavy convective cloudiness, with scales of the order of few hundred kilometers, which are separated by regions of relatively clear skies. The strength of the ITCZ is also quite variable in both space and time. It is particularly persistent and well defined over the Pacific and Atlantic oceans between about 5°N and 10°N latitude, and occasionally appears over the Pacific Ocean between 5°S and 10°S [*Holton*, 1979]. The convective activity in the ITCZ manifests itself often as heavy cloud clusters which appear to be moving as a wave pattern with a typical eastward propagation velocity of 8-10 m/s, the so called Madden-Julian oscillation (MJO) with a typical period of about 40-50 days [*Madden and Julian,* 1971, 1994].

The rising motion in deep convection must be compensated by subsidence in the environment if an overall mass balance is to be maintained. Only a fraction of about 0.01 of the convective areas in the tropics is covered by active convective cells. This means that for an average vertical ascending velocity of 1 m/s [*Balsley et al*, 1988, *Gage et al.,* 1991] in the cumulus towers this implies a compensating subsidence of 0.01 m/s over the trough zone.

Over certain regions of the tropics, especially the Indonesian archipelago, deep convective transport can be so vigorous that it even can penetrate into the stratosphere which provides an important mechanism to inject tropospheric trace gases (including water vapor) into the stratosphere [e.g. *Newell and Gould-Stewart,* 1981]. In this way deep convection is feeding the upward transfer of the stratospheric Brewer-Dobson circulation [e.g. *Brewer,* 1949, *Andrews et al.,* 1987]. In this context deep convection in conjunction with the cold- trap at the tropical tropopause ($\approx$ -80°C) is also the most likely mechanism that determines the stratospheric water vapor content [e.g. *Kley et al*, 1982].

2.1.3   Water Vapor and Deep Convection

Deep convection, together with large scale subsidence, is involved in one of the most prominent regulating mechanism that determines the climate whereby water vapor together with clouds is of crucial importance. However, water vapor and cloud feedback also constitute the largest uncertainties in quantifying the climate system and its future changes [*IPCC,* 1996, 2001]. Water vapor feedback is the interaction between surface temperature, water vapor and the Earth's radiation balance. While it is clear that evaporation from the surface in combination with convective processes is ultimately responsible for the flux of water vapor to the atmosphere, and precipitation is the sink, it is less clear, what are the processes that control the water vapor concentration in the UT [e.g. *Held and Soden,* 2000].

Complication thereby is that the control processes are strongly influenced by water vapor itself through feedback mechanisms caused by radiative forcing and moist convection whereby clouds play a crucial role. The large-scale distribution of water vapor in the tropics is dependent on the properties of deep convection [*Betts*, 1990]. However, an adequate understanding of the anatomy of moist convection and how it interacts with the large scale flow still does not exist. Much of our uncertainty in predicting future climate arises from a poor understanding of how water vapor behaves in the atmosphere and the role that clouds may play.

Figure 2.6 shows a histogram of relative humidity values as a function of atmospheric pressure, obtained from radiosonde observations over the tropical western Pacific Ocean [*Spencer and Braswell*, 1997]. The higher pressure levels below 700 hPa are moist, with relative humidities (RH) of 70-90%, as would be expected for the turbulent boundary layer with the tropical ocean as a moisture source. However, immediately above the boundary layer frequent instances of much drier conditions, with a peak in the frequency distribution near 15% RH between 500 and 250 hPa are the norm. This sharp decrease in RH rules out the possibility of large scale upward transport of water vapor from the boundary layer. This separation of humidity regimes is clear evidence of the very different processes controlling boundary layer versus free tropospheric humidity [*Sun and Lindzen*, 1993]. Above pressure levels of 250 hPa the relative humidity exhibits enhanced values peaking at about 35% (RH with respect to saturation over liquid water). The primary source of this upper tropospheric moisture in the convectively active regions of the tropics is most likely the vertical convective transport of condensed water plus the subsequent convective detrainment with eventual evaporation of hydrometeors [e.g. *Betts*, 1990, *Sun and Lindzen,* 1993]. Detrainment (the opposite of entrainment) is a process whereby air and cloud particles are transferred from the organized convective updraft to the surrounding atmosphere.
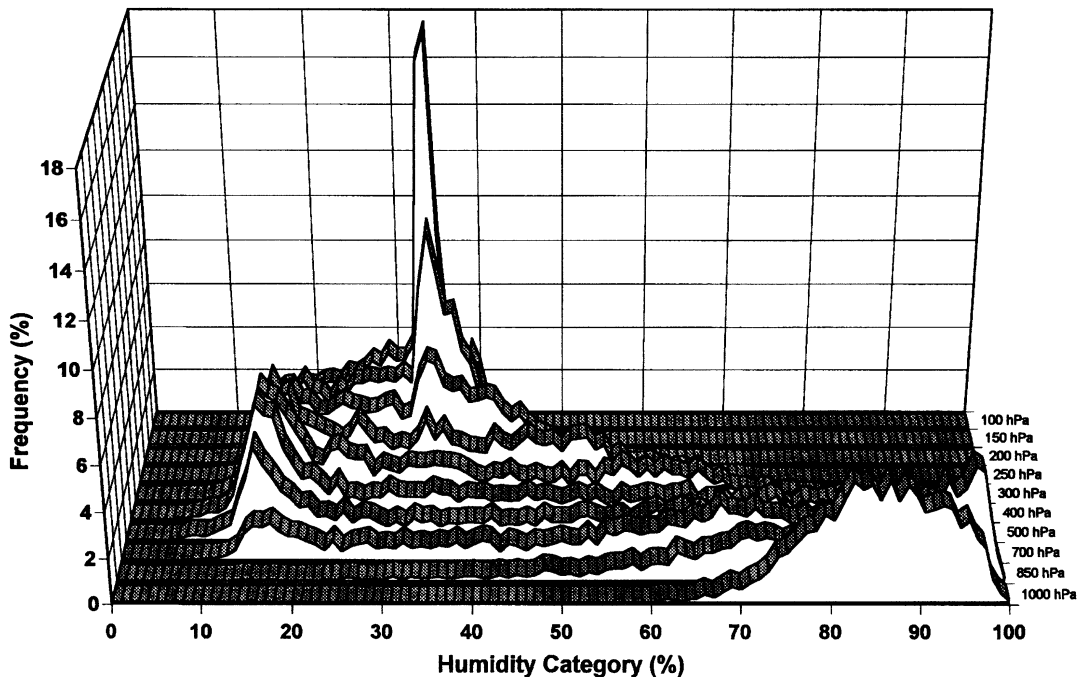
Figure 2.6 : *Frequency histograms of relative humidities (with respect to saturation over liquid water) at pressure levels from 1000 to 100 hPa for a total of 1600 radiosonde ascents at Yap, Koror, Ponape, and Majuro in the tropical western Pacific during January-May of 1994 and 1995. [From Spencer and Brasswell, 1997]*

Convection in the tropics also generates widespread and often upper level anvil clouds, which generate precipitation and can moisten the sub-saturated air below through evaporation of falling hydrometeors. The outflow region of deep convection is also a region of widespread compensating subsidence. In non-convective regions in the tropics the air appears to be relatively dry. Subsidence decreases the relative humidity through compressional heating. Hence the dualism exist that detrainment and evaporation of anvil precipitation act to moisten the tropical environment while compensating subsidence dries the tropical environment. At

the present a controversy exist whether an increase of SST will also cause an enhancement of water vapor in the upper troposphere [e.g. *Inamdar and Ramanathan*, 1994, 1998] or will have a drying effect [e.g. *Lindzen,* 1989, *Sun and Lindzen,* 1993]. Convective cloud systems which transport water vapor aloft may carry moisture to higher elevations but there is also evidence that microphysical processes and cloud dynamics may dry the upper troposphere. However, the possible mechanisms are still poorly understood.

The processes controlling the vertical mass fluxes in the deep convection and precipitation efficiency are not well known for tropical meso-scale convective systems. At present, it is not clear whether deep convection acts to dry or moisten the upper troposphere and even more uncertain is its response in a warmer climate [e.g. *Webster,* 1994]. An additional difficulty is that an analysis of the local tropical thermodynamic water vapor feedback can be misleading, since large scale horizontal advection is an important part of the global moisture budget.

2.1.4 Can Large Scale Subsidence Dry The Tropics?

An important point for the understanding of the water vapor feedback in tropical climate is to recognize that the tropics can be divided in convective (ascending) and non-convective (subsiding) regions. Only a small fraction of the tropics is subject to direct moistening by nearby deep convection. This can be clearly seen from the global distribution of outgoing long wave radiation (OLR) shown in Figure 2.7.
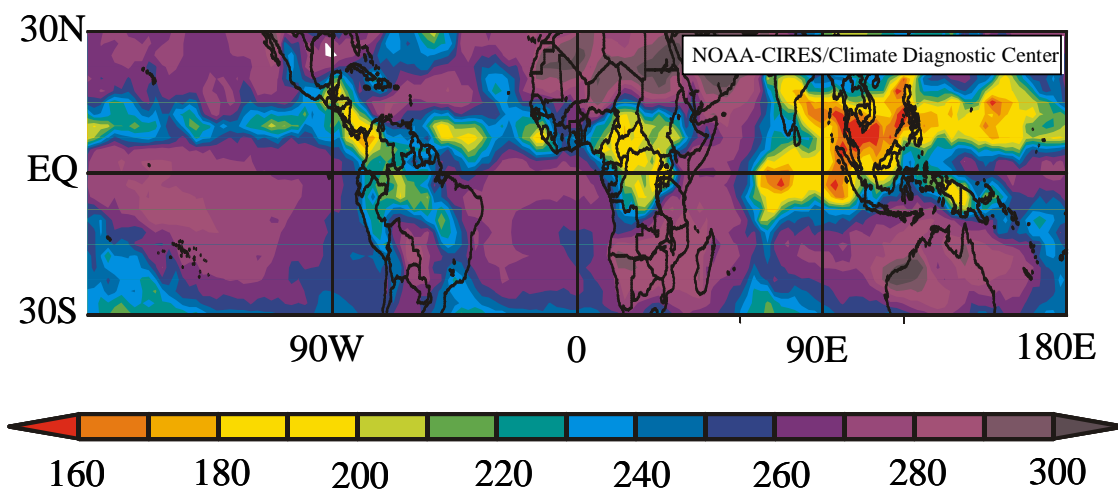
Figure 2.7: Global distribution of OLR (in W/m^2) from NCEP re-analysis over period between 26 and 30 September 1988. (Image provided by the NOAA-CIRES Climate Diagnostics Centre, Boulder, Colorado, URL= http://www.cdc.noaa.gov)

Regions in the tropics with low OLR, typical below 250 W/m^2 indicating cold cloud top temperatures of high level cumulonimbus clouds, i.e. deep convective activity, while high OLR indicates warm temperatures, which means no upper level clouds, i.e. suppressed convection [e.g. *Waliser and Graham*, 1993]. Three regions with strong convective activity (OLR below about 250 W/m^2) are confined to the narrow zonaly oriented ITCZ band, the warm pool region with the highest sea surface temperatures in the tropical western Pacific and equatorial Pacific, and the continental tropical regions in South America and Africa. These regions cover about one third of the tropics, while the rest of the tropical free atmosphere must

get its moisture by some more indirect means. The convective region is characterized by mean ascent where the resulting adiabatic cooling balances the latent heat release due to precipitation. Non-convective regions are characterized by mean descent, with the resulting adiabatic warming balancing infrared radiative cooling.

In the tropics, outgoing long wave radiation (OLR) is very sensitive to changes in upper tropospheric water vapor content. The lower tropospheric moisture content is very high, such that the long wave radiation emitted by the Earth's surface is fully absorbed (optically thick) - most notably by water vapor with a corresponding high water vapor emissivity. Therefore, small changes in lower tropospheric moisture content have little influence on either the local tropical OLR or on downwelling long wave radiative flux to the surface. The net radiative flux is more sensitive to changes in water vapor amount in the upper troposphere where the water vapor mixing ratio is low and the infrared absorption is far from being optically thick.
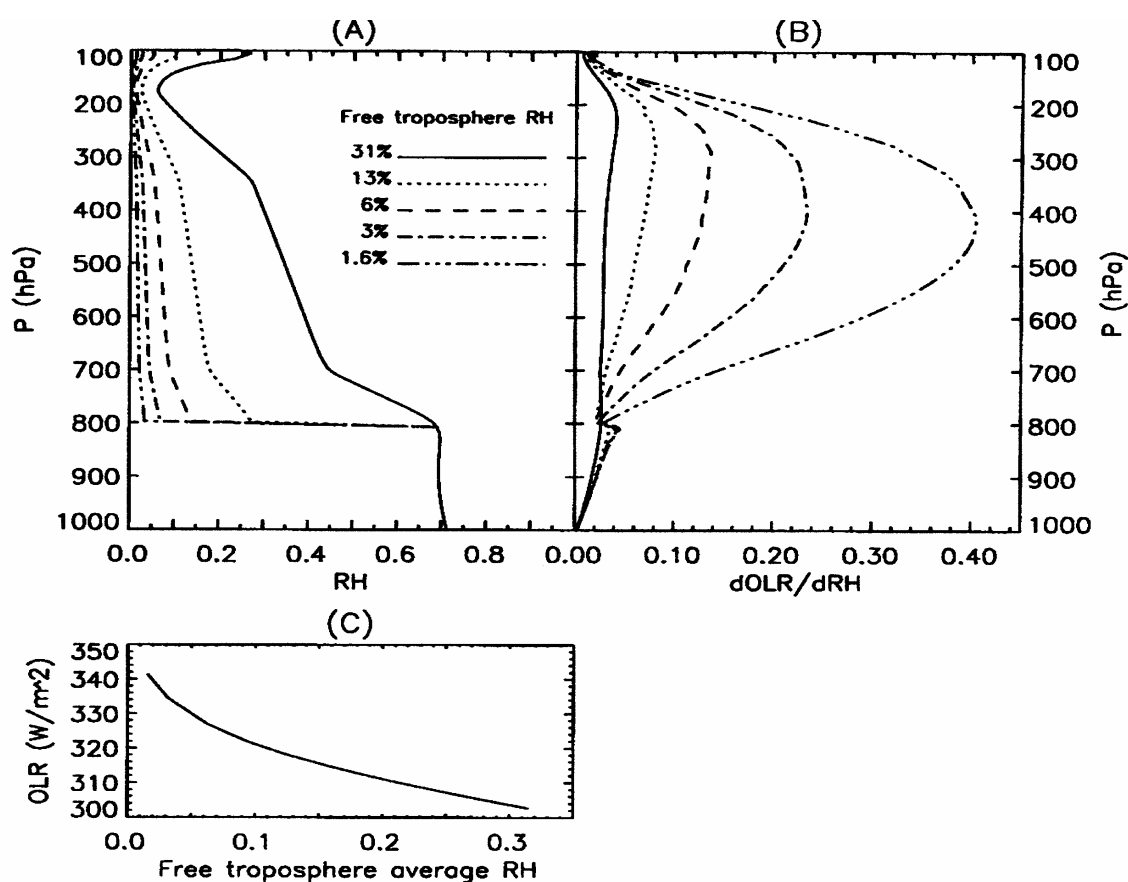
Figure 2.8: (a) Progressive humidity profiles computed by reducing a standard tropical free tropospheric specific humidity between 800 and 100 hPa by multiplicative factors of 1.0, 0.4, 0.2, 0.1, and 0.05. This results in height weighted average relative humidities in the free troposphere of 31%, 13%, 6%, 3% and 1.6%, respectively. (b) Sensitivity of OLR to additative changes of RH of 3% in 10 hPa thick layers as a function of the humidity profiles shown in (a). (c.) The non-linear dependence of clear sky OLR over this range of free tropospheric RH. Source: Spencer and Braswell, 1997.

The sign of the tropical water vapor feedback is therefore strongly dependent on the response of upper tropospheric humidity to a change of the surface temperature [*Lindzen*, 1995]. Spencer and Braswell [1997] who calculated the OLR for clear sky conditions at progressive drier vertical RH-profiles derived from a standard tropical profile [See Figure 2.8] also demonstrated this. The figure shows clearly the non-linear sensitivity of OLR to RH changes such that OLR for the drier troposphere is most sensitive to small fluctuations in RH.

In a dry *free* troposphere at pressures below 800 hPa and at relative humidities between 10 % and 30 % the OLR is reduced by more than 15 W/m^2. Taking into account that a doubling of CO_2 concentration from pre-industrial values would reduce the Earth's OLR by about 3.7 W/m^2 [*IPCC*, 2001], this shows the crucial importance of knowing the humidity of the upper troposphere. Lindzen [1995] who showed that humidity fluctuations at 10% RH have about three times as much impact on OLR as do fluctuations around 90% RH has addressed the non-linear relationship of OLR and humidity in the upper troposphere. If low relative humidities cover a large fraction of the tropics, then the mechanisms that control the UT humidity levels of these dry zones is of importance to understanding the global radiation budget. *Pierrehumbert* [1995] argued that dry air in the tropics might regulate the tropical climate even to a larger degree than cloudiness.

Mapes et al., [2001] using a radiative transfer model showed that under cloudless (clear sky) conditions the upper troposphere dries very rapidly as shown in Figure 2.9 which shows the evolution of the vertical RH-profile if the atmosphere would be subjected to diabatic heating due to subsidence. At 10 km altitude the air can dry from saturation to dry values, clearly below 30% RH, within a period of less than 2-3 days of subsidence. An interesting question thereby also arises in how far the dry air entraining into the Cb-convection can have a regulating effect on the intensity of deep convection?
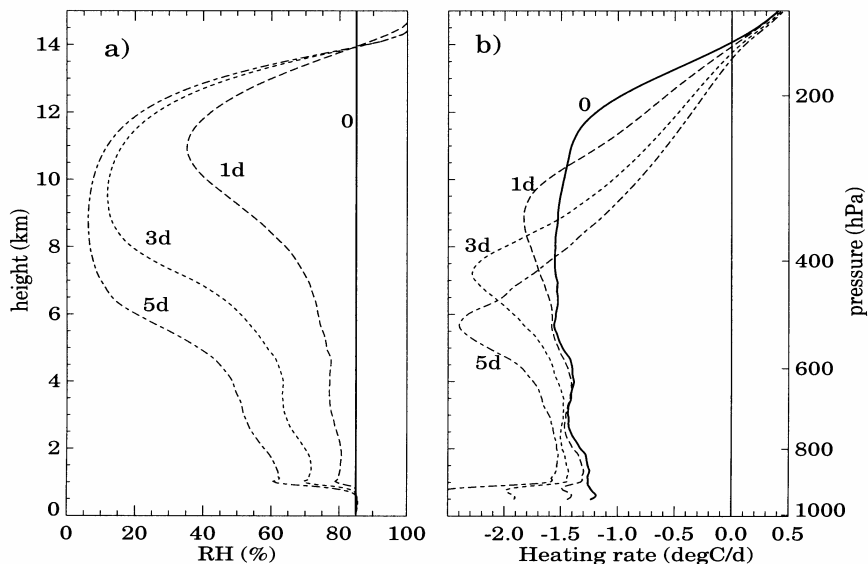
Figure 2.9: *Evolution of vertical relative humidity profile under cloudless conditions and subject to diabatic subsidence (left diagram), corresponding evolution of the radiative cooling profile [Source: Mapes et al., 2001]*

2.2 Photochemistry of Ozone in the Remote Marine Tropics

2.2.1 Introduction

A considerable number of global studies, reported over the last two decades, have shown that much of the ozone in the troposphere is of photochemical origin [e.g. *Fishman, Solomon and Crutzen*, 1979, *Liu et al.,* 1980, *Jacob et al., 1993, Müller and Brasseur,* 1995, *Roelofs et al.*, 1997, *Levy et al.,* 1997, *Wang et al.,* 1998]. These studies suggested that the amount of ozone that is photochemically produced (3500-4500 Tg/yr) largely balance the chemical loss (3400-4100 Tg/yr). Transport into and out of the troposphere caused by stratospheric input (400-800 Tg/yr) and dry deposition (500-1200 Tg/yr), respectively, are of comparable magnitude. An important contributor to the regional but also global ozone budget is situated in the tropics and is related to biomas burning activities [e.g. *Crutzen and Andreae*, 1990]

In the free troposphere, due to lower air densities, lower temperatures and lower water vapor abundance (i.e. lower OH-concentrations) at higher altitudes, the photochemistry of ozone generally proceeds much slower relative to that within the PBL. In addition, fast reacting VOC's are largely absent compared to more slowly reacting substances such as carbon monoxide, methane and some oxygenated hydrocarbons (e.g. acetone) [*Singh et al.,* 1994, 1995]. Furthermore, in the free troposphere the photochemical lifetime of ozone becomes long, in excess of several months in the altitude region close to the tropopause. Therefore, it is clear that in addition to photochemistry, knowledge of atmospheric transports in general and of vertical ozone transport in particular, is a prerequisite for the establishment of the ozone distribution in the free troposphere.

Finally, in the middle/upper troposphere the concentration of ozone is strongly influenced by ozone transport from the stratosphere, which involves complex processes on the synoptic as well as the global scale [*Danielsen, 1968, Danielsen and Mohnen,* 1977, *Holton et al.,* 1979]. Overall, stratosphere-troposphere exchanges in combination with tropospheric horizontal and vertical transport conspire to create a large variability of ozone on short to long time scales in the upper troposphere. This has made it impossible up to the presence to demonstrate by direct observations that in situ formation of ozone does have an effect on the ozone distribution in the free troposphere.

Knowledge of the concentration and sources of NO_X and their local, regional, and global distribution on a temporal and spatial scale is thereby of primary importance for a better understanding of the photochemistry of ozone and its contribution to the budget of tropospheric ozone. The net photochemical production or destruction of ozone depends critically on the NO-concentration [*Crutzen*, 1979, 1988, *Liu et al.*, 1980]. Due to the relatively short life time of the order of one day and the large variety of sources [e.g. *Ehhalt et al.,* 1992] tropospheric NO_X-mixing ratios are highly variable ranging from a few pptv over remote areas to more than four orders of magnitude larger values over urban regions. Besides, of upper air emissions of NO_X by lightning or aircraft, most of the NO_X-sources like fossil fuel combustion, biomass burning and soil emissions are located over the continent [e.g. *Ehhalt et al.,* 1992, *Horowitz and Jacob*, 1999]. Although research about the fate of nitrogen oxides has progressed strongly during last two decades, there are still large deficiencies in the knowledge about the tropospheric budget and distribution of NO_X. [*Carroll and Thompson*, 1995].

The remote marine troposphere in the tropics is characterized by low NMHC concentrations [e.g. *Rudolph,* 1988, *Rudolph and Johnen,* 1990, *Koppmann et al.,* 1992, *Donahue and Prinn,* 1993] and low NO_X-levels: only a few pptv in the PBL [e.g. *McFarland et al,* 1979, *Ridley et al.,* 1987, *Rohrer et al.,* 1992, *Torres and Thompson, 1993*] and 50-200 pptv in the free troposphere [e.g. *Drummond et al.,* 1988, *Rohrer et al,* 1997, *Emmons et al.,* 1997]. This means that the in-situ photochemical fate of ozone in the marine tropics is predominantly determined by the oxidation of CO and CH_4 in conjunction with a moderate to poor NO_X (<200 pptv) environment while the contribution of NMHC-photochemistry is of minor significance [e.g. *Thompson,* 1993].

2.2.2 Sources and Sinks of Ozone.

The primary natural source of tropospheric ozone located in the upper stratosphere where ozone is formed from photolytic dissociation of oxygen molecules into atomic oxygen by solar ultraviolet radiation and subsequent reaction with oxygen molecules (R1 and R2).

$$O_2 \;+\; h\nu \quad (\lambda<240\,nm) \quad \longrightarrow \quad O(^3P) \;+\; O(^3P) \qquad [R1]$$

$$O_2 \;+\; O(^3P)+\; M \quad \longrightarrow \quad O_3 \qquad +\; M \qquad [R2]$$
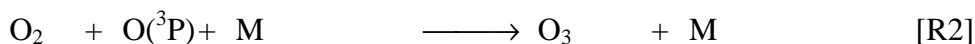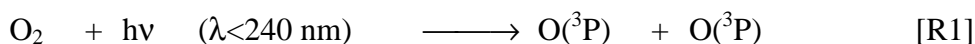
The earliest view assumed that stratospheric ozone is transferred by atmospheric dynamics into the troposphere and destroyed at the surface with no intervening chemistry [e.g. *Regener,* 1949, *Junge,* 1963]. However, the stratospheric ozone flux, estimated as 200-500 Tg O_3 /yr. [e.g. *Danielsen,* 1968, *Danielsen and Mohnen,* 1977], is not balanced by the surface deposition flux of about 500-1000 Tg O_3 /yr. [e.g. *Fabian and Pruchniewicz,* 1977, *Galbally and Roy*, 1980]. The reaction mechanism R1, R2 is not active in the troposphere due to the absence of short wave ultraviolet solar radiation, which is absorbed by the stratospheric ozone and oxygen. However, in the troposphere ozone can be formed via the photolytic dissociation of nitrogen dioxide (NO_2) by solar radiation producing atomic oxygen, which recombines then with oxygen molecules [R2] to form ozone:

$$NO_2 \quad +\; h\nu \quad (\lambda<410\,nm) \quad \longrightarrow \quad NO \quad +\; O(^3P) \qquad [R3]$$
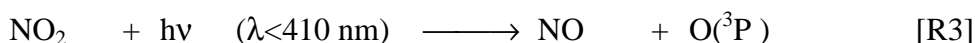
This photochemical production of ozone is in rapid photostationary state through the chemical destruction of ozone via reaction with nitric oxide (NO):

$$O_3 \quad +\; NO \quad \longrightarrow \quad NO_2 \quad +\; O_2 \qquad [R4]$$
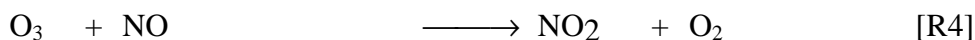
However, the NO_2 that is necessary for a net ozone production originates from the oxidation of nitric oxide (NO) during the atmospheric oxidation of CO (carbon monoxide), CH_4 (methane) and NMHC (non methane hydrocarbons) according to the net reaction scheme:

$$CO, CH_4, NMHC + NO + h\nu \quad \longrightarrow \quad NO_2 \quad +\; products \qquad [R5]$$
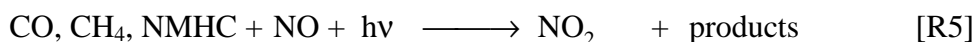
The mechanism [R5] was first identified in the early 1950's by *Haagen-Smit et al*. [e.g. 1952, 1953] studying the Los Angeles summer smog.

In the beginning of the 1970's after the prediction of a vigorous radical chemistry in the troposphere by *Levy* [1971], *Crutzen* [1973, 1974] and *Chameides and Walker* [1973] proposed that in these photo-oxidation mechanisms reactive radicals such as the hydroxyl (OH) and hydroperoxyl (HO_2) radical play an important role with OH radicals initiating the oxidation of CO, CH_4 and most NMHC's. In the troposphere hydroxyl radicals are primarily

produced from the photodissociation of ozone due to solar ultraviolet radiation in the presence of water vapor according the reaction scheme R6 to R9:

$$O_3 \quad + \quad h\nu\,(\lambda<320\ nm) \quad \longrightarrow \quad O_2 \quad + \quad O(^1D) \qquad [R6]$$

$$O(^1D) \quad + \quad M \quad \longrightarrow \quad O(^3P\,) \quad + \quad M \qquad [R7]$$

$$O(^3P\,) \quad + \quad O_2 + \quad M \quad \longrightarrow \quad O_3 \quad + \quad M \qquad [R8]$$

$$O(^1D) \quad + \quad H_2O \quad \longrightarrow \quad 2\,OH \quad + \quad M \qquad [R9]$$
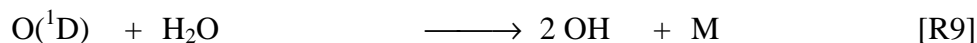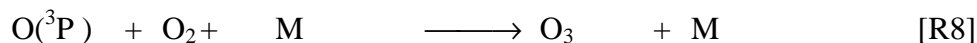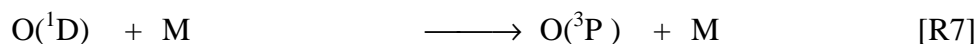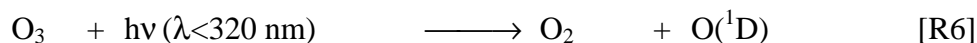
Within the oxidation mechanisms of CO, CH_4, and NMHC the NO_X (= NO + NO_2) act as a catalyst regarding the photochemical production of ozone [*Crutzen,* 1979] as is shown by the oxidation mechanisms of CO and CH_4 respectively:

$$CO \quad + \quad OH \quad + \quad O_2 \quad \longrightarrow \quad CO_2 \quad + \quad HO_2 \qquad [R10]$$

$$HO_2 \quad + \quad NO \quad \longrightarrow \quad NO_2 \quad + \quad OH \qquad [R11]$$

$$NO_2 \quad + \quad h\nu \quad (\lambda<410\ nm) \quad \longrightarrow \quad NO \quad + \quad O(^3P) \qquad [R3]$$

$$O_2 \quad + \quad O(^3P) + \quad M \quad \longrightarrow \quad O_2 \quad + \quad M \qquad [R2]$$

_____

Overal: $CO \quad + \quad 2\,O_2 \quad + \quad h\nu \quad \longrightarrow \quad O_3 \quad + \quad CO_2 \qquad [R12]$

$$CH_4 \quad + \quad OH \quad \longrightarrow \quad CH_3 \quad + \quad H_2O \qquad [R13]$$

$$CH_3 \quad + \quad O_2 \quad + \quad M \quad \longrightarrow \quad CH_3O_2 \quad + \quad M \qquad [R14]$$

$$CH_3O_2 \quad + \quad NO \quad \longrightarrow \quad CH_3O \quad + \quad NO_2 \qquad [R15]$$

$$CH_3O \quad + \quad O_2 \quad \longrightarrow \quad HO_2 \quad + \quad CH_2O \qquad [R16]$$

$$HO_2 \quad + \quad NO \quad \longrightarrow \quad NO_2 \quad + \quad OH \qquad [R11]$$

$$2\,NO_2 \quad + \quad h\nu \quad (\lambda<410\ nm) \quad \longrightarrow \quad 2\,NO \quad + \quad 2\,O(^3P) \qquad [R3]$$

$$2\,O_2 \quad + \quad 2\,O(^3P) \quad + \quad M \quad \longrightarrow \quad 2\,O_3 \quad + \quad M \qquad [R2]$$

_____

Overal: $CH_4 \quad + \quad 4\,O_2 + \quad h\nu \quad \longrightarrow \quad 2\,O_3 \quad + \quad CH_2O \quad + H_2O \qquad [R17]$
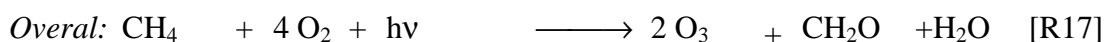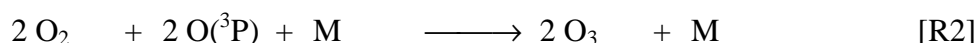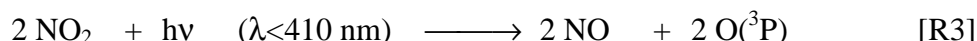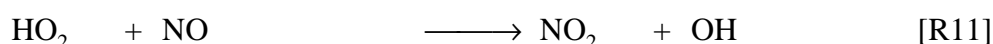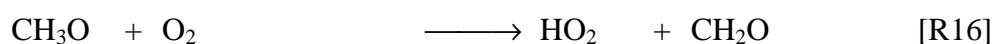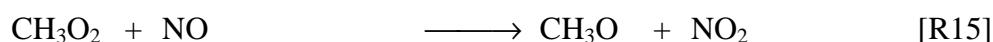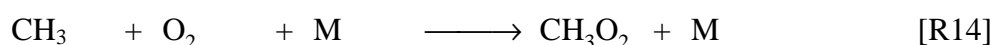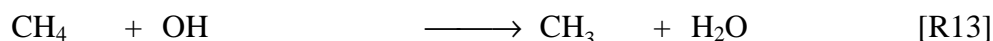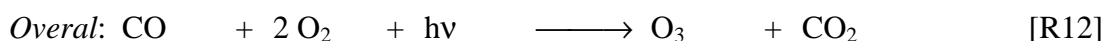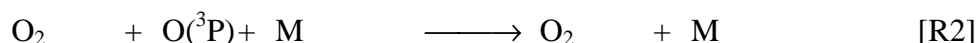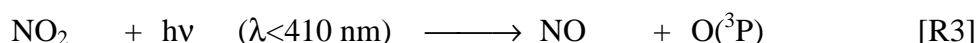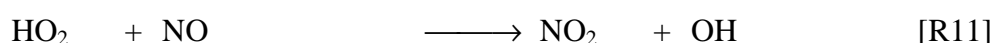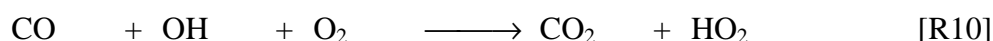
An additional source of HO_X constitutes the further oxidation of formaldehyde (see next section).

The photochemical formation of ozone from the oxidation of NMHC proceeds in a similar way but according more complex reaction mechanisms [e.g. *Finlayson-Pitts and Pitts,* 1997].

Paradoxically, HO_X-radicals are not only involved in the photochemical formation of ozone but also jointly responsible for the photochemical destruction of ozone. Besides of its photolysis in the presence of water vapor [R6 to R9] ozone can also be destroyed by its reaction with OH [R14] and HO_2 [R15], respectively:

$$O_3 \quad + \quad OH \quad \longrightarrow \quad O_2 \quad + \quad HO_2 \qquad [R18]$$

$$O_3 \quad + \quad HO_2 \quad \longrightarrow \quad 2\,O_2 \quad + \quad OH \qquad [R19]$$
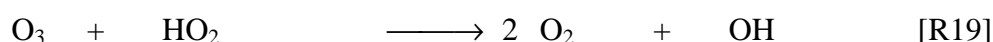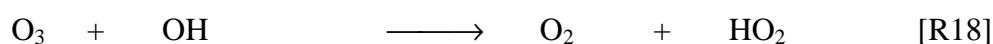
Apart of these photochemical sinks, in the PBL ozone can also be removed by dry deposition to the surface.

$$O_3 \quad + \quad \text{Dry Deposition.} \longrightarrow \quad \text{Products} \qquad [R20]$$
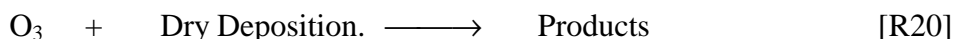
Because the photolysis of ozone in the presence of water vapor is simultaneously the primary source of HO_X driving the photochemistry of ozone, the crucial role water vapor plays in the photochemical fate of ozone is obvious.

2.2.3 Role of HO_X and NO_X

The photochemical formation of ozone from the oxidation of CO, CH_4, and NMHC compete with reactions that can deplete HO_X, CH_3O_2 or NO_X radicals and thus limit the chain length of the oxidation mechanisms for CO [R12] and CH_4 [R17]). In the first stage, HO_X-radicals are predominantly removed by self-reaction of HO_2 [R21] and OH [R22], cross-reaction of OH with HO_2 [R23] and reaction of OH with NO_2 [R24]:

$$HO_2 \quad + \quad HO_2 + M, H_2O \longrightarrow \quad H_2O_2 \quad + O_2 + M, H_2O \quad [R21]$$

$$OH \quad + \quad OH \ + M \quad \longrightarrow \quad H_2O_2 \quad + M \qquad [R22]$$

$$OH \quad + \quad HO_2 \quad \longrightarrow \quad H_2O \quad + O_2 \qquad [R23]$$

$$OH \quad + \quad NO_2 + M \quad \longrightarrow \quad HNO_3 \quad + M \qquad [R24]$$
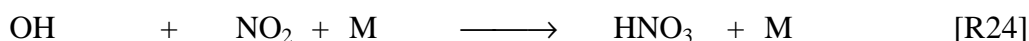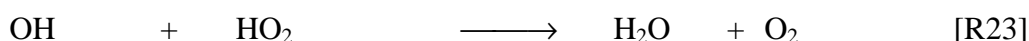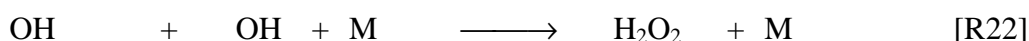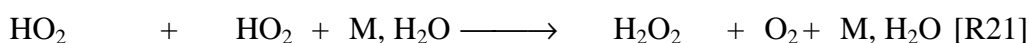
The formed hydrogen peroxide, still a reservoir of HO_X-radicals, can be photolyzed [R25], react with OH [R26], or be removed heterogeneously by aerosols, clouds or rain [R27]:

$$H_2O_2 \quad + \quad h\nu \quad \longrightarrow 2 \ OH \qquad [R25]$$

$$H_2O_2 \quad + \quad OH \quad \longrightarrow \quad H_2O \quad + HO_2 \qquad [R26]$$

$$H_2O_2 \quad + \quad \text{Heterogeneous} \longrightarrow \quad \text{Products} \qquad [R27]$$
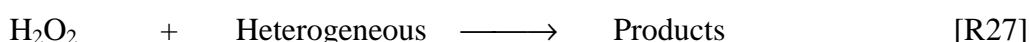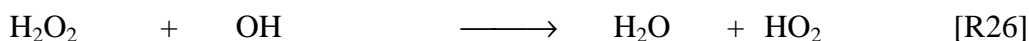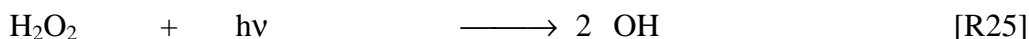
Thereby HO_X can be recycled [R25] but also removed [R26, R27] from active photochemistry. In a similar way, the CH_3O_2-radical reacts whereby the formed methyl peroxide is an additional reservoir for HO_X and CH_3O_2 radicals while further reaction can recycle but also remove HO_X or CH_3O_2 from active photochemistry:

$$CH_3O_2 \quad + \quad CH_3O_2 \quad \longrightarrow \quad CH_3OH + CH_2O \qquad [R28]$$

$$CH_3O_2 \quad + \quad CH_3O_2 \quad \longrightarrow 2 \ CH_2O \quad + HO_2 \qquad [R29]$$

$$CH_3O_2 \quad + \quad HO_2 \quad \longrightarrow \quad CH_3OOH + O_2 \qquad [R30]$$

$$CH_3OOH \ + \quad h\nu \quad + O_2 \quad \longrightarrow \quad CH_2O \quad + HO_2 \qquad [R31]$$

$$CH_3OOH \ + \quad OH \quad + O_2 \quad \longrightarrow \quad CH_2O \quad + OH \ + H_2O \ [R32]$$

$$CH_3OOH \ + \quad OH \quad + O_2 \quad \longrightarrow \quad CH_3O_2 \quad + H_2O \qquad [R33]$$

$$CH_3OOH \ + \quad \text{Heterogeneous} \ \longrightarrow \quad \text{Products} \qquad [R34]$$

$$CH_3OH \quad + \quad OH \quad \longrightarrow \quad \text{Products} \qquad [R35]$$
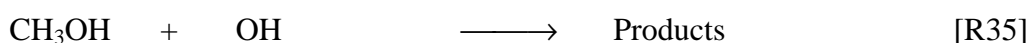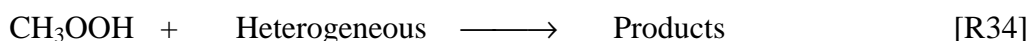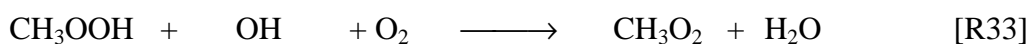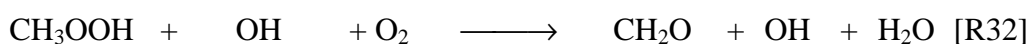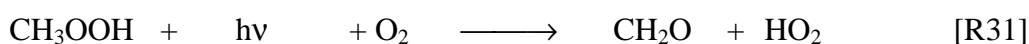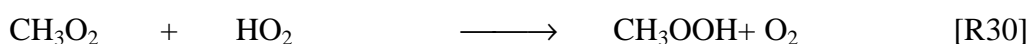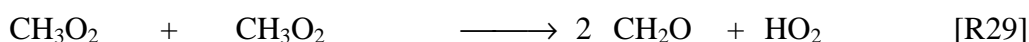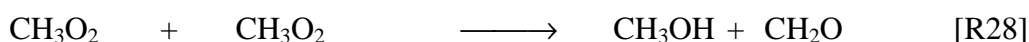
An additional source of HO_X radicals constitutes the photochemical degradation of formaldehyde:

$$CH_2O \quad + \quad h\nu \qquad \longrightarrow \qquad H_2 \quad + \quad CO \qquad [R36]$$

$$CH_2O \quad + \quad h\nu \quad + 2\,O_2 \longrightarrow 2\,HO_2 \quad + \quad CO \qquad [R37]$$

$$CH_2O \quad + \quad OH \quad + \quad O_2 \longrightarrow \quad HO_2 \quad + \quad CO \quad + \quad H_2O \quad [R38]$$

$$CH_2O \quad + \quad \text{Heterogeneous} \quad \longrightarrow \quad \text{Products} \qquad [R39]$$
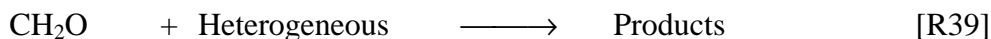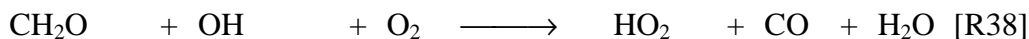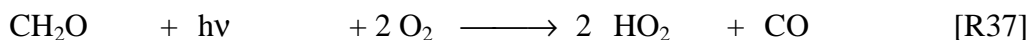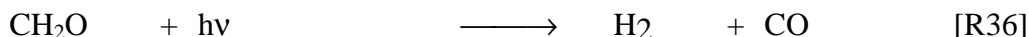
However, depending on the concentration of NO the final oxidation of methane can yield a net sink of HO_X in NO poor air or a net source of HO_X in NO rich air [*Logan et al.,* 1981, *Crutzen et al.*, 1988)]. However, CH_4 oxidation contributes only about 20 % to the net sink of HO_X [*Logan et al.,* 1981]. Although the reaction of OH with NO_2 [R24] contributes only significant losses of HO_X for NO_X levels above 200 pptv it constitutes the major sink for NO_X via the heterogeneous removal and wash out of HNO_3 [R40]:

$$HNO_3 \quad + \quad \text{Heterogeneous} \quad \longrightarrow \quad \text{Nitrates} \qquad [R40]$$

However, in the upper troposphere NO_X can recycle through UV-photolysis of HNO_3 [R41] or reaction with OH with HNO_3 [R42]:

$$HNO_3 \quad + \quad h\nu \qquad \longrightarrow \qquad OH \quad + \quad NO_2 \qquad [R41]$$

$$HNO_3 \quad + \quad OH \quad + \quad M \quad \longrightarrow \quad H_2O \quad + \quad NO_2 \quad +M \qquad [R42]$$

Furthermore, NO_2 and HO_2 are in thermal/photolytic equilibrium with HO_2NO_2 through reactions [R43], [R44], and [R45]. However, as a temporary reservoir of NO_X and HO_X this reaction chain is only in the upper troposphere of significance:

$$HO_2 \quad + \quad NO_2 \qquad \longrightarrow \qquad HO_2NO_2 \qquad [R43]$$

$$HO_2NO_2 \quad \text{Thermal} \quad \longrightarrow \quad HO_2 \quad + \quad NO_2 \qquad [R44]$$

$$HO_2NO_2+ \quad h\nu \qquad \longrightarrow \qquad OH \quad + \quad NO_2 \qquad [R45]$$

Eventual losses of ozone or NO_X by the formation of N_2O_5 from reactions of O_2 with NO_2[2] and the additional removal by heterogeneous reactions, are negligibly small due to the low NO_X concentrations (NO_X<200 pptv) in marine remote regions [*Drummond et al.,* 1988, *Rohrer et al.*, 1992] and will not be considered here.

The atmospheric lifetimes of peroxides and formaldehyde are sufficiently long ($\approx$few days) such that through fast convective transport these substances can be injected in the UT and subsequent photochemical degradation can provide an additional primary source of HO_X and may alter the chemical composition of the UT significantly. [e.g. *Chatfield and Crutzen*, 1984, *Prather and Jacob*, 1997, *Cohan et al.,* 1999].

---

[2] N_2O_5 is formed from reaction of O_3 with NO_2:

$\quad NO_2 \quad + \quad O_3 \quad \longrightarrow \quad NO_3 \quad + \quad O_2$

$\quad NO_2 \quad + \quad NO_3 \quad \longleftrightarrow \quad N_2O_5 \; \textit{(thermal equilibrium)}$

$\quad N_2O_5 \quad + \quad \text{Het.} \quad \longrightarrow \quad \text{Products}$
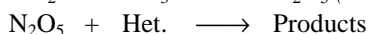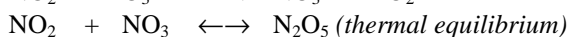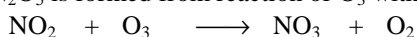
This is a typical night time mechanism because during day time NO_3 is very low due to its fast photolysis resulting back into NO_2 and $O(^3P)$. The latter forms with oxygen via R2 instantly O_3 again

2.2.4 Role of Oxygenated Hydrocarbons

Although some progress has been made by in-situ measurements of OH and HO_2 in the middle/upper troposphere recently, large deficiencies exist in the understanding and quantification of the processes governing the HO_X-radicals and their impact on in-situ photochemistry of ozone. Recent in-situ measurements of OH and HO_2 in the upper troposphere have shown [*Jaeglé et al*., 1997, *Wennberg et al*., 1998] that the observed HO_X concentrations are larger than what model studies have suggested in which photolysis of ozone in the presence of water vapor [R6-R9] was the only primary source of HO_X.

A key issue here is the role of the photochemistry of peroxides and carbonyls, which provide additional primary sources of HO_X-radicals and thus increase the rate of photochemical ozone formation in the free troposphere [e.g. *Chatfield and Crutzen, 1984*, *Singh et al.,* 1995, *Prather and Jacob*, 1997, *Cohan et al.,* 1999]. Studies [*Wennberg et al*., 1998, *Jaeglé et al*., 1998, *Folkins et al*., 1997, 1998] have shown that the observed HO_X concentrations in the UT are higher than what they would be if R6-R9 were the only primary HO_X source. However, the enhancement of the HO_X concentration depends on the ratio of the mixing ratio of peroxides or carbonyls to water vapor. Since the water vapor mixing ratio is a strongly decreasing function of altitude, the HO_X enhancement by photolysis of peroxides or carbonyls is relatively more important in the upper than in the middle troposphere [*Crawford et al.,* 1999].

Employing a global chemistry-transport model *Müller and Brasseur* [1999] quantified the importance of the acetone, and of some minor primary HO_x sources, in the troposphere. Their model results indicated that R6-R9 constitutes the single most important source of HO_X in the lower and middle troposphere while, in the upper troposphere, photochemistry of oxygenated hydrocarbons represents a large source of HO_X, which could even dominate in regions with low water vapor levels. Further, they estimated that the ozone production rate in the upper troposphere is typically between 2 and 10 times larger than chemical ozone losses.

2.2.5 In-Situ Production and Destruction: Threshold NO_X

Photochemical production of ozone from reactions R11 and R15 can be expressed as:

$$P_{O_3} = [NO] * \{k_{11} * [HO_2] + k_{15} * [CH_3O_2]\} \qquad [2.1]$$

During daytime NO and NO_2 are within a few minutes in photostationary state through the reaction chain R4, R11, R15 and R3. The concentration ratio of NO to NO_2, R_{NOX}, is determined by the photostationary state of NO_X:

$$R_{NOX} = \frac{[NO]}{[NO_2]} = \frac{k_3}{\{k_4 * [O_3] + k_{11} * [HO_2] + k_{15} * [CH_3O_2]\}} \qquad [2.2]$$

In the remote troposphere R_{NOX} is predominantly determined by the reaction chain R3 and R4. The ozone production rate is expressed in relation to NO_X as:

$$P_{O_3} = \left\{ \frac{R_{NOX}}{(1 + R_{NOX})} \right\} * [NO_X] * \{k_{11} * [HO_2] + k_{15} * [CH_3O_2]\} \qquad [2.3]$$

The photochemical destruction rate is:

$$D_{O_3} = L_{O_3} * [O_3] \qquad [2.4]$$

Whereby the relative loss rate of ozone, L_{O3} is:

$$L_{O_3} = J_{Eff,O(1D)} + k_{23} * [OH] + k_{19} * [HO_2] + \{k_{20}\} \qquad [2.5]$$

Thereby $J_{Eff, O1D}$ represents the effective photolysis rate of ozone in the presence of water vapor [R6-R9]:

$$J_{Eff, O(1D)} = \frac{k_9 * [H_2O]}{k_7 * [M] + k_9 * [H_2O]} * J_{O(1D)} \qquad [2.6]$$

In general $k_{7*}[M] >> k_9 * [H2O]$, such that $J_{Eff, J(O1D)}$ simplifies to:

$$J_{Eff,O(1D)} \cong \frac{k_9}{k_7} * J_{O(1D)} * \mu_{H_2O} \qquad [2.7]$$

whereby μ_{H2O} is the volume mixing ratio of water vapor,

It is obvious that the primary HO_X-production rate from the photolysis of ozone in presence of water vapor increases almost proportionally with increasing mixing ratio of water vapor, μ_{H2O} and the UV-photolysis frequency of O_3, $J(O1D)$ ($=k_6$).

The relative loss rate of ozone due to dry deposition within the PBL, k_{20}, can be expressed as:

$$k_{20} \cong \frac{v_{d,O_3}}{H_{PBL}} \qquad [2.8]$$

($v_{d,O3}$ = dry deposition velocity of ozone; H_{PBL} = height of the PBL)

The reactions governing the photochemistry of ozone involving the photochemical oxidation of CO and CH_4 in the remote marine troposphere are summarized in Table 2.1. In how far a net production or destruction of ozone will occur in situ depends largely on the actual strength of the individual sources and sinks described above. Of crucial importance is the actual concentration of NO_X, which finally determines the strength of the photochemical ozone production while water vapor in combination with the photolysis of ozone is strongly responsible for the primary production of HO_X. Furthermore, photochemical products like CH_2O, H_2O_2 and CH_3OOH in case of convective transport might provide additional primary HO_X-radicals at higher altitudes.

Figure 2.10 shows chemical box model simulations of the variations of the formation and losses of ozone from the oxidation of CO and CH_4 as a function of NO_X at different altitudes (Z=0, 5, 10, and 15 km) for two different latitude conditions: equator and 30°N respectively. The displayed parameters (incl. the calculated concentrations of OH and HO_2) are 24h-diurnal averages. The following parameters were employed: Reaction rate constants from *Jet Propulsion Laboratory-JPL Evaluation Number 14* [2003], rate constant for heterogeneous

removal rate constants from *Logan et al.* [1981], and diurnal varying latitude and altitude dependent photolysis rates at 0^oN and 30^oN for 21 September (equinox-conditions) are from *Röth* [1992]. $[O_3]$, [CO]-and $[CH_4]$-concentrations were fixed at 40 ppbv, 100 ppbv and 1.74 ppmv, respectively. Temperature was determined for a lapse rate of 6.5 K/km and a surface temperature of 303 K and 293 K at 0^oN and 30^oN respectively, while the H_2O volume mixing ratio was determined for 75% relative humidity (below 273 K with respect to ice). The calculations were made at four fixed concentrations of CH_2O, H_2O_2 and CH_3OOH ranging between very low and rather high levels (0.008, 0.04, 02, and 1.0 ppbv) to demonstrate the influence of additional primary HO_X production from CH_2O, H_2O_2 and CH_3OOH increasing the levels of HO_x and thus increasing ozone formation.

The chemical box model simulations [See Figure 2.10] show the following significant and characteristic features with regard to the behavior of HO_X and the corresponding ozone formation and losses as a function of NO_X:

- The OH and HO_2 concentrations resulting from the balance of recycling, production and destruction decrease both by about an order of magnitude between lower and upper troposphere at comparable CH_2O, H_2O_2 and CH_3OOH mixing ratios

- HO_2 concentrations are rather insensitive to NO_X for values less than about 0.1-0.2 ppbv and majorly limited by its self reaction [R21], while at higher NO_X-levels HO_2 decreases due to the dominating influence of its reaction with NO [R11].

- Only for NO_X for values less than about 0.005-0.010 ppbv OH is independent of NO_X, but is an increasing function of NO_X in the range from 0.01-1 ppbv while at higher NO_X-levels OH is depleting due to the dominating removal by its reaction with NO_2 [R24].

- Increasing influence of CH_2O, H_2O_2 and CH_3OOH on OH and HO_2 at higher altitudes due to much lower water vapor content and thus depleting primary HO_X-production from $O(1D)+H_2O$ [R6-R9] with increasing altitude. It also clearly shows the increasing effect on the photochemical production of ozone

- In the lower troposphere up to 5 km altitude, however, OH and HO_2 are rather insensitive to changes of CH_2O, H_2O_2 and CH_3OOH, particularly in the tropics with its high water vapor content. This is also the region where the ozone losses [2.5] are most significant and can dominate ozone formation by far in case of low NO_X (<10-pptv).

- At NO_X-levels below 0.1-0.2 ppbv the photochemical losses of ozone are insensitive to NO_X. In the lower troposphere, the ozone losses are dominated by photolysis of ozone in presence of water vapor [R6-R9] and reaction with HO_2 [R19], while at higher altitudes the latter reaction and the reaction with OH [R23] are of importance. However, the relative loss rates are getting slow, less than 1% per day at altitudes above 10 km

- In the middle/upper troposphere at NO_X levels above 10-20 pptv photochemical formation of ozone is much larger than its concurrent losses. More than 70% of the ozone production is contributed by the reaction of NO with HO_2 [R11] and less than 30% by NO with CH_3O_2 [R15]. At moderate NO_X mixing ratios below 0.2-1.0 ppbv, depending on altitude, the ozone formation is almost linearly increasing with NO_X according equation [2.3] while at larger NO_X it decreases again due to the very strong decrease of HO_2.

22
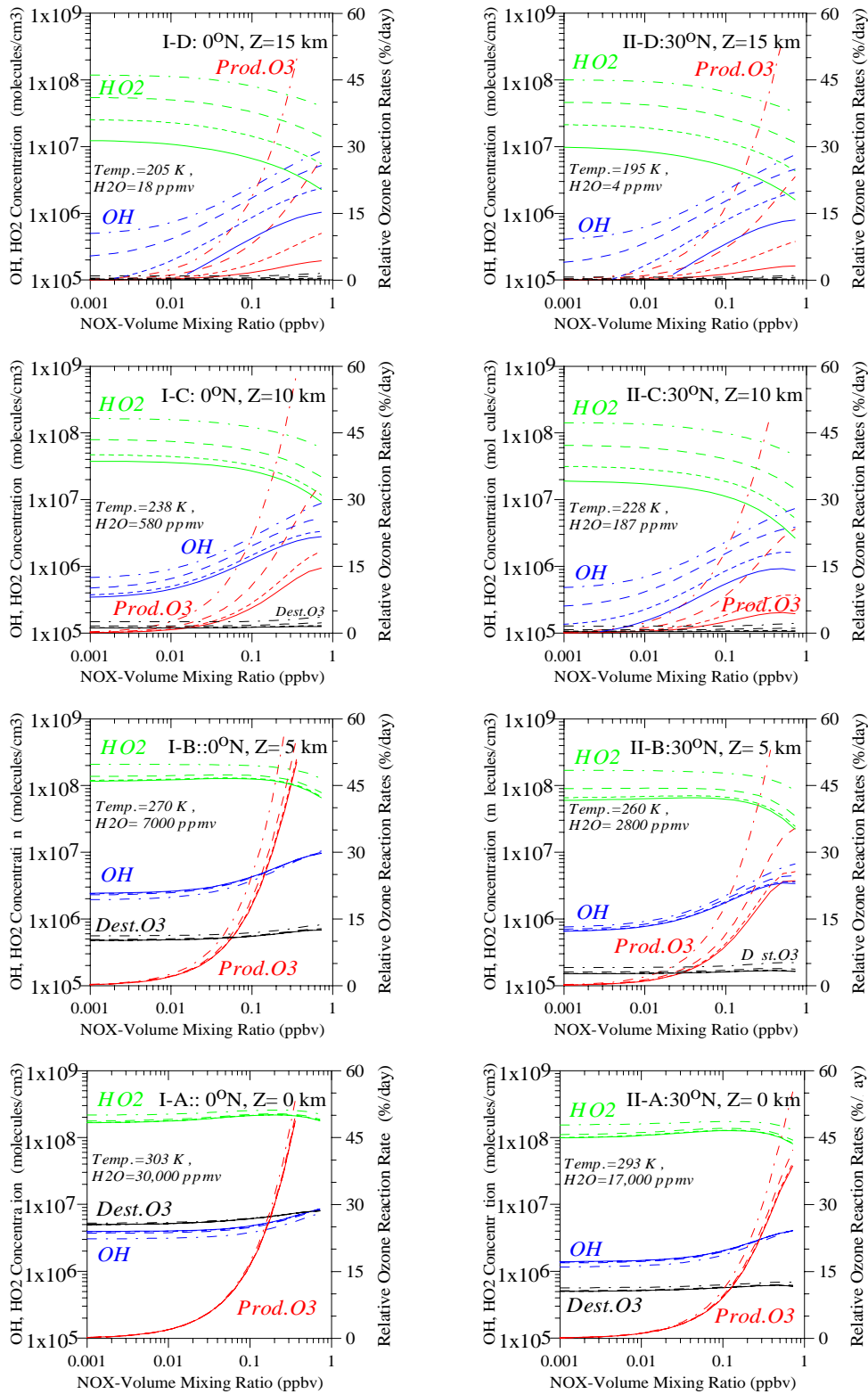
Figure 2.10: *Chemical box model simulations of the variations of the concentrations of OH (blue), HO₂ (green), and the relative rates of formation (red) and losses (black) of ozone (% per day) as a function of NO_X at different altitudes (Z=0, 5, 10, and 15 km) at equator (left diagrams) and 30°N (right diagrams) for fixed mixing ratio's of $CH_2O=H_2O_2=CH_3OOH= 0.008$ ppbv (solid), 0.04 ppbv (fine-dashed), 0.2 ppbv (dashed), 1 ppbv (dashed/dotted). The displayed parameters are 24h-diurnal averages. More details about box-model see text.*

The results show clearly the strong and critical influence of NO_X on the photochemical fate of ozone. However, no detailed knowledge about the spatial and temporal distribution of NO_X exists from the the Central Atlantic region, such that it is not possible to obtain a direct good estimate of the actual photochemical ozone production according equation 2.3. Therefore, an indirect approach is used to estimate the potential of air masses for in-situ photochemical production of ozone in relation to its total losses.

A hypothetical threshold concentration for NO_X, $[NO_X]_{Thres}$, is defined here as the concentration of NO_X for which production of ozone according to equation 2.3 just balances the ozone loss L_{O3} (equuation 2.5). $[NO_X]_{Thres}$ is expressed as:

$$[NO_X]_{Thres} = \left\{ \frac{(1+R_{NOX})}{R_{NOX}} \right\} * \left\{ \frac{L_{O_3} *[O_3]}{\{k_{11}*[HO_2]+k_{15}*[CH_3O_2]\}} \right\} \qquad [2.9]$$

From the box model simulations it is seen that at $NO_X < 200$ pptv the concentration of HO_2 as well as the total losses of ozone, L_{O3}, are both insensitive to variations in NO. For the actual NO_X concentration, $[NO_X]_{Act}$, the corresponding actual production rate of ozone P_{O3} has been derived from equations 2.3 and 2.9 and expressed in terms of the total ozone losses $L_{O3,Tot}$ as follows:

$$P_{O_3} = \left\{ \frac{[NO]_{Act}}{[NO]_{Thres}} \right\} * L_{O_3} *[O_3] = \left\{ \frac{[NO_X]_{Act}}{[NO_X]_{Thres}} \right\} * L_{O_3} *[O_3] \qquad [2.10]$$

The ratio of the actual and the (hypothetical) threshold concentration of NO_X is a measure of the strength of the photochemical production of ozone compared to its losses. The ratio can be interpreted as a sensitivity criterion with regard to the classification of in-situ net photochemical production or destruction of ozone. The net relative change of ozone is expressed as:

$$P_{O_3} - D_{O_3} = \left\{ \frac{[NO_X]_{Act}}{[NO_X]_{Thres}} - 1 \right\} * L_{O_3} *[O_3] \qquad [2.11]$$

2.2.6 Locations of Photochemical Sources and Sinks of Ozone

According to *Jacob et al* [1996] the ozone budget in the tropical troposphere is exclusively controlled by photochemistry while input from the stratosphere and dry deposition are only of minor importance. The conclusions are drawn from results obtained from a study of intensive biomass burning events during the Southern African Fire Atmospheric Research Initiative/Transport and Atmospheric Chemistry near the Equator-Atlantic (SAFARI/TRACE-A), conducted in September and October 1992. It was shown that the locations of the major photochemical sources and sinks are totally different. The photochemical sources of ozone are generally located over the continents, particularly in urbanized areas and regions with strong biomass burning activities, while the photochemical sinks are in the MBL over the remote areas of the tropical oceans [e.g. *Jacob et al.*, 1996, *Lelieveld and Dentener*, 2000].

Deep convection constitutes a very efficient mechanism to redistribute trace gases from their source region near the surface to the upper troposphere followed by fast horizontal transport spreading the trace gases over vast areas [e.g. *Gidel,* 1983, *Chatfield and Crutzen*, 1984].

Deep convection is the major driving mechanism that can distribute emissions from biomass burning events, which occur over limited areas of the tropical continents, so that they can have a large scale chemical impact over large regions of the tropical oceans [e.g. *Crutzen and Andreae*, 1990, *Pickering et al.*, 1996, *Thompson et al.*, 1996].

Figure 2.11 show the Walker circulation and its role in the tropospheric ozone balance in the tropics. Deep convective motions over South America, southern Africa, and Oceania (rising branches of the Walker circulation) inject NO_X from combustion, soils, and lightning to the upper troposphere, driving additional ozone production. Subsequently, the air subsides over the ocean and net ozone loss takes place in the lower troposphere due to low NO_X concentrations and high humidities. In how far ozone from stratosphere-troposphere exchange (STE) play a role is an open question.
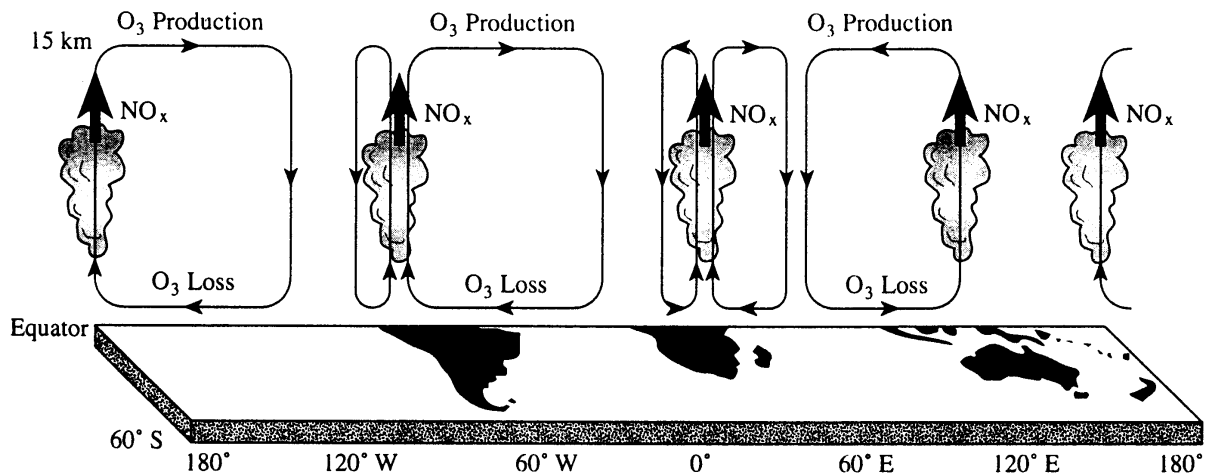
Figure 2.11: *Schematic depiction of the fate of ozone in the tropical troposphere. For details, see text. Source: Jacob et al., 1996.*

Table 2.1: *List of reactions governing the photochemistry of ozone involving the photochemical oxidation of CO and CH4 in the remote marine troposphere:*

O_2	+	hν	(λ<240 nm)	$\longrightarrow$		$O(^3P)$	+	$O(^3P)$	[R1]
O_2	+	$O(^3P)$	+ M	$\longrightarrow$		O_3	+	M	[R2]
NO_2	+	hν	(λ<410 nm)	$\longrightarrow$		NO	+	$O(^3P)$	[R3]
O_3	+	NO		$\longrightarrow$		NO_2	+	O_2	[R4]
O_3	+	hν	(λ<320 nm)	$\longrightarrow$		O_2	+	$O(^1D)$	[R6]
$O(^1D)$	+	M		$\longrightarrow$		$O(^3P)$	+	M	[R7]
$O(^3P)$	+	O_2	+ M	$\longrightarrow$		O_3	+	M	[R8]
$O(^1D)$	+	H_2O		$\longrightarrow$	2	OH	+	M	[R9]
CO	+	OH	+ O_2	$\longrightarrow$		CO_2	+	HO_2	[R10]
HO_2	+	NO		$\longrightarrow$		NO_2	+	OH	[R11]
CH_4	+	OH		$\longrightarrow$		CH_3	+	H_2O	[R13]
CH_3	+	O_2	+ M	$\longrightarrow$		CH_3O_2	+	M	[R14]
CH_3O_2	+	NO		$\longrightarrow$		CH_3O	+	NO_2	[R15]
CH_3O	+	O_2		$\longrightarrow$		HO_2	+	CH_2O	[R16]
O_3	+	OH		$\longrightarrow$		O_2	+	HO_2	[R18]
O_3	+	HO_2		$\longrightarrow$	2	O_2	+	OH	[R19]
O_3	+	Dry deposition.		$\longrightarrow$		Products			[R20]
HO_2	+	HO_2	+ M, H_2O	$\longrightarrow$		H_2O_2	+	O_2	+ M, H_2O [R21]
OH	+	OH	+ M	$\longrightarrow$		H_2O_2	+	M	[R22]
OH	+	HO_2		$\longrightarrow$		H_2O	+	O_2	[R23]
OH	+	NO_2	+ M	$\longrightarrow$		HNO_3	+	M	[R24]
H_2O_2	+	hν		$\longrightarrow$	2	OH			[R25]
H_2O_2	+	OH		$\longrightarrow$		H_2O	+	HO_2	[R26]
H_2O_2	+	Heterogeneous		$\longrightarrow$		Products			[R27]
CH_3O_2	+	CH_3O_2		$\longrightarrow$		CH_3OH	+	CH_2O	[R28]
CH_3O_2	+	CH_3O_2		$\longrightarrow$	2	CH_2O	+	HO_2	[R29]
CH_3O_2	+	HO_2		$\longrightarrow$		CH_3OOH	+	O_2	[R30]
CH_3OOH	+	hν	+ O_2	$\longrightarrow$		CH_2O	+	HO_2	[R31]
CH_3OOH	+	OH	+ O_2	$\longrightarrow$		CH_2O	+	OH	+ H_2O [R32]
CH_3OOH	+	OH	+ O_2	$\longrightarrow$		CH_3O_2	+	H_2O	[R33]
CH_3OOH	+	Heterogeneous		$\longrightarrow$		Products			[R34]
CH_3OH	+	OH		$\longrightarrow$		Products			[R35]
CH_2O	+	hν		$\longrightarrow$		H_2	+	CO	[R36]
CH_2O	+	hν	+ 2 O_2	$\longrightarrow$	2	HO_2	+	CO	[R37]
CH_2O	+	OH	+ O_2	$\longrightarrow$		HO_2	+	CO	+ H_2O [R38]
CH_2O	+	Heterogeneous		$\longrightarrow$		Products			[R39]
HNO_3	+	Heterogeneous		$\longrightarrow$		Nitrates			[R40]
HNO_3	+	hν		$\longrightarrow$		OH	+	NO_2	[R41]
HNO_3	+	OH	+ M	$\longrightarrow$		H_2O	+	NO_2	+ M [R42]
HO_2	+	NO_2		$\longrightarrow$		HO_2NO_2			[R43]
HO_2NO_2	+	Thermal		$\longrightarrow$		HO_2	+	NO_2	[R44]
HO_2NO_2	+	hν		$\longrightarrow$		OH	+	NO_2	[R45]

Chapter 3

Ozone-Humidity Soundings

3.1 Introduction

To measure the vertical distributions of ozone and meteorological parameters such as pressure, temperature and relative humidity, balloon borne electrochemical ozone sondes in combination with radiosondes were flown from aboard the RV-"Polarstern" during the cruises ANT-V/5 (March/April 1987) and ANT-VII/1 (September/October 1988) over the Central Atlantic. Ozone sondes are small, lightweight and compact balloon borne sondes. In an electrochemical cell the reaction of ozone with potassium iodine in aqueous solution is used to measure continuously the ozone concentration. The sensing device is interfaced to a standard meteorological radiosonde for data transmission to the ground station and is flown on a small rubber weather balloon.

This chapter gives an overview of the instrumental and operational aspects as well as an evaluation of the performance of the ozone/humidity sounding system used during the two cruises aboard the RV "Polarstern". In the first part the different components of the sounding system like the ozone sonde, the weather radiosonde and the electronic interface for digital coupling and transmission of the signals of both sondes are described. In addition, the operational aspects of the ozone-radio sonde like preparation, instrumental checks, and data processing are described. Finally, an evaluation of the instrumental performance of the electrochemical ozone sensor and the pressure, temperature and humidity sensor of the radiosondes is given. The evaluation is based on theoretical and experimental studies addressing the precision and accuracy of the different sensors of the sonde under the typical conditions encountered during both cruises. The experimental studies are reported separately in Annex A of this thesis.

3.2 Instrumental Aspects

3.2.1 Set-up of the Sounding System

The set up of the ozone sounding system deployed during both cruises is shown in Figure 3.1 [*Smit et al.*, 1989-B, 1994-B]. The balloon flight package consists of the following components:

1) Ozone sonde of the ECC-5A-type (Science Pump Corporation, USA).

2) Standard meteorological radiosonde for measuring pressure, temperature and relative humidity of the RS80-type (Vaisala, Finland).

3) Microcomputer controlled sonde data interface board (type H, TMAX, Boulder CO, USA) for in-flight coupling and digital processing of all measured parameters as digital coded data stream of two-tone signal modulated on the UHF-transmitter (400-406 MHz) of the RS80-radiosonde.

4) A 600 gram hydrogen filled latex balloon (type-TA600, Totex, Japan)

5) A small parachute with a diameter of 1m to slow the descent rate after burst of the balloon

The ground station (see Figure 3.1) established aboard the ship consists of:

a)   UHF-Antenna (Omni directional type RM-20, Vaisala, Finland)

b)   Conventional 400-406 MHz UHF-receiver (type UR-15, Vaisala, Finland) for receiving and demodulating the digital coded data stream of two tone signals of the sonde

c)   Modem (type UTU-XT/P, Kantronics, USA) for converting the two tone data stream into a hexadecimal coded data frame of ASCII-characters

d)   Personal Computer for further processing and reduction of the sonde data

27 m	Balloon (TA-600)	Diameter	1.5 m
		Volume	2.5 m^3
		Weight	680 g
1 m	Parachute	Diameter	1.5 m
		Weight	100 g
7 m	Ozone Sonde (ECC-5A) +	Volume	10 dm^3
	Sonde Data Interface (TMAX)	Weight	680 g
	Radiosonde (RS80-15)	Volume	0.7 dm^3
	[Pressure , Temperature, Relative Humidity]	Weight	300 g

Ascent   Descent

Ground Station

| 403 Mhz UHF-Receiver | → | Modem | → | Personal Computer | → | Data Storage |
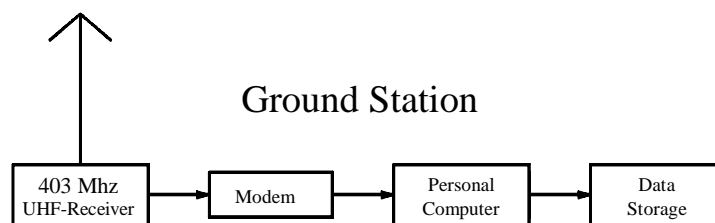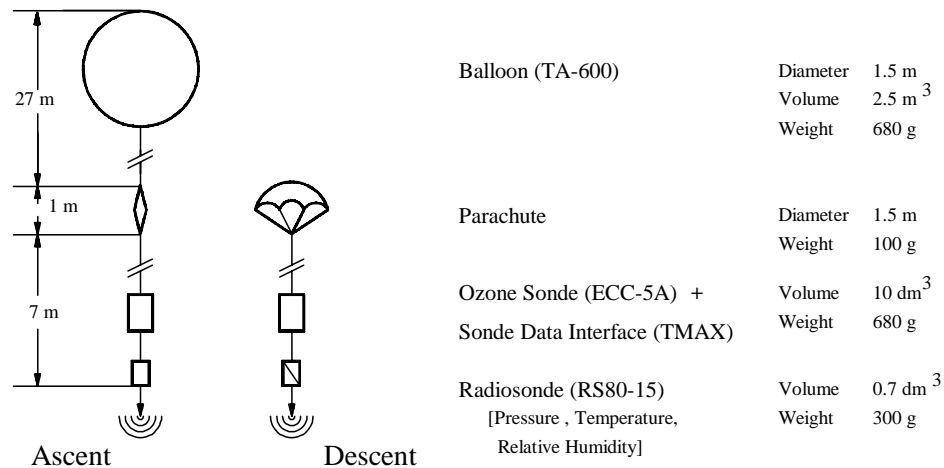
Figure 3.1: *Set up of ozone sounding system*

3.2.2 Ozone Sonde: Electrochemical Concentration Cell

The main component of the ozone sonde is an ozone sensor of the ECC-5A type (Science Pump Corporation, USA), which is based on the electrochemical method after *Komhyr* [1969, 1971] and generates an electrical current proportional to the mass flow rate of ozone through the sensing solution. A small motor driven gas sampling pump [*Komhyr,* 1967] forces ambient air through the ozone sensor. By knowing the volumetric gas flow rate and its temperature the measured electrical current can be converted to the ozone concentration. A schematic diagram of the ECC-5A ozone sonde is shown in the left panel of Figure 3.2.

The ECC-ozone sensor is based on the Iodine/Iodide redox reaction by ozone, which is performed in an electrochemical cell (see right panel of Figure 3.2). The cell consists of two half cells, made of Teflon, which serve as the cathode and anode chamber, respectively. Both half-cells contain a platinum mesh serving as electrodes. They are immersed in a KI-solution of different concentrations. An ion bridge in order to provide an ion pathway and to prevent mixing of the cathode- and anode electrolytes links the two chambers together.

The ECC does not require an external electrical potential. In contrast to the Brewer-Mast type of electrochemical ozone sensor [*Brewer et al.,* 1960], the ECC gets its driving electromagnetic force from the difference in the concentration of the KI-solution in the cathode- and anode chamber, 0.06 and 8.0 Mol/l respectively. When ozone is pumped through the cathode solution (lower KI-concentration), there will be an increase of I_2 according the redox reaction:

$$2 \, KI \quad + O_3 + H_2O \qquad \longrightarrow \qquad I_2 \qquad + O_2 \quad + 2 \, KOH \qquad \text{[R51]}$$
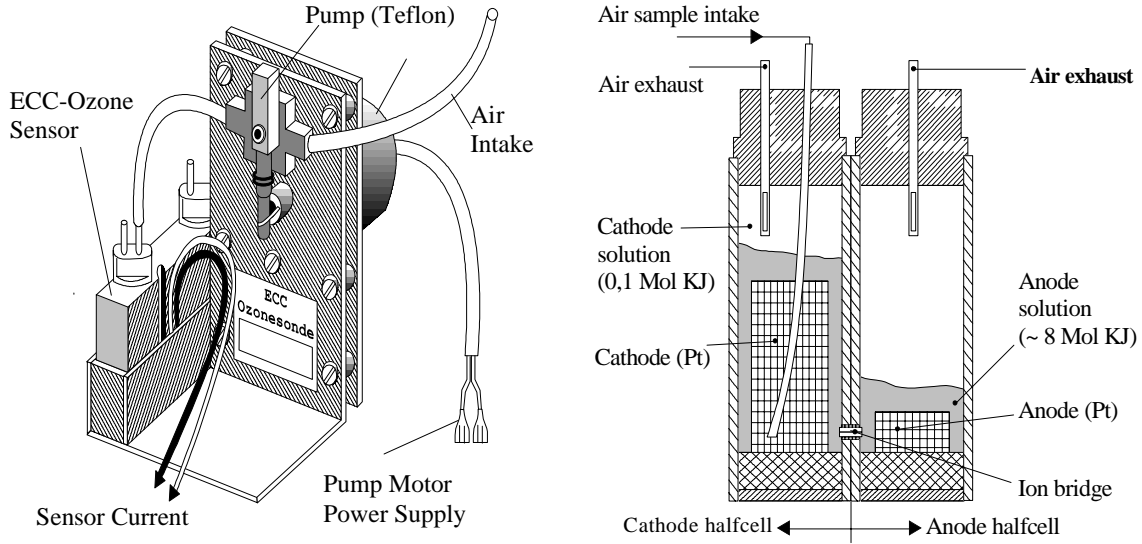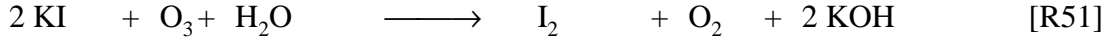
Figure 3.2: Scheme of Electrochemical Concentration Cell (ECC) ozone sonde of type ECC-5A (left) and sensing cell (right)

In the vicinity of the cathode, I_2 will be converted to I^- ions, while in the vicinity of the anode, I^- is converted to I_2, such that the overall cell reaction is

$$3 \, I^- \quad + I_2 \qquad \longrightarrow \qquad I_3^- \quad + 2 \, I^- \qquad \text{[R52]}$$
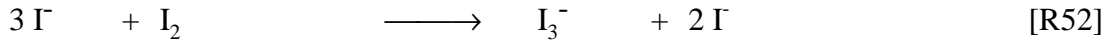
thereby one ozone molecule causes two electrons to flow in the external circuit. This electrical current is thus directly related to the uptake rate of ozone in the cathode chamber and is determined by the relation:

$$P_{O3,ECC} = C_{ECC} \cdot I_{O3,ECC} \qquad \text{[3.1]}$$

whereby $P_{O3,ECC}$ = Pressure of ozone, [mPa]

$I_{O3,ECC}$ = Electrical current due to sampled ozone, [μA]

The conversion coefficient C_{ECC} is determined by:

$$C_{ECC} = 0.04307 \cdot \eta_{ECC} \cdot \frac{T_{ECC}}{\Phi_{V,ECC}} \quad [\textit{Komhyr}, 1969] \qquad \text{[3.2]}$$

whereby η_{ECC} = Conversion efficiency of the ECC-sensor

T_{ECC} = Temperature of air sampling pump, [K]

$\Phi_{V,ECC}$ = Volumetric flow rate of air sampling pump, [ml/s]

Although the conversion efficiency η_{ECC} is the overall result of the influences of several different parameters, it is mainly determined by the absorption efficiency $\alpha_{O3,ECC}$ of gaseous O_3 in the liquid phase and the chemical conversion of O_3 into I_2 given by the stoichoimetric factor $S_{O3/I2}$ of reaction. The conversion efficiency η_{ECC} can be expressed by:

$$\eta_{O3,ECC} \cong \alpha_{O3,ECC} \cdot S_{O3/I2} \qquad [3.3]$$

whereby $\alpha_{O3,ECC}$ = Absorption efficiency of O_3 into the sensing (cathode) solution
                 $S_{O3/I2}$ = Stoichiometry of the conversion of O_3 into I_2

The ECC-sensor is designed such that a full absorption of O_3 by the sensing solution ($\alpha_{O3,ECC} \cong 1$) in combination with a one to one conversion of O_3 into I_2 ($S_{O3/I2} \cong 1$) by reaction R51 is achieved [*Komhyr,* 1969].

The electrical current measured by the ECC-sonde is fed into the current to voltage converter on the sonde data interface board (see also Section 3.2.4). The overall electrical current, $I_{M,ECC}$, measured by the ECC-sonde is a superposition of the ozone current, $I_{O3,ECC}$ and the background current, $I_{B,ECC}$:

$$I_{O_3,ECC} = I_{M,ECC} - I_{B,ECC} \qquad [3.4]$$

whereby $I_{M,ECC}$ = Overall electrical current measured by ECC-sensor

             $I_{O3,ECC}$ = Electrical current measured by ECC-sensor due to ozone

             $I_{B,ECC}$ = Electrical current measured by ECC-sensor due to background

The background current that varies for individual ozone sensors is determined at ground just before flying the sonde. The temperature of the air sampling pump (T_{ECC}) is measured in flight by a thermistor, which is connected to the sonde data interface board. The volumetric pump flow rate ($\Phi_{V,ECC}$) is determined at ground.

The power supply for the electrical motor of the sampling pump is provided by a battery package of seven serially connected Lithium dry cells (type BR 2/3A, Panasonic). In contrast to wet batteries this battery type has the advantage of relative high power (1000 mAh) and no emission of oxidizing/reducing gases like H_2S or SO_2. The latter can have a detrimental effect on the ECC-sensor performance [*Schenkel et al.,* 1982]. In addition, the battery package is supplied with a 12 V voltage regulator to ensure a constant rotation speed (volume flow rate) of the pump.

3.2.3   Meteorological Radiosonde: RS80

The radiosonde is of the type RS80-15 of Vaisala (see Figure 3.3). The RS80 is small sized (55x147x90 mm), light weighted (200 g) and has sensors for pressure (P), temperature (T) and relative humidity (U) which are all electronic capacitive devices:

♦ The pressure sensor (Barocap®) is a small aneroid capsule with capacitive transducer plates inside. The external diameter of the capsule is 35.5 mm and the weight of the complete assembly only 5 g. The sensor is mounted inside the radiosonde package. To correct for temperature influences an additional temperature sensor mounted inside the sensor housing of the Barocap. The resolution of the pressure sensor is 0.1 hPa.

♦ The temperature sensor (Thermocap®) is based on temperature dependent dielectric ceramic material. The sensor (2.5 x ϕ 1.5 mm) is coated with an electrically grounded thin film of aluminium to minimize radiation errors. The resolution of the sensor is 0.1K

♦ The humidity sensor (Humicap®, type A) is a thin film capacitor on a glass substrate. A hydroactive polymer whose capacitance depends on the amount of water vapor adsorbed is used as dielectric between two electrodes. The sensor is small (4x4x0.2 mm) whereby the polymer film is only 1 micron thick. The surface electrode is porous for air humidity. An aluminized cap protects the sensor from direct rain and radiation effects. The sensor reading is relative humidity with respect to liquid water with a resolution of 0.2 %.
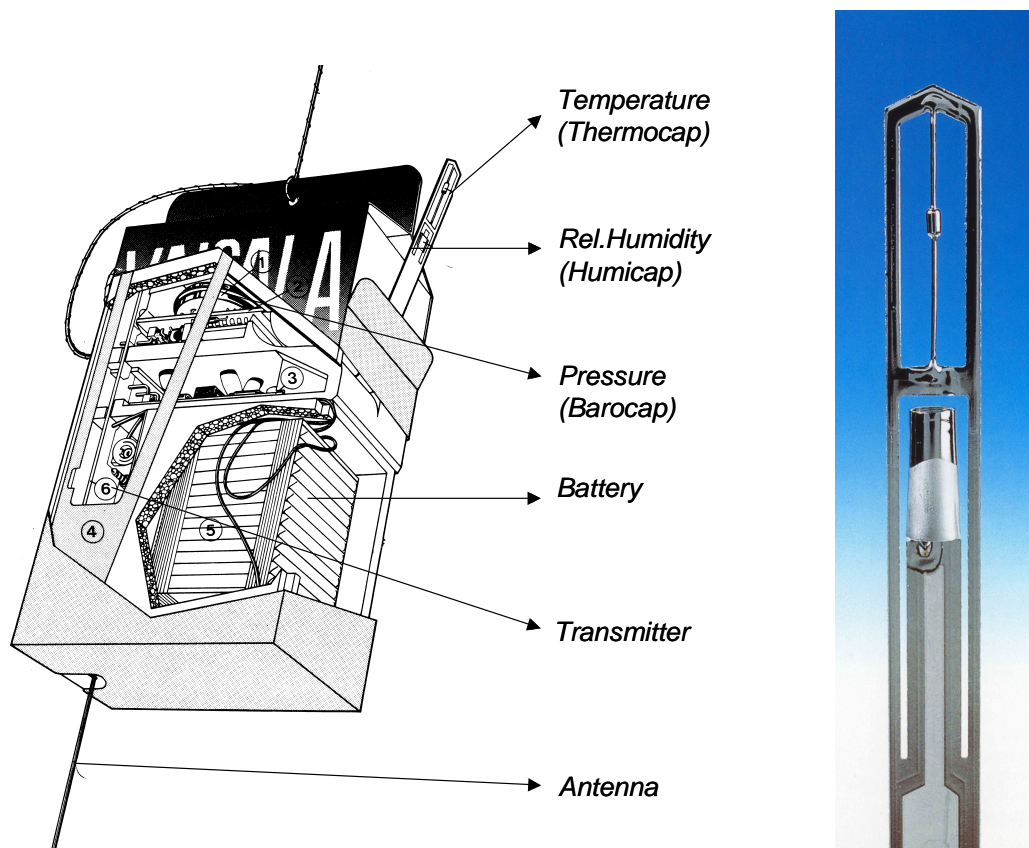
Figure 3.3: RS80-15 Radiosonde of Vaisala, Finland (Left) with sensor boom (Right)

The PTU (pressure, temperature, relative humidity) transducer signals are converted within an electronic multiplexed oscillator circuit into frequencies varying between 7 and 10 KHz. Next to these three signal frequencies of the PTU sensors, additionally three supporting signal frequencies (one for the temperature measurement of the pressure transducer and two references) are incorporated in the electronic multiplexer circuit. At normal operation the six analogue signal frequencies are modulated on the UHF-transmitter (403 MHz) of the radiosonde and transmitted to the ground station for further data processing. In the concept presented here the frequencies are however intercepted before modulation on the transmitter and fed to the sonde data interface board to be digitized. A battery package of nine serially connected Lithium dry cells (type BR 2/3A, Panasonic) with a -18V voltage regulator supplies the radiosonde together with the sonde data interface board.

3.2.4   Mechanistic Behavior of Humicap-A Humidity Sensor

The Humicap-A sensing element of the RS80-humidity sensor consists of a hydroactive polymer film as dielectric whose capacitance depends on the relative humidity [*Salasma and Kostamo,* 1975]. Although, the Humicap-A sensor is extensively used world wide in the radiosounding networks for weather forecasting, little is known about the theory of operation of the hydroactive polymer film of the sensor. *Denton et al.* [1985] suggested that the water vapor molecules within the cavities of the polymer film are in thermodynamic equilibrium with the water molecules adsorbed on the hydroactive surface of the walls of the cavities. This water adhesion is characterized by physical adsorption through the "weak" Van der Waals interaction of water molecules with the hydrophylic groups of the polymer molecules [*Matsuguchi et al.*, 1998]. It was assumed that the adsorbed water exists as a very thin film of liquid water on the surface of the polymer.

Denton et al. [1985] showed experimentally that the number of water molecules adsorbed by the hydroactive polymer film $N_{W,Ads}$ is proportional to the relative humidity in the gas phase RH_G. Similarly to *Anderson* [1995] a "physical adsorption film vapor pressure model" is used to explain why the Humicap-A sensor responds to relative humidity. The porous polymer material acts as a hydroactive sponge whereby the water molecules in the polymer material are in a reversible thermodynamically equilibrium with the gas phase, i.e. the rate of adsorption of molecules onto the surface is exactly counterbalanced by the rate of desorption of molecules into the gas phase [*Anderson,* 1995].

At constant temperature T the number of water molecules $N_{W,Ads}$ adsorbed in the solid phase is in equilibrium with the water vapor pressure P_{WV} in the gas phase and can be expressed as:

$$N_{W,Ads} = K_W \cdot P_{WV} \qquad [3.5]$$

The equilibrium constant K_W is temperature T dependent and can be described by[3]:

$$\frac{\partial(Ln(K_W))}{\partial T} = \frac{\Delta H_{Ads}}{RT^2} \qquad [3.6]$$

whereby ΔH_{Ads} is the adsorption enthalpy of water vapor which is released in case water vapor is adsorbed from the gas phase onto the surface of the polymer material. R is the gas constant. After integration of equation 3.6 yields

$$K_W = K_{W0} \cdot Exp\left[\frac{-\Delta H_{Ads}}{R}\left(\frac{1}{T} - \frac{1}{T_0}\right)\right] \qquad [3.7]$$

whereby K_{W0} is the equilibrium constant at temperature T_0.

Substituting equation 3.7 into equation 3.5 and expressing the water vapor pressure P_{WV} in terms of relative humidity RH_G [4] the number of adsorbed molecules in the polymer film is:

---

[3] The effect of temperature on the equilibrium between the water vapor pressure in gas phase and the number of water molecules in the solid phase can be derived from the Gibb-Helmholtz equation $\frac{\partial(\Delta G/T)}{\partial T} = \frac{-\Delta H}{T^2}$ through substituting the free enthalpy $\Delta G = -RT \bullet Ln(K_W)$ [*Daniels and Alberty*, 1979].

$$N_{W,Ads} = K_{W0} \cdot Exp\left[\frac{-\Delta H_{Ads}}{R}\left(\frac{1}{T} - \frac{1}{T_0}\right)\right] \cdot RH_G \cdot P_{WVS} \qquad [3.8]$$

whereby P_{WVS} is the water vapor partial pressure over liquid at temperature T which can be expressed by the Clausius-Clapeyron equation

$$P_{WVS}(T) = P_{WVS}(T_0) \cdot Exp\left[\frac{-\Delta H_{Evap}}{R}\left(\frac{1}{T} - \frac{1}{T_0}\right)\right] \qquad [3.9]$$

whereby $P_{WVS}(T_0)$ is the water vapor partial pressure at temperature T_0.

Substituting equation 3.9 into equation 3.8 yields:

$$N_{W,Ads} = K_{W0} \cdot P_{WVS}(T_0) \cdot RH_G \cdot Exp\left[\frac{-\left(\Delta H_{Ads} + \Delta H_{Evap}\right)}{R}\left(\frac{1}{T} - \frac{1}{T_0}\right)\right] \quad [3.10]$$

whereby the factor $K_{W0} \cdot P_{WVS}(T_0)$ represents the number of water vapor molecules adsorbed under saturated water vapor conditions at temperature T_0.

The dielectric properties of the water molecules adsorbed in the polymer material are close to these of free water [*Denton et al.,* 1985] such that the corresponding change of capacitance ΔC_W of the sensor film due to the uptake of moisture is proportional to $N_{W,Ads}$ and can be expressed as:

$$\Delta C_W(T) = \Delta C_{WS}(T_0) \cdot RH_G \cdot Exp\left[\frac{-\left(\Delta H_{Ads} + \Delta H_{Evap}\right)}{R}\left(\frac{1}{T} - \frac{1}{T_0}\right)\right] \qquad [3.11]$$

whereby $\Delta C_{WS}(T_0)$ represents the change of capacitance due to the uptake of moisture under saturation conditions at temperature T_0.

Adsorption is an exothermic process such that ΔH_{Ads} have negative values while evaporation is an endothermic process with positive values for ΔH_{Evap}. The van der Waals' forces causing physical adsorption are the same type as those that cause the condensation of a gas to form a liquid such that the adsorption enthalpy ΔH_{Ads} is of the same order of magnitude than the condensation enthalpy of water that is equal to the evaporation enthalpy of water but opposite of sign.

Observations below the freezing point of water have shown that the Humicap sensor still responds to relative humidity with respect to liquid water. The implication of this behavior is that the water does not experience a sudden phase change within the material at temperatures below the freezing point of water. Indeed, for a capacitive device, such a phase change would have a very marked effect on the dielectric constant of the water film, which would cause a

---

[4] The conventional definition of relative humidity is $RH_G = \frac{P_{WV}}{P_{WVS}} \bullet 100\%$ whereby P_{WVS} is the saturation water vapor partial pressure with respect to liquid water at temperature T

large jump in sensor output during the phase change [*Anderson*, 1995]. Such a jump has never been observed at low temperatures down to -90°C.

Virtually the relative humidity sensor would be independent of the temperature in case the adsorption enthalpy ΔH_{Ads} of water vapor would exactly counter balancing the evaporation enthalpy ΔH_{Evap} of water such that the temperature dependent exponential factor in equation 3.11 would reduce to one. However, in practice ΔH_{Ads} and ΔH_{Evap} will not completely counterbalance each other such that a remaining temperature dependence represented by the exponential factor in equation 3.11 has to be expected.

3.2.5   Sonde Data Interface: Data Transmission

In corporation with TMAX (Boulder CO, USA) a data interface board for coupling the signals of the ozone sonde and radiosonde was developed. A scheme of the board (TMAX-H) is shown in Figure 3.4.
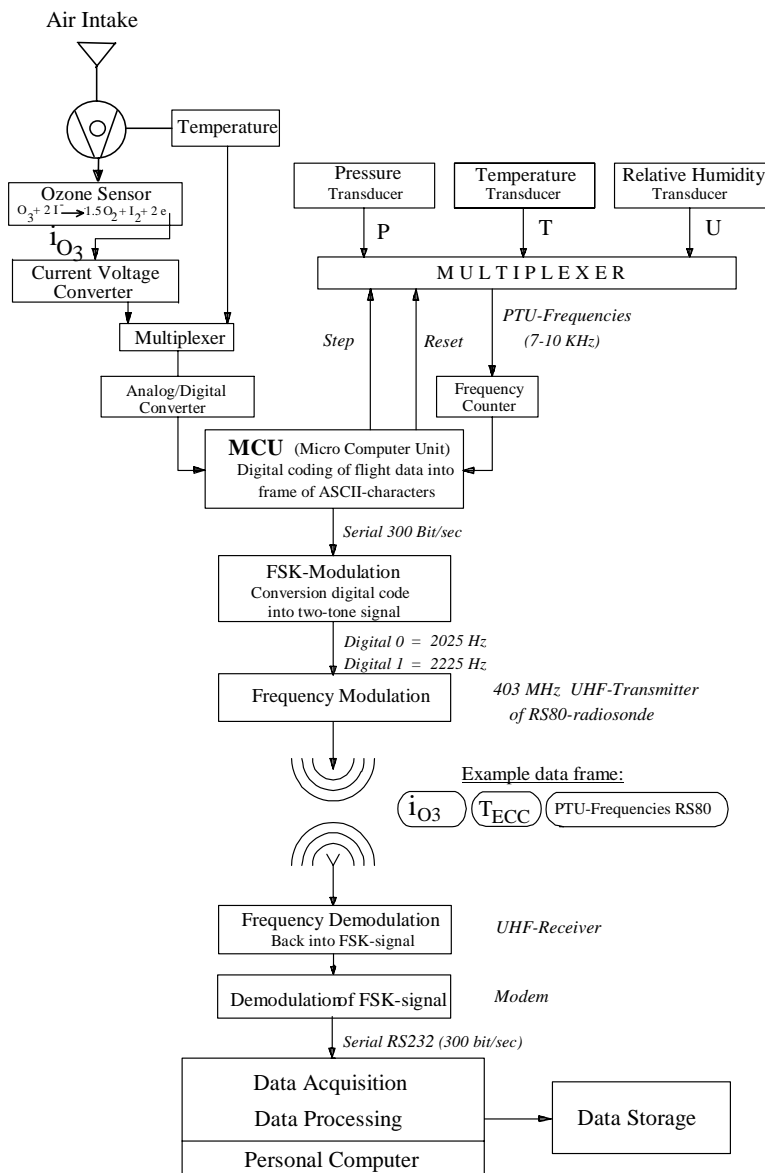
Figure 3.4: *Data transmission of ozone sounding system: TMAX-H sonde data interface board*

The basis of this microcomputer controlled interface is to convert all measured analogue signals, such as the ozone current, the temperature of the gas sampling pump and the six frequencies of the RS80 radiosonde, into a digital coded data stream. Modulated as a two tone signal on the UHF-transmitter of the RS80 sonde the data stream is transmitted to the ground station for further data processing. The main device is a microcomputer unit (MCU), Motorola type 68705R3 [1].

The current of the ECC-sensor, I_{ECC}, is fed via an I/V-(Current to Voltage) converter into the multiplexed ADC (=Analogue Digital Converter) input channel of the MCU. If the 8 bits ADC is saturated the gain of the I/V-converter is switched by a scaling factor such that a dynamic range of 11 bits is obtained. I_{ECC} can be measured up to 10 μA with a resolution of 0.01μA.

The temperature of the ECC-sensor, T_{ECC}, measured by a thermistor (type UUA41J1, Fenwal Electronics, USA; accuracy is +/-0.2^{o}C at 25°C) is also fed into the ADC of the MCU. T_{ECC} can be measured between -20 ^{o}C and +80 ^{o}C with a resolution of 0.4^{o}C.

The six frequency signals (7-10 KHz) of the radiosonde are fed into a programmable timer for analogue to frequency counting, whereby the time period is measured over a fixed number of N-cycles (N=4000). The electronic multiplexer of the radiosonde is controlled by the MCU via a step and reset signal sequence coming from the MCU. The total sampling time for the determination of the six frequencies is about 3.5 sec. The accuracy of the frequency determination is better than 0.1 Hz and does not have any significant influence on the overall accuracy of the measured meteorological parameters.

The MCU collects the four multiplexed input ADC-signals (I_{ECC}, T_{ECC} and the two spare channels) plus the six signal frequencies of the RS80 and formats them into a digital ASCII, 11 bits-NRZ (= Non Return to Zero) data stream that is put on the output line of the MCU. The digital NRZ-data stream is converted into a FSK tone signal (FSK = Frequency Shifted Key) of 2025 and 2225 Hz as the digital zero- and one-bit respectively. In addition, the data stream is frequency modulated on the 403 MHz transmitter of the RS80 radiosonde and telemetered to the ground station at a baud rate of 300 bits/s.

At the ground station, a conventional UHF-receiving equipment is used to demodulate the telemetry signal back into the data stream of FSK-tone signals. A modem converts the data stream back into the hexadecimal coded data format of ASCII characters and via a RS232-serial port the data are fed into a personal computer for further data processing. Every 7 seconds a complete set of measured parameters is received in form of a hexa-decimal coded data frame of totally 72 ASCII characters.

Beside of the simultaneous measurements of the ozone concentration, pressure, temperature and relative humidity, the use of this sonde data interface board enables the simultaneous measurement of the actual temperature of the air sampling for a more accurate determination of the ozone concentration. The use of digital coded data in a two tone signal transmission by the telemetry of the radiosonde has the additional advantage of being less sensitive to telemetry noise compared with the conventional method using analog coded data transmission.

---

[1] The Motorola 68705R3 is a complete 6800 type of computer with following specifications:
RAM=112 bytes, EPROM=3.8 Kbytes, own clock generator, interrupts =4, 4 multiplexed ADC-channels (8 bit), programmable timer, in-and output lines=24.

3.3   Flight Operation

3.3.1   Pre flight: Preparation and Instrumental Checks

Each ozone sounding is made with a new instrument, which has therefore to be characterized well prior to flight. Consistency of the flown instruments with regard to their quality and characteristics, but also uniform operating procedures, is a prerequisite to assure consistent sonde measurements. Therefore, before every flight the different components of the sonde were carefully prepared and checked in the laboratory aboard the ship, mainly following the guidelines of *Komhyr* [1986] for the ECC-ozone sonde and of *Vaisala* [1988] for the RS80-radiosonde, respectively.

3.3.1.1   ECC-Ozone Sonde

The performance of the ECC-ozone sensor is checked for response time, conversion efficiency by comparison with an ozone reference, background current at ozone free air and volumetric flow rate of the gas sampling pump.

During the first cruise (ANT-V/5) commercial equipment (Type TSC-1, Science Pump Corporation, USA), recommended in the operation handbook of *Komhyr* [1986], was used to prepare and check the ozone sondes. However, this instrument showed three major disadvantages:

a) The conversion efficiency of the sensor was only checked by comparison with another ECC-sensor as reference cell and thus not really by an independent method as reference for the measurement of ozone.

b) The ozone free air for determining the background current was obtained by pumping laboratory air through a hopcalite/charcoal filter that was probably not efficient enough to purify the laboratory air from impurities. Oxidizing/reducing impurities can interfere with the ECC-ozone measurements [*Schenkel et al.,* 1982].

c) The accuracy of the analog current meter of the sensor current was only 0.05-0.1 μA and is thus not sufficient for an accurate measurement of the background current of the ECC-sensor that was in the same range of 0.05-0.1 μA.

Therefore, during the second cruise (ANT-VII/1) a couple of changes in the equipment for instrumental checks of the ECC-sensor were made. As ozone reference served an UV-photometer with integrated ozone generator (1008 RS type, Dasibi Corporation, USA). The gas flow system was operated with synthetic air, purified by a Pt-catalyst plus a charcoal/molecular sieve trap. The conversion efficiency of the ECC-sensor was determined for ozone pressures up to 25 mPa corresponding to atmospheric ozone values up to an altitude of 30 km. Further, the sensor current was measured by an electrometer amplifier (Type 617, Keithley Corporation, USA) with an accuracy better than 0.005 μA.

The volumetric flow rate of the gas sampling pump was determined with a burette tube by measuring the displacement time needed for a soap bubble to pass through a well defined volume of the burette. The observed pump flow rate was corrected for the moistening effect of the initially dry air when flowing through the cathode sensing solution and the soap bubbler itself. At a room temperature of $20^{\circ}C$ with a saturation water vapor pressure of 25 hPa a correction of about -2.5 % was applied to the observed flow rates. The accuracy of the determination of the volumetric flow rate was better than ±2 ml/min [*Smit and Kley*, 1998].

The results of the performance checks of the flown ECC-sondes are listed in Table 3.1. As an indication of quality assurance the statistical scattering of the individual sondes occurs only in a narrow bandwidth, which ensures a rather good reproducibility of the performance of the individual, flown ECC-sonde.

Sounding experiments made in an environmental simulation chamber, reported in detail in Annex A-1, have shown that the most accurate results are achieved when the measured ozone sensor current is corrected for the background current (see equation 3.4) which is determined before exposure of the ECC-sensor with ozone. As shown in Table 3.1 the background current measured before exposure with ozone is about 30 percent lower compared with the background current measured after exposure with ozone [*Johnson et al*., 2002].

Cruise [Number of Samples]	*ANT-V/5* March/April 1987 [25]		*ANT-VII/1* Sept/Oct 1988 [40]		*ANT-V/5 +* *ANT-VII/1* [65]	
Checked Parameter	Mean	Standard Deviation	Mean	Standard Deviation	Mean	Standard Deviation
Response Time [1], τ_{ECC} , at T=20°C, [sec]	31	3.0	29	1.9	30	2.5
Conversion Efficiency [2], η_{ECC} [unity]	--	--	1.00	0.01	--	--
Background Current, $I_{B,ECC}$ [µA] Before exposure with ozone After exposure with ozone	0.07 0.09	0.03 0.03	0.06 0.09	0.02 0.02	0.07 0.09	0.03 0.02
Vol. Flow Rate Pump, $\Phi_{V,ECC}$, [sccm/min]	210	5	226	8	220	10

Table 3.1:   *Overview of the results of the instrumental pre-flight checks of the ECC-ozone sensors flown during the ANT-V/5 and ANT-VII/1 cruises*

---

[1] The exponential response time τ_{ECC} on a downward response is defined as the time required that the signal S(t) is decayed by a factor 1/e of its initial value S(0) , whereby S(t) = S(0) * Exp[-t/τ_{ECC}]

[2] The conversion efficiency of the ECC-sensor, η_{ECC}, is defined here as the ratio of the ozone signal measured by the ECC-sensor compared to the UV-photometer, respectively, and is obtained from a linear regression fit of the ECC-sensor output as a function of the readings of the UV-photometer

3.3.1.2   RS80-Radiosonde

Prior to launch, the RS80-radiosonde was checked in the laboratory aboard the ship using the ground check equipment GC22 (Vaisala) and following the guidelines of the manufacturer [*Vaisala*, 1985]. The PTU-signals of the radiosonde were checked at ambient pressure and temperature, measured by a reference barometer (accuracy: ±0.2 hPa) and a thermometer (accuracy: ±0.2 ºC) respectively and at zero relative humidity (humidity sensor of RS80 had been put in a box with molecular sieve as desiccating agent). The results of the ground checks of the flown RS80-radiosondes are summarized in Table 3.2. The results of the individual instrumental checks of the radiosondes are included in the post flight data processing to correct the raw radiosounding data.

Cruise [Number of Samples]	*ANT-V/5* March/April 1987 [25]		*ANT-VII/1* Sept/Oct 1988 [40]		*ANT-V/5 +* *ANT-VII/1* [65[	
Checked Parameter: Differences of Radiosonde - Reference	Mean	Standard Deviation	Mean	Standard Deviation	Mean	Standard Deviation
Pressure: [hPa]	-2.3	0.5	-0.8	1.0	-1.64	2.0
Temperature: [K]	0.1	1.0	0.3	0.2	0.2	0.2
Relative Humidity: [%]	-1.0	1.0	0.2	0.5	-0.1	0.9

Table 3.2: *Overview of the results of the instrumental pre-flight checks of the pressure, temperature and relative humidity sensors of the RS80-radiosondes flown during the ANT-V/5 and ANT-VII/1 cruises*

3.3.1.3   Sonde Data Interface Board

The I/V-converter to measure the ozone sensor current is checked with a calibrated current source at well defined currents: 1.00, 2.50, 5.00 and 8.00 µA with accuracy better than 1 %. All checked I/V-converters agreed very well with the current source such that the accuracy of the I/V-converter is better than 1 % at currents between 1 and 8 µA. At currents below 1 µA the accuracy of the I/V-converter is limited by its resolution corresponding to ±0.01 µA. The thermistor for measuring the temperature of the gas sampling pump (T_{ECC}) is checked against the same reference thermometer (accuracy: ± 0.2 ºC) as used for the temperature ground check of the radiosonde. The results of these checks are summarized in Table 3.3.

Cruise [Number of Samples]	ANT-V/5 March/April 1987 [25]		ANT-VII/1 Sept/Oct 1988 [40]		ANT-V/5 + ANT-VII/1 [65]	
Checked Parameter: Differences: Interface board - Reference	Mean	Standard Deviation	Mean	Standard Deviation	Mean	Standard Deviation
Temperature pump T_{ECC} [K]	0.7	0.8	0.8	0.5	0.8	0.6

Table 3.3: *Overview of the results of the instrumental pre-flight checks of the sonde data interface boards flown during the ANT-V/5 and ANT-VII/1 cruises*

3.3.1.4 Outdoor Checks at Compass and Helicopter Deck

After preparation and about 30 minutes prior to launch, a performance check of the sonde under ambient atmospheric conditions was conducted at the front of the ship on the compass deck (21 m asl, asl = above sea level,) by in-situ comparison of the sonde readings with ozone measurements of ambient air. The latter being continuously carried out aboard the ship. The meteorological parameters (temperature, pressure and relative humidity) were all measured in the vicinity of the compass deck, using standard meteorological instrumentation and recorded by the integrating data system (=INDAS) of the ship. The concentration of ozone near the surface was monitored with an UV-photometer (1008 AH-type, Dasibi Corporation, USA) during both cruises. The air intake line (Teflon, 4 mm i.d., 8 m length, flow rate 3 l/min) extended about 4 m beyond the reeling of the upper, compass deck (21 m asl.) to avoid contamination from ship emissions.

In Table 3.4 the results of this in-situ comparison are listed as differences between the parameters measured by the sonde and the corresponding references. The observed levels of pressure, temperature, relative humidity and ozone were thereby in the ranges of 1010-1035 hPa, 285-302 K, 40-95 % and 10-55 ppbv, respectively. The sonde values include the corrections obtained from the ground check procedure (see section 3.3.1). The sonde data of ozone and pressure agreed very well with the readings of their corresponding references, while the sonde readings of temperature and relative humidity differed significantly, particularly during the ANT-V/5 cruise. The latter probably for the following reasons: The enhanced temperature observed by the sonde in combination with the lower relative humidity measured by the sonde was caused by a heating effect of the air close to the ship hull which is relatively warm due to absorbed solar radiation (tropics/sub tropics) encountered during both cruises. This effect is clearly seen by considering the specific humidity, which is not sensitive to air temperature variations. Comparing the relative deviations of the sonde readings of the relative humidity with the derived relative deviations of the specific humidity sonde readings it is seen that the sonde measures the specific humidity quite well within 5 % compared to the references. Similar findings were obtained from the final instrumental checks made at the helicopter deck just prior to the launch of the sondes (see Table 3.5). Reference instruments are the same as used for the checks made at the compass deck

Cruise [Number of Samples]	ANT-V/5 March/April 1987 [25]		ANT-VII/1 Sept/Oct 1988 [40]		ANT-V/5 + ANT-VII/1 [65]	
Differences of Sonde - Reference	Mean	Standard Deviation	Mean	Standard Deviation	Mean	Standard Deviation
Ozone, mixing ratio [ppbv]	2.0	2.6	-0.2	2.0	0.8	2.4
ΔP = Pressure [hPa]	1.1	0.8	-0.5	0.7	0.3	0.8
ΔT =Temperature [K]	3.0	1.7	1.0	0.8	1.8	1.5
ΔU =Relative Humidity [%]	-11	9	-5.4	5.0	-7.7	7.5
ΔS=Specific Humidity [g/kg]	0.05	1.0	-0.17	0.6	-0.08	0.8
$\Delta U / U$	-0.17	0.15	-0.07	0.07	-0.11	0.12
$\Delta s / s$	0.006	0.11	0.013	0.05	-0.005	0.08
$\Delta O_3 / O_3$	0.06	0.11	-0.001	0.07	0.03	0.10

Table 3.4: *Overview of the results of the instrumental pre-flight checks of the sondes at the compass deck after sonde preparation and prior to launch during ANT-V/5 and ANT-VII/1.*

Cruise [Number of Samples]	ANT-V/5 March/April 1987 [25]		ANT-VII/1 Sept/Oct 1988 [40]		ANT-V/5 + ANT-VII/1 [65[	
Differences of Sonde - Reference	Mean	Standard Deviation	Mean	Standard Deviation	Mean	Standard Deviation
ΔO_3=Ozone, mix. ratio [ppbv]	0.6	2.2	-1.2	1.9	-0.4	2.2
ΔP= Pressure [hPa]	1.5	0.8	-0.4	1.1	0.4	1.4
ΔT= Temperature [K]	2.6	1.7	1.3	0.7	1.8	1.4
ΔU=Relative Humidity [%]	-11	8	-5.5	4.0	-7.8	6.4
ΔS=Specific Humidity [g/kg]	-0.1	1.2	-0.01	0.6	-0.05	0.9
$\Delta U / U$	-0.15	0.11	-0.07	0.05	-0.10	0.09
$\Delta S / S$	-0.004	0.14	0.003	0.05	0.001	0.1
$\Delta O_3 / O_3$	0.02	0.1	-0.04	0.05	-0.01	0.08

Table 3.5: *Overview of the results of the instrumental pre-flight checks of the sondes at the helicopter deck just prior to their launches during the ANT-V/5 and ANT-VII/1.*

3.3.2 In-Flight Operation

Directly after the final checks at the compass deck had been made, the sondes were launched from the helicopter deck (12 m asl.) at the back of the ship. The total weight of the flight package was about 1660 g, whereby the weight of the payload of the gondola was about 1000 g and the balloon (inclusive H_2-filling) weighted 660 g. The free lift of the flight package was about 1200 g such that an ascent velocity of about 5 m/sec and a bursting altitude of about 29 km were achieved (see Table 3.7).

During ascent and descent of the sonde the measured data were transmitted to the ground station aboard the ship. The received signal of the sonde was decoded back via the modem and fed into the personal computer and stored on-line together with the actual flight time as raw data for the following post flight data processing

3.3.3 Post Flight Data Processing

After each flight the recorded raw sounding data were processed under inclusion of the corrections resulting from the ground check procedures described in Section 3.3.1. The ozone pressure was derived from the measured ECC-current ($I_{M,ECC}$) using equations 3.1 and 3.2 (see Section 3.2.2). Based on laboratory studies made in the environmental simulation chamber, as reported in Annex A-1, a new method of background correction was applied. Simulations of vertical ozone soundings made in the chamber under realistic atmospheric conditions of pressure, temperature and ozone concentrations have shown that the most accurate results are achieved with full subtraction of the background current at each pressure [*Smit et al,* 1994-A].

In other words, the background current is independent of the oxygen pressure. This is in contrast to the conventional method of background correction, prescribed by *Komhyr* [1986] and customary applied worldwide. Komhyr assumes that the background current is dependent of the oxygen pressure, getting negligibly small contribution to the overall signal in the middle/upper troposphere and above. However, laboratory studies [*Thornton et al.,* 1982, 1983] do not show any oxygen dependence of the background current. Therefore, at each pressure the measured ozone sensor current $I_{M,ECC}$ is corrected by a full subtraction of the background current that was determined at the groundcheck before exposure with ozone.

The simulation experiments (See Annex A-1) have shown that in case of tropospheric ozone measurements not to use any correction based on total ozone column measurements. Therefore, the ozone sonde data presented in this thesis have not been normalized to any spectroscopic measurement of the total ozone column density.

The volumetric gas sampling pump is a constant displacement type pump whereby the pumping efficiency varies with ambient air pressure and depends on pump leakage, the pump dead volume and the back pressure exerted on the pump by the sensing cathode solution through which gas is forced [*Komhyr,* 1967]. This means that the effective volumetric flow rate $\Phi_{V,ECC}$ is given by:

$$\Phi_{V,ECC} = \Phi_{V,ECC,Ground} \cdot \eta_{Pump} \qquad [3.5]$$

whereby: $\Phi_{V,ECC,Ground}$ = Volumetric flow rate of pump as determined at ground check

η_{Pump} = Efficiency of pump which is pressure dependent

The pump efficiency is a function of ambient air pressure which has been determined by several investigators [*Komhyr,* 1986, 1995 and *Torres,* 1981] is shown in Figure 3.5.

The loss of pump efficiency is increasing with altitude it becomes significant only in the middle stratosphere at altitudes above 30 km. In the troposphere and in the lower stratosphere below 20 km altitude the loss of efficiency is smaller than 1 percent. Up to an altitude of 30 km the losses of pump efficiencies as determined by *Komhyr et al.* [1986 and 1995] and *Torres* [1981] are smaller than 2-3 percent. Only in the upper stratosphere above 30 km the losses get significant larger than 3-5 percent. The ozone sonde data obtained during the two Polarstern cruises did not exceed altitudes above 30 km, such that the corrections for losses of pump efficiency are marginally small. In the final processing of the ozone sonde data pump efficiency corrections were included by using the middle curve as reported by *Komhyr* (1986) shown in figure 3.5 while the curves labelled Torres [1981] and Komhyr et al. [1995] mark lower and upper limits of the pump efficiency as reported.
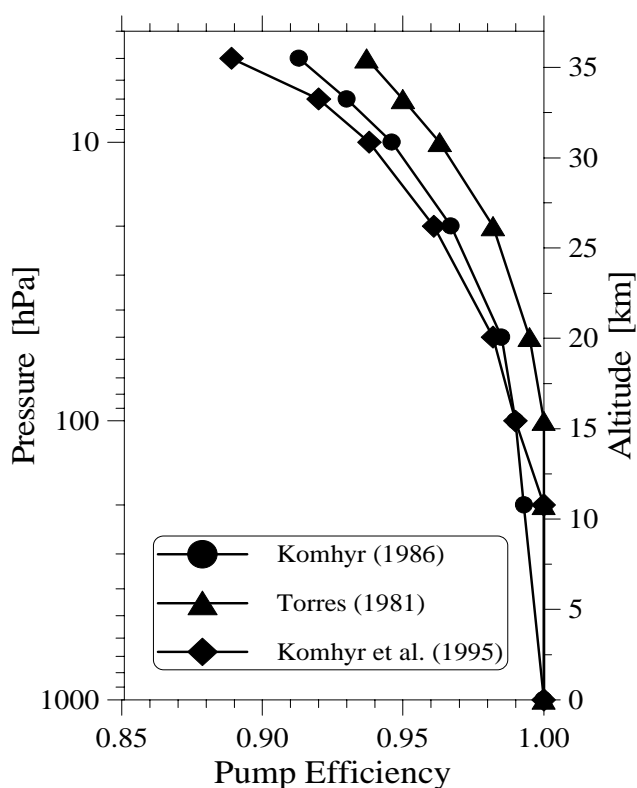
Figure 3.5: *Pump efficiency of the ECC-sensor as a function of ambient air pressure c.q. altitude as determined by Komhyr (1986= ●, 1995= ◆) and by Torres (1981= ▲).*

The measured signals of the RS80-radiosonde are processed according to the standard procedure described by the manufacturer [*Vaisala,* 1988] with one exception for the thermal behavior of the Humicap-A humidity sensor at low temperatures. Relative humidity measurements made with the Humicap-A sensor are known to be unreliable at temperatures below 250 K [e.g. *Elliott and Gaffen*, 1991]. This can be expected from the fact that the reliability of the calibration curve provided by the manufacturer (Vaisala, Helsinki, Finland) for every Humicap-A sensor is limited because is it only based on calibrations made at 20^oC and 0^oC [*Vaisala,* private communication]. This means that using this calibration curve at lower temperatures together with the temperature dependence of thin film capacitive RH sensing elements as demonstrated in Section 3.2.4 (See Equation 3.11) considerable

inaccuracies of relative humidity at low temperatures can be expected. Field investigations comparing Humicap-A humidity measurements to an accurate frost point hygrometer [*Kley et al,* 1997, *Miloshevich et al.,* 2001] showed a dry bias that increases with decreasing temperatures. Significantly low biases of up to -30% relative humidity values at -65°C resulted. Twin sounding comparisons of two RS80-radiosondes flown simultaneously at the same gondola showed that the in-flight precision of the Humicap-A sensor is better than ±(1-2)% [See Annex-A-2, Table A-2-2], independent of the relative humidity and the air temperature.

Based on the excellent precision of the Humicap-A and the systematic dry bias observations made by Kley et al. [1997] together with laboratory investigations made in the environmental simulation chamber a correctional scheme for the dry bias observed below 240 K is developed. The results of these investigations are reported in detail in Annex-A-3. The scheme to correct the frost point temperature derived from Humicap-A readings are listed in Table 3.6.

Temperature Range in K	Correction to frost point temperature: $\Delta T_{F,C}$ in K
$T > 240$ K	$\Delta T_{F,C} = 0$
205 K $\leq T \leq 240$ K	$\Delta T_{F,C} = -0.186 \bullet T + 44.6$
$T < 205$ K	$\Delta T_{F,C} = +6.5$

Table 3.6: *Correctional scheme of frost point temperature derived Humicap-A sensor reading at low temperatures obtained from comparison with frost point hygrometer [See Annex-A-3].*

The uncertainty of the corrected Humicap-A derived frost point temperature is estimated to be ±3K according to the standard deviation of the differences between Humicap-A and FPH. The corresponding corrected relative humidity readings of the Humicap-A have an uncertainty factor of about ± 0.3 of the corrected values.

At low temperatures the Humicap-A sensor suffers a humidity lag due to large response times. At an ascent rate of 5 m/s the response time (height resolution) of the Humicap-A strongly increases at lower temperatures: It is at 293 K ≈1 s (5 m), at 230 K ≈ 1min (300 m) and at 200 K ≈10 min (3 km) [*Antikainen and Paukkunen.,* 1994]. Below 200 K the humidity lag is larger than 3 km and strong smoothing (integrating) effects of actual humidity structures occur. The large humidity lag may cause the humidity values observed above the tropopause, in the lower stratosphere, to be far too high. In general, the performance of the Humicap-A sensor is not reliable above the tropopause and Humicap-A measurements made in the stratospheric region were therefore excluded from further investigation.

For evaluation water vapor data obtained from RH-measurements the water vapor saturation pressure over a plane surface of liquid water (P_{WVS} (T) has been used, since relative humidity with respect to liquid water is the usual measure in the scientific community. P_{WVS} (T) with respect to liquid water but also with respect to ice is derived using the *Goff- Gratch* (1946) formulation as recommended by the World Meteorological Organization [*WMO-Report No.8,* 1983] and adapted to the International Temperature Scale 1990 (ITS-90) [*Sonntag,* 1994].

The water vapor saturation partial pressure with respect to a plane surface of liquid water or ice is respectively:

$$P_{WVS}(T) = Exp\left[\frac{a}{T} + b + c \cdot T + d \cdot T^2 + e \cdot Ln(T)\right], \text{ where } P_{WVS} \text{ is in Pa, T in K.}$$

For liquid water the constants are:

a = -6096.9385, b = 21.2409642, c = -2.711193E-2, d = 1.673952E-5, and e = 2.433502

For ice the constants are:

a= -6024.5282, b=29.32707, c= 1.0613868E-2, d= -1.3198825E-5, and e = -0.49382577

The post-flight data consist of a set of vertical profiles of the measured parameters such as flight time, ozone concentration, meteorological parameters (pressure, temperature and relative humidity) and the two instrumental temperatures of the sonde (temperature of pressure transducer and gas sampling pump, respectively). Additionally the geometric altitude has been calculated step by step as the cumulative sum of the height difference between two successive pressure levels using the hydrostatic equation [e.g. *Holton*, 1979] [5] .

Beside of the elimination of erratic data due to telemetry noise no further data filtering is applied. Although during ascent as well as descent of the sonde data were taken, only ascent data are used in this thesis. The statistics of some flight parameters of the soundings made during both cruises are summarized in Table 3.7.

The temperature T_{ECC} of the pump with values of about 300-310 K is relatively high during the ascent of the sondes. This evokes the question in how far these enhanced temperatures can influence the conversion efficiency of the ECC-sensor due to a stronger evaporation of the sensing solution in the cathode half-cell of the sensor. However, laboratory experiments have shown that even at these enhanced temperatures within the operational period during the ascent of the sonde (< 2 hours), the conversion efficiency (η_{ECC}) of the ECC-sensor is still better than 95 %. The experiments showed that during the operation of the ECC-sensor the sensing solution will evaporate and thus the absorption efficiency will decrease but simultaneously the stoichiometry of the conversion of O_3 into I_2 is increasing due to an increase of the concentration of KI in the sensing solution. Both effects compensate during the first two hours of flight operation of the sensor, such that the conversion efficiency will keep close to unity during ascent of the sonde.

Response tests of the ECC-sensor made in the laboratory at these enhanced sensor temperatures have yielded response times of less than 20 s. They are substantially smaller compared to the response time of 30 s obtained from the ground checks reported in section Table 3.1 (see Section 3.1.1.1). At higher temperatures the ECC's show a faster response due to a faster mass diffusion of I_2 in the vicinity of the cathode surface in the sensing solution [*Komhyr et al.* 1971]. At a response time of 20 seconds in combination with an ascent velocity

---

[5]Hydrostatic equation is defined as $\Delta Z = \frac{R}{g} * \frac{T_{i+1}^V + T_i^V}{2} * Ln\left(\frac{P_i}{P_{i+1}}\right)$, whereby R= gas constant, g= gravity

constant, T^V= virtual tamperature, P= pressure and indices i and i+1 are representing the two succeeding pressure levels

of 5 m/s the overall height resolution of the ozone measurements made with the ECC will be about 100 m.

On a few occasions, the balloon drifted through the ship's engine exhaust plume just after launch. This caused transient erratic readings that were discarded. The ozone sensor recovered, however, within 1-2 minutes after passage through the exhaust fumes.

Erratic data above 10 km between 3°N and 15°N were recorded during the first cruise (ANT-V/5). This was probably caused by a Saharian dust storm encountered in the upper troposphere that deteriorated a proper performance of the ECC-ozone sensor. These erratic data were discarded from the final ozone data set.

During the second part of the first cruise (ANT-V/5) three twin soundings were performed to investigate the precision of the vertical profiles of ozone, pressure, temperature and relative humidity measured by the ECC/RS80-sonde. The results of these twin flights are reported in Annex A-2.

Cruise Flight parameters	ANT-V/5 March/April 1987		ANT-VII/1 Sept/Oct 1988		ANT-V/5 + ANT-VII/1	
Flight Parameter	Mean	Standard Deviation	Mean	Standard Deviation	Mean	Standard Deviation
Ascent Velocity : [m/s]	5.1	0.5	4.5	0.3	4.7	0.5
Burst Altitude : [km]	28.2	1.4	30.2	1.4	29.4	1.7
Recovery of data transmission : [%]	0.74	0.2	0.82	0.09	0.8	0.2
Height resolution of data transmission : [m]	50	50	40	6	45	40
Temperature of pressure transducer ,T_{RS80} : [K]	261	8	263	5	262	7
Temperature of pump, T_{ECC} : [K]	307	6	301	4	303	5

Table 3.7: *Overview of the statistics of some in-flight parameters as obtained from the ozone soundings made from aboard the RV „Polarstern" during the ANT-V/5 and ANT-VII/1 cruises.*

3.4 Performance of ECC-Ozone Sonde and RS80-Radiosonde

3.4.1 Introduction

Despite the fact that since more than 30 years a large number of balloon ozone soundings ($\approx$2000 soundings/year) have been flown world wide, relatively little has been done concerning the quality assurance (=QA) of sounding data. Only a limited number of laboratory and field studies have been performed in the past [e.g. *Attmanspacher and Dütsch*, 1970 and 1981, *Hilsenrath et al.*, 1986, *Kerr et al.*, 1994]. Most of these studies have focused on the performance of the ECC-sonde in the stratosphere and only a sparse number of studies also addressed the more specific sonde performance in the troposphere [*Beekmann et al.*, 1994, 1995, *Reid et al.*, 1996]. The uncertainty in sonde measurements of tropospheric ozone concentrations is relatively high since the signal to noise ratio is low due to the much lower ozone values in the troposphere than in the stratosphere and the relatively large contribution from the background current to the signal. Up to now only rough estimates about the reliability of the sounding data below the tropopause could be made [*SPARC*, 1998)]. No sonde validation studies existed to assess the data quality of vertical sounding data of tropospheric ozone obtained in remote regions such as the maritime regions of the tropics and southern hemisphere which are usually characterized by relatively low tropospheric ozone concentrations throughout the entire troposphere. [*Smit et al.*, 1989-A, 1990, *Kley et al.*, 1996].

In case of the RS80-radiosonde, which is operational since 1980 [*Antikainen and Hyvonen*, 1983], it is even more concerning that the use of this type of weather sonde for scientific research purposes has not been systematically investigated [*Schmidlin*, 1982]. Intercomparisons organized by the WMO (=World Meteorological Organization) only assess the performance of radiosondes with regard to their specific needs in the worldwide weather forecasting networks [e.g. *Nash and Schmidlin*, 1987]. Since standard meteorological humidity sensors are not validated above 5000 m altitude, so that their accuracy and precision are not well known a dramatic lack in case of the humidity measurements made by radiosondes is apparent [e.g. *Elliott and Gaffen*, 1991, *Gaffen*, 1993],.

This section reports about the instrumental performance of the ECC-ozone sensor and the humidity, temperature and pressure sensors of the RS80-radiosonde deployed during the ANT-V/5 (March/April 1987) and ANTVII/1 (September/October) cruises. First, in a theoretical analysis the overall uncertainty of the ECC-ozone sensor as a function of altitude is estimated and the performance of the ECC/RS80-sonde is given. In addition, based on three experimental studies (See technical reports in Annex-A) an evaluation of the performance of the ECC/RS80-sonde is given.

3.4.2 Instrumental Uncertainties of the ECC-Ozone Sensor

As shown in Section 3.2.2 the ozone pressure measured by the ECC-sensor is a function of the measured sensor current ($I_{M,ECC}$), the background current ($I_{B,ECC}$), the conversion efficiency ($\eta_{O3,ECC}$), the temperature of the gas sampling pump (T_{ECC}) and the volumetric flow rate ($\Phi_{v,ECC}$):

$$P_{O_3} = P_{O_3} \left(I_{M,ECC} , I_{B,ECC} , \eta_{O_3,ECC} , T_{M,ECC} , \Phi_{V,ECC} \right) \qquad [3.6]$$

The instrumental uncertainty of the ECC-ozone sonde for the measurement of ozone is a composite of the contributions of the individual uncertainties of the different instrumental parameters listed above. Some of the contributions depend on air pressure, such that the overall uncertainty of the ozone measurement will be a function of pressure i.e. altitude.

3.4.2.1 Error Propagation

Applying Gaussian law of error propagation [*Bevington and Robinson,* 1992] to the functional relation between P_{O3} and the parameters $I_{M,ECC}$, $I_{B,ECC}$, T_{ECC}, $\Phi_{V,ECC}$ and $\eta_{O3,CC}$, defined by equations 3.1 , 3.2 and 3.4 the overall relative uncertainty of P_{O3} is expressed as :

$$\frac{\Delta\,P_{O3}}{P_{O3}} = \sqrt{\left(\frac{\Delta\,C_{ECC}}{C_{ECC}}\right)^2 + \frac{\left(\Delta\,I_{M,ECC}\right)^2 + \left(\Delta\,I_{B,ECC}\right)^2}{\left(I_{M,ECC} - I_{B,ECC}\right)^2}} \qquad [3.7]$$

whereby the relative uncertainty of the conversion factor C_{ECC} is given as:

$$\frac{\Delta\,C_{ECC}}{C_{ECC}} = \sqrt{\left(\frac{\Delta\,\eta_{O3,ECC}}{\eta_{O3,ECC}}\right)^2 + \left(\frac{\Delta\,T_{ECC}}{T_{ECC}}\right)^2 + \left(\frac{\Delta\,\Phi_{V,ECC}}{\Phi_{V,ECC}}\right)^2} \qquad [3.8]$$

The relative uncertainty of the conversion efficiency, $\eta_{O3,ECC}$ is determined by the contributions of the absorption efficiency $\alpha_{O3,ECC}$, the stoichiometric factor $S_{O3/I2}$ and their uncertainties:

$$\frac{\Delta\,\eta_{O3,ECC}}{\eta_{O3,ECC}} = \sqrt{\left(\frac{\Delta\,\alpha_{O3,ECC}}{\alpha_{O3,ECC}}\right)^2 + \left(\frac{\Delta\,S_{O3/I2}}{S_{O3/I2}}\right)^2} \qquad [3.9]$$

The relative uncertainty of the effective volumetric pump flow rate $\Phi_{V,ECC}$, which is determined by the contributions from the uncertainty of the determination of the flow rate $\Phi_{V,ECC,Ground}$ at the ground check and the uncertainty of the pump efficiency η_{Pump} at lower air pressures, can be expressed by applying equation 3.5 as:

$$\frac{\Delta\,\Phi_{V,ECC}}{\Phi_{V,ECC}} = \sqrt{\left(\frac{\Delta\,\Phi_{V,ECC,Ground}}{\Phi_{V,ECC,Ground}}\right)^2 + \left(\frac{\Delta\,\eta_{Pump}}{\eta_{Pump}}\right)^2} \qquad [3.10]$$

From equations 3.7, 3.8, 3.9 and 3.10 it is seen that the contributions of the parameters like the conversion efficiency ($\eta_{O3,ECC}$), the pump temperature (T_{ECC}) and the pump flow rate ($\Phi_{V,ECC}$) is the sum of the squares of the relative uncertainties of the individual parameters. The contributions of the measured sensor current ($I_{M,ECC}$) and the background current ($I_{B,ECC}$) are slightly more complicated. The square of the difference of both parameters in the denominator in equation 3.6 shows clearly the sensitivity of the overall relative uncertainty of the ozone pressure to these two parameters in case that both are of the same order of magnitude. In the next section the individual contributions of the different parameters to the overall uncertainty of P_{O3} are discussed.

3.4.2.2 Error Contributions of η_{ECC} , T_{ECC} , $\Phi_{V,ECC}$, $I_{M,ECC}$, and $I_{B,ECC}$

The relative uncertainty of the conversion factor C_{ECC}, given by equation 3.8, is composed of the individual contributions from $\eta_{O3,ECC}$, T_{ECC} and $\Phi_{V,ECC}$ as follows:

(i) $\eta_{O3, ECC}$

In the $P_H = 7$ buffered $[KI] = 0.01$ Mol/l sensing cathode solution the stoichoimetry of the conversion reaction of ozone into iodine is 1.00 with an uncertainty of about ±0.03 *Dietz et al*., 1973], while the initial absorption efficiency of gaseous O_3 into the sensing solution will be 1.00 with an uncertainty of ±0.01. This means that according to equation 3.7 the initial relative uncertainty of the conversion efficiency $\eta_{O3,ECC}$ at ground will be close to ±0.03. Laboratory studies, as reported in section Annex A-1 have shown further that during the first two flight hours, i.e. at pressures above 25 hPa, the conversion efficiency remains close to unity with an uncertainty of ±0.03. This means that the contribution of the overall conversion efficiency of ozone into iodine is independent of altitude, at least during the first two hours of flight operation.

(ii) T_{ECC} :

The uncertainty of the temperature measurement, T_{ECC}, of the gas sampling pump is smaller than ±1.0 K as obtained from the groundcheck of the sonde data interface board (see Section 3.3.1.3: Table 3.3). During flight the levels of T_{ECC} vary only between 295 and 305 K (see Section 3.3.3: Table 3.6), such that at an uncertainty of T_{ECC} of ±1.0 K the corresponding relative uncertainty of T_{ECC} will be smaller than ±0.3 % and can thus be neglected as an altitude dependent contribution. However, there are two temperature effects which have to be taken into account with respect to the measurement and use of the temperature of the gas sampling pump T_{ECC} for the determination of the ozone concentration. Firstly, due to frictional heating effects the air inside the pump piston is approximately warmed by 1-2 K [*Komhyr et* al., 1995] and thus causes an underestimation of the measured ozone values of about 0.7 %. Secondly, laboratory experiments in the environmental simulation chamber in Jülich have shown that under tropospheric/stratospheric conditions the temperature of the incoming sampling air is 1-2 K lower than the actual measured temperature T_{ECC} of the pump. This is caused by an incomplete thermalization of the incoming sampling air to the actual temperature of the inner part of the pump. The two temperature effects, caused by friction and thermalization respectively, are of the same magnitude but opposite of sign and will compensate eachother.

(iii) Φ_V :

The uncertainty of the volumetric pump flow rate is determined to a major part by the accuracy (±2 ml/min) of the soap film displacement measuring technique used at the ground check of the ozone sonde (see Section 3.3.1.1). This means that for a volumetric flow rate of about 210-230 ml/min the relative contribution of the uncertainty of the flow rate determination will be below ±1 %. An additional contribution is due to the loss of pump efficiency at lower ambient pressures and the uncertainty of the experimentally achieved correction factors as reported in section 3.3.3. The uncertainty of this pump efficiency correction factor was estimated to be about half of the difference between the lower and upper limit of the pump efficiencies as determined by *Komhyr* [1995] and *Torres* [1981] shown in Figure 3.5 (see Section 3.3.3). The equation for the overall relative uncertainty of the pump flow rate is given in equation 3.9.

48

The overall relative uncertainty of the conversion factor C_{ECC} is weakly dependent on ambient air pressure, i.e. altitude, and mainly due to the uncertainty of the pump efficiency correction at lower pressures. The ratio $\Delta C_{ECC} / C_{ECC}$ slightly increases with altitude with values of ± 0.03 at the surface, ± 0.035 at 15 km, ± 0.04 at 25 km, and ± 0.045 at 30 km.

(iv) $I_{M,ECC}$

The most sensitive part of the overall relative uncertainty of P_{O3} is due to the magnitude of the measured sensor current $I_{M,ECC}$, the background current $I_{B,ECC}$ and their uncertainties $\Delta I_{M,ECC}$ and $\Delta I_{B,ECC}$ respectively.

The uncertainty of the measured sensor current ($I_{M,ECC}$) is mainly determined by the accuracy of the current measurement by the sonde data interface board (see Section 3.3.1.3), such that for currents above 1 µA the uncertainty of $I_{M,ECC}$ (12 bit resolution) is about ± 1 percent of the measured value, while for currents below 1 µA the uncertainty will be about ± 0.01 µA.

(v) $I_{B,ECC}$:

Figure 3.6 shows the influence i.e. fraction of the background current to the measured ozone current as a function of altitude for ozone profiles that are typically encountered at mid latitudes (left diagram) and in the tropics (right diagram), respectively. It is seen that the contribution of the background current, at typical values of 0.05-0.1 µA to the measured current with typical values of 0.2-1 µA (=0.7-4 mPa ozone) in the troposphere, is large enough to have a significant influence on the accuracy of the ozone measurements, especially in the middle and upper troposphere.
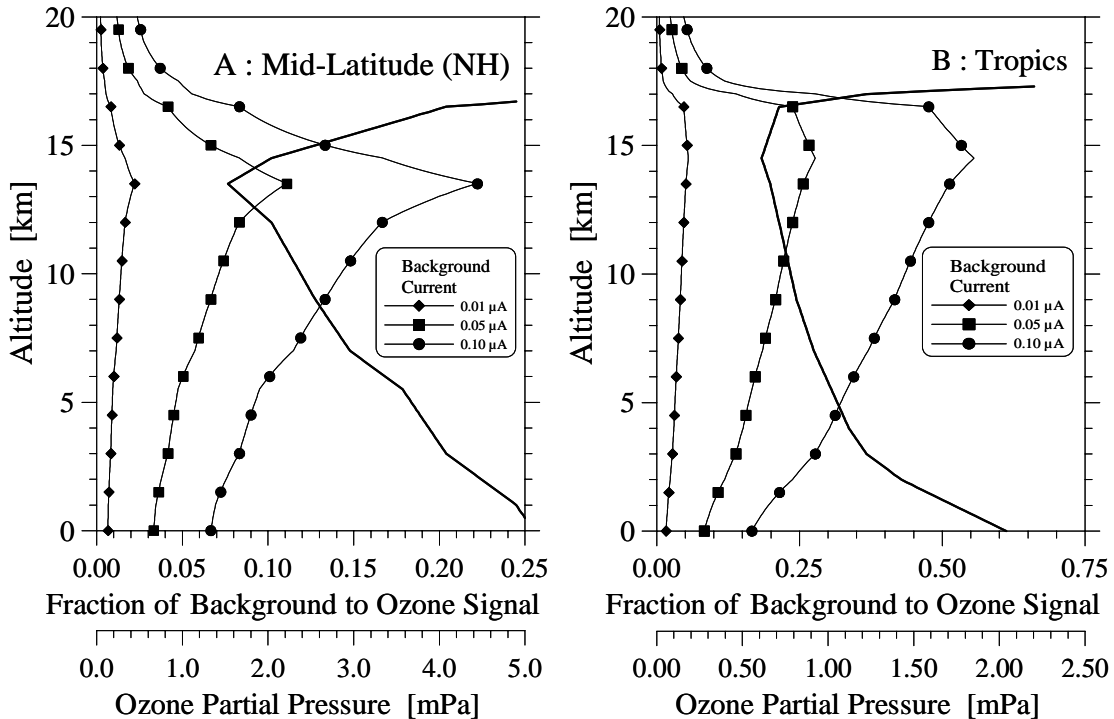

Figure 3.6: *Contribution of the background current of the ECC-ozone sensor as fraction of the vertical profile of ozone (fat solid line) for background values of 0.01 µA (♦), 0.05 µA (■) and 0.1 µA (●) at mid-latitudes (A-panel) and in the tropics (B-panel).*

In particular, tropical profiles of ozone under conditions of high convective activity with a high tropopause at 18 km and a low tropopause temperature that are characterized by extremely low ozone values in the middle and upper troposphere [Smit et al., 1991, Kley et al., 1996] are sensitive to the magnitude of the background current and its accuracy.

3.4.2.3 Overal Uncertainty

The contributions of the individual uncertainty sources are put together into the overall relative uncertainty of P_{O3} according the equations 3.6 to 3.9. Figure 3.7 show the overall relative uncertainty of P_{O3} as a function of altitude estimated for typical mid-latitudinal and tropical conditions respectively. The overall uncertainty has been calculated for three different hypothetical values of the uncertainty of the background current determination, namely $\Delta I_{B,ECC} = \pm 0.01$ µA, ± 0.02 µA, and ± 0.05µA, while for the background current itself a typical value of 0.1 µA is valid. It is clearly seen that for uncertainties of the background current larger than ± 0.02 µA this contribution will become large and can even dominate the overall uncertainty of P_{O3} in the middle/upper troposphere, particularly in the tropics.

Figure 3.8 shows the fractions of the individual contributions of the three main uncertainty sources like conversion efficiency C_{ECC}, measured ozone current $I_{M,ECC}$ and background current $I_{B,ECC}$ to the overall uncertainty of the ECC-ozone sensor as a function of altitude as estimated for two different uncertainties of background current (± 0.01 µA and ± 0.05 µA respectively) under typical mid-latitudinal and tropical conditions, respectively. It is clearly seen that in the stratosphere the dominant uncertainty source will be the conversion factor C_{ECC}, while in the troposphere the overall uncertainty is governed by the uncertainties of the background current $I_{B,ECC}$ and the measured ozone current $I_{M,ECC}$.
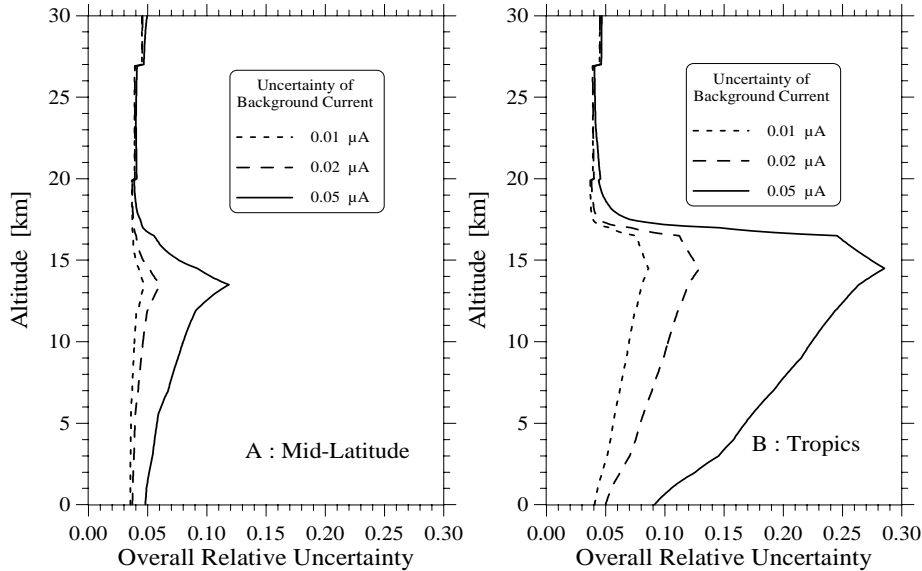

Figure 3.7: *Estimation of the overall relative uncertainty of ozone measurements made with an ECC-sensor as a function of altitude calculated according Gaussian law of error propagation for three different uncertainty levels of the background current (±0.01 µA, ±0.05 µA and ±0.05 µA) under typical mid latitudinal (A-panel) and tropical (B-panel) conditions.*
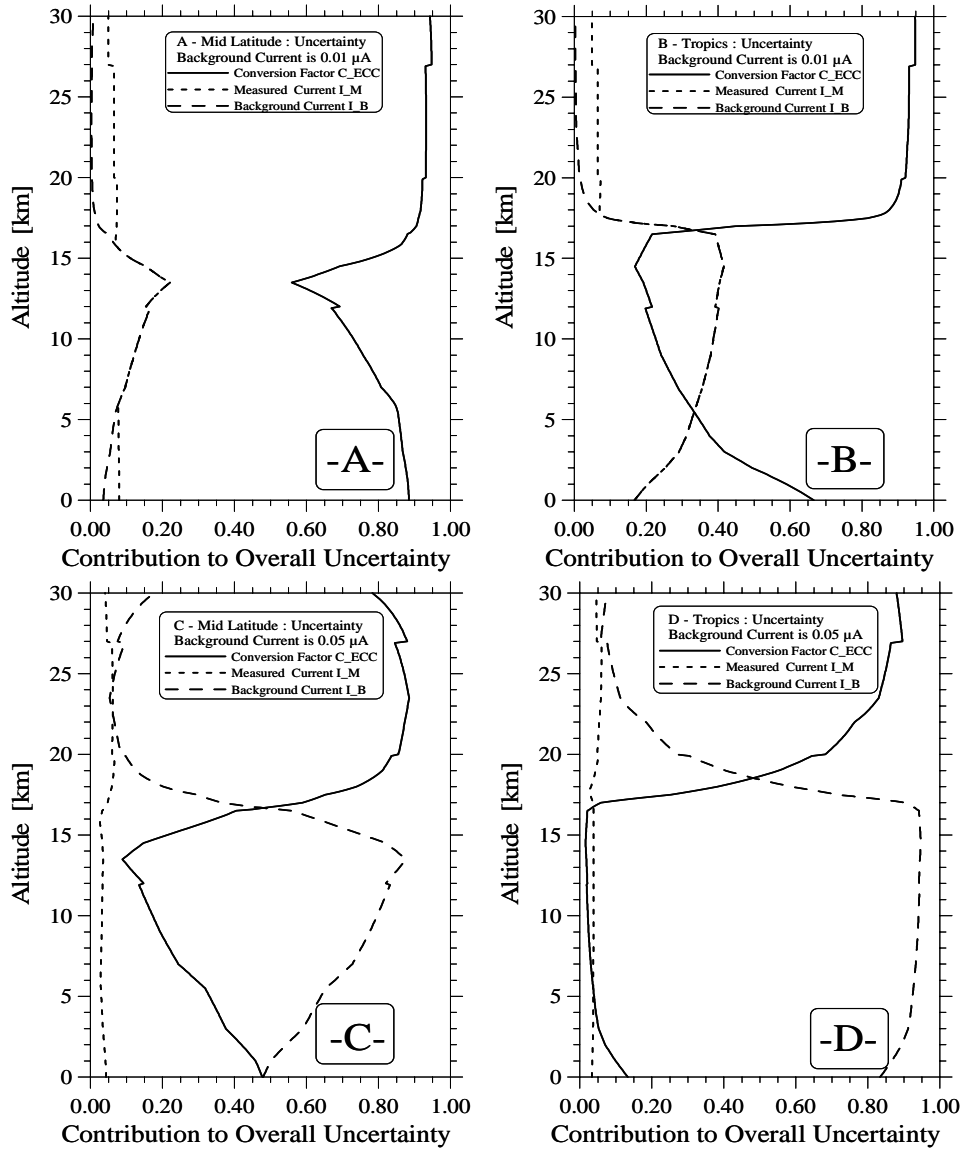
Figure 3.8: *Estimate of the fractional contributions from the three main uncertainty sources (conversion efficiency C_{ECC}, measured ECC current $I_{M,ECC}$ and background current $I_{B,ECC}$) to the overall uncertainty of the ECC-ozone sensor as a function of altitude calculated for two different uncertainties of background current (± 0.01 µA and ± 0.05 µA) under typical mid-latitudinal conditions (A- and C-panel) and typical tropical conditions (B- and D-panel).*

Particularly at uncertainties of the background current with values larger than ± 0.02µA this will become the dominant uncertainty source for the measurement of P_{O3}. This was the case during the first ANT-V/5 cruise in March/April 1987 for which the background current could only be measured with an accuracy of about 0.05 µA due to the limited resolution of the electrometer used for the measurement of the background current during the ground check just before launch. However, during the second cruise ANT-VII/1 in September/October 1988 a more accurate electrometer (accuracy better than ± 0.005 µA) was used to determine the background current. For the tropospheric part of the vertical ozone profiles measured with the ECC-sensor this means that during the second cruise the overall uncertainty of P_{O3} had significantly improved compared with the results obtained during the first cruise.

In Table 3.8 an overview of the overall uncertainties of P_{O3} - sonde measurement estimated for ANT-V/5 cruise (uncertainty background current ≈ ± 0.05 µA) and ANT-VII/1 cruise (uncertainty background current ≈ ± 0.01 µA) are listed for mid-latitudinal as well as tropical conditions at different altitude ranges. The propagation of the most significant sources of instrumental uncertainties show clearly that for the stratospheric part of the vertical ozone profiles the overall uncertainty of ozone measured with the ECC sensor is below 5 % and is governed by the conversion factor C_{ECC}. In the troposphere the overall uncertainty is dominated by the uncertainty of the background current, especially at values exceeding 0.02 µA. The negative influence of large uncertainties of the background current is most evident in the middle/upper troposphere, particularly in the tropics with its low ozone concentrations. For background currents that are not exceeding 0.1 µA and determined with an accuracy better than 0.01µA the overall relative uncertainty of the measurement of ozone with the ECC sensor in the troposphere is better than ±(4-7)%. This means that a precision of the ECC-ozone sensor of ±(4-7)% in the troposphere and ±(4-6)% in the lower/middle stratosphere was achieved. The above analysis shows the importance of the proper processing of the background current for tropospheric ozone measurements made with the ECC-sensor, particularly in the tropics. The above analysis shows the importance of the proper processing of the background current for tropospheric ozone measurements made with the ECC-sensor, particularly in the tropics.

	ANT-V/5 - Cruise [Background Uncertainty ± 0.05 µA]		ANT-VII/1 - Cruise [Background Uncertainty ± 0.01 µA]	
Altitude Range	Mid Latitude	Tropics	Mid Latitude	Tropics
20 - 25 km	±4%	±5%	±4%	±5%
TP - 20 km	±5%	±6%	±4%	±6%
10 km - TP	±8%	±20%	±5%	±7%
5 - 10 km	±6%	±17%	±4%	±4%
0 - 5 km	±5%	±12%	±4%	±4%

Table 3.8: *Overview of the overall uncertainties of P_{O3} - sonde measurement estimated for ANT-V/5 cruise (uncertainty background current ≈ ± 0.05 µA) and ANT-VII/1 cruise (uncertainty background current ≈ ± 0.01 µA) is listed for mid-latitudinal as well as tropical conditions at different altitude ranges. TP = Tropopause*

3.4.3   Evaluation: Precision and Accuracy of ECC/RS80-Sondes

Different validation studies addressing the performance of the different sensors of the ECC- and RS80 sonde, reported in Annex A, have been conducted in the field and in the laboratory. Annex-A-1 deals with sonde validation experiments conducted under controlled laboratory conditions at the environmental simulation facility established at Forschungszentrum Jülich (FZJ). A temperature and pressure controlled vacuum chamber enables to investigate the performance of different types of airborne ozone, humidity, temperature and pressure sensors

under realistic atmospheric conditions with accurate reference instruments [*Smit et al,* 2000]. In Annex-A-2 investigations specifically addressing the in-flight precision of the ECC/RS80-sonde obtained from two sets of three twin soundings in the field are reported. Annex-3 describes the results of investigations about the performance of the humidity Humicap-A sensor at low temperatures. Results of experiments at zero and saturated humidities made in the environmental simulation chamber are presented. In addition, the results of a field intercomparison of the Humicap-A sensor with an accurate balloon borne frost point hygrometer are reported.

In this section a summary of these investigations about the performance of the ECC/5A-ozone sondes and RS80-radiosondes in terms of precision and accuracy of the different sensors is presented. For the ECC-ozone sensor the major results are listed in Table 3.9. For the ECC-ozone sensor it is seen that the precisions estimated from the different approaches (theory, field and laboratory) agree rather well in the troposphere. In the stratosphere, however, the theoretical approach rather overestimates the uncertainty compared with the twin-soundings and the simulation experiments. This is probably due to an overestimate of the uncertainty of the pump flow efficiency at lower pressures (See Section 3.3.3). From evaluating the results listed in Table 3.9, a synthesis is listed in Table 3.10.

	Precision Theoretical [*Section 3-3*]		Precision In-Flight [*Annex A-2*]	Precision Simulation Exp. [*Annex A-1*]		Accuracy Simulation Exp. [*Annex A-1*]	
Altitude	Mid-Latitude	Tropics	Mid-Latitude	Mid-Latitude	Tropics	Mid-Latitude	Tropics
20-25 km	±0.6 mPa ±4%	±0.7 mPa ±5%	±0.4 mPa ±3%	±0.3 mPa ±2%	±0.4 mPa ±3%	±0.5 mPa ±3%	±0.6 mPa ±5%
TP-20 km	±0.3 mPa ±4%	±0.3 mPa ±6%	±0.3 mPa ±4%	±0.15 mPa ±2%	±0.2 mPa ±4%	±0.3 mPa ±4%	±0.5 mPa ±9%
10 km-TP	±0.15 mPa ±5%	±0.04 mPa ±7%	±0.15 mPa ±5%	±0.09 mPa ±3%	±0.04 mPa ±7%	±0.18 mPa ±6%	±0.1 mPa ±19%
5-10 km	±0.13 mPa ±4%	±0.04 mPa ±4%	±0.15 mPa ±4%	±0.10 mPa ±3%	±0.03 mPa ±3%	±0.25 mPa ±7%	±0.1 mPa ±10%
0-5 km	±0.11 mPa ±4%	±0.06 mPa ±4%	±0.1 mPa ±3%	±0.08 mPa ±3%	±0.07 mPa ±5%	±0.10 mPa ±4%	±0.14 mPa ±10%

Table 3.9: *Overview of the results about the precision and accuracy of the ECC/5A-ozone sensor obtained from different experimental approaches, theory, laboratory and field that are reported in section 3.3, Annex-A-1 and Annex-A-2. TP = Tropopause.*

Table 3.11 summarizes the major results obtained from validation studies on the performance of the pressure (P) and temperature (T) sensors of the RS80-radiosonde. In general, the precision of the P-and T-sensor of the RS80-radiosonde determined from twin soundings are in good agreement with the precision obtained from the simulation experiments. The performance of the P-and T-sensor is rather good for vertical profiling up to at least 25 km altitude. Based on the accuracy of the P-, and T-sensor the accuracy of the determination of

altitude is about ± 75 m at 0-5 km, ± 100 m at 5-10 km, ± 150m at 10-15 km, ± 200 m at 15-20 km, ± 250 m at 20-25 km [*Lenhard,* 1970, *Rieker,* 1976].

| | ECC-Ozone Sensor | | | |
| | Precision | | Accuracy | |
Altitude	Mid-Latitude	Tropics	Mid-Latitude	Tropics
20-25 km	±0.4 mPa ±(2-3)%	±0.5 mPa ±(3-4)%	±0.6 mPa ±(3-4)%	±0.7 mPa ±(5-6)%
TP-20 km	±0.25 mPa ±(2-4)%	±0.25 mPa ±(4-5)%	±0.4 mPa ±(4-5)%	±0.6 mPa ±(8-10)%
10 km-TP	±0.12 mPa ±(3-5)%	±0.04 mPa ±(6-8)%	±0.22 mPa ±(5-7)%	±0.1 mPa ±19%
5-10 km	±0.12 mPa ±(3-4)%	±0.03 mPa ±(3-4)%	±0.30 mPa ±(6-8)%	±0.1 mPa ±10%
0-5 km	±0.1 mPa ±(3-4)%	±0.07 mPa ±(4-5)%	±0.12 mPa ±(4-5)%	±0.14 mPa ±10%

Table 3.10: *Summary of the assessment of the results of the experimental studies addressing precision and accuracy of the ECC/5A-ozone sensor listed in Table 3.2. TP=Tropopause.*

| | Pressure (Barocap-sensor RS80-Radiosonde) | | | Temperature (Thermocap-Sensor RS80-Radiosonde) | | |
| | Sounding Simulation Experiments *[Annex-A-1]* | | Twin-Soundings *[Annex-A-2]* | Sounding Simulation Experiments *[Annex-A-1]* | | Twin-Soundings *[Annex-A-2]* |
Altitude	Precision	Accuracy	Precision	Precision	Accuracy	Precision
20-25 km	±0.4 hPa ±(0.8-1.3)%	±0.9 hPa ±(2-3)%	±0.3 hPa ±(0.6-1)%	---	---	±0.5 K ±0.25%
TP-20 km	±0.5 hPa ±(0.5-1)%	±0.8 hPa ±(0.8-1.6)%	±0.3 hPa ±(0.3-0.6)%	---	---	±0.3 K ±0.1%
10 km-TP	±0.6 hPa ±(0.3-0.5)%	±1.1 hPa ±(0.7-1.3)%	±0.5 hPa ±(0.3-0.5)%	±0.4 K ±0.15%	±1.4 K ±0.5%	±0.2 K ±0.07%
5-10 km	±0.5 hPa ±(0.07-0.2)%	±2.5 hPa ±(0.4-1.1)%	±0.7 hPa ±(0.1-0.3)%	±0.3 K ±0.1%	±0.8 K ±0.3%	±0.2 K ±0.08%
0-5 km	±0.4 hPa ± < 0.1%	±2.4 hPa ±(0.2-0.4)%	±0.6 hPa ± < 0.1%	±0.2 K ±0.1%	±0.5 K ±0.2%	±0.2 K ±0.07%

Table 3.11: *Overview of the results about the precision and accuracy of pressure and temperature sensor of the RS80-radiosonde obtained from laboratory and field experiments which are reported in detail in Annex-A-1 and Annex-A-2 respectively. TP = Tropopause.*

Table 3.12 shows an overview of the precision and accuracy of the Humicap A humidity sensor of the RS80 radiosonde obtained from the twin soundings (see Annex A-2) and the field/laboratory investigations (see Annex-A-3). The results are in good agreement which each other. After the use of the correctional scheme for the dry bias at low temperatures it can be stated that tropospheric relative humidity measurements made with the Humicap-A sensor have a relative uncertainty of ±1% (Z=0-5 km), ±20% (Z=5-10 km) and ±30% (Z=10 km up to the tropopause) relative humidity (with respect to ice at T<273K). In general, the performance of the Humicap-A sensor is not reliable above the tropopause and Humicap-A measurements made in the stratospheric region are thus excluded from further investigations (see Annex-A-3, Section A-3.3).

	Simulation Experiments *[Annex-A-3]*		Twin-Sounding *[Annex-A-2]*	Comparison with Frost Point Hygrometer *[Annex-A-3]*	After Use of Correction Scheme *[Annex-A-3]*
Altitude	Precision Rel.Hum. [%]	Bias as Frost Point Temp. [K]	Precision Rel.Hum. [%]	Bias as Frost Point Temp. [K]	Accuracy as Frost Point Temp. [K]
10 km-TP	±(1-2)%	-(1-5) K	±(1-2)%	-(0.5-6) K	±3 K
5-10 km	±(1-2)%	-(0-1) K	±(1-2)%	-(0-0.5) K	±2 K
0-5 km	±1%	0 K	±(1-2)%	0 K	±1 K

Table 3.12: *Overview of the results on precision and accuracy of the Humicap-A sensor of the RS80-radiosonde obtained from laboratory and field experiments, which are reported in Annex-A-2 and Annex-A-3 respectively. TP = Tropopause.*

Chapter 4

Ozone and Humidity Distribution Observed over the Central Atlantic Ocean during ANT-V/5 & ANT-VII/1

4.1 Introduction

Vertical ozone soundings were performed over the Central Atlantic between 36°S and 52°N during two scientific cruises aboard the research vessel "Polarstern" operated by the Alfred Wegener Institute, Bremerhaven, Germany. The first cruise, ANT-V/5, tracked from Puerto Madryn, Argentina (43°S, 65°W) to Bremerhaven, Germany (54°N, 8°E) between 19. March and 18. April 1987. The second cruise, ANT-VII/1, was from Bremerhaven to Rio Grande do Sul, Brazil (32°S, 52°W) between 14. September and 9. October 1988. The tracks of both cruises are shown in Figure 4.1. Between 30°S and 50°N both cruises track the same route, mainly along the 30°W meridian in 30°S and 30°N.
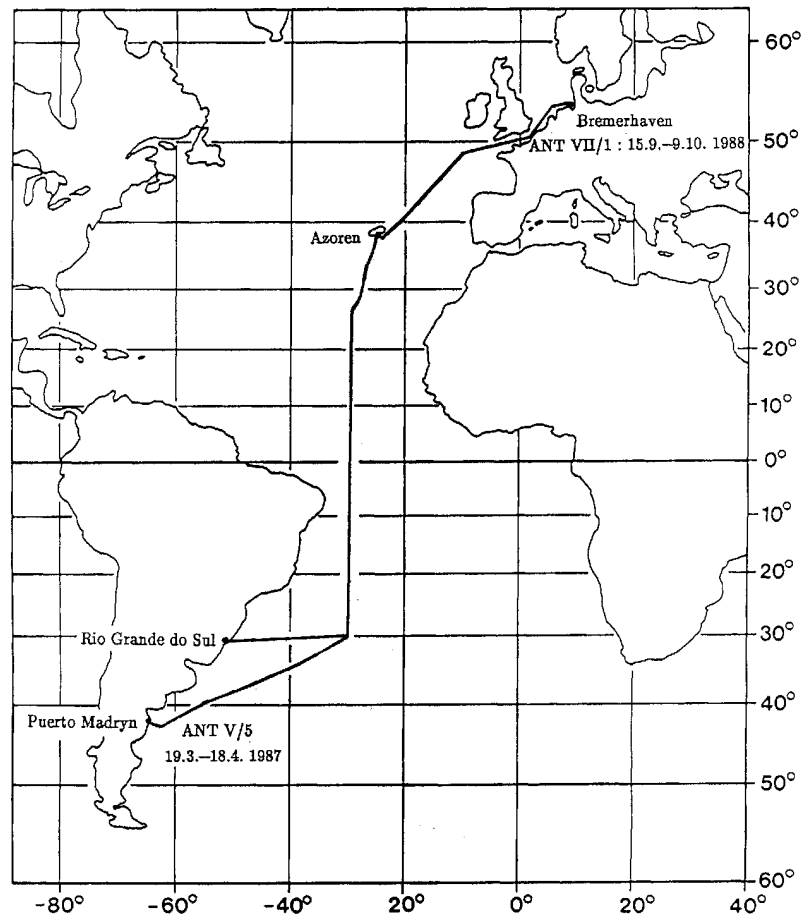

Figure 4.1 : *Cruise tracks of the RV "Polarstern": First cruise ANT-V/5 from Puerto Madryn (Argentina) to Bremerhaven (Germany) between 19. March and 19. April 1987. Second cruise: ANT-VII/1 from Bremerhaven to Rio Grande do Sul, Brazil between 14. September and 9. October 1988.*

During the second cruise the ozone sounding program was part of an atmospheric research program for monitoring a comprehensive set of trace gas concentrations and meteorological parameters involved in tropospheric chemistry. An overview of the general features, the atmospheric measurements made, the techniques employed and the characterization of the origin of air masses encountered from synoptic data have been reported by *Platt et al.* [1992].

During both cruises comprehensive sets of meteorological parameters (air and water temperature, pressure, relative humidity, wind velocity, wind direction, etc.) were monitored near the surface using standard instrumentation and were recorded by INDAS. Synoptic surface observations (every 4 hour) were made by the weather service aboard the ship. During both cruises meteorological rawinsondes using the Omega Navaid wind finding (WS80-15N, Vaisala Ltd., Finland) for measuring the vertical profiles of pressure, temperature, relative humidity, wind velocity and wind direction with a latitudinal resolution of 1-2 degrees were flown by the weather service. The actual weather synoptics encountered during both cruises are described in detail *by Behr et al.* [1990] for the ANT-V/5-cruise and by *Behr et al.* [1989] for the ANT-VII/1-cruise respectively.

A total of 25 simultaneous ozone/humidity soundings were performed during the 1987-cruise (ANT-V/5) between 36°S and 47°N with a latitudinal spacing of 2 to 4 degrees. During the 1988-cruise (ANT-VII/1) 40 sondes were flown between 30°S and 52°N with a latitudinal resolution of about 1.5 to 2.5 degrees. The dates, launch times and geographical locations of the individual ozone/humidity soundings are listed in Table 4.1.

All individual vertical profiles of ozone and the simultaneously measured meteorological parameters such as pressure, temperature and relative humidity have been published as a technical report [*Smit et al.*, 1991]. For each cruise two typical examples of vertical profiles of ozone, temperature and relative humidity measured in the SH and NH are displayed in Figure 4.2. For cruise ANT-V/5 the ozone profile obtained in the SH at 9°30' S, 30 °W (Flight No.9: Diagram-A) show very low ozone mixing ratio of 10 ppbv near the surface and a relatively steep gradient throughout the troposphere. This in contrast to the profile obtained in the NH at $33^{o}30'$ N, $27^{o}12'$W (Flight No.23: Diagram-B) which is characterized by fairly high ozone values of 50-60 ppbv and relative weak vertical gradients. The examples of cruise ANT-VII/1, both taken in the sub-tropics (SH: Flight No.83: Diagram-C and NH: Flight No.62: Diagram-D) show in the SH yet much larger ozone values than during the cruise ANT-V/5 and are comparable to the values obtained in the NH. Both profiles show surface ozone values of about 30 ppbv with a sharp increase (vertical gradient) to about 50 pbbv just above the PBL and fairly uniform values of 50-70 ppbv in the middle/upper troposphere. From the simultaneously measured humidity profiles it seen that in the free troposphere the variations of ozone and humidity are mainly negatively correlated. In this report relative humidities are with respect to liquid water for temperatures above 273 K and with respect to ice below 273 K.

In the context of this thesis, it is the intention to present and to discuss the large scale features of the ozone and water vapor distribution over the Central Atlantic observed during the two cruises. To present the large scale latitudinal distribution of tropospheric ozone and water vapor, the following procedure of data reduction was employed:

1. The individual vertical profiles of the measured parameters: ozone, pressure, temperature and relative humidity, were made vertically equidistant with a vertical spacing of 250 m by calculating the weighted mean over the different height intervals.

2. For each measured parameter the resulting equidistant vertical profiles, obtained at different latitudes, were concatenated to a data set representing their latitudinal/vertical distribution sampled during the two cruises.

Cruise ANT-V/5 in March/April 1987				
Flight No.	Date	Time (UTC)	Latitude	Longitude
1	23-3-1987	18:00	-36:00	-45:00
2	24-3-1987	17:45	-34:15	-40:18
3	25-3-1987	17:25	-32:30	-35:42
4	26-3-1987	17:45	-30:30	-31:18
5	27-3-1987	17:30	-27:12	-30:00
6	28-3-1987	17:23	-22:48	-30:00
7	29-3-1987	14:50	-18:30	-30:00
8	30-3-1987	14:00	-13:54	-30:00
9	31-3-1987	15:15	-09:30	-30:00
10	01-4-1987	16:10	-05:06	-30:00
11	02-4-1987	16:00	00:06	-30:00
12	03-4-1987	14:30	04:18	-30:00
13	03-4-1987	23:10	05:06	-30:00
14	05-4-1987	17:35	13:30	-30:00
16	06-4-1987	15:35	18:18	-30:00
17	07-4-1987	01:00	19:24	-30:00
18	07-4-1987	15:28	22:48	-30:00
19	08-4-1987	15:35	27:18	-30:00
20	08-4-1987	15:35	27:18	-30:00
21	09-4-1987	14:15	29:54	-28:30
22	10-4-1987	15:10	33:30	-27:12
23	10-4-1987	15:10	33:30	-27:12
24	12-4-1987	20:30	40:54'	-21:12'
25	13-4-1987	09:40	42:54'	-18:54'
26	13-4-1987	13:25	43:30'	-18:12'
27	13-4-1987	17:35	44:18'	-17:12'
28	13-4-1987	20:47	44:36'	-16:48'
29	14-4-1987	14:20	47:00'	-13:42'
30	14-4-1987	14:20	47:00'	-13:42'

Table 4.1: *Date, launch time (UTC) and geographical location of the individual ozone/humidity- soundings made from aboard the RV-"Polarstern" during the cruises ANT-V/5 (March/April 1987) and ANT-VII/1 (September/October 1988).*
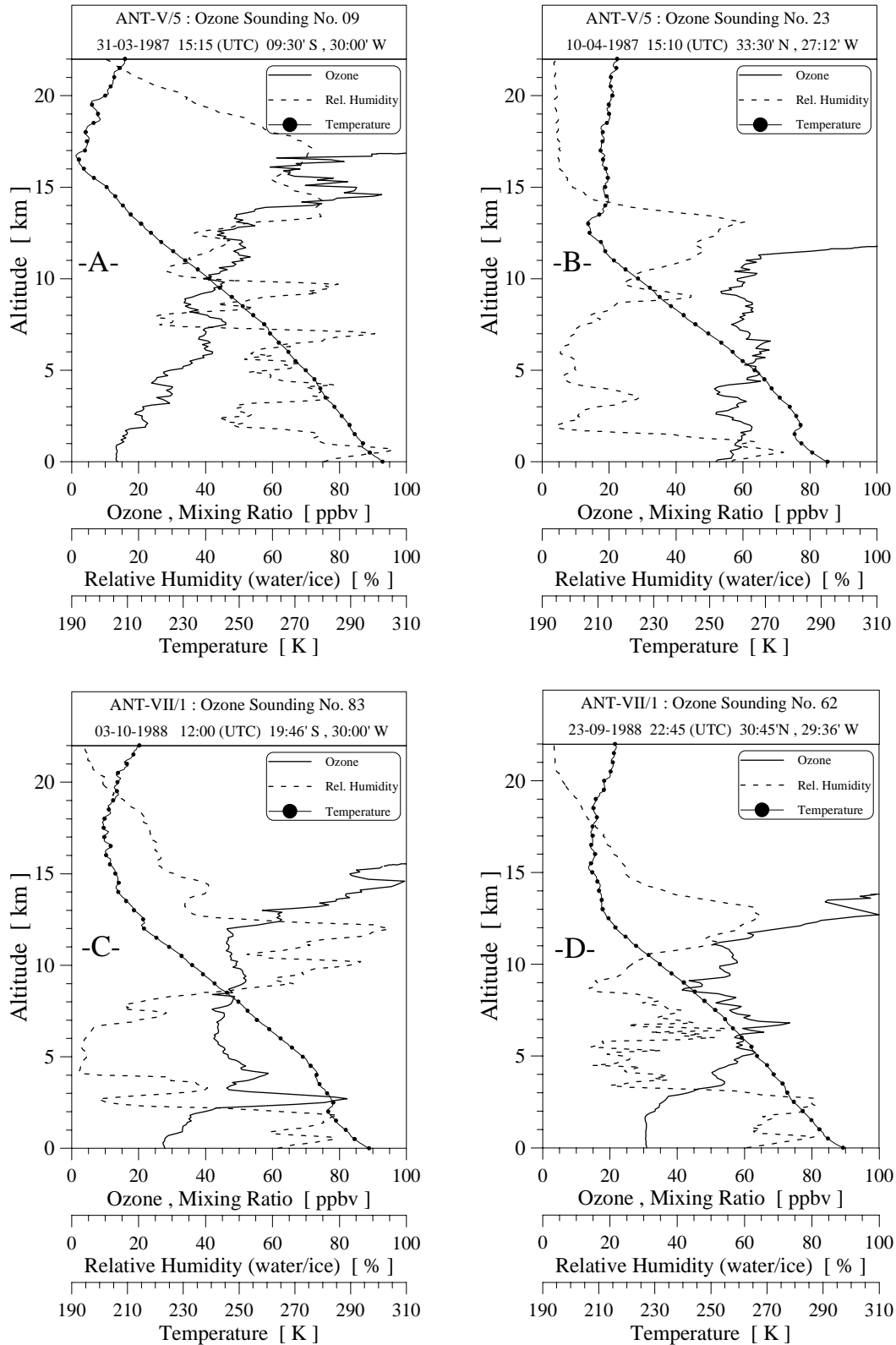
Cruise ANT-VII/1 in Sep/Oct 1988				
Flight No.	Date	Time (UTC)	Latitude	Longitude
50	16-9-1988	19:40	52:24	03:24
51	17-9-1988	14:55	50:06	-02:12
52	18-9-1988	10:05	47:27	-07:36
53	18-9-1988	22:00	45:48	-10:30
54	19-9-1988	10:00	44:06	-13:33
55	19-9-1988	21:45	42:24	-16:18
56	20-9-1988	22:00	40:54	-18:51
57	21-9-1988	10:25	39:30	-21:24
58	21-9-1988	21:45	38:18	-23:48
59	22-9-1988	14:20	37:07	-26:00
60	23-9-1988	11:45	32:54	-28:24
61	23-9-1988	16:11	31:48	-29:00
62	23-9-1988	22:45	30:45	-29:36
63	24-9-1988	12:15	28:15	-30:00
64	24-9-1988	21:15	26:03	-30:00
65	25-9-1988	12:10	22:37	-30:00
66	26-9-1988	02:00	19:27	-30:00
67	26-9-1988	11:30	17:13	-30:00
68	26-9-1988	21:30	15:00	-30:00
69	27-9-1988	11:50	11:51	-30:00
70	27-9-1988	18:35	10:18	-30:00
71	28-9-1988	01:15	08:48	-30:00
72	28-9-1988	10:40	06:33	-30:00
73	28-9-1988	16:30	05:12	-30:00
74	28-9-1988	22:30	04:01	-30:00
75	29-9-1988	11:50	01:12	-30:00
76	29-9-1988	22:40	-01:01	-30:00
77	30-9-1988	11:45	-03:51	-30:00
78	30-9-1988	23:00	-06:18	-30:00
79	1-10-1988	11:45	-09:06	-30:00
80	1-10-1988	19:15	-10:45	-30:00
81	2-10-1988	15:00	-15:03	-30:00
82	2-10-1988	22:30	-16:42	-30:00
83	3-10-1988	12:00	-19:46	-30:00
84	3-10-1988	22:30	-22:06	-30:00
85	4-10-1988	12:25	-25:18	-30:00
86	4-10-1988	22:15	-27:33	-30:00
87	5-10-1988	11:45	-30:04	-30:36
88	5-10-1988	23:00	-30:24	-33:36
89	6-10-1988	12:30	-30:48	-36:30

Figure 4.2: *Vertical profiles of ozone (solid line), temperature (dotted line) and relative humidity (dashed line) obtained from ozone/humidity-soundings made during ANT-V/5 [Diagram-A : 9º30'S, 30ºW at 29-3-1987 (FLH-No. 9); Diagram-B: 33º30'N, 27º12'W at 10-4-1987 (FLH-No.23)] and ANT-VII/1 [Diagram-C: 19º46'S, 30ºW at 3-10-1988 (FLH-No.83; Diagram-D: 30º45'N, 29º 36'W at 23-9-1988 (FLH-No.62)].*

4.2 Latitudinal Variations of Ozone and Water Vapor in the PBL

Figure 4.3 shows the latitudinal variations of the surface pressure continuously recorded with 10 minutes time resolution during ANT-V/5 and ANT-VII/1 cruises. In the equatorial trough region the surface pressure decreases towards the equator and has minimum values of about 1012 hPa in the inter tropical convergence zone (ITCZ) which is located between 4^oN and 10^oN [*Behr et al,* 1989 and *Behr et al*., 1990]. The pressure decrease towards the ITCZ is more pronounced in the NH than in the SH.
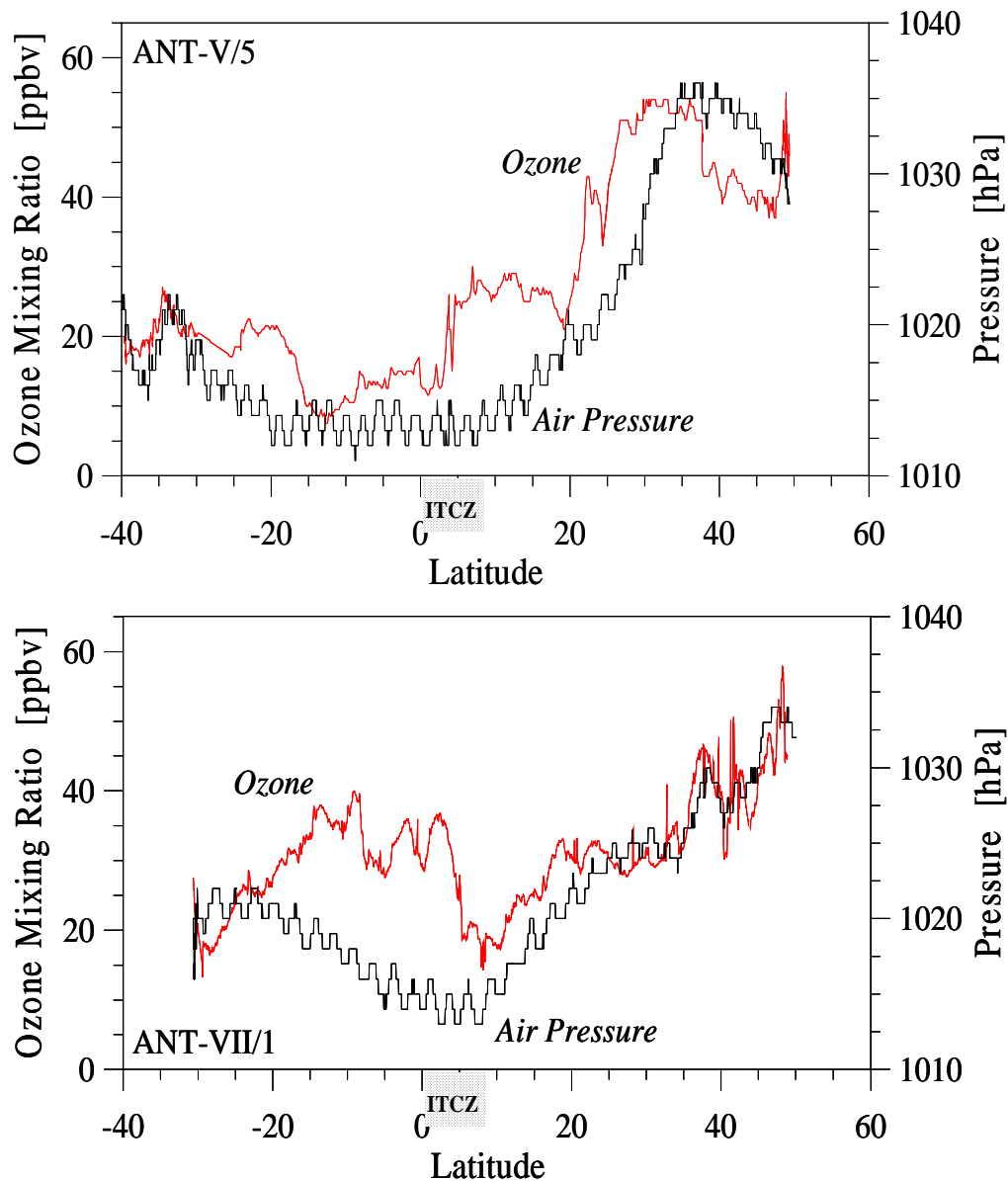

Figure 4.3: *Latitudinal variations of surface pressure (black line) recorded by INDAS and surface mixing ratio of ozone (red line) monitored with UV photometer (1008 AH type, Dasibi Inc., for details see section 3.3.1.4) during ANT-V/5 cruise (upper diagram) and ANT-VII/1 cruise (lower diagram). Location of the ITCZ between 4^oN and 10^oN from Behr et al, 1990 for ANT-V/5 cruise and Behr et al., 1989 for ANT-VII/1 cruise.*

The corresponding surface air temperature and relative humidity monitored by INDAS are shown in Figure 4.4. During both cruises the air temperature in NH and SH increases towards the ITCZ. During ANT-VII/1 cruise, maximum values were observed at the north of the ITCZ at 10°N, while during ANT-V/5 cruise the highest temperatures were measured in the SH between 0°S and 20°S. The relative humidity fluctuated between 60% and 80% with enhanced spikes close to saturation that corresponded with rain events [*Behr et al,* 1989 and *Behr et al.*, 1990].
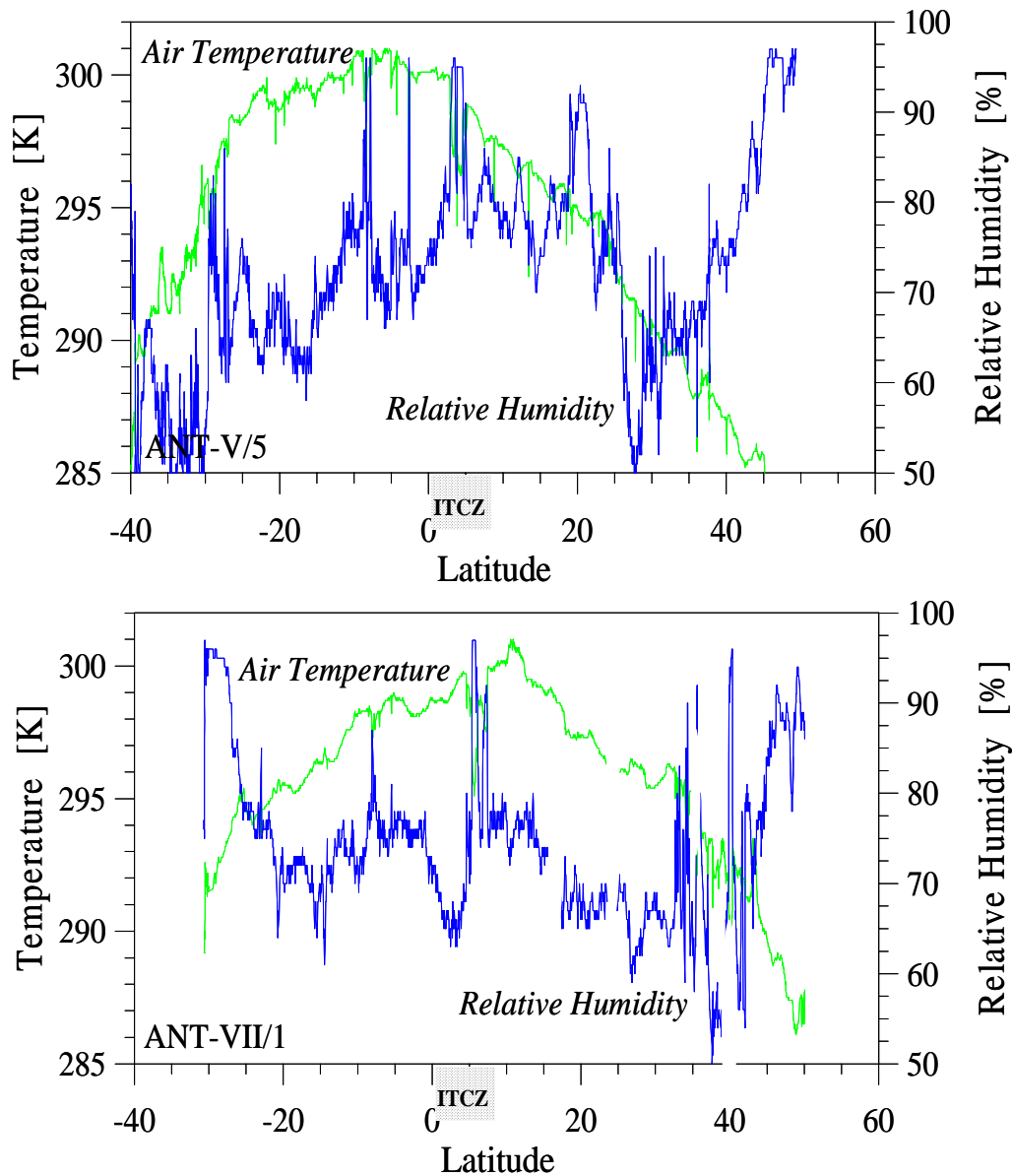

Figure 4.4: *Latitudinal variations of surface temperature (green line) and relative humidity (blue line) as recorded by INDAS during ANT-V/5 cruise (upper diagram) and ANT-VII/1 cruise (lower diagram).*

Figure 4.5 displays the latitudinal variations of the planetary boundary layer (PBL)-height for both cruises. The PBL-height was determined from the vertical slope of potential temperature using the individual sounding profiles. In the extra-tropics, the PBL-height varied between 1

and 2 km while inside the Inter Tropical Convergence Zone (ITCZ) a distinct PBL was not identifiable due to strong convective processes and associated rapid vertical mixing.

For these cases the PBL-height has been assumed to be virtually 2.5 km. The location of the ITCZ was determined from synoptic observations by the weather service aboard the ship (ANT-V/5: *Behr et al.,* 1990 and ANT-VII/1: *Behr et al.,* 1989).
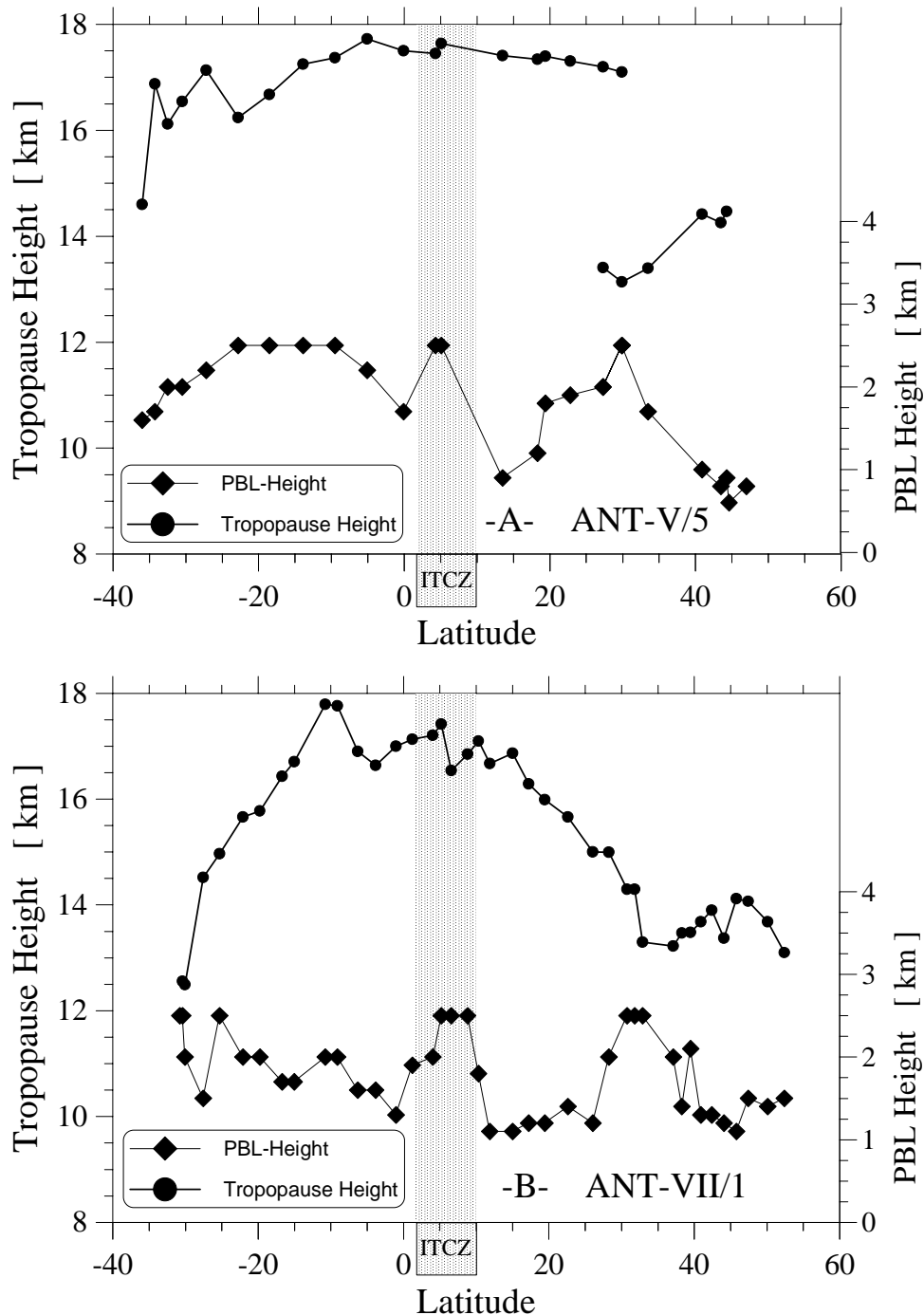

Figure 4.5: *Latitudinal variations of the heights of the planetary boundary layer (◆ + solid line) and tropopause (● + solid line) derived from the vertical ozone/humidity-soundings (see text) made during the cruises ANT-V/5 (Diagram A) and ANT-VII/1 (Diagram B). Symbols mark individual soundings*

Latitudinal variations of height averaged mixing ratios of ozone and water vapor for the PBL are presented in Figure 4.6. Comparing the latitudinal variations of surface ozone obtained from ozone sondes and INDAS displayed in the Figure 4.6 and 4.4, respectively, it is concluded that the large scale variations observed with the ozone sondes clearly maps the large scale variations recorded with the UV-photometer at the compass deck of the ship (for details see Section 3.3.1.4)
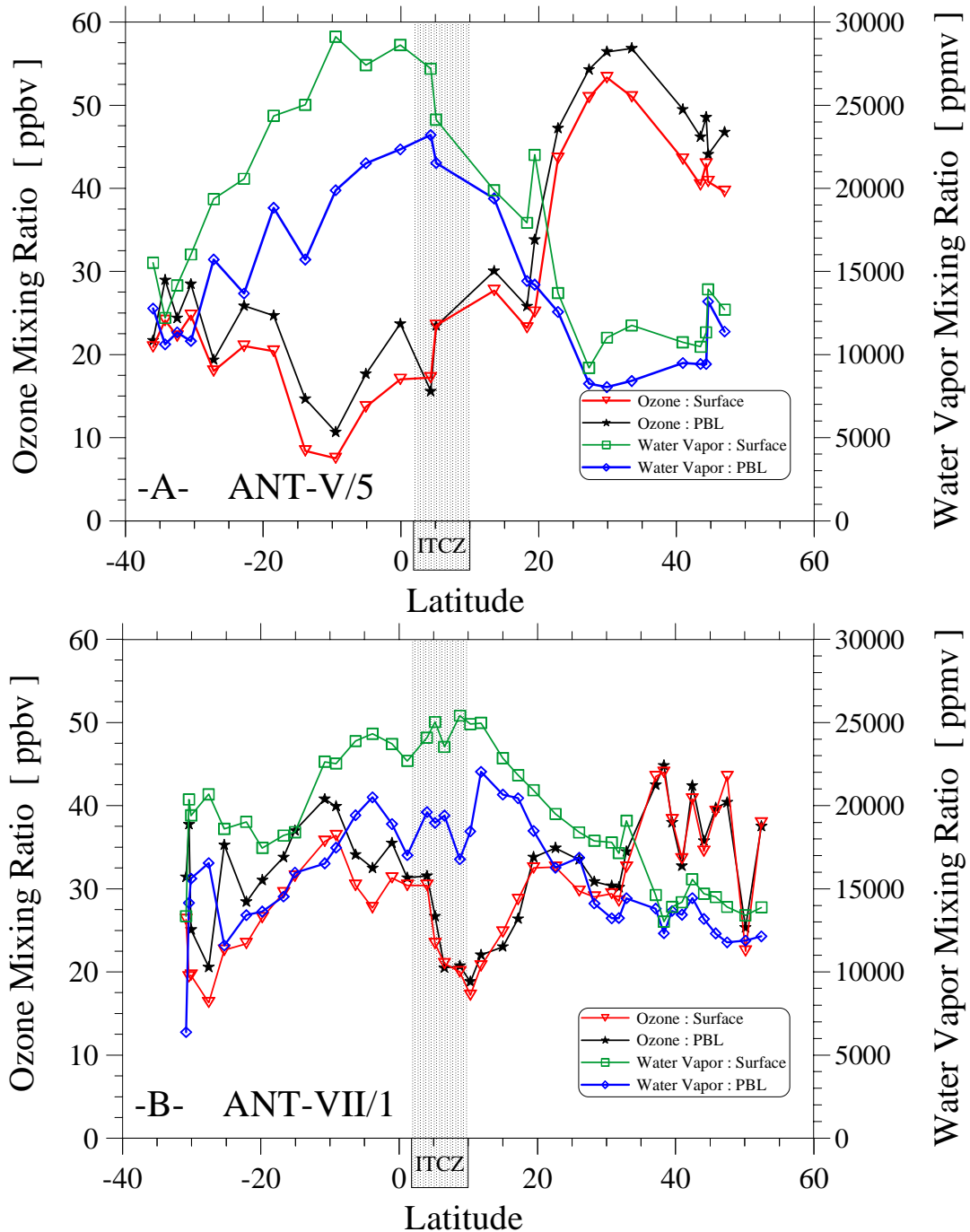

Figure 4.6: Latitudinal variations of mixing ratios of ozone and water vapor near the surface (O3 =∇-symbols and dashed line and H2O = symbols and dotted/dashed line) and averaged over the planetary boundary layer (O3 = ∗ symbols and solid line and H2O = ◊ symbols and dashed line) derived from vertical ozone/humidity-soundings made during the cruises ANT-V/5 (Diagram-A) and ANT-VII/1 (Diagram-B). Symbols mark individual soundings.

The general features of the latitudinal ozone variations within the PBL and the concurrently measured water vapor variations are summarized as follows:

- Surface ozone and PBL-averages of ozone mixing ratios are virtually identical.

- Extremely low mixing ratios of ozone were observed in the tropics during both cruises. In 1987, a minimum of about 10 ppbv was centered near 10^oS. In 1988, the minimum was 20 ppbv, centered at 10^oN. The ozone minima were accompanied by maximum water vapor mixing ratios of 30000 ppmv and 25000 ppmv, respectively.

- A strong north-south ozone gradient, spanning a range of more than 45 ppbv, was apparent during the 1987-cruise. The largest mixing ratios were found near 30^oN. From there on ozone decreased with latitude down to a value of 10 ppbv at 10^oS.

- During the 1988 cruise, the northern and southern hemisphere ozone mixing ratios were similar with values around 30-40 ppbv in the extra-tropics separated by a 20 degree wide ozone minimum. This minimum was co-located with the ITCZ.

- Towards the equator water vapor shows a latitudinal increase from extra-tropical values of 10000-15000 ppmv to tropical values of 25000-30000 ppmv.

- Relative humidity is varying between 60 and 80 % in tropics as well as in extra-tropics and is not correlated with ozone

- Latitudinal variations of ozone within the PBL are negatively correlated with the accompanying variations of the water vapor mixing ratio

4.3 Latitudinal Variations of Tropospheric Columns of Ozone and Water Vapor

The features observed within the PBL are similar to the ones seen for the entire troposphere. This is displayed in Figure 4.7 showing the latitudinal variations of the abundance of tropospheric ozone (in DU[6]) and water vapor (in kg/m^2) in a vertical column between the surface and the tropopause. The tropospheric columns are obtained from individual vertical profiles as the integrating sum over the height interval between the surface and the tropopause. Tropopause heights (See Figure 4.5) were determined from the vertical temperature profiles following the guide lines of the WMO [7]. Unfortunately, for the ANT-V/5 cruise between 3^oN and 15^oN, no tropospheric ozone column data could be derived due to missing ozone data above 8 km altitude (See Section 4.2).

For both cruises the shape of the large-scale latitudinal distribution of the total tropospheric columns of ozone and water vapor are similar to the distributions that were observed within the PBL. The most striking features of the latitudinal distribution of the tropospheric columns of ozone and in conjunction with water vapor are:

- During cruise ANT-V/5 in the NH, outside of the ITCZ, the tropospheric ozone content with column values of 45-50 DU is almost a factor two larger than the 25-30 DU observed in the SH. The opposite is seen for the water vapor content which is larger in the SH than

---

[6] The column ozone abundances are expressed in Dobson units; 1 DU= 2.69×10^{16} molecules O_3 cm^{-2}.

[7]Tropopause height according to the guidelines of the World Meteorological Organization (WMO), is defined as the lowest height above which the temperature decrease is smaller than 2 K/km over a height interval of at least 1 km.

the NH. This is in contrast to the cruise ANT-VII/1 where in the NH as well as in the SH, exterior the ITCZ, the columns of tropospheric ozone had comparable values between 30 and 40 DU. The water vapor contents in both hemispheres were of equal magnitude varying between 25 and 35 kg/m2.

- In the ITCZ very pronounced maxima of water vapor columns with values of 50-55 kg/m^2 were seen, in coexistence with extremely low ozone contents of 20-25 DU (ANT-VII/1-cruise). A similar feature was seen at 9°S during cruise ANT-V/5.

- During the ANT-V/5 cruise at 30°N a very high tropospheric ozone column density of 56 DU was observed.
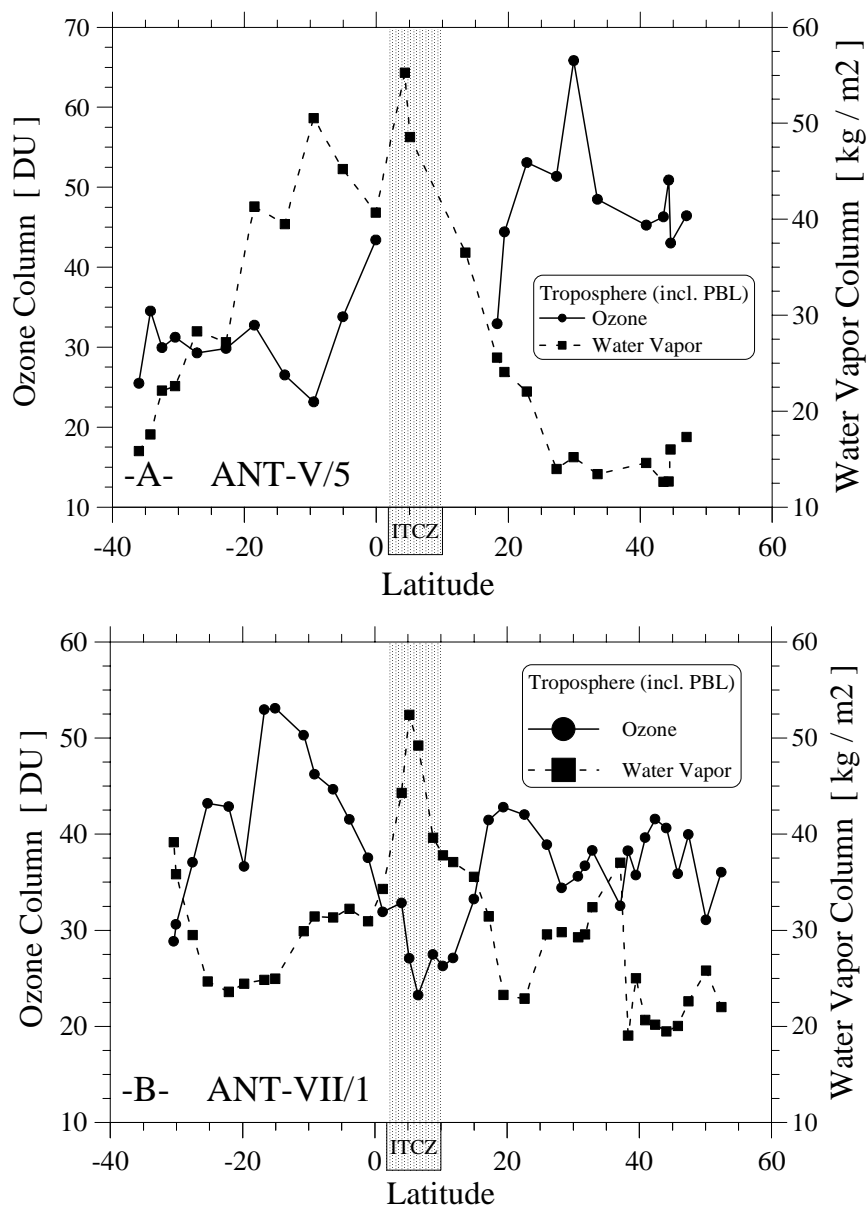

Figure 4.7: *Latitudinal variations of tropospheric columns of ozone (• symbol and solid line) and water vapor (■ symbol and dashed line) derived from ozone/humidity-soundings made during ANT-V/5 (Diagram-A) and ANT-VII/1 (Diagram-B). Symbols mark individual measurements. Note: Tropospheric columns include PBL.*

The latitudinal variations of ozone and water vapor content in the PBL as well as over the entire troposphere were negatively correlated. This fact reveals itself from a display of the latitudinal distribution of the free tropospheric (i.e. region between top of PBL and tropopause) contents of ozone and water vapor as shown in Figure 4.8.
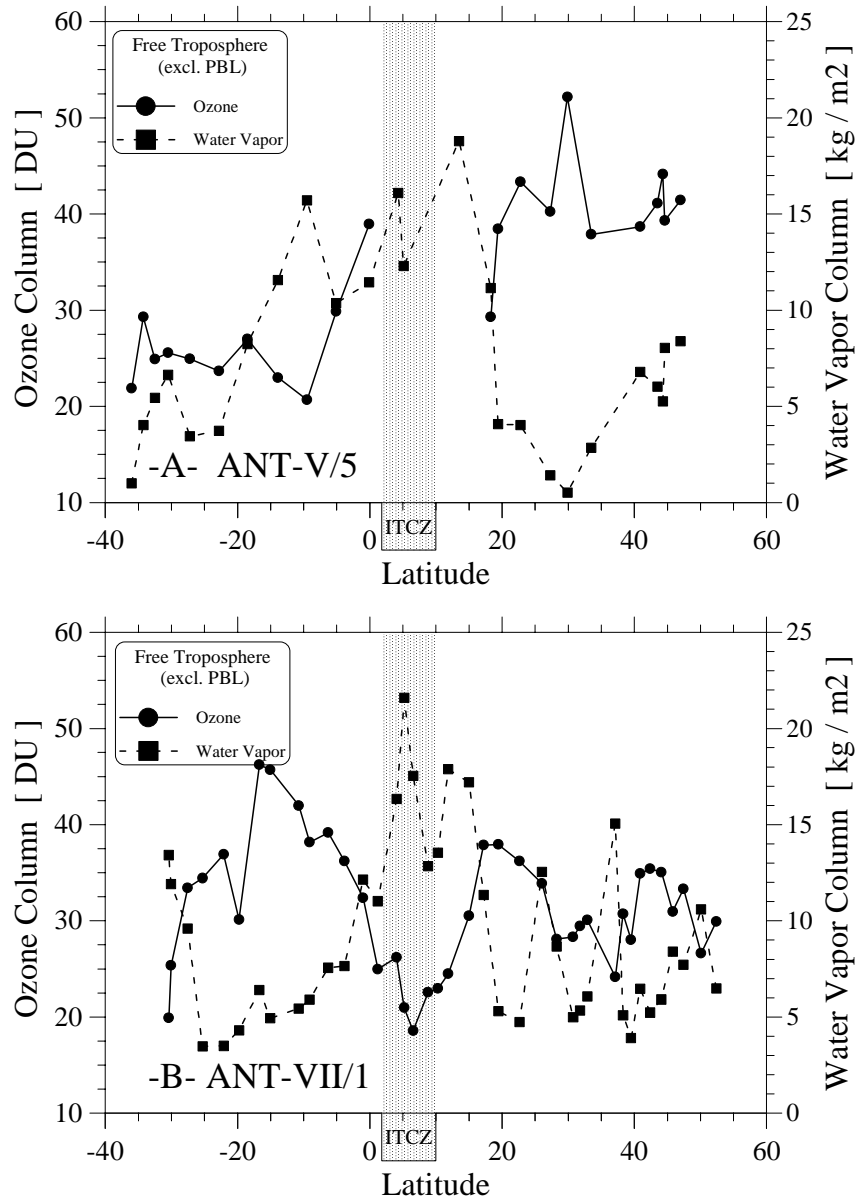

Figure 4.8: *Latitudinal variations of columns of free-tropospheric ozone (● symbol and solid line) and water vapor (■ symbol and dashed line) derived from ozone/humidity-soundings made during ANT-V/5 (Diagram-A) and ANT-VII/1 (Diagram-B). Symbols mark individual measurements. Note: Free tropospheric columns exclude PBL.*

4.4 Cross Sections of Latitude/Altitude Distributions of Ozone and Water Vapor

Detailed pictures of the latidude-height cross sections of ozone and water vapor mixing ratios plus relative humidity in the meridional plane between the surface and 20 km altitude are shown as contour plots in Figures 4.9, 4.10 and 4.11. The cross sections are based on a large number of independent measurements (4000: ANT-V/5, 1987 and 6000: ANT-VII/1, 1988), which are fairly uniformly spaced in altitude and latitude (for data reduction see section 4.1).

In the latitudinal direction the resolution is about 3-4 degree for the 1987-cruise and about 2 degree for the 1988-cruise while the height resolution is around 100 m. This is much better than the width of the observed features

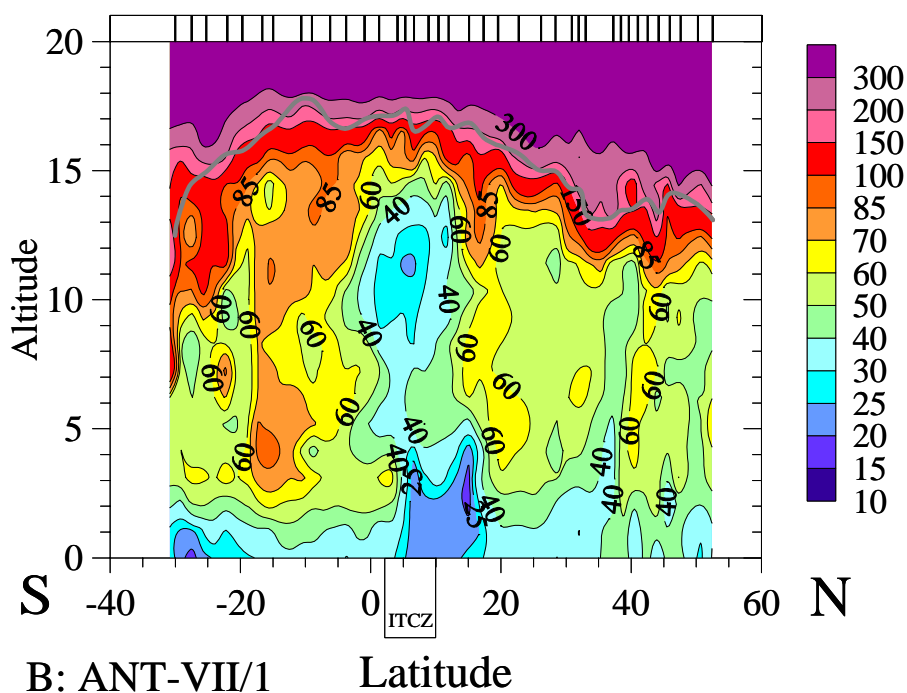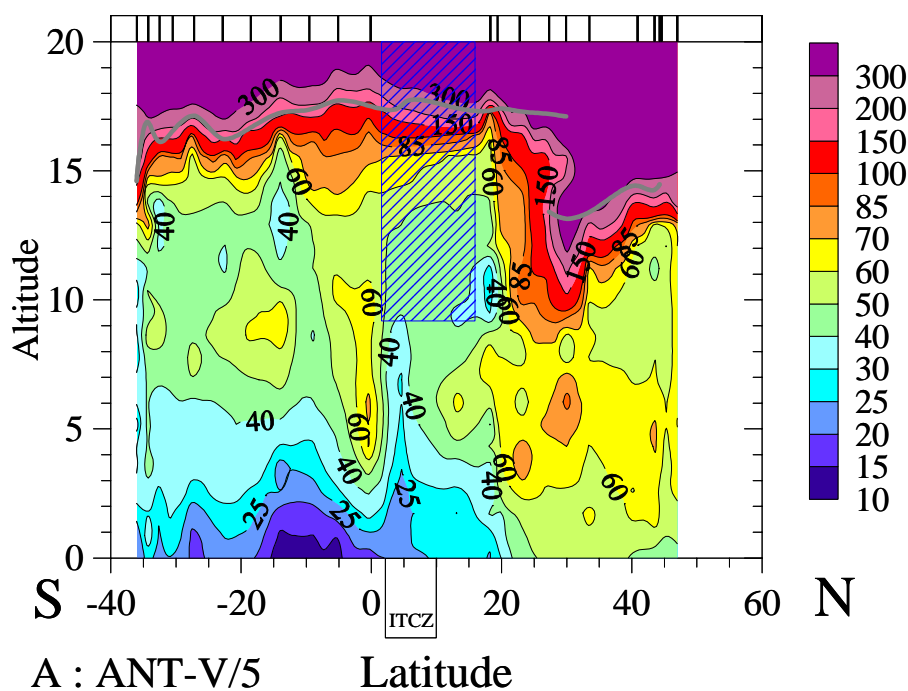**Figure 4.9:** *Cross section of the latitude/altitude distribution of ozone mixing ratio (in ppbv) over the Central Atlantic Ocean derived from ozone/humidity-soundings made during ANT-V/5 (Diagram A) and ANT-VII/1 (Diagram B) mainly along the 30ºW meridian. Short bars along the top of the diagram indicate latitudes of vertical soundings. The thick black/grey line indicates location of the tropopause*

Figure 4.10: *Cross section of the latitude/altitude distribution of water vapor mixing ratio (in ppmv) over the Central Atlantic Ocean derived from ozone/humidity-soundings made during ANT-V/5 (Diagram A) and ANT-VII/1 (Diagram B) mainly along the $30^{o}W$ meridian. Short bars along the top of the diagram indicate latitudes of vertical soundings. The thick black/grey line indicates location of the tropopause.*
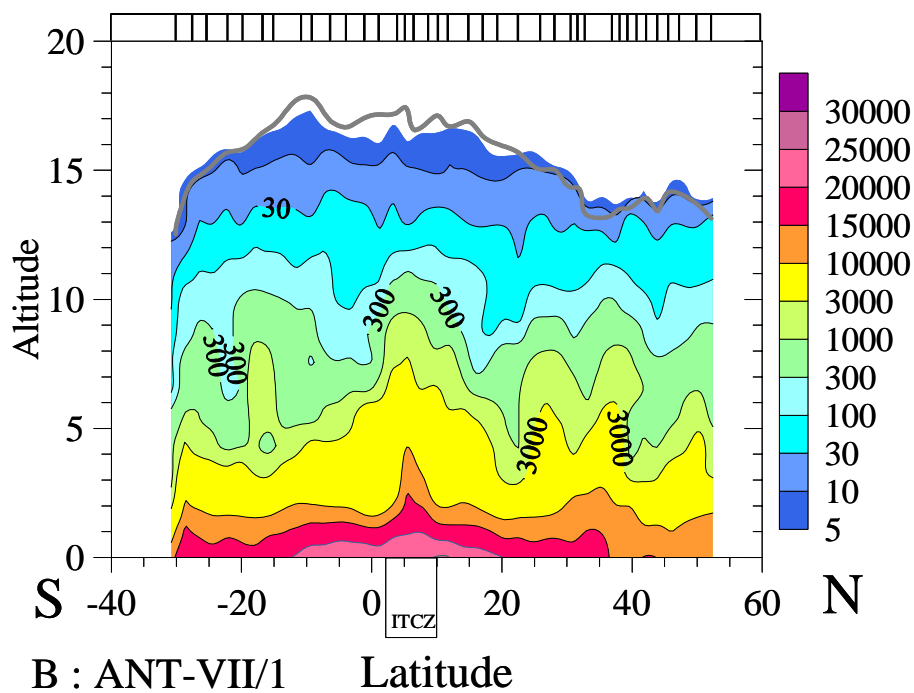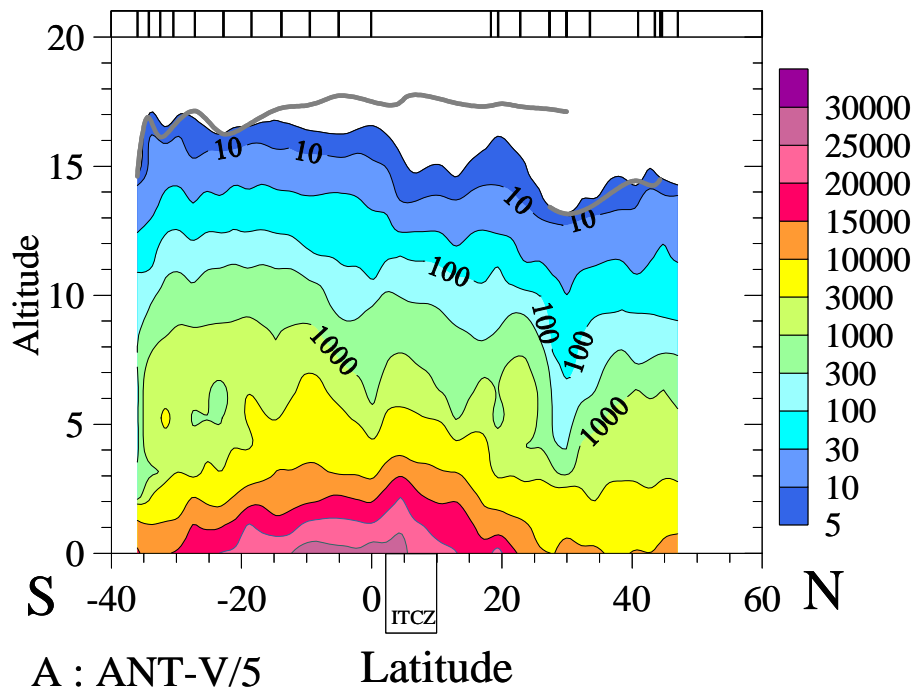
Prominent features observed from cross sections of ozone (Figure 4.9: Diagram A) and water vapor (Figure 4.10: Diagram A) of cruise ANT-V/5 are:

- Exterior to the ITCZ the observed mixing ratios of ozone were lower in the SH than in the NH.

- In the SH the vertical gradients of ozone were much stronger, throughout the entire troposphere compared to the NH, where the vertical gradients were very weak.

- In the SH at 10^oS above a surface minimum of 9 ppbv, low mixing ratios of ozone were found throughout the entire troposphere. Accompanying water vapor mixing ratio show enhanced values.

- In the region of the ITCZ, the low mixing ratios of ozone observed in the PBL, extend to the free troposphere up to an altitude of at least 10 km (no data were obtained above). Similar to the feature at 9^oS, enhanced water vapor mixing ratios were found over the ITCZ region.

- At the equator, just exterior the ITCZ, relatively high values of ozone in the lower/middle troposphere were observed at flight No.10.

- At around 30^oN a double tropopause at 12.5 and 16.5 km altitude, respectively, was found. High ozone values of stratospheric origin, as represented by their isolines, together with low water vapor contour lines penetrate deeply into the troposphere, down to 10 km. Air masses beneath the top of PBL and Tropopause are characterized by high ozone (50-80 ppbv) and relatively low water vapor mixing ratios.

For the ANT-VII/1 cruise the characteristic features of cross sections of ozone (Figure 4.9: Diagram-B) and water vapor (Figure 4.10, Diagram B) are:

- Ozone variations outside of the ITCZ in the SH were slightly larger compared to those of the NH.

- Exterior to the ITCZ a strong vertical gradient in the lower troposphere with ozone increasing from about 30 ppbv within the PBL up to values of 60-70 ppbv at 5 km altitude is apparent. The gradient is very pronounced in the SH between 15^oS and 20^oS. Between 5 and 10 km altitude only a weak gradient is seen, while in the upper troposphere above the tropopause the gradient is stronger, likely due to the influence of stratospheric ozone.

- In the tropical region of the ITCZ a well defined cellular structure of low ozone values of 20-40 ppbv extending throughout the entire troposphere is found. The contour of the cell is marked by the horizontal contraction of isolines of 40, 50 and 60 ppbv respectively. Just outside the cell the ozone values are about a factor 1.5 to 2 larger than the values encountered within the cell. Water vapor shows the opposite behavior: high mixing ratios of water vapor within the cell and relatively low mixing ratio contouring the regions outside of the cell.

The most pronounced feature of the large scale variations of the meridional distributions of ozone, obtained during both cruises, is the negatively correlated relation with the corresponding variations of the water vapor distribution: relatively high mixing ratios of ozone go in hand with relatively low mixing ratios of water vapor and vice versa. This feature is observed in the PBL as well as in the free troposphere.

Cross sections of latitude/altitude distributions of relative humidity are displayed in Figure 4.11. Compared with the co-existing ozone distributions shown in Figure 4.9 it is evident that, in the free troposphere, low ozone is related to relative humidities close to saturation and high ozone levels with low relative humidities. However, one exception is identified for the ANT-VII/1 cruise: high ozone values in the upper troposphere in the SH between the equator and 30^oS coexisted with relatively wet air masses, close to saturation.
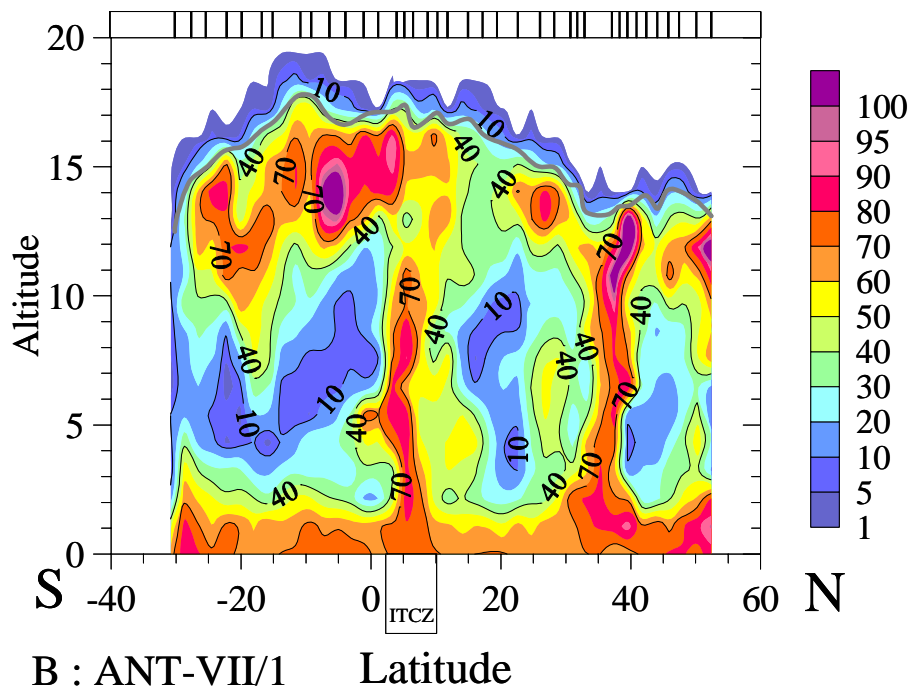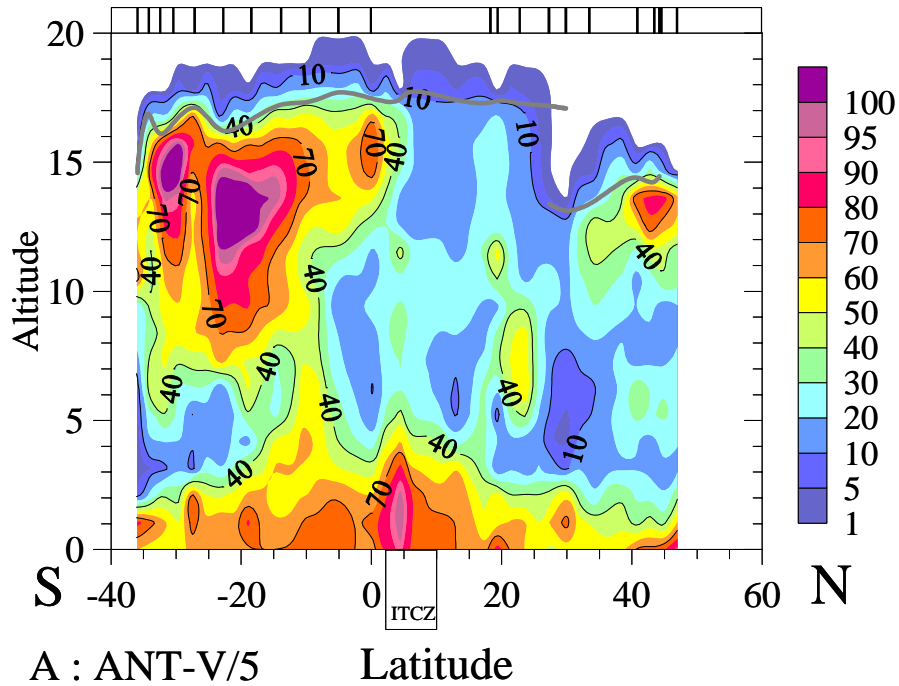
Figure 4.11: *Cross section of the latitude/altitude distribution of relative humidity (in %) over the Central Atlantic Ocean derived from ozone/humidity-soundings made ANT-V/5 (Diagram A) and ANT-VII/1 (Diagram B) mainly along the $30^{o}W$ meridian. Short bars along the top of the diagram indicate latitudes of ozone/humidity soundings. The fat grey line indicates location of the tropopause. Relative humidities are with respect to liquid water for temperatures above 273 K and with respect to ice below 273 K.*

Chapter 5

Tropospheric Ozone over the Central Atlantic Ocean

5.1   Low Tropospheric Ozone in the MBL and Free Troposphere

5.1.1   Comparison with Other Measurements

One of the prominent large-scale features seen in the meridional distributions of ozone, obtained during the cruises ANT-V/5 and ANT-VII/1, is the latitudinal decrease of ozone in the tropical region towards the ITCZ with minimum values in the vicinity of the equator (see Figure 4.9). This feature extends from the surface throughout the whole troposphere. The vertical ozone profiles observed in the inter tropical convergence (ITCZ) region mainly exhibit low mixing ratios in the marine boundary layer (MBL), enhanced values in the middle troposphere, decreasing values towards the upper troposphere and a subsequent increase towards the tropopause and above [*Smit et al.,* 1991].

Few investigators have reported vertical ozone distributions of the free troposphere over tropical oceans where low ozone values in the free troposphere and latitudinal decrease towards lower latitudes were observed over the MBL as well as in the free troposphere [*Kley et al.,* 1996, *Weller et al.,* 1996, *Thompson et al.*, 2000]. Particularly intriguing were the extremely low ozone mixing ratios observed in the MBL and upper troposphere with values below 10 ppbv as obtained from ozone soundings made in the equatorial Pacific in March 1993 [Kley et al., 1996]. Since 1998, the SHADOZ (=Southern Hemisphere Additional Ozone Sondes) network of ozone sounding stations, mainly located in the tropics, provides a climatology of the vertical distribution of ozone in the tropical belt through regular balloon soundings [*Thompson et al.* 2003]. The SHADOZ-stations located in the Atlantic region show low values throughout the entire troposphere in the March/April period and enhanced ozone values in the free troposphere in the September/October period thus mapping the typical features of the observations made during the ANT-V/5 and ANT-VII/1 cruises, respectively.

Within the MBL, minimum values of 10 ppbv at 10ºS during March/April 1987 and 15 ppbv at 10ºN during September/October 1988 were observed (see Figure 4.3). Very low values observed within the tropical marine boundary layer (MBL) have been also reported over the Atlantic Ocean [*Stallard et al.*, 1975, *Winkler,* 1988, *Piotrowicz,* 1989, 1990], Indian Ocean [*Johnson et al.,* 1990, *Rhoads et al.*, 1997] and Pacific Ocean [*Routhier et al.,* 1980, *Liu et al.,* 1983, *Piotrowicz et al.,* 1986, 1991, *Thompson et al.,* 1993]. However, the only climatology of the latitudinal distribution of ozone in the MBL over the Atlantic Ocean was reported by Winkler [1988] from a series of surface measurements made on board of several research vessels between 83ºN and 76ºS spread over a period of 10 years (1977-1986). Figure 5.1 shows the Winkler climatology of surface ozone for March/April- and September/October and the corresponding ozone surface measurements during ANT-V/5 and ANT-VII/1 respectively. Although the values of ozone given by Winkler are mostly somewhat lower, the general features of the latitudinal variations for March/April are in good agreement with that shown in Figure 5.1. The Winkler climatology also shows very low values of O_3 in the SH with a tropical minimum of around 10 ppbv at 10ºS and a latitudinal gradient towards this minimum in the SH and NH. However, Winkler did not find the sharp increase of ozone, observed during ANT-V/5 in the NH between 20ºN and 30ºN. A comparison of the distribution reported by Winkler for the September/October-period shows the same general features for

the NH as we have observed, but differs for the SH, especially between the ITCZ and 20°S. In the NH, Winkler's data also show a strong latitudinal gradient between 20°N and the ITCZ, where O_3 reaches its minimum. However, southwards the ITCZ, Winkler's ozone climatology show almost no latitudinal gradient in contrast to the increase of ozone we measured between the ITCZ and 20°S from 18 ppbv up to 40 ppbv.
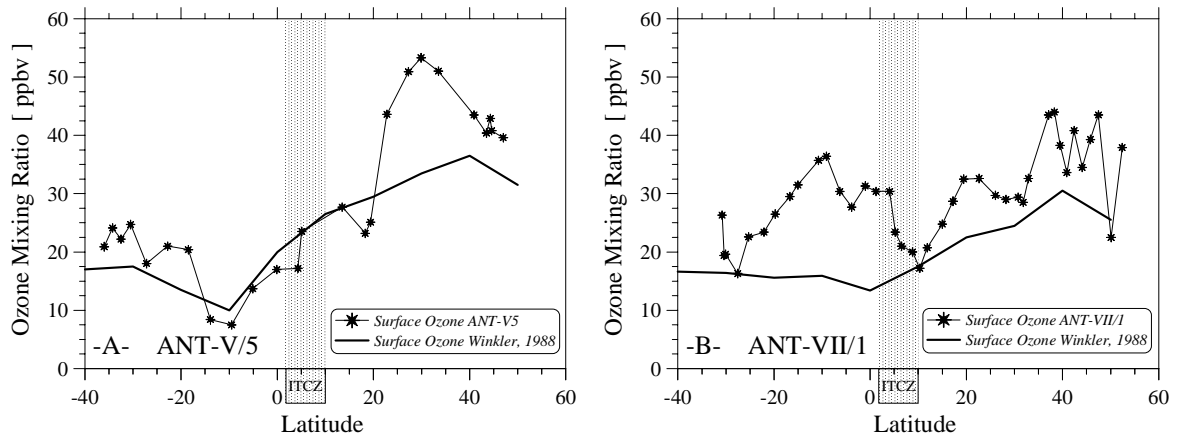

Figure 5.1: *Latitudinal distribution of ozone in the MBL over the Atlantic Ocean derived from a climatology reported by Winkler [1988] compared with surface ozone observed during ANT-V/5 (March/April 1987) and ANT-VII/1 (Sept./Oct. 1988)*

5.1.2 Cause for the ITCZ Ozone Minimum

Destruction of ozone due to dry deposition to the ocean surface is insufficient to explain the low concentrations of ozone observed within the MBL in the equatorial regions over the oceans [*Liu et al.,* (1983)]. Liu et al. suggested that, over the equatorial region over the Pacific Ocean, the existence of photochemical sinks has a much more significant influence on the distribution of tropospheric ozone in the region of the ITCZ than outwards of this region. In the tropics there is less total overhead ozone than elsewhere (see Figure 5.2) so more UV-B radiation penetrates and increases the UV-photolysis rate of ozone in the troposphere [R6].
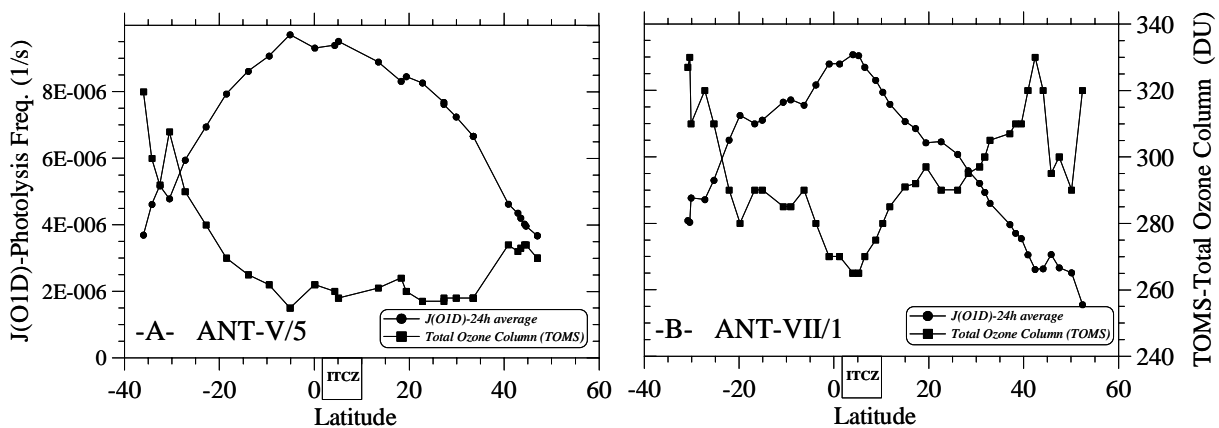

Figure 5.2: *Latitudinal variations of the total ozone column from TOMS (■ symbol) and J(O^1D)-24h average (● symbol) derived from empirical relation between solar angle and overhead ozone column reported by Hofzumahaus et al [1992]. Panel-A: ANT-V/5 and panel B: ANT-VII/1. Symbols mark individual ozone soundings.*

In conjunction with the high humidity in the tropics (see Figure 4.3) the photochemical losses of ozone [R6-R9, R23, and R24] are promoted. In studies by *Ridley et al.* [1992] and *Schultz et al,* [1999] it was shown that over the equatorial Pacific photochemical destruction of ozone dominates photochemical production [R11 and R15]. The photochemical ozone formation strongly depends on the mixing ratio of NO_x. In the remote tropical marine boundary layer (MBL) extremely low mixing ratios of NO of about 5-10 pptv are routinely observed near the surface [e.g. *McFarland et al,* 1979, *Ridley et al.*, 1987, *Harris et al.,* 1992, *Rohrer and Bruening.,* 1992, *Torres and Thompson,* 1993] such that ozone destruction significantly dominates over concurrent production (see Chapter 2, Section 2.2.5: Figure 2.12). For the case of the equatorial MBL over the Atlantic as encountered during the ANT-VII/1, cruise the strength of the different chemical sources and sinks of ozone are estimated as follows:

> Using a measured UV-photolysis rate constant of ozone of about $8x10^{-6}$ s^{-1} (24h average obtained from continuous measurements made during ANT-VII/1 by *Hofzumahaus et al.,* [1992]) and a mixing ratio of water vapor of about 25000 ppmv loss rates of ozone due to its UV-photolysis in the presence of water vapor [R6-R9], $L_{O3,J(O1D)} \approx 13$ % per day are obtained. In comparison, destruction of ozone in the MBL by dry deposition to the ocean surface yields only a relative loss rate, $L_{O3, Dep} < 3$ %/day at a deposition velocity of 0.05 cm/s [*Galbally et al.,* 1980, *Lenschow et al.,* 1982] and PBL-height of about 1500 m. Relative ozone losses from reaction with OH [R23] and HO_2 [R24] are estimated for typical conditions in the equatorial MBL to be about 4.5 % per day[8]. At a typical NO_x mixing ratio of 10 pptv, the photochemical formation of ozone is about 6% per day for $NO+HO_2$ [R11] and 3% per day for $NO+CH_3O_2$ [R15]. This finally results in a net relative ozone loss rate of about 11 % per day.

The above example clearly demonstrates that substantial net losses of ozone occur over the remote tropical MBL. Of those, the UV-photolysis of ozone in presence of water vapor governs the photochemical fate of ozone in this region. In how far these losses are limited to the MBL or also affect the ozone distribution in the free troposphere and in how far photochemical formation plays a counter part, causing the enhanced ozone values, is subject for a more detailed analysis as follows: At the onset, the question is posed whether the observed minimum feature of the ozone distribution in the MBL and free troposphere are caused by photochemistry, dynamics or by a combination of both? In questioning this, it is not the intention of this thesis to investigate the tropical ozone budget on a global or regional scale, but to stay constrained to the question of how well ozone can be used as a tracer to map the morphology of the tropical Hadley or Walker circulation patterns. In other words, how well can a chemical chemical analysis address the question whether ozone is a quantitative proxy for a description of vertical transport such as deep convection and subsidence? If the answer is yes it would follow that ozone could serve as a quasi-conservative tracer for the vertical water vapor transport and its meridional distribution in the free troposphere. The analysis proceeds in two steps:

1. Characterization of the photochemical changes of ozone as function of latitude and altitude. This necessitates an estimate of the actual strength of the individual photochemical sources and sinks of ozone.

---

[8] The following parameters were observed during the cruise: diurnal averages of O_3=20ppbv, H_2O_2=1.5 ppbv [*Jacob and Klockow.,* 1992], CH_3OOH=1.5 ppbv [estimated value], CH_2O=1.0ppbv [*Harris et al.,* 1992], CO= 100 ppbv and CH_4=1.7ppmv [*Koppmann et al.,* 1992], and NO_x=10pptv [*Harris et al.,* 1992, *Rohrer and Bruening,* 1992]. Using the photochemical box model, described in section 2.2.5, at equinox conditions diurnal averages [OH] $\approx$ 1.5xE6 mol/cm3 and [HO_2]$\approx$ 2.0xE8 mol/cm3 the relative losses of ozone through its reaction with OH and HO_2, $L_{O3,OH}$, and $L_{O3,HO2}$ are estimated as 1 % per day and 3.5 % per day, respectively

2. Comparison of the time scales of photochemical changes of ozone with the characteristic time scales of horizontal and vertical transport of the tropical Hadley-circulation.

5.2   Photochemical Fate of Ozone

5.2.1   Photochemical Box Model to Estimate the Sources and Sinks of Ozone

As shown in Section 2.2.5 the strength of the individual photochemical sources and sinks of ozone depends critically on the actual concentrations of NO_X while the key role of HO_X radicals are strongly linked to water vapor, CO, CH_4 but also species like CH_2O, H_2O_2, and CH_3OOH which act as latent buffers of odd hydrogen. Important aspects thereby is in how far in-situ a net production or destruction of ozone will occur and on what characteristic time scale these photochemical changes of ozone take place in the MBL as well as in the free troposphere? Therefore, the photochemical box model, described in section 2.2.5, is used to estimate the strength of the individual photochemical sources and sinks of ozone at different latitudes and altitudes for conditions that are typical for the two cruises.

In the model calculations for $[O_3]$, $[H_2O]$, pressure, and temperature the actual observations obtained from the ozone soundings are used, while $[CH_4]$=1.74 ppmv is fixed. For the MBL region surface measurements of NO_X [*Harris et al.* 1992, *Rohrer and Bruening*, 1992], CO [*Koppmann,* private communication], CH_2O [*Harris et al.,* 1992], H_2O_2 [*Jacob and Klockow,* 1992] have been used. Further, in the MBL $[CH_3OOH]$ has been assumed to be equal to H_2O_2 [*Slemr and Tremmel,* 1994]. Unfortunately, for the free troposphere no simultaneously measured data exist for the concentrations of NO_X, CO, CH_2O, H_2O_2, and CH_3OOH so that their concentrations had to be substituted from a sparse number of observations from other missions made over the Central Atlantic or Central Pacific. Figure 5.3 shows the latitude/altitude cross-sections of the mixing ratios of NO_X, CO, CH_2O, H_2O_2, and CH_3OOH, respectively used in the model simulations at different latitudes and altitudes.

As far as the NO_X-and CO-distributions for the free troposphere are concerned the vertical profiles of NO obtained during the Atlantic bounded aircraft missions of STRATOZ-III [*Drummond et al.* 1988, *Marenco et al.,* 1989)] and TROPOZ-II [*Rohrer et al.*, 1997] were used. The vertical profiles, mainly measured along the coastline of the African and American continent, do not represent typical marine conditions and therefore only vertical profiles with prevailing wind directions coming from the ocean have been considered. The above cited NO-measurements show in the free troposphere show an increase of the mixing ratio of NO with altitude in the tropical regions between 30 °S and 30 °N with values of 5-20 pptv in the lower troposphere (2-5 km), 10-40 pptv in the middle troposphere (5-10 km) and 30-70 pptv in the upper troposphere between 10 and 12 km were observed. The CH_2O-distribution from TROPOZ-II mission [*Arlander et al.*, 1995] is used. For the H_2O_2 and CH_3OOH distribution data measured from aircraft over the South Atlantic and Pacific [*O'Sullivan et al.,* 1999] are used. PAN-chemistry is omitted since its chemistry in the remote tropics it is assumed to be of minor importance [*Rudolph et al.,* 1987, *Müller and Rudolph,* 1992].

Diurnally varying latitude and altitude dependent photolysis rate constants for equinox-conditions (21 September) were taken from *Röth* [1992] whereby the actual overhead ozone column (see Figure 5.2) was obtained from the Total Ozone Mapping Spectrometer (TOMS) satellite observations [Nimbus-7 TOMS ozone database version 7, *McPeters and Beach,* 1996]. Good agreement between the calculated $J_{O(1D)}$ and J_{NO2} and corresponding surface observations [*Hofzumahaus et al.,* 1992, and *Brauers et al.,* 1992] for the ANT-VII/1 cruise was achieved. The photolysis rate constants are calculated for clean marine background air

with low aerosol load and almost cloudless sky. Although both cruises were made under almost equinox conditions, north of 20°S, the values of $J_{O(1D)}$ are about 10 to 15 percent larger for March/April 1987 than for September/October 1988. The lower overhead ozone column densities in March/April 1987 exclusively cause this[9]. Within the ITCZ, the values of $J_{O(1D)}$ are reduced due to cloudiness by about 30 percent, according the measurements of $J_{O(1D)}$ made during ANT- VII/1 cruise [*Hofzumahaus et al.,* 1992].
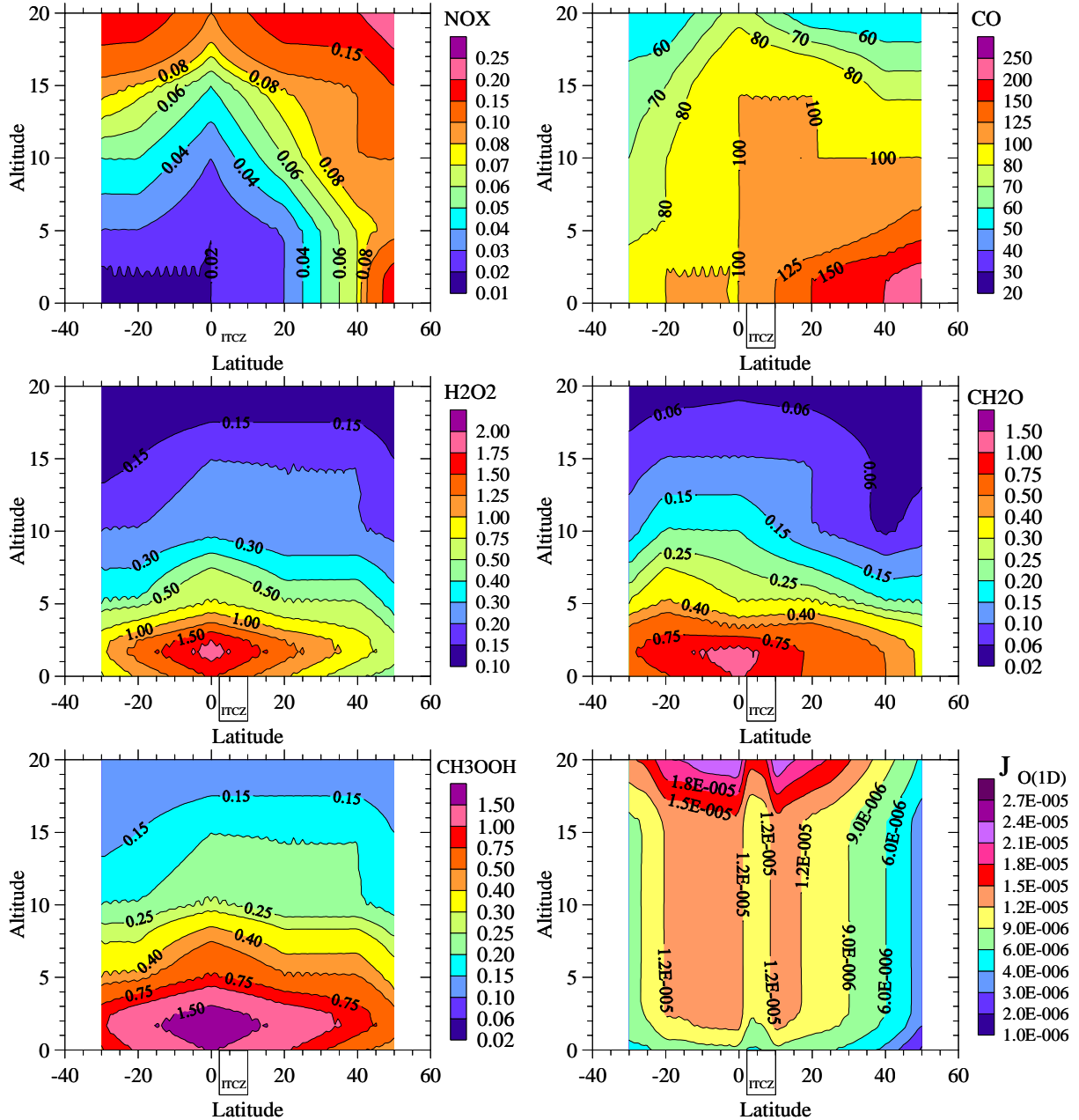
Figure 5.3: *Cross sections of the meridional/altitude distribution of the mixing ratio of NO$_X$, CO, H$_2$O$_2$, CH$_2$O, and CH$_3$OOH (all in ppbv) used as input data in the photochemical box model calculations (for details see text) Panel on the bottom right: Cross section of the meridional/altitude distribution of the calculated $J_{O(1D)}$ photolysis rates (in s^{-1}) as 24h-diurnal averages for the ANT-VII/1 condition (for details see text).*

---

[9] $J(O1D) = 1.74E\text{-}4 * Exp[-5.87*OC_{O3} *Sec(\zeta)]$ (s^{-1}) [Hofzumahaus, 1992], whereby ξ = solar zenith angle and OC_{O3} = overhead ozone column in DU (Dobson Unit)

5.2.2 Destruction of Ozone

5.2.2.1 Ozone Losses due to its UV-Photolysis

Figure 5.4 shows the latitude/altitude cross section of the diurnal (24h) average of the relative loss rate of ozone from photolysis ($L_{O3,J(O1D)}$) for March/April 1987 (left panel) and September/October 1988 (right panel) as determined according to equation 2.7 for the appropriate distributions of water vapor (Figure 4.7) and calculated $J_{O(1D)}$ (Figure 5.3).
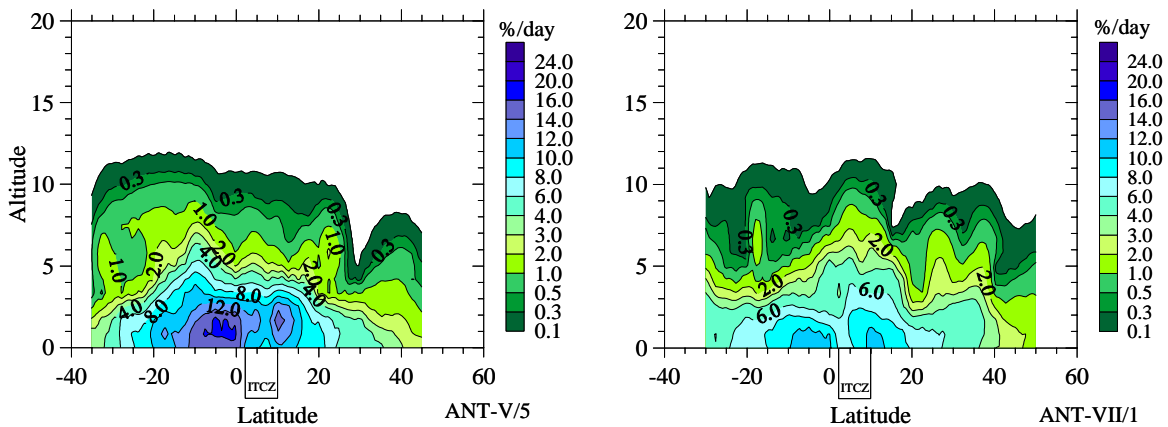

Figure 5.4: *Cross sections of the meridional/altitude distribution of the calculated diurnal average (24h) of the relative loss rate of ozone (in percent per day) by its photolysis in presence of water vapor ($L_{O3,J(O1D)}$) for March/April 1987 (left panel) and September/October 1988 (right panel), respectively (for details see text).*

Within the MBL the photochemical losses of O_3 due to UV-photolysis in the presence of water vapor dominates the O_3 loss from dry deposition in the region between 30°S and 30°N[10]. Just outwards of this region, there is a sharp decrease of photochemical O_3 losses due to a strong decrease of $J_{O(1D)}$ and the lower mixing ratios of water vapor towards higher latitudes. However, in the tropical region near the equator the photochemical losses strongly increase towards the meteorological equator to a maximum in the vicinity of the ITCZ, which yields a photochemical O_3 lifetime of less than one week. In this region significant losses are not limited to the MBL but extend to the free troposphere up to an altitude of about 6 km. This is mainly caused by the high water vapor content above the MBL from active cumulonimbus (Cb) convection. Despite maximum water vapor concentrations in the center of the ITCZ, the photochemical ozone losses at the outskirts of the ITCZ because of a reduced $J_{O(1D)}$ photolysis rate from the cumulonimbus clouds in this region.

In the free troposphere, particularly over the trade wind region, which are characterized by large-scale subsidence, the water vapor content decreases exponentially with altitude with a scale height of about 2-3 km in the free troposphere. Furthermore, just above the temperature inversion at an altitude of 1.5-2 km the mixing ratio of water vapor stepwise decreases by almost a factor 3 compared to that in the MBL. These facts result in a drastic decrease of the photochemical ozone losses of ozone.

---

[10] Loss by dry deposition to the ocean surface yields only a relative loss rate, $L_{O3, Dep} < 3$ %/day at a deposition velocity of 0.05 cm/s [*Galbally et al.,* 1980, *Lenschow et al.,* 1982] and PBL-height of about 1500m.

5.2.2.2 Ozone Losses by HO$_X$-Radicals

Figure 5.5 displays the latitude/altitude cross-sections of the diurnally averaged (24 hours) concentrations of OH and HO$_2$ for both cruises. From these OH and HO$_2$ distributions, together with the corresponding O$_3$-distributions, the latitude/altitude cross sections of the diurnal averages (24 hours) of the relative ozone loss rates by its reaction with OH and HO$_2$ were derived and are shown in Figure 5.6.
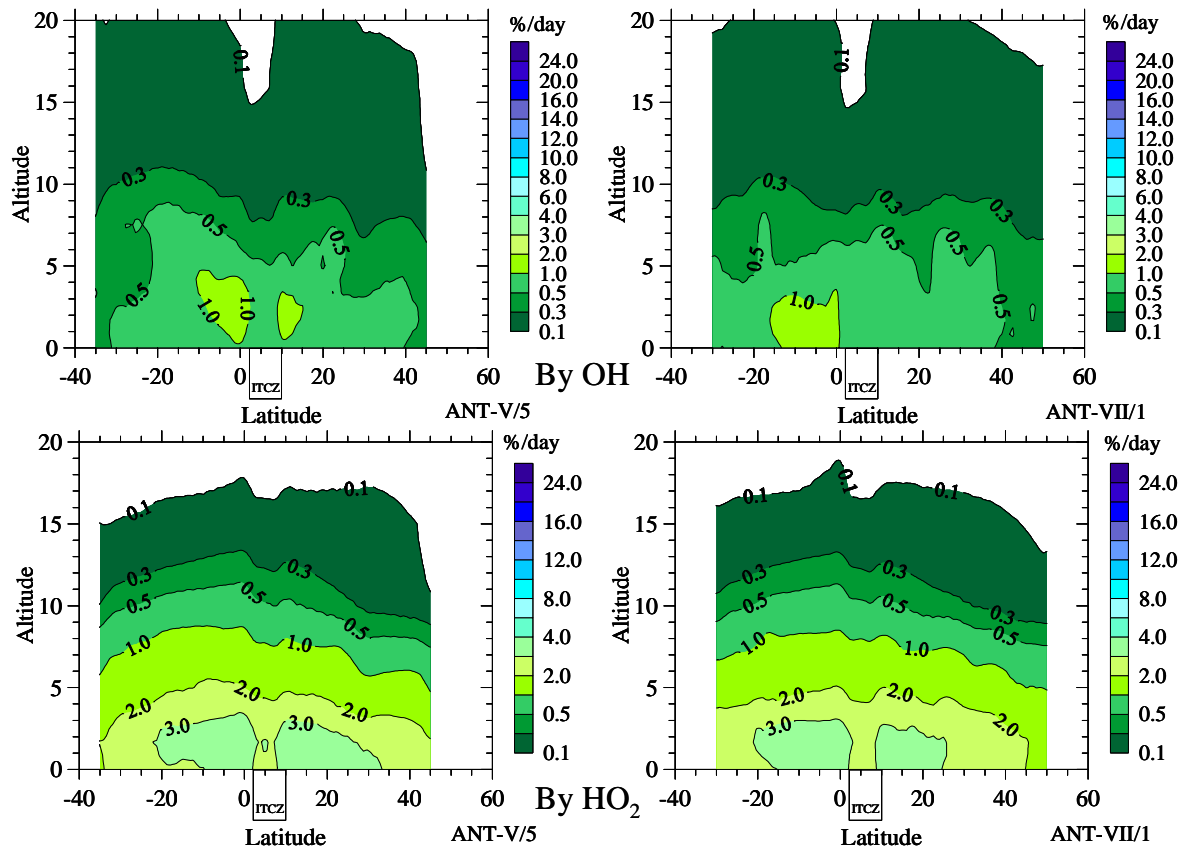

Figure 5.5: *Cross-sections of the meridional/altitude distribution of the calculated diurnal average (24h) of the OH- and HO$_2$-radical mixing ratio (in pptv) for March/April 1987 (upper panels) and September/October 1988 (lower panels), respectively (for details see text)*

The figure shows that the photochemical losses of ozone by HO$_2$ reaction are about a factor two larger in the MBL and lower troposphere than those from the loss by the OH reaction, while both are of equal magnitude in the middle and upper troposphere. Taking into account that the concentration of HO$_2$ and OH are both a function of L$_{O3,J(O1D)}$ it is clear that the slope of the contour lines of L$_{O3,\,OH}$ and L$_{O3,\,HO2}$, are similar to the corresponding contour plot of L$_{O3,J(O1D)}$.

In the tropical region the strong UV-photolysis of ozone in the presence of enhanced values of the mixing ratio of water vapor provides the major ozone sink in the lower troposphere. However, reactions of ozone with HO$_X$-radicals constitute also a significant contribution to the ozone loss in the lower troposphere with a relative influence that becomes stronger with increasing altitude and which finally provides the dominant ozone sink in the upper troposphere.
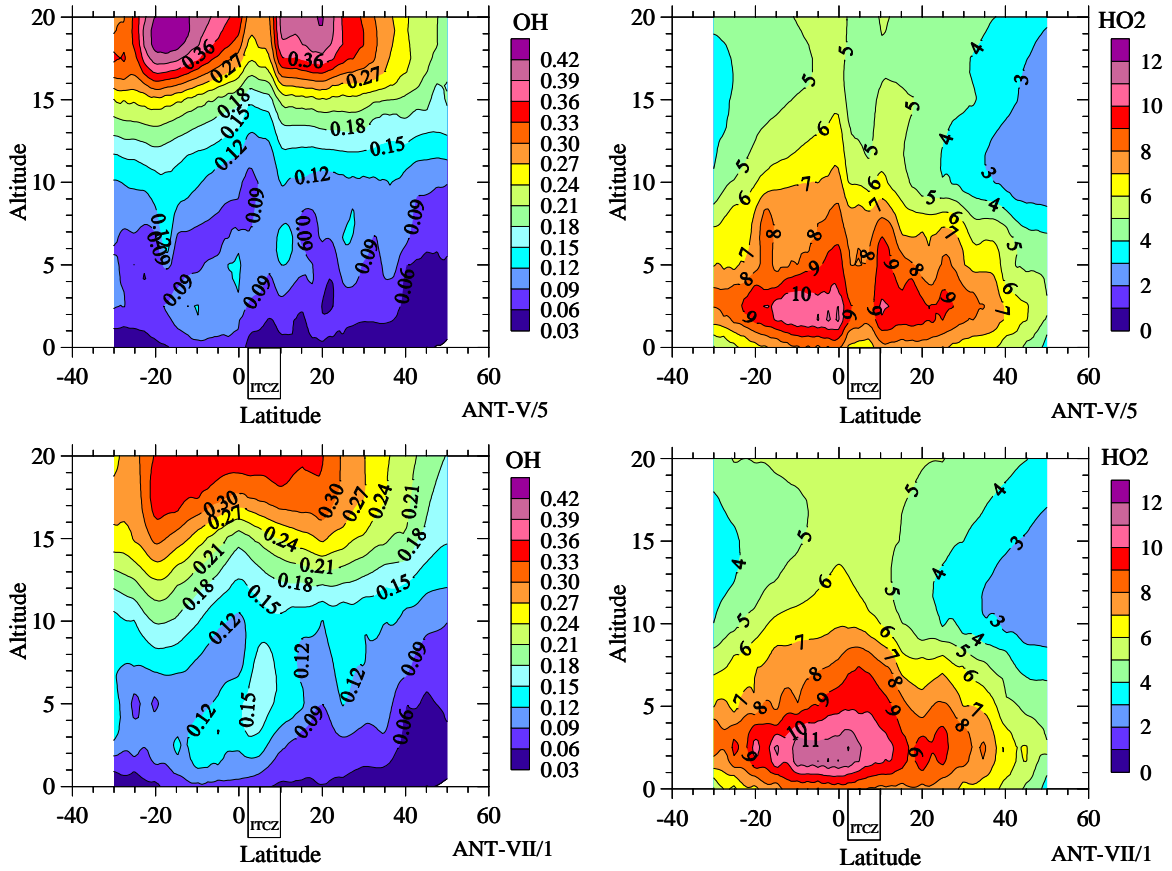
Figure 5.6: *Cross sections of the meridional/altitude distribution of the calculated diurnal average (24h) of the relative loss rate of ozone (percent per day) by its reaction with OH-radicals ($L_{O3,\ OH}$) and HO$_2$-radicals ($L_{O3,\ HO2}$) for March/April 1987 (left panels) and September/October 1988 (right panels), respectively (for details see text)*

5.2.2.3 Total Losses of Ozone

The latitude/altitude cross sections of the diurnal (24h) average of the total relative loss rates of ozone, $L_{O3,Tot}$, are shown in Figure 5.7. $L_{O3,Tot}$ is presented as sum of the photochemical loss rates $L_{O3,J(O1D)}$, $L_{O3,\ OH}$ and $L_{O3,\ HO2}$, while for the region within the MBL the contribution by dry deposition (3 percent per day) is also included.

From these contour plots it is seen that in the tropical regions the resulting atmospheric lifetime of ozone in the lower troposphere is less than 1-2 weeks. It is obvious that high concentrations of water vapor in combination with high solar UV-radiation in the tropics provides a strong photochemical ozone sink in the lower troposphere. Within the MBL between 30°S and 30°N the photochemical loss by far dominates the loss from dry deposition to the ocean surface. The photochemical ozone loss increases towards the equator and maximizes in the vicinity of the ITCZ. Following the decrease of water vapor with altitude the relative loss rate of ozone decreases drastically in the middle and upper troposphere with a corresponding increase of the photochemical ozone lifetime to more than 100 days in the UT.
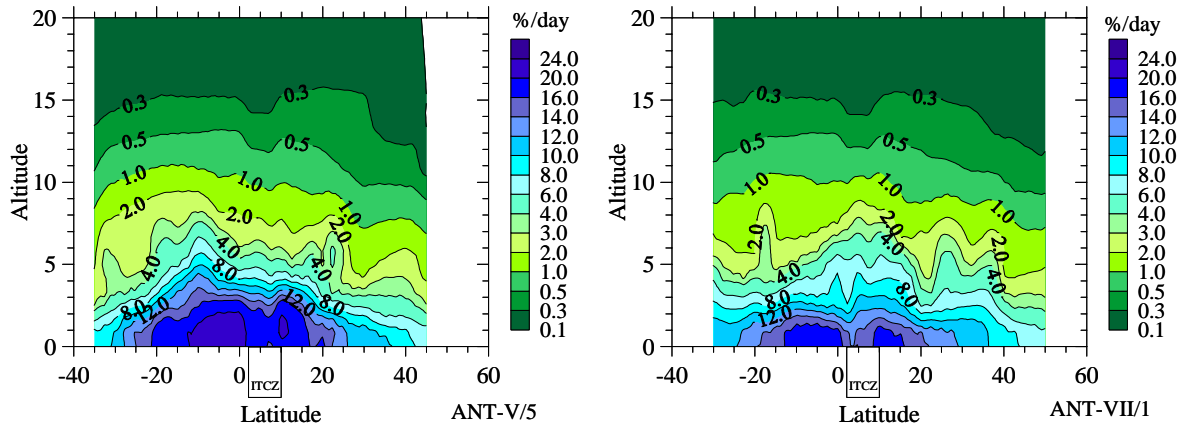
Figure 5.7: *Cross sections of the meridional/altitude distribution of the calculated diurnal average (24h) of the total relative loss rate of ozone (percent per day) by its photolysis in presence of water vapor $L_{O3,J(O1D)}$, its reactions with OH ($L_{O3, OH}$) and HO$_2$-radicals ($L_{O3, HO2}$) for March/April 1987 (left panel) and September/October 1988 (right panel), respectively. For the region within the MBL the contribution by dry deposition (3 percent per day) is included (for details see text)*

5.2.3 Production of Ozone

The question of how much a slow photochemistry in the middle and upper troposphere can have a significant influence on the measured ozone distributions must be treated in conjunction with an assessment of the concurrent photochemical formation rates which are critically related to [NO$_X$]. The latitude/altitude cross sections of the calculated diurnal average of the relative production rate of ozone for both cruises is calculated, based on the assumed cross sections of NO$_x$ (Figure 5.3) and are presented in Figure 5.8. In the free troposphere, the gross formation rates are less than 2-4 % per day throughout the entire troposphere. In the tropics the formation rates are slightly higher due to the higher HO$_X$ concentrations.
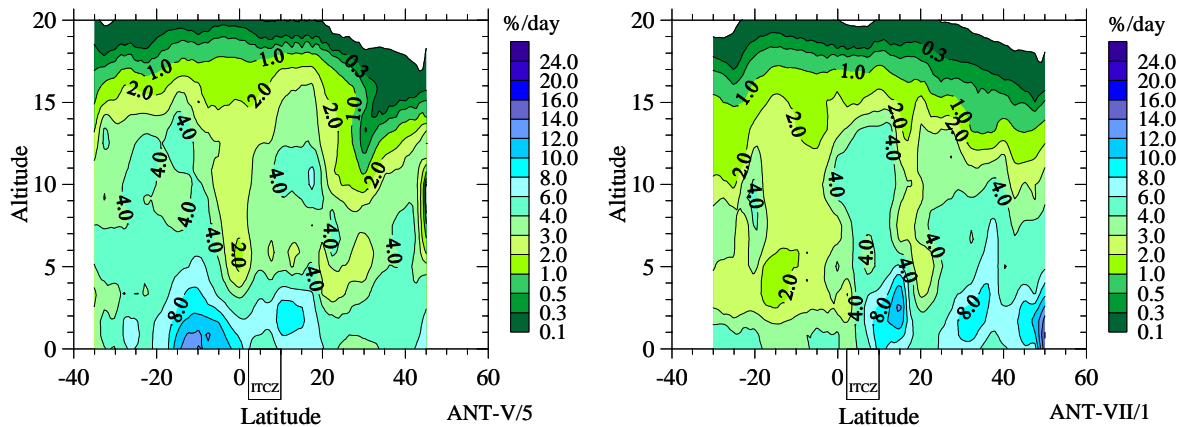

Figure 5.8: *Cross sections of the meridional/altitude distribution of the calculated diurnal average (24h) of the relative formation rate of ozone (percent per day) for March/April 1987 (left panel) and September/October 1988 (right panel), respectively (for details see text).*

5.2.4   Net Production or Destruction of Ozone: Assessment

Figure 5.9 show cross sections of the calculated threshold concentration $[NO_X]_{Thres}$ for the NO_X concentration, defined as the concentration of NO_X for which ozone production just balances the total ozone loss $[NO_X]_{Thres}$ was calculated according Equation 2.9 (See Chapter 2, Section 2.2.5). In order to show the sensitivity of the NOX-threshold criterion with regard to the classification of in-situ net photochemical ozone production or destruction, the ratio of the actual to the (hypothetical) threshold concentration of NO_X was calculated and presented as cross section in Figure 5.10. This ratio, calculated according equation 2.10 (see Chapter 2, Section 2.2.5) represents the ratio of photochemical production and destruction of ozone.

Figure 5.9: *Cross sections of the meridional/altitude distribution of the calculated diurnal average (24h) of the threshold NO_X mixing ratio (in ppbv) for March/April 1987 (left panel) and September/October 1988 (right panel), respectively (for details see text)*

Figure 5.10: *Cross sections of the meridional/altitude distribution of the ratio of the estimated NO_X-concentration (see FigureF-DIS-1-1A) and calculated threshold NOX-concentration (see Figure F-DIS-1-12A) for March/April 1987 (Upper panel A) and September/October 1988 (Lower panel B), respectively (for details see text*Cross sections of the net changes of ozone are shown in Figure 5.9.

The classification of regions with net photochemical production or destruction of ozone is very similar for both cruises. The figure shows that, in the MBL and lower troposphere up to about 5 km altitudes, there is a net destruction of ozone, which is of significant strength in the MBL. In the middle and upper troposphere between 40^oS and 50^oN the actual NO_X-mixing ratio's shown in Figure 5.3 are significantly larger than the estimated low threshold NO_X-mixing ratios estimated from the model calculations (See Figure 5.9). Therefore, it is expected that net photochemical formation of ozone will always occur. However, the photochemical conversion rates are rather slow with only a couple of percent per day or even less in the middle and particularly in the upper troposphere.

Cross sections of net changes of ozone are shown in Figure 5.11. Within the tropical MBL over the Central Atlantic ozone losses dominate the production of ozone by more than a factor of 2-3 in the SH and NH. In the trade wind regions, there is a strong net photochemical destruction of about 3-6 percent per day at 30 ^{o}N/S that increases towards the ITCZ to 12-15 percent per day in the equatorial region. In the free troposphere, the photochemical fate of ozone changes from a net destruction in the lower troposphere into a net production in the upper troposphere while in the middle troposphere destruction more or less balances production. However, the net (positive) relative changes of ozone becomes very small at higher altitudes with values of about 1-3 % per day at 10 km to values below 1 % per day near the tropopause.
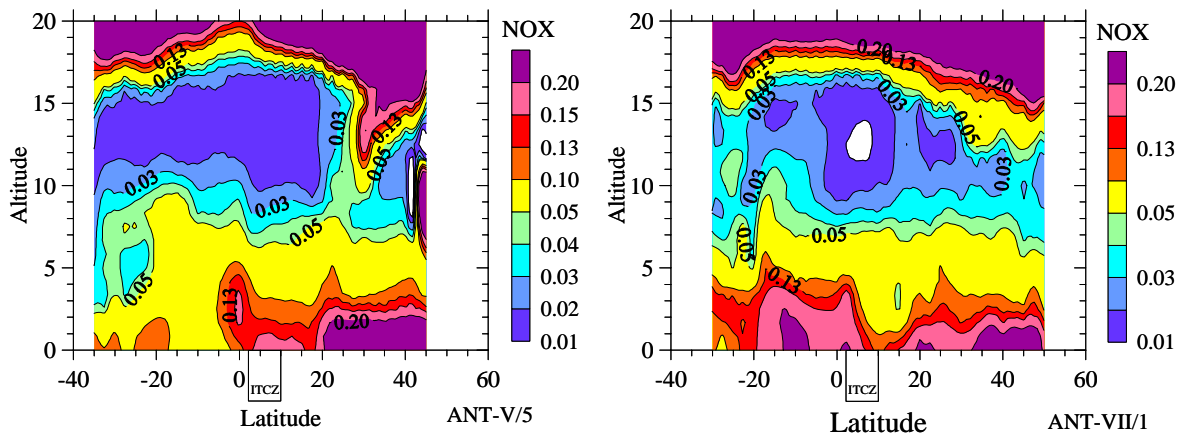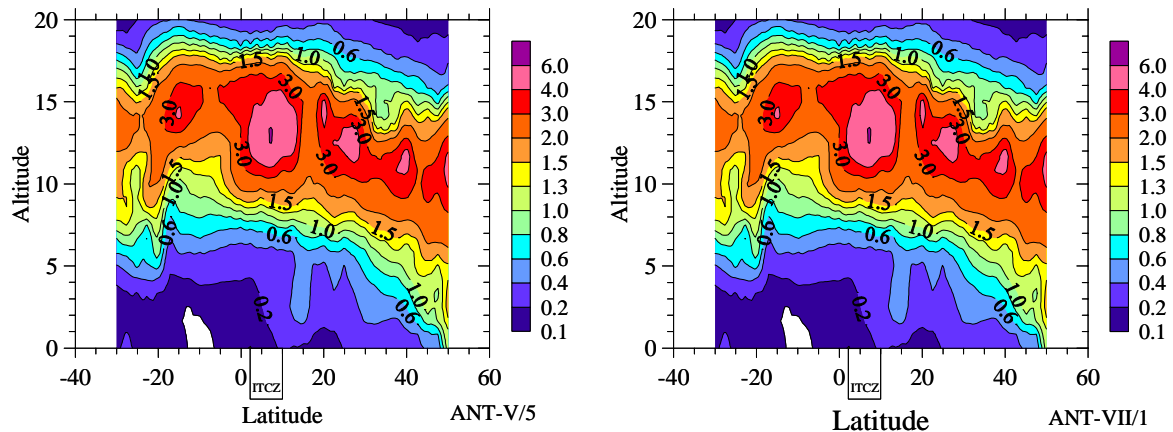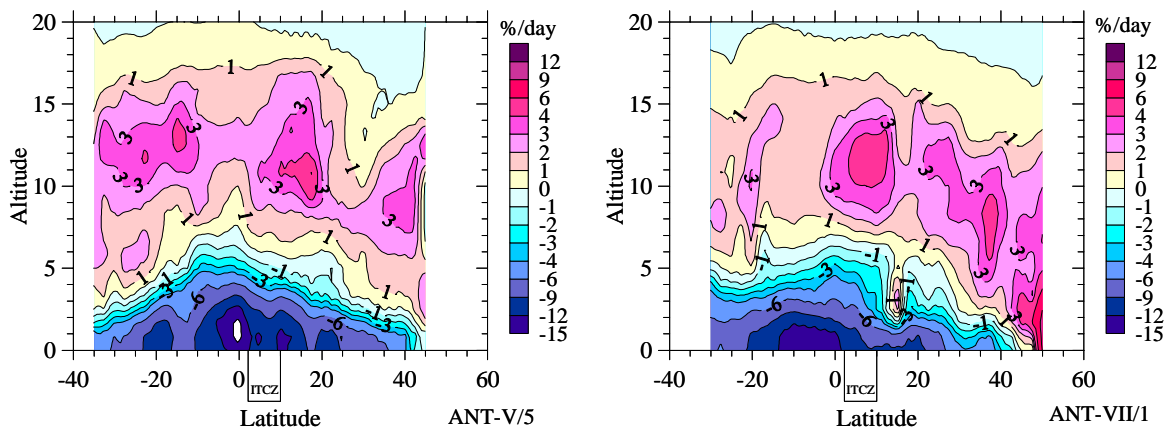

Figure 5.11: *Cross sections of the meridional/altitude distribution of the calculated diurnal average (24h) of the net relative rate of ozone changes (percent per day) for March/April 1987 (left panel) and September/October 1988 (right panel), respectively (for details see text).*

It is obvious that in the remote marine tropical regions a change from a pronounced photochemical ozone loss in the lower troposphere to a net photochemical production, increasing with altitude occurs. Even so, the net relative change of ozone decreases with altitude. This translates to a photochemical ozone lifetime of about 5-10 days in the lower troposphere, increasing to 30-50 in the middle, and up to more than 50-100 days, in the upper troposphere.

5.3   Photochemistry Versus Transport of Ozone

In order to assess how far in-situ photochemistry can have significant effects on the observed ozone distributions and can compete with transport it is necessary to characterize the specific transport, i.e. residence times of air parcels in the different regions over the Central Atlantic.

5.3.1   Horizontal Winds in Troposphere

From the synoptical weather analyses made aboard the ship during both cruises[*Behr et al.,* 1990, *Behr et al.,* 1990] it is known that during both missions the equatorial trough with the ITCZ (3-10 ^{o}N) was situated north of the equator between 0° and 15°N. The regions north and south of the equatorial trough were characterized by the classical situation of two anticyclonic systems centered at 30°N, 20°W in the NH and at 30°S, 20°W in the SH.

The synoptic wind speeds observed from board the research vessel are shown in Figure 5.12 for the latitudinal variation of the surface winds and Figure 5.13 for the latitude/altitude cross section of the horizontal wind up to 20 km altitude obtained from the rawin soundings.
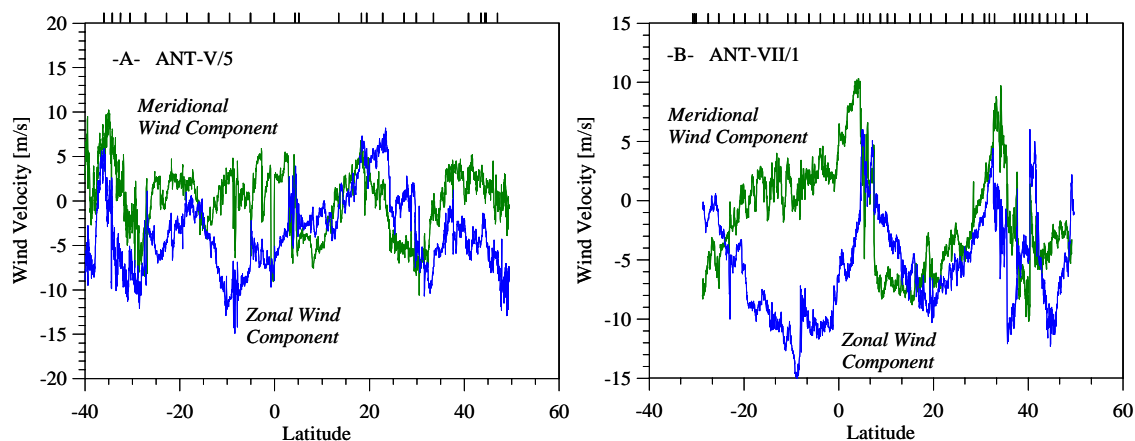
Figure 5.12*: Latitudinal variation of meridional component (green line) and zonal component (blue line) of the surface wind recorded by INDAS during ANT-V/5 (left diagram) and ANT-VII/1 (right diagram)*

In the marine boundary layer (MBL) typical NE-winds in the NH and SE-winds in the SH are directed towards the ITCZ (Figure 5.12). From the latitude/altitude cross sections of the meridional and zonal wind components, shown in Figure 5.13, it is seen that the lower and middle troposphere in the equatorial region towards the ITCZ was governed by easterly flowing winds with wind speeds of about 2-10 m/s. However, outside the equatorial region westerly flowing winds were dominating with wind speeds of 15-20 m/s in the middle/lower troposphere and increasing to values of 30-35 m/s in the upper troposphere. Very pronounced was the sub-tropical jet stream centered at 20°N encountered during the ANT-V/5 cruise in March/April 1997.

Zonal Wind Component

Meridional Wind Component
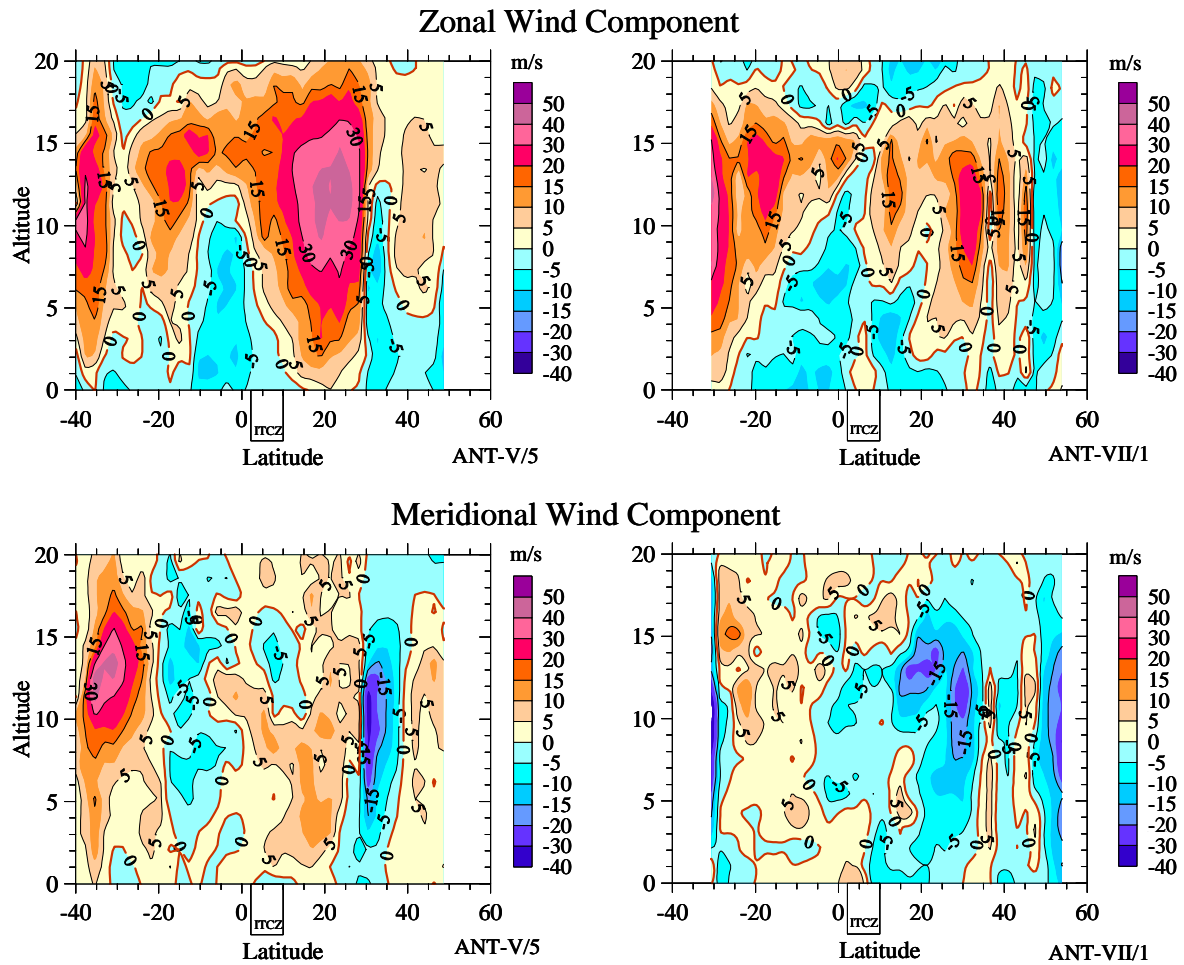
Figure 5.13:*Cross section of the meridional/altitude distribution of zonal wind component (m/s, positive values point in easterly direction) and meridional wind component (m/s, positive values point in southern direction) over the Central Atlantic Ocean derived from rawin-soundings made during ANT-V/5 (left panels) and ANT-VII/1 (right panels) mainly along the 30°W meridian.*

5.3.2 Ozone during Transport in MBL in Trade Wind Regions

Trade wind velocities of 5-10 m/s towards the ITCZ were observed such that the typical transport time for air masses flowing from the subtropical regions (30°N and 20°S) towards the ITCZ (4°N-10°N) was about 4-7 days. This means that with destruction rates of about 10-15 % per day significant net losses of ozone of 50-100 % occurred during its transport by the trade winds from the sub-tropics to the equatorial trough region. Due to the strong temperature inversion of more than 2-3°C at the top of the MBL, the transport of ozone from the free troposphere into the MBL is a slow diffusion process as indicated by the increasing vertical gradient of ozone just above the MBL in the trade wind regions (see Figure 4.6). Therefore, it can be concluded that photochemical destruction processes provided an effective sink mechanism, which was responsible for the low ozone values observed near the surface and the latitudinal decrease of ozone towards the ITCZ.

5.3.3 Ozone in Active Cb-Convection Within the Equatorial Trough Region

The equatorial trough zone is characterized by strong upward transport due to a relative small number of deep convective cells (so called "hot towers") with vigorous vertical transport

inside [see Section 2.1.1]. Inside of a cumulonimbus convective cell, an air parcel will be fast upward transported with upwards velocities varying between 1-10 m/s, strongly depending on the actual in-situ buoyancy of the air parcel transported aloft [e.g. *Cotton and Anthes*, 1989, *Holton*, 1979]. This means that surface air is transported aloft to the middle/upper troposphere in less than about one hour. However, only less than 1 percent of the ITCZ area, at any given moment, is covered with active deep convective cells rising from the subcloud layer that consists of cumulus clouds extending up to about 3-4 km altitude (See section 2.1.2). It is therefore most likely that the MBL air after entering the equatorial trough zone can stay for a longer period before being transported aloft by an event of a Cb-convection. For example in case of the ANT-VII/1 mission the residence time of an air parcel inside the equatorial trough after entering the equatorial trough zone between $0°$ and $15°N$ with a trade wind velocity of typically 3m/s (see Figure 5.12) will be more than 3 days[11]. This is long enough that additional significant depletion of ozone by net photochemical destruction of 30-45 % may occur. This explains the sudden drop of the ozone mixing ratio from about 30 ppbv down to 20 ppbv after entering the equatorial trough zone observed during the ANT-VII/1 mission in September/October 1988. Above the sub-cloud layer the ozone levels measured in the middle and upper troposphere inside the equatorial trough is not significantly influenced by photochemistry due to the much lower conversion rates of less than 2-4 % per day at these higher altitudes compared to the fast vertical transport associated with the Cb-convection.

5.3.4   Ozone Under Large Scale Subsidence Exterior the Equatorial Trough Region

The trade wind belts as part of anti-cyclonic weather systems (see Section 5.3.1) are characterized by overal subsidence motion in the free troposphere. The vertical velocity, w, can thereby be inferred from hydrostatic stability in conjunction with the adiabatic heating due to the subsidence and the balancing radiative cooling in the absence of any strong diabatic heating, [*Holton,* 1979], as follows:

$$w \bullet (\Gamma_d - \Gamma) = \frac{\partial Q}{\partial t} \qquad\qquad [5.1]$$

whereby $\frac{\partial Q}{\partial t}$ is radiative heating rate, Γ_d ($=g/c_p$) and Γ ($=-\partial T/\partial z$) are the dry and actual lapse rate respectively.

Estimates of subsidence velocities at different altitudes are listed in Table 5.1. Thereby, typical climatological values for the balancing radiative cooling rates $\partial Q/\partial t$ are taken from *Dopplick* (1972) while actual lapse rates were obtained from the measured temperature profiles. Subsidence velocities of about 0.5-1 km/day in the free troposphere are calculated, such that the typical vertical transport time for large scale diabatic descent under clear sky from the middle/upper into the lower troposphere will be less than 1-2 weeks.

From the cross sections of the meridional and zonal wind components, shown in Figure 5.13, it is seen that the horizontal wind velocities in the free troposphere are generally larger than 5-10 m/s. This means that within the domain of interest over the Central Atlantic covered by

---

[11] The residence time τ_{ETZ} of an air parcel within the equatorial trough zone (ETR) from $4°N$ to $20°N$ (Length $L_{ETR} \approx 1750$ km) was estimated by assuming mass balance, i.e. that the entering air mass flux by the trade winds (w_{trade}) with a velocity of 3m/s over a PBL height of 1km into the equatorial trough is equal to the average updraft air mass flux inside the trough, expressed as: $\tau_{ETR} = L_{ETR} / 2$ x w_{trade}

30°S-30°N and 0°W and 60°W the horizontal transport in the free troposphere is on a time scale of less than 1 week. It is obvious that in the free troposphere the typical times of photochemical changes of ozone of several weeks are much slower than the typical transport times of large scale subsidence north and south of the equatorial trough area. This means that in the free troposphere there will be no significant changes of ozone due to photochemistry during horizontal transport of the subsiding air inside the tropical region over the Atlantic region.

Altitude [Km]	Radiative Heating Rate [°C/day]	Actual Lapse Rate [K/km]	Subsidence Velocity [Km/day]	Relative Photochemical Ozone Changes [%/day]
14	-1.0	8.5	-0.8	+(2-3)
8	-1.5	8.0	-0.8	+(1-2)
5	-1.5	7.5	-0.6	-(1-2)
2	-2.0	6.5	-0.6	-(3-4)

Table 5.1: *Typical subsidence velocities at different altitudes for clear sky conditions in the tropics (30°S – 30°N) taken typical radiative heating rates from Dopplick [1972] and actual lapse rates from ozone soundings. Relative photochemical ozone changes are taken from Figure 5.9*

It is concluded that in the free troposphere, and particularly within the tropical region between 30°S and 30°N, the dynamical structure of the latitudinal ozone distributions are determined by transport and, conversely, that photochemical processes during the transport are insignificant. The opposite is the case in the MBL of the trade wind regions where photochemical destruction processes play a major role and provide an effective sink that is responsible for the low ozone values near the surface and its latitudinal decrease towards the ITCZ. The consequences are that the morphology of the observed ozone distributions of ozone was controlled by the uplifting of ozone-poor air to the middle and upper troposphere through Cb-convection within the region of the ITCZ and by slanted subsidence of ozone rich air from the upper troposphere into the lower troposphere outside of the ITCZ region. This is clearly seen during ANT-VII/1 mission in September/October 1988 (Figure 4.6) where the low ozone values of the troposphere over the equatorial trough zone (0-20°N) are caused by the uplifting of ozone depleted air through Cb convection and enhanced ozone mixing ratios in the troposphere outside the trough zone.

5.3.5   The Influence of Large-Scale Transport

Although, the enhanced ozone values in the free troposphere outside of the trough zone do not appear to have been caused by in-situ photochemical production, they could nevertheless have a photochemical origin. It cannot be excluded that those were photochemically produced over the continents of South America or Africa, followed by large-scale transport towards the region over the Central Atlantic. Also, they could have a stratospheric origin (see Section 2.2.6). The ANTVII/1 cruise where remarkably high ozone mixing ratios were observed in the SH, particularly between 5°S and 20°S (Figure 4.3) gives a strong hint for photochemical

production. As Figure 4.6 shows high ozone values between 5°S and 30°S extending from the surface throughout the entire troposphere up to about 15 km altitude. Simultaneous measurements of NO_X, HNO_3, CO, and NMHC made in the MBL underlying these air masses, indicated that photochemically aged air masses were probed that some time ago must have possessed the potential for photochemical ozone production. The indications for this can be seen in the enhanced concentrations of HNO_3 of about 50-100 pptv [*Papenbrock et al.,* 1992] and CO of about 100-130 ppbv [*Koppmann, private communication*], which coexisted, with relatively low concentrations of NO_X of less than 20 pptv [*Rohrer and Brüning,* 1992, *Harris et al.,* 1992] and NMHC [*Koppmann et al.,* 1992]. Since in-situ production of the ozone in the MBL can be discounted the origin of the enhanced ozone levels in the MBL air at these latitudes must be have occurred in the overhead air masses. Transport to the surface may have occurred relatively slow as indicated by the strong vertical ozone gradient, just above the MBL. The ozone being probably photochemical in origin and having been transported down from the middle/upper troposphere implies that the air must have experienced emissions of ozone precursors at least once in its photochemical history.

Now, it is well known that in the tropical Atlantic region enhanced tropospheric ozone values are often largely associated with biomass burning emissions which maximize in austral spring (September/October), the dry season in the SH [e.g. *Crutzen and Andreae,* 1990]. Tropospheric ozone columns retrieved from satellite data show enhanced values over the southern hemisphere Atlantic between equator and 30°S during the austral spring [*Fishman et al.,* 1990, *Kim et al.*, 1996]. Several studies have analyzed atmospheric transports over the SH tropical Atlantic Ocean and their influence on observed ozone distribution. On the basis of a three-dimensional backward trajectory analysis, *Krishnamurti et al.* [1993] suggested that high ozone abundances over the eastern Atlantic result from transports of biomass burning products from South America by high altitude westerly winds as well as transport from Africa by lower altitude easterly winds, followed by accumulation of ozone under the influence of an anticyclone near the west coast of central Africa. However, *Krisnamurti* also concluded that there is considerable subsidence over the tropical southern Atlantic, such that stratospheric influences can also be a significant factor in contributing the enhanced ozone concentrations. Similar conclusions can be drawn from the results of the measurement campaign "Southern African Fire Atmospheric Research Initiative/Transport and Atmospheric Chemistry near the Equator-Atlantic (SAFARI/TRACE-A)", conducted in September/October 1992 [*Thompson et al*, 1996].

To study the origin of the enhanced ozone concentrations observed over the SH tropical Atlantic Ocean during ANT-VII/1 *Roelofs et al.* [1997-b] used a coupled chemistry-general circulation model. Although the focus of the study was to investigate the influence of biomass burning over the tropical Atlantic, also more generally the contributions of stratosphere-troposphere exchange (STE) and photochemistry to the measured ozone distribution in both hemispheres were addressed. The general circulation model (GCM) used in the study is the European Center Hamburg Model, version 4 (ECHAM-4) which is coupled to a tropospheric chemistry model that considers CH_4-CO-NO_X-HO_X chemistry, emissions of NO and CO, dry deposition of O_3, NO_2, HNO_3, and H_2O_2, and wet deposition of HNO_3, and H_2O_2. A detailed description of the study is beyond the scope of this thesis but the major results and conclusions derived from it are:

- Simulated wind fields in the region agree well with ECMWF analyses presented by *Krishnamurti et al* [1993].

- The SH (sub) tropical Atlantic Ocean, photochemically produced ozone is largely associated with biomass burning emissions which maximize in September/October, the dry season in the SH.
- The model results show that in the MBL, relatively unpolluted marine air is transported from the southeast. Above the MBL, between about 2 and 5 km altitude, relatively ozone rich air is transported into the region from the east where the African biomass burning regions are located. Above 5 km, ozone levels are influenced by westerlies, which advected air from the South American biomass burning regions.
- Photochemical destruction of ozone with about 1-4 ppbv prevails over the ocean in the lower troposphere while in the upper troposphere there is a net photochemical formation of ozone of about 1 ppbv per day.
- Between 5^oS and 20^oS tropospheric ozone levels are dominated by photochemical aged air while transport from the stratosphere is of minor importance. However, between 20^oS and 30^oS about 50% of the tropospheric column ozone is determined by transport from the stratosphere.
- Photochemical production of ozone due to biomass burning emissions is majorly restricted to the source regions over the continents, which is clearly seen in Figure 5.14 showing the longitudinal distribution of the calculated net ozone production/destruction rate along 6^oS. The model simulates relatively strong net ozone production over South America and Africa, form about 50 ppbv per day near the surface to about 4 ppbv per day between 8 and 12 km. However, the zonal convective outflow show moderate production rates of less than 1-2 ppbv per day and are comparable with the estimates for in-situ production made in Section 5.2.4.
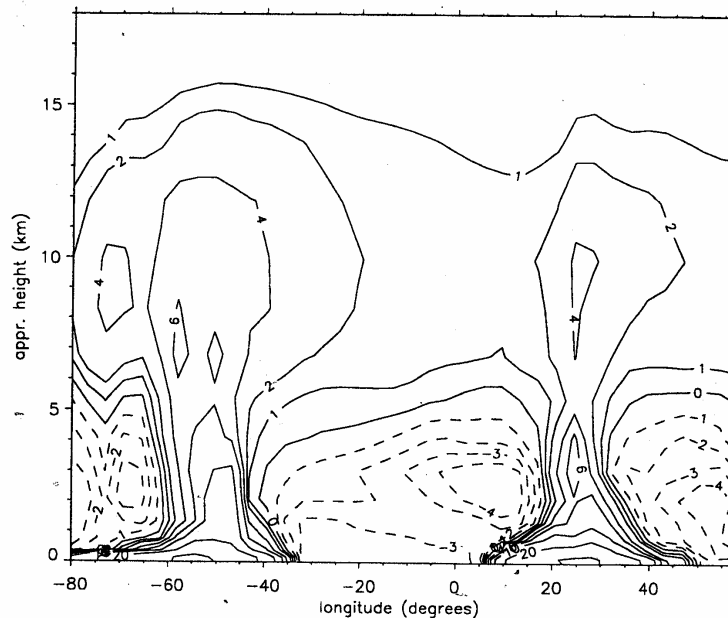
Figure 5-14: *Longitudinal cross section of simulated ozone production/destruction rates (ppbv per day) for the month September 1988 at approximately 6^oS obtained with the ECHAM 4 general circulation model coupled with CH_4-CO-NO_X-HO_X chemistry model [Roelofs et al, 1997-b].*

- Absolute ozone levels over the SH tropical Atlantic Ocean appear to be generally underestimated by the model. It is likely that the model underestimates photochemical production of ozone because higher hydrocarbons released by biomass burning have

not been considered. Particularly the emissions of reactive hydrocarbons can lead to a more efficient in situ production of ozone near the source regions of the biomass burning. Although this photochemistry is fast it is only efficient near the source region over the continents before lifted up by convection and followed by zonal transport in the middle and upper troposphere.
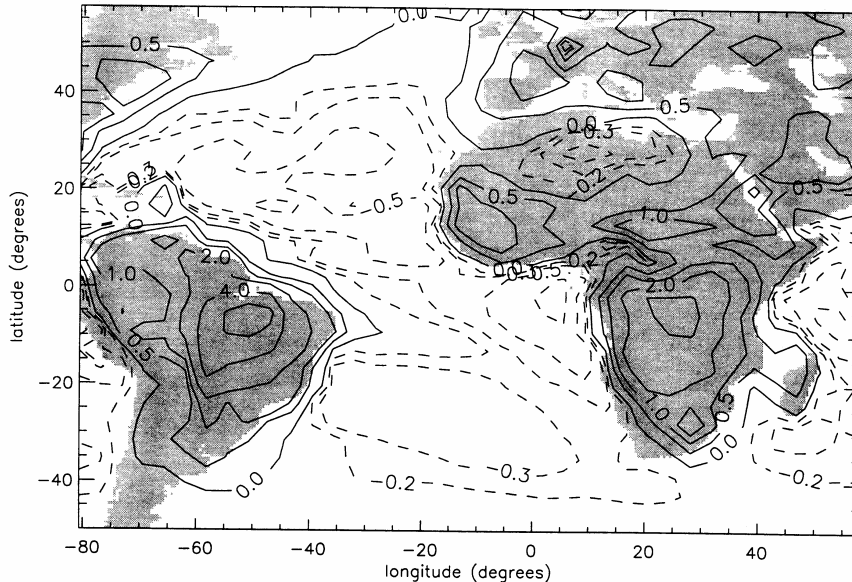
- Calculated ozone production/destruction rates, integrated over the troposphere for the entire region of the Atlantic Ocean (See Figure 5.15) show that net ozone production is limited to the continents, while net destruction prevails over the oceans.

Figure 5-15: *Simulated column integrated ozone production rate (solid contour lines) or destruction rate (dashed contour lines) in DU per day for the month September as obtained with the ECHAM 4 general circulation model coupled with CH4-CO-NOX-HOX chemistry model [Roelofs et al, 1997].*

- The enhanced ozone concentrations north and south of the ITCZ are also produced by the model and indicate that these are due to downward ozone transports from the tropopause region or even the stratosphere.

Thus the modeling study shows that the observed enhanced ozone values likely have a photochemical origin, but that most of this ozone had already been produced in the vicinity of the source regions over the continents before it was transported to the Central Atlantic region at 30°W. This is an interesting result because it shows that the production of ozone is largely restricted to the continental regions with minor amounts produced in the upper troposphere during transport over the oceans while the major ozone destruction proceeds in the MBL over the oceans (see Figure 5.15).

5.3.6   Tropospheric Ozone Maps Tropical Motions Over Remote Oceans

Since air masses transported in the MBL with the Passat winds, steadily loose ozone by photochemical depletion towards the ITCZ ozone deficient air inside the ITCZ is lifted by Cb-convection into the upper tropical troposphere. After an air mass has left the marine boundary layer in a forced Cb-ascent, the ozone chemical conversion time becomes long, in excess of

30-100 days. Active or recent deep convection marks its appearance in the upper tropical troposphere by very low ozone mixing ratios. Ozone values as low as those near the surface are understandable if subcloud layer air is lifted in the core of undiluted Cb-convection. The equivalence of surface and top of the troposphere ozone mixing ratio forms an excellent indicator for the nature and the intensity of the transfer process [*Kley et al.,* 1996]. The large scale extent of deep convection becomes apparent through the morphology of the ozone cross section given the isolines of low ozone mixing ratio of 20-40 ppbv extending into the upper troposphere while on the other hand contour lines of high ozone penetrating deep into the lower/middle troposphere indicate diabatic subsidence processes.

Within the domain of interest of tropical motion systems that are active over the equatorial Atlantic between 30^oS and 30^oN and the bordering continents (South America and Africa) the time scale of horizontal transport is typically about 1 week. This means that the impact of the relatively slow local ozone photochemistry with relative changes less than about ±(1-3) % per day, depending on altitude, will not significantly change the ozone content during this large scale subsidence. On a time scale of approximately 1 week the impact of local photochemistry is estimated to be less than 10% with regard to the observed morphology of ozone in the middle/upper troposphere up to about 14 km altitude. This is confirmed by the results of the coupled chemistry-general circulation model analysis presented in the previous section which show that most of the ozone in air masses of large scale subsidence over the Central Atlantic originated from the upper troposphere or even stratosphere. It is therefore concluded that within tropical motion systems in marine environments with characteristic time scales of the order of 1 week ozone can be used as a quasi-chemical inert tracer to map the dynamics of deep convection associated with entrainment and detrainment processes in conjunction with large scale subsidence.

Chapter 6

Deep Convection and Subsidence over the Central Atlantic Ocean

6.1   Introduction

To study deep convection and its influence on the humidity distribution it is important to understand processes like entrainment and detrainment in conjunction with large scale subsidence (see Chapter 2). From the shape of the isolines of the reported water vapor distributions (see Figures 4.7 and 4.8) it is only possible to describe the dynamics of the tropical circulation in a phenomenological way. Due to the processes of condensation of water vapor and evaporation of hydrometeors the water vapor in itself cannot be considered as a conservative tracer in describing processes like deep convection or large scale subsidence. Even during subsidence of air evaporation of hydrometeors, which are originating from the outflow of the upper tropospheric anvil clouds [*Sun et al.,* (1993)], can occur. It is obvious that the water vapor distribution alone cannot give enough quantitative information about the dynamical structure interior as well as exterior of the deep convective regions. Therefore water vapor is not sufficient as tracer for mapping the dynamics of the tropical motion systems.

Although several tools exist to diagnose deep convection, they all contain very little information about the dynamical structure of deep convection and its affect on the surrounding atmosphere. In this chapter ozone is used as a quasi-conservative tracer to map the dynamical structure of deep convection and its consequences on the humidity distribution in- and outside the Cb-convection. The investigations will be limited and focused on the situation as encountered during the second mission (ANT-VII/1), which showed a clear mesoscale cluster of deep convective cells in the ITCZ

6.2   Diagnostic Tools to Study Deep Convection and Subsidence

6.2.1   Sea Surface Temperature and Threshold for Deep Convection

Why deep tropical convection occurs when and where remains somewhat of an enigma. Convection preferentially tends to occur over warm moist surfaces. Although large areas in the tropics are known to have significant amounts of stored energy available for convection, convective areas represent only a small fraction. The problem then is to identify these areas. *Graham and Barnett* [1987] suggested the existence of a minimum threshold sea surface temperature (SST) of approximately 300K for the onset of deep convection in the tropical oceans as a necessary condition, but not a sufficient one. Figure 6.1 shows the latitudinal distribution of the SST measured by the ship during ANT-V/5 (left diagram) and ANT-VII/1 (right diagram). It is obvious that with regard to this threshold SST of 300 K rather large areas have the potential for the onset of deep convection (ANT-V/5: 25^oS - 8^oN and ANT-VII/1: 10^oS - 20^oN). However, as is shown in the next sections only a small fraction of these areas actually revealed active convection.

6.2.2   Outgoing Long Wave Radiation and Deep Convective Activity

Measurements of outgoing long wave radiation (OLR) from satellite broadband radiometers represent a measure of convective activity [e.g. *Wielicki and Green,* 1989]. OLR is an indicator of both how warm the earth's surface is and the degree of transparency of the

overhead atmosphere. Warm surfaces radiate more in the longwave range. Low values of OLR are typically due to clouds in the atmosphere. The radiation from below the clouds gets trapped by them and it is the temperature of the cloud top, which determines the amount of OLR such that for optically thick clouds OLR is an indicator of cloud top temperature. When OLR is low, cold cloud tops indicate the presence of upper level clouds, i.e. cumulonimbus convection in the region [*Wielicki and Green,* 1989], which will reduce OLR by about 50-100 W/m^2 compared to clear sky OLR [*Harrison et al.*, 1990].
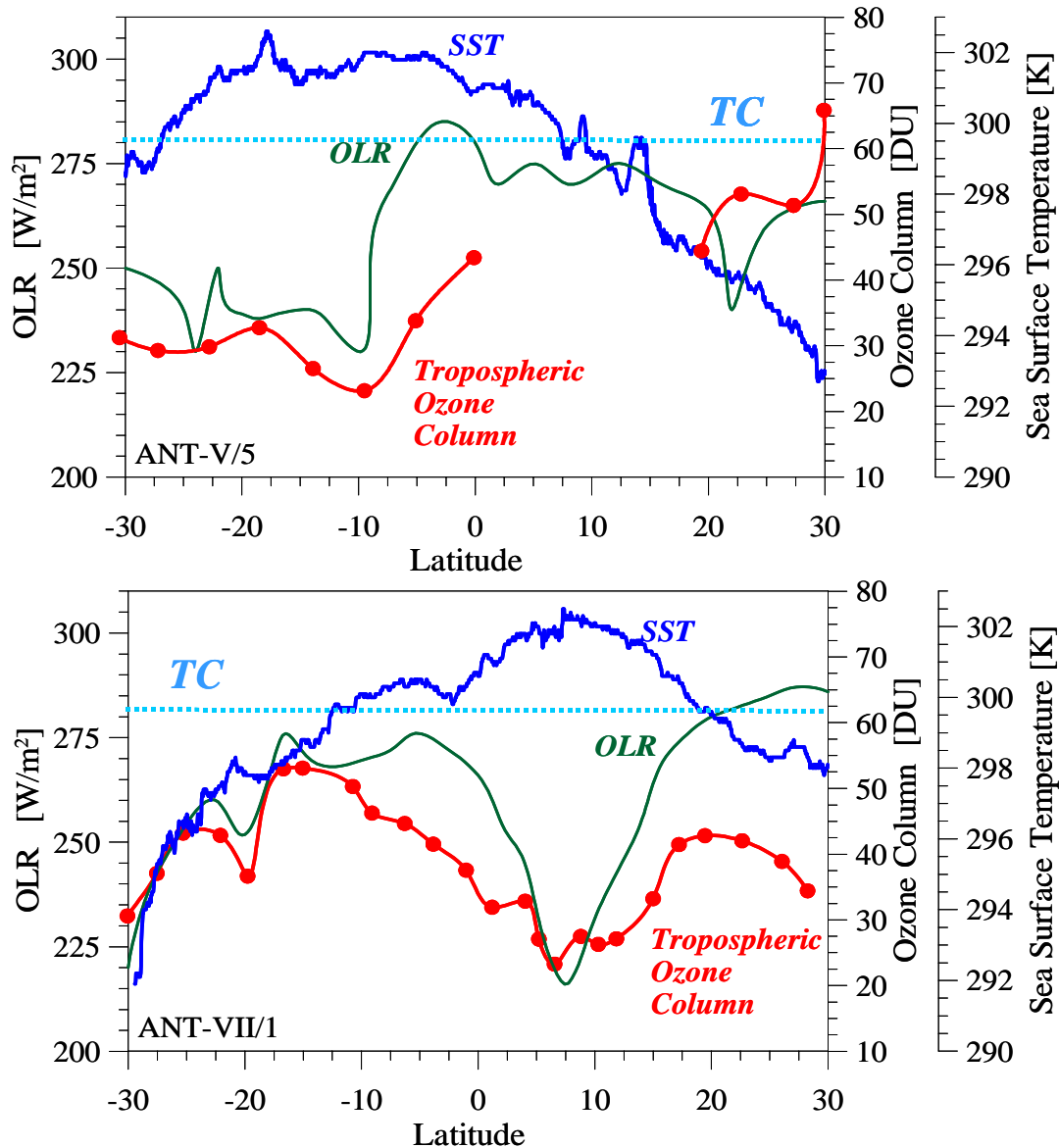
Figure 6.1: *Latitudinal distribution of SST (Sea Surface Temperature, blue curve from ship measurements), tropospheric ozone column (red curve, derived from ozone soundings), and OLR (Outgoing Longwave Radiation, green curve, averaged over 25°W to 35°W from satellite data provided by the NOAA-CIRES Climate Diagnostics Centre, URL= http://www.cdc.noaa.gov) for the two cruises ANT-V/5 (upper panel) and ANT-VII/1 (lower panel). The light blue dotted lines (TC-labelled) represent the threshold SST for the onset of deep convection (see text). No tropospheric ozone columns during ANT-V/5 between 0 and 20°N due to erratic ozone soundings.*

Figure 6.2 shows the temporal evolution of the OLR between 30°S and 30°N centered along the 30°W meridian as derived from satellite observations. Regions of deep convective activity are indicated by OLR values typically below about 250 W/m^2. During the ANT-V/5 cruise between 10°S and 30°S OLR values below 240 W/m^2 indicate the presence of upper level clouds, i.e. deep convective activity, while the ITCZ (5°-10°N) show high OLR values, i.e. no indication of upper level clouds were present during the passage of the research vessel. This is in contrast to the situation during ANT-VII/1 where the ITCZ region (5°-10°N) shows OLR values below 220 W/m^2 and thus clear evidence for the presence of deep convective activity.
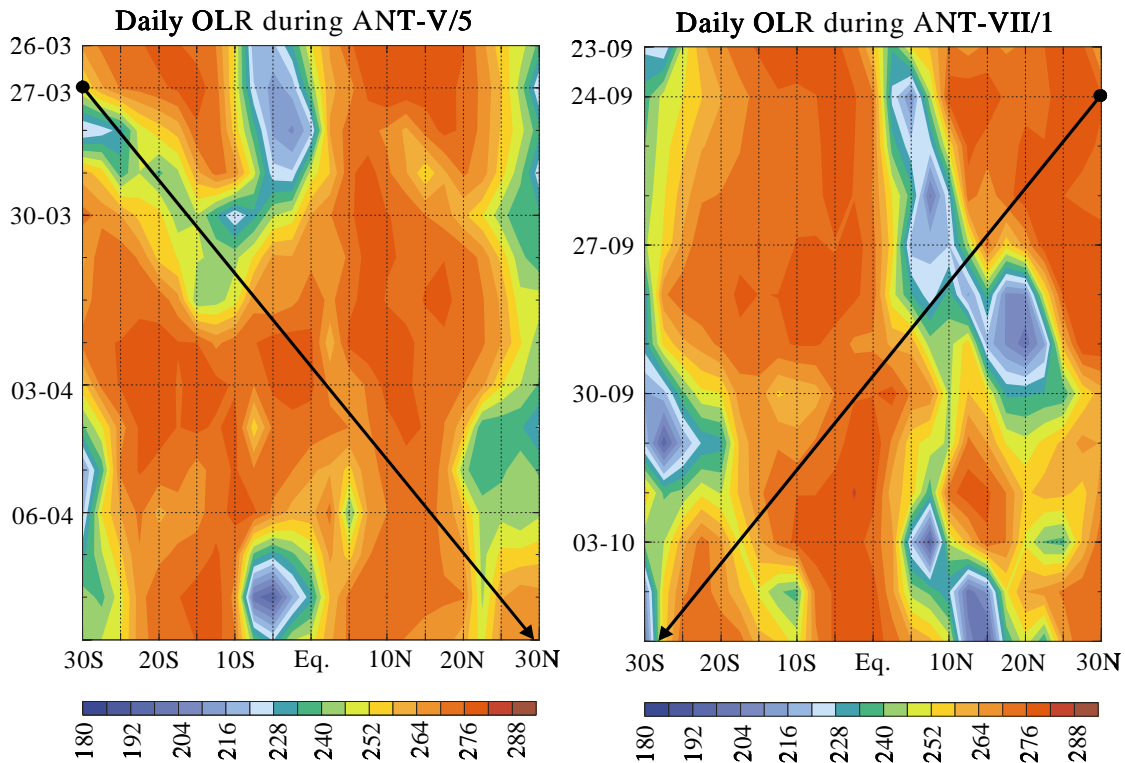
Figure 6.2: *Temporal evolution of the OLR (outgoing longwave radiation, W/m^2) between 30°S and 30°N centered along 30°W meridian (averaged over 25°W to 35°W) for the two cruises ANT-V/5 (left panel) and ANT-VII/1 (right panel). The thick black line represents the cruise track of the RV "Polarstern". (Images provided by the NOAA-CIRES Climate Diagnostics Centre, URL= http://www.cdc.noaa.gov)*

Figure 6.1 also demonstrates that low OLR values, i.e. recent active convection, are associated with low tropospheric ozone columns, while high OLR (no convection) corresponds to high tropospheric ozone columns. In particular, Figure 6.1 suggest a positive correlation between OLR and tropospheric ozone column for ANT-VII/1.

However, OLR is an integral quantity covering the entire infrared spectrum between 5 and 50 μm and thus not a quantitative measure of the radiation temperature itself. Therefore, in the tropics low OLR values can only be an indicator of the presence of high altitude clouds, i.e. deep convective activity, but OLR is not specific to cloud types and cannot resolve temporal and spatial patterns [e.g. *Waliser and Graham*, 1993]

6.2.3   Moist Static Energy

Another tool to investigate deep convection is moist static energy (Q_{MS}) and its vertical distribution (see also Chapter 2, Section 2.1.2). Moist static energy is the total energy of a unit mass of air, when kinetic energy is omitted as a small quantity, and expressed as:

$$Q_{MS} = g \cdot z + c_p \cdot T + L \cdot q \qquad\qquad [6.1]$$

whereby g•Z is potential energy (g acceleration of gravity, Z height); c_p•T is specific enthalpy (c_p specific heat at constant pressure, T temperature) and L•q (L latent heat of condensation, q specific humidity). For a convective element rising without external heat or cold sources, neglecting horizontal pressure gradients (i.e. kinetic energy) and assuming steady state, the first law of thermodynamics may be stated in the form:

$$dQ_{MS} = g \cdot dz + c_p \cdot dT + L \cdot dq = 0 \qquad\qquad [6.2]$$

In case of an undisturbed ascent (i.e. no entrainment) the moist static energy will be conserved and thus be constant over the entire ascent.

Figure 6.3 shows the cross sections of moist static energy derived from the pressure, temperature and relative humidity measurements of the ozone/humidity soundings made during ANT-V/5 (left diagram) and ANT-VII/1 (right diagram) cruise.
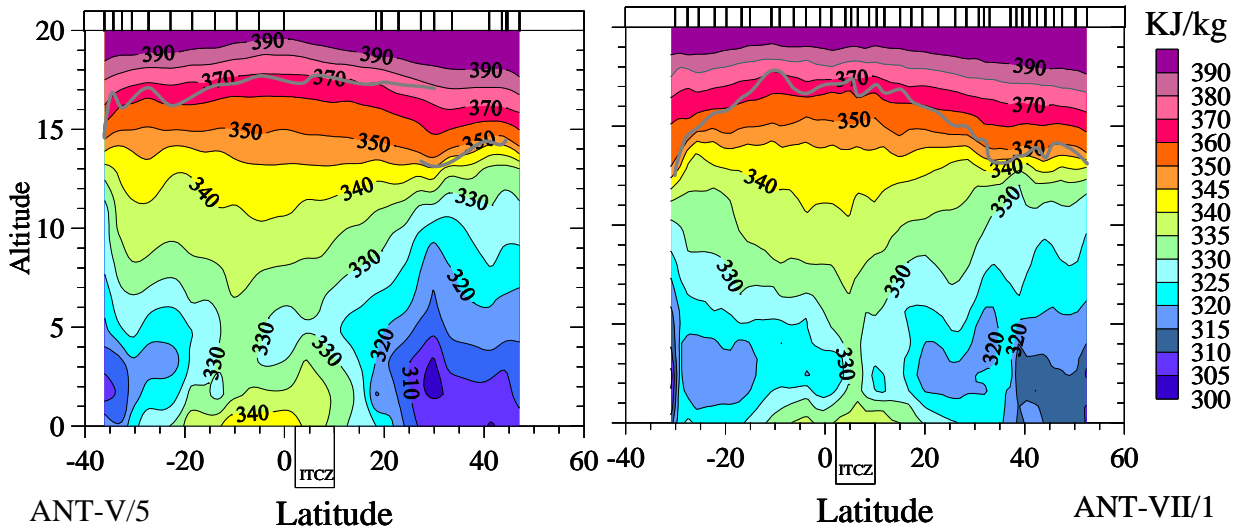
Figure 6.3: *Cross section of the latitude/altitude distribution of moist static energy (in KJ/kg) over the Central Atlantic Ocean derived from ozone/humidity-soundings made during ANT-V/5 (Diagram A: March/April 1987) and ANT-VII/1 (Diagram B: September/October 1988) mainly along the 30°W meridian. Short bars along the top of the diagram indicate latitudes of ozone/humidity soundings. The fat grey line indicates the location of the tropopause.*

Characteristic is the mid-tropospheric minimum observed over the entire latitude region of the tropics between 30°S and 30°N. It is seen that even in the centre of the deep convective areas as identified by OLR-values below 240W/m^2 at around 10°S during ANT-V/5 and between 5°N and 12°N during ANT-VII/1 (see Figure 6.1), the moist static energy has a mid tropospheric minimum, albeit a small one. This means that the moist static energy over vertical columns is not conserved. This mid tropospheric minimum holds not only for the results from the two ship cruises but also virtually for all tropical radiosonde observations

[*Riehl,* 1979]. As suggested by the name, moist static energy does not provide information about the dynamical structure of deep convection and in particular not in the upper troposphere. In order to approach the subject of Q_{MS} from a different angle it is noted that the observations of the minimum of Q_{MS} in the middle troposphere goes hand in hand with enhanced ozone mixing ratios between 30°S and 30°N. This crucially important fact will be discussed in Chapter 6.8.

6.2.4 Tropospheric Ozone as a Conservative Tracer

As it was shown in chapter 5 ozone is chemically a quasi inert tracer in the middle and upper troposphere of the ITCZ for time scales of less than 1-2 weeks. One to two weeks is typical for mesoscale tropical motion systems [e.g. *Holton,* 1979, *Hastenrath*, 1995]. This means that ozone can also be used as a conservative tracer of deep convection. Since relatively low values of ozone are encountered near the surface of about 10-20 ppbv, caused by the strong photochemical sink which is predominantly active in the MBL of the whole trade winds region plus in the lower 3-4 km of the equatorial trough, ozone can be used as a tracer for describing the dynamical structure of a mesoscale cluster of deep convective cells and for the subsidence regime directly exterior of the deep convective cell. In the tropical regions between 30°S and 30°N the free tropospheric part of the meridional distribution of ozone (Figure 4.9) reflects the results of the dynamics of vertical transport processes.

Cruise ANT-V/5 in March/April 1987:

During the first cruise (ANT-V/5) uplifting was observed in the SH at 10°S whereby the lowest ozone value of 10 ppbv near the surface had been found. The fact that ozone mixing ratios increase from 10 ppbv near the ground to values around 50-60 ppbv in the upper troposphere indicates a strong horizontal confluence (entrainment) of ozone rich air into the vertical advective transport of ozone deficient air. No direct uplifting above 9 km altitude could be observed in the ITCZ. This was due to erratic ozone readings between 5°N and 15°N that were caused by Saharian dust (see Chapter 3, Section 3.3.3). From the high values of OLR (see left panel of Figure 6.1), together with the low RH values, (see Figure 4.8, Chapter 4) it is not very likely that recent deep convective activity had taken place during the passage of the ship through the ITCZ. Above 4-5 km altitude the air was even extremely dry with RH values well below 10-20%, which suggests strong subsidence. Below 4 km altitude the air was relatively wet with values of 70-100% RH and low ozone mixing ratios. Together with the heavy cumulus cloud coverage observed [*Behr et al.*, 1989] this implies that in the lower troposphere including the MBL it is most likely that shallow convection had taken place

Cruise ANT-VII/1 in September/October 1988:

As suggested by the strong upward sloping of the cross section of contour lines of low ozone mixing ratios evidence for large-scale active deep convection is clearly apparent inside the ITCZ (see Figure 4.6). Large scale uplifting of air masses, caused by deep convection is commonly associated with the rising branch of the Hadley cell circulation. It is shown in chapter 5 (See Sections 5.3.2 & 5.3.3) that the MBL in the trade wind regions and over the convective regime are also the regions of the highest, photochemical ozone losses and, therefore, the regions of the relatively lowest ozone mixing ratios throughout the entire troposphere. Within the Hadley circulation, air masses are transported by the trade winds from regions north and south of the ITCZ into the equatorial trough by horizontal confluence and then transported to the upper troposphere. Cb-convection lifts ozone deficient air into the upper troposphere where it displaces air with higher ozone mixing ratios. This almost classical

situation of Cb convection in the equatorial trough will be subject for a more detailed investigations in the remaining part of this chapter.

6.3 Deep Convection in the Equatorial Trough Zone during ANT-VII/1

6.3.1 Mesoscale Clusters of Deep Convective Cells

A detailed view about the convective activity over the Central Atlantic during ANT-VII/1 is shown in Figure 6.4 representing the evolution of the large scale distribution of OLR during the passage of the equatorial trough region. Using low OLR (<240 Wm-2) as an identifier of convective cloudiness it is clear from figure 6.4 that over the Central Atlantic between the equator and 15°N clusters with heavy convective cloudiness exist.
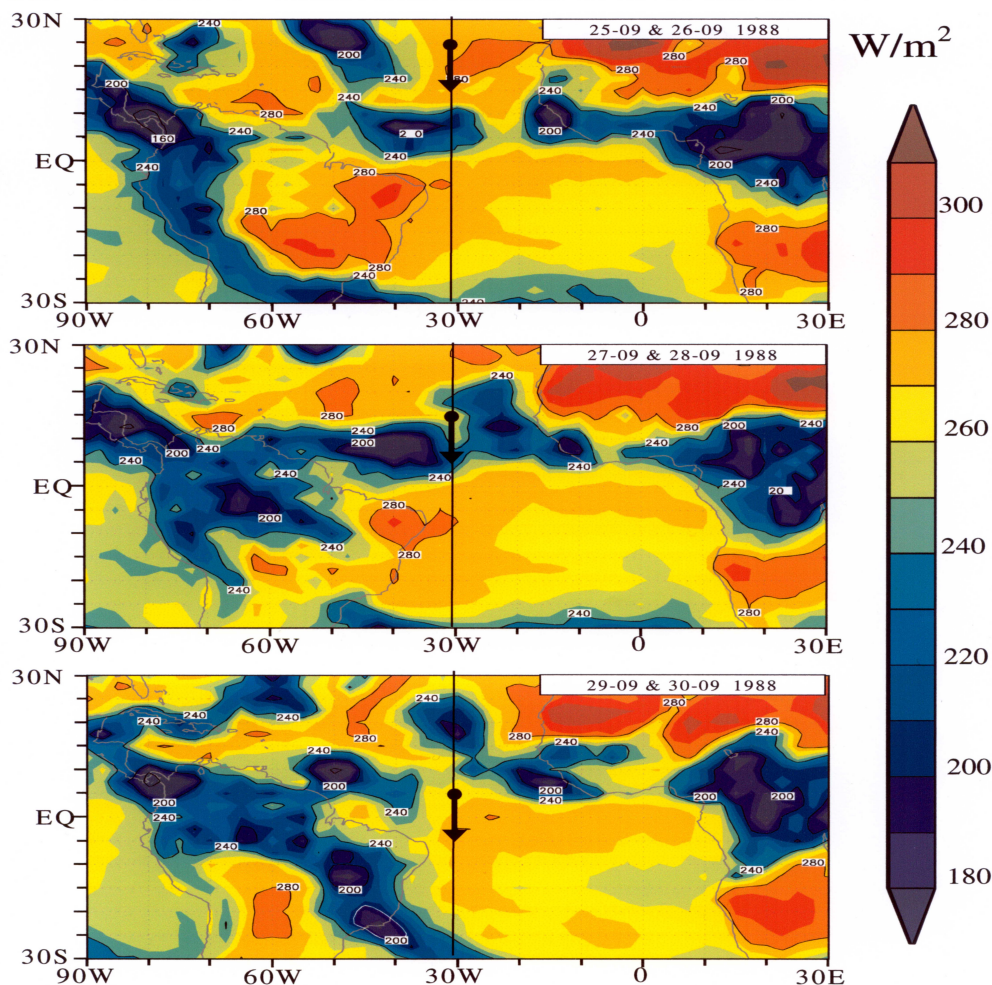
Figure 6.4: *Large scale distribution of OLR (in W/m^2) in the tropics between 90°W and 30°E derived from NCEP re-analysis presented as two day averages for 25./26. (upper panel), 27./28. (middle panel) and 29./30. (lower panel) September 1988, respectively during the passage of the equatorial region during ANT-VII/1. (Images provided by the NOAA-CIRES Climate Diagnostics Centre, Boulder, Colorado, URL= http://www.cdc.noaa.gov). The arrow in each panel marks the section of the cruise track covered for the two days concerned.*

A mesoscale cluster of heavy cloudiness, associated with deep convective cells, was encountered during the passage of the equatorial trough in the period of 27 and 28 September

1998. This mesoscale cluster of deep convective cells is embedded in a mesoscale convective system (MCS). Further it is seen in Figure 6.4 that the Central Atlantic Ocean is bordered by large mesoscale convective systems that are located over South America and Central Africa.

6.3.2   Ozone Morphology: Mesoscale Convective Cell

The meridional structure of the tropical ozone distribution (see Figure 6.5) shows a clear picture of the dynamics involved, that is deep convection inside the equatorial trough and subsidence to the exterior.
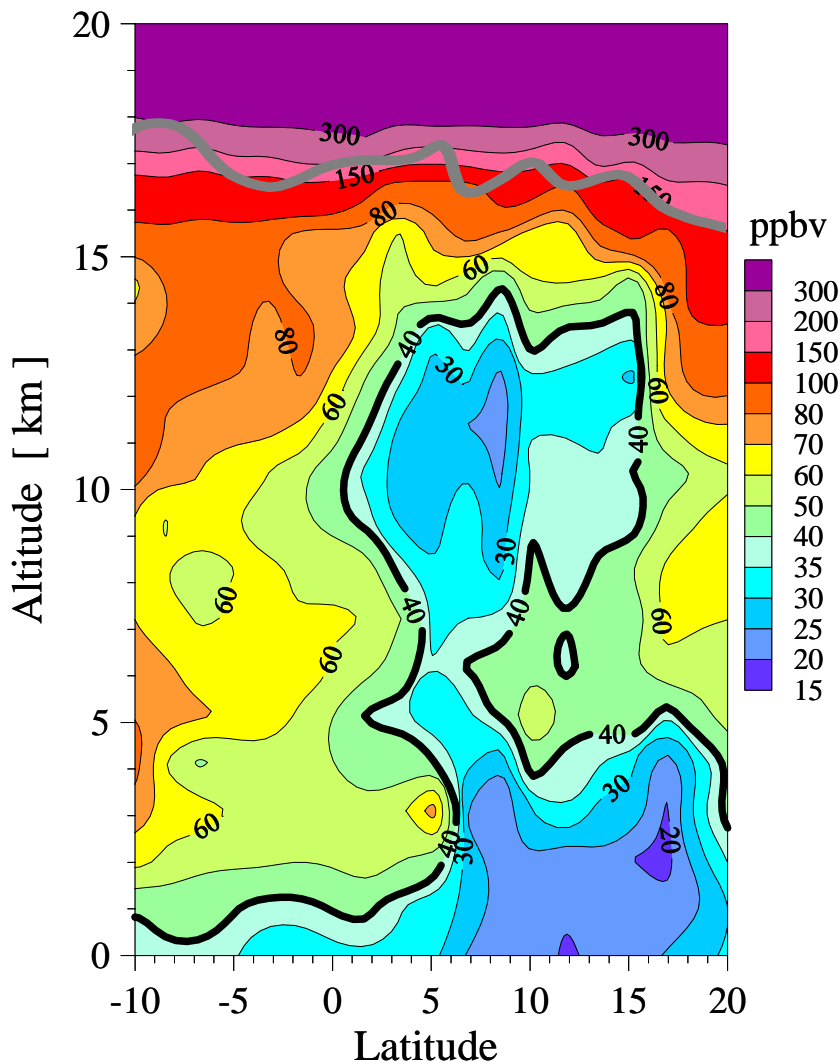
Figure 6.5: *Cross section of the meridional/altitude distribution of ozone mixing ratio (ppbv) over the Central Atlantic derived from ozone/humidity-soundings made during ANT-VII/ (September/October 1988) in the tropical region along the 30°W meridian. The fat grey line is the tropopause and the fat black line the contour of the MCC (Mesoscale Convective Cell)*

Within the ITCZ air from deep convection is dynamically uplifted from the surface up to the upper troposphere. This upward transport is the result from a relative small number of vigorous deep cumulus convective cells in which the air ascends pseudo-adiabatically in the cores of large cumulonimbus clouds, so called "hot towers". Despite the fact that these hot towers occupy only a small fraction less than 1% [e.g. *Riehl*, 1979] of the total area of the tropics, even of a convectively active region like the ITCZ, they provide a very effective vertical transport mechanism. The meridional ozone cross section shows (Figure 6.5) mixing

ratio of ozone in the lower troposphere are about 20 ppbv and levels of about 30-40 ppbv in the middle and upper troposphere.

However, from the eight individual vertical ozone profiles obtained in the equatorial trough (1°S and 15°N), during ANT-VII/1, and displayed in Figure 6.6, it is clearly seen that in the middle troposphere enhanced ozone values of about 50-70 ppbv were observed. Four individual vertical ozone profiles (Panels B-E) measured within the center of the ITCZ between 3°N and 10°N show fairly constant ozone mixing ratios of about 20 ppbv in the lower part of the soundings. Outside of the ITCZ (panels A, and F - H) the values in proximity of the surface were about 30 ppbv whereas in the middle troposphere (4-8 km altitude) mixing ratios increased to levels of about 50-60 ppbv. In the upper troposphere between 10 and 14-15 km altitude ozone first decreased to values of about 40 ppbv while above 14 km altitude ozone increased very rapidly to stratospheric values of 100 ppbv and more. However, between the lower and mid tropospheric part of those soundings enhanced ozone values of about 50-70 ppbv were observed over height intervals of 1-4 km. These enhanced ozone values go hand in hand with sharply lower relative humidity. This feature indicate the existence of layers of air that originated in the upper parts of the troposphere. The existence of this quasi-separation of very low ozone layers in the lower from the upper troposphere is a strong indication that none of soundings, displayed in Figure 6.6, had entered an active hot tower because if they had a constant or perhaps very slow monotonic increase of the ozone mixing ratios with height would have resulted. In fact, the probability for a sounding to occur inside a hot tower is low considering the very small cross sectional areas of hot towers (<25 km^2), and also the sum of all momentarily active hot towers occupy only a small fraction ($\approx$0.01) of the MCS area in the equatorial trough zone which implies that the chance for a sondes to enter a hot tower is very small. In addition, chances for survival of sonde going uo in a hot tower per se very small due to the extremely strong updraft velocities and heavy precipitation, which would have likely destroyed those sondes. All in all this finally means that the measured profiles and the resulting cross sectional picture of the ozone distribution in the equatorial trough zone show a map of the overal net effect of deep convection and that the cause for the enhanced ozone layers in the middle troposphere remains unexplained up to this point.

How then are the enhanced ozone mixing ratios in the middle troposphere of the convective region generated? A likely scenario starts from non-convective regions with subsidence of air masses from the upper troposphere. Strong subsidence is clearly demonstrated by the very dry troposphere over the convectively suppressed troposphere. Now, assume that convection starts, ozone deficient air is lifted from the sub cloud layer, bypassing the middle troposphere, and expelled over the height range that the convection reaches. This height range is 9-13 km over the tropical Atlantic Ocean. This process would, depending on the intensity, extent and frequency of the convection events, generate a vertical O_3 distribution similar to what is observed. However, if the convection is assumed to prevail over a large area, say, over the size of a synoptic disturbance like here in the equatorial trough, then, the entrainment of middle tropopsheric air requires a further supply of ozone rich air to retain the enhanced mid-tropopsheric ozone mixing ratio's observed inside the equatorial trough region. Because photochemical production of ozone is too slow (See chapter 5), an ozone source, located outside of the convective region, is required that supplies ozone to the middle troposphere of the convective region. Since transport from non-convective to the convective region, caused by radiative cooling in clear air,must be inclined, the ozone source to the middle troposphere of the convective region must be the upper troposphere, or even the stratosphere, of non-convective regions.

Figure 6.6 (Panels A-D): *Vertical profiles of ozone (thick solid line), temperature (dotted line), relative humidity (thin solid line) and moist static energy (thick broken line) obtained during ANT-VII/1*
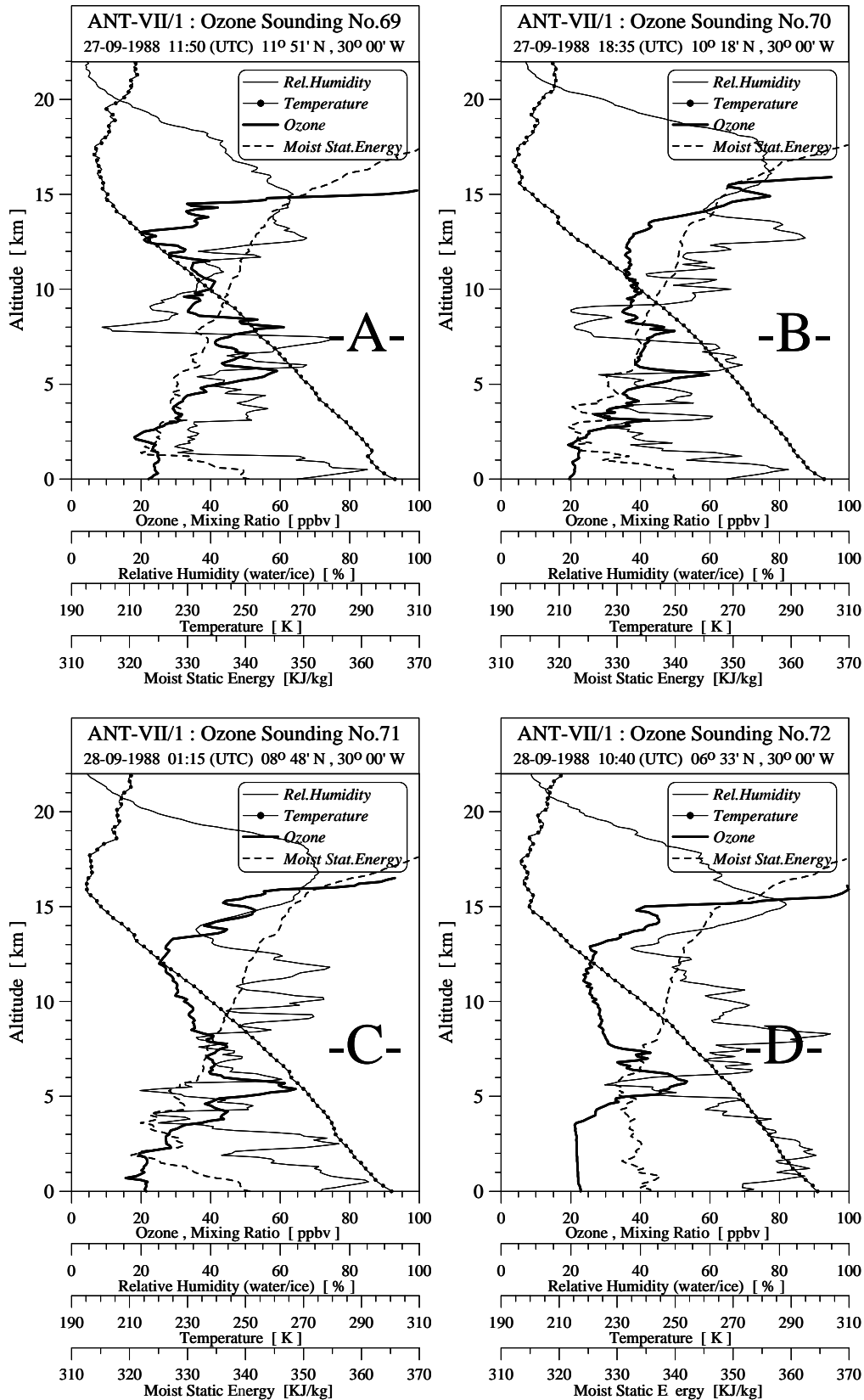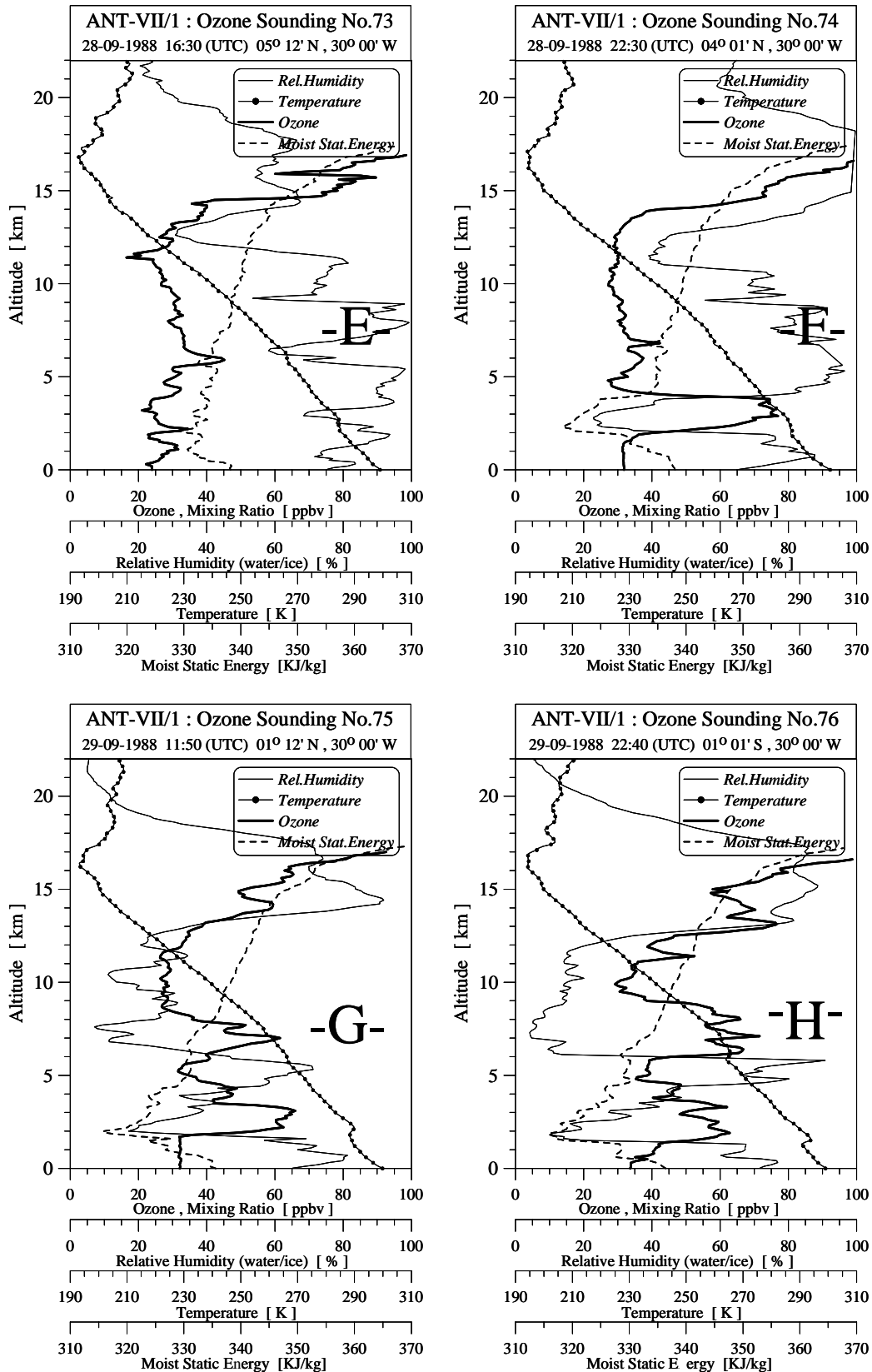
Figure 6.6 Continued (Panels E-H): *Vertical profiles of ozone (thick solid line), temperature (dotted line), relative humidity (thin solid line) and moist static energy (thick broken line) during ANT-VII/1*

The ozone cross section (Figure 6.5) suggests that the cross sectional extent of a large convective cell in the equatorial trough between 0 and 20ºN can be approximately contoured by the 40 ppbv isoline. This area will be abbreviated as MCC (Mesoscale Convective Cell) and its border represented by the fat contour line in figure 6.5. The envelope of MCC virtually describes the overall extension of a mesoscale cluster of cumulonimbus convective cells. The shape of the 40 ppbv contour line shows that layers with enhanced ozone values, observed in individual profiles, are caused by the confluence of air masses with high ozone levels into the MCC. This confluence appears as kind of a constriction of the MCC in about 3-7 km altitude. This means that the convergence of air masses is not only limited to the MBL but extends up to an altitude of 6-7 km.

6.3.3 Temperature Structure and "Mixing Barrier" at 14 km Altitude

The cross-section of the temperature distribution in the tropical region (see Figure 6.7) shows no significant differences between the inside or the outside the equatorial trough zone. Even inside the equatorial trough region with active deep convection the horizontal temperature variability is rather small. It is observed that in typical cumulus convection the differences between the temperatures inside the uplifting air parcel (T) and the "undisturbed" surrounding air (T_S) is generally small and of the order of magnitude of 1-2ºC [*Rogers and Yau*, 1992]. This indicates that even in synoptic disturbances, like the mesoscale convective cluster encountered in the equatorial trough during ANT-VII/1, slow radiative subsidence over large areas is sufficient to compensate for the fast convective upward flow over small areas [e.g. *Holton*, 1979].

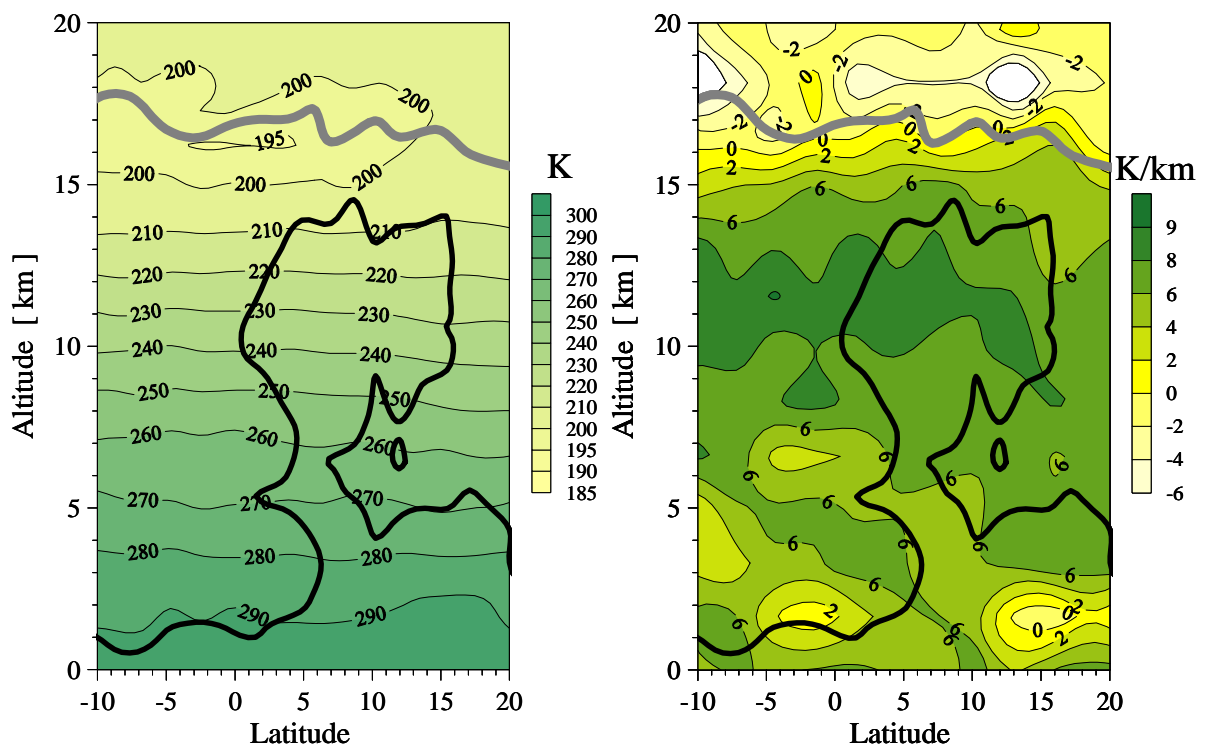
Figure 6.7: *Cross sections of the latitude/altitude distribution of temperature (left diagram) and lapse rate (right diagram) over the Central Atlantic derived from ozone/humidity-soundings made during ANT-VII/1 in the tropical region along the 30ºW meridian. The fat grey line is the tropopause and the fat black line the 40 ppbv ozone contour line of the MCC (Mesoscale Convective Cell)*

The atmospheric lapse rate (defined as –dT/dz) is shown in the right diagram of Figure 6.7. In the lower troposphere the lapse rates are moist adiabatic with values near 5-6 K/km, then veer toward the dry adiabatic lapse rate of about 9-10 K/km above about 8 km altitude. This resembles the fact that above 8 km altitude the water content becomes scarce. However, strong infrared emission by water vapor cools up to about 13-14 km altitude achieving a zero net heating level [12] (See also Chapter 2, Figure 2.9). At this altitude level the lapse rates begin to decrease again which corresponds with the top of the deep convective cell marked by the 40 ppbv ozone mixing ratio.

During ANT-VII/1 the deep convection clearly did not penetrate above 14 km altitude. This is also anticipated from thermodynamic reasoning since it is near the altitude at which the moist static energy (Q_{MS}) become equal to the highest moist static energy realized in the marine boundary layer (See right diagram of Figure 6.3: QMS $\approx$ 345-350 KJ/kg). This is near the maximum altitude which an air parcel from the marine boundary layer can reach by undiluted, non overshooting ascent [*Reid and Gage*, 1981]. This is in agreement with the recent knowledge that most tropical convection does not extend above about 14 km altitude [e.g. *Highwood and Hoskins,* 1998, *Folkins et al.,* 1999]. Based on ozone sonde observations made over Samoa, *Folkins*, in fact used the term "barrier of vertical mixing" to describe the rapid falloff of convective detrainment above 14 km altitude.

Between $\approx$14 km and the tropical tropopause at $\approx$17 km, there is a transition zone, the so called Tropical Transition Layer (TTL) in which air starts to assume more and more the physico-chemical characteristics of stratospheric air [*Sherwood and Dessler, 2000*]. This is also reflected in the vertical ozone distribution observed during ANT-VII/1 (See Figure 6.5) whereby ozone rapidly increases with altitude. However, it is unclear whether the ozone enhancements observed in the TTL have a photochemical origin attributed to net production during slow ascent through positive radiative heating [*Folkins et al.,* 1999] or a stratospheric origin associated with breaking equatorial Kelvin waves which result in a downward mixing of stratospheric air into the upper troposphere [*Fujiwara et al.,* 1998]. However, on the other hand, it is also well known that convection can occasionally reach the altitude of the tropopause or even higher [*Danielsen,* 1993]. The still unresolved question is whether the relatively infrequent penetrations above about 14 km altitude are sufficient to influence the physics and chemistry of the atmosphere above this level.

6.3.4   Humidity in Relation to Entrainment and Detrainment

Figure 6.8 shows the meridional distribution of relative humidity for the equatorial region between 10°S and 20°N for the ANT-VII/1-mission. From the shape of the contour lines of the relative humidity, particularly of the contour lines of sub-saturated values of 60 - 90 % RH at 1-2 km altitude, it is clearly depicted that the convergence of moisture is nevertheless limited to the convective boundary layer of the trades. This part of the convergence, namely the converging trade wind flow in the convective planetary boundary layer, is mainly responsible for the convergence of moisture in the ITCZ and provides the necessary latent heat supply to maintain the deep convection in the ITCZ.

The fact that the ozone mixing ratio in the MCC above the region of convergence are higher as in the lower part near the surface implies a substantial entrainment of low/mid tropospheric air into the MCC and, consequently, that the rising saturated, ozone deficient, air parcels in

---

[12] Above Z$\approx$14 km ($\approx$200 hPa) the emission from water vapor becomes less important than the emission from CO_2 because the saturation water vapor pressure is so very low at the low temperatures above 200 hPa.

the hot towers are diluted by mixing in of surrounding air with relatively higher ozone levels. From the slope of the individual profiles presented in Figure 6.6 it is seen that the increase of ozone in the middle/upper part of the MCC mainly occur just above the layer with the enhanced ozone values in the middle troposphere, while stays fairly constant in the upper part. From the detailed cross section of ozone and relative humidity (Figures 6.5 and 6.8) it is also seen that the entrainment of air with enhanced ozone values of 50-70 ppbv is accompanied with low relative humidities of 20-40% RHI.

Because the mid-tropospheric air is relatively dry, this entrainment will require considerable evaporation of liquid water to bring the mixture of cloud and environment air to saturation. It will thus reduce the buoyancy of the cloud air, and may in fact produce negatively buoyant convective downdrafts if there is sufficient evaporative cooling.
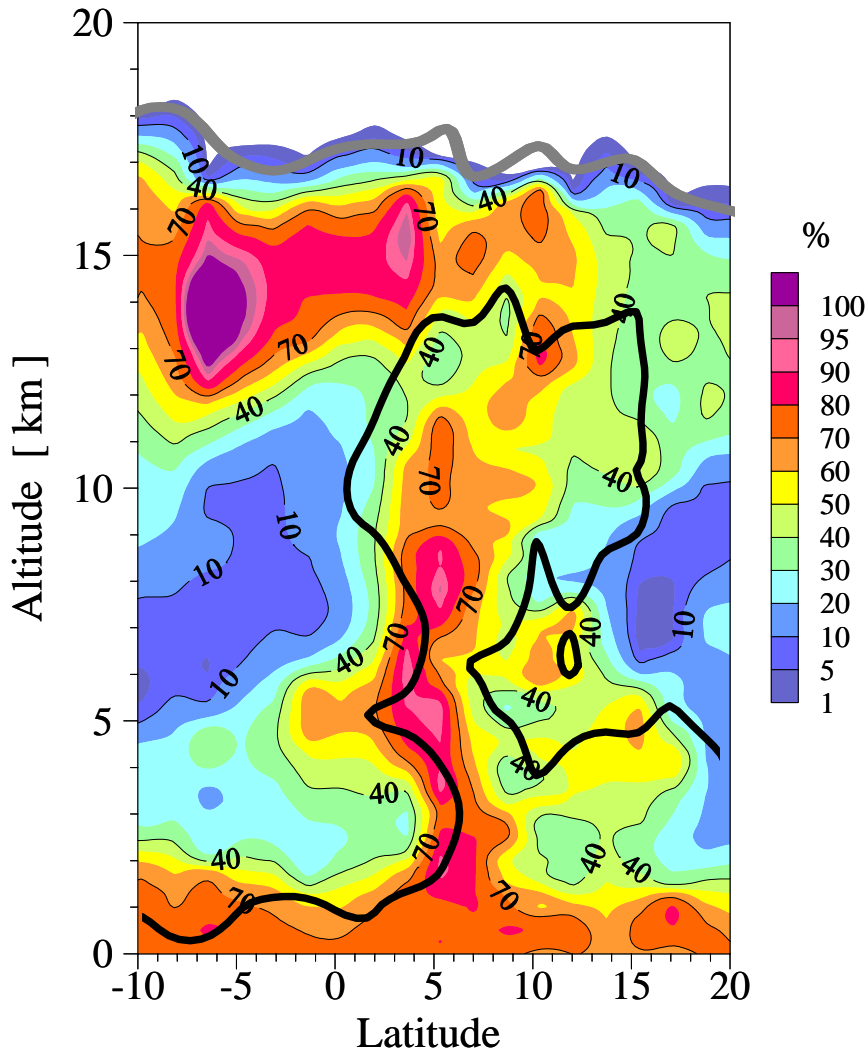
Figure 6.8: *Cross section of the latitude/altitude distribution of relative humidity over ice over the Central Atlantic derived from ozone/humidity-soundings made during ANT-VII/ in the tropical region along the 30°W meridian. The fat grey line is the tropopause and the fat black line the 40 ppbv ozone contour line of the MCC (Mesoscale Convective Cell)*

As a buoyant parcel ascends, mixing typically occurs through the parcel boundaries as a result of turbulent motions, which is called entrainment. Since the environmental air with temperature T_e and water vapor mixing ratio q_e is typically cooler and drier than a rising saturated parcel with temperature T and water vapor mixing ratio q_s , entrainment will lower

the buoyancy B of the parcel ($B \approx (T-T_e)/T$)) and reduce the amount of condensed water through evaporation to remain saturated conditions. The evaporative cooling caused by entrainment will decrease the buoyancy. Thus, the equivalent potential temperature θ_e in an entraining convection cell will decrease with height z than remaining constant according [e.g. *Holton*, 1992]:

$$\frac{1}{\theta_e} \cdot \frac{d\theta_e}{dz} = -\frac{1}{M} \frac{dM}{dz} \cdot \left[\frac{L_c}{c_p \cdot T} \cdot (q_s - q_e) + \frac{T - T_e}{T} \right] \qquad [6.3]$$

whereby L_C is the latent heat per unit mass of air in the cloud, c_p is specific heat at constant pressure while M is the mass of saturated cloud air and dM/dz is the change of mass through entrainment with altitude.

To achieve positive buoyancy, c.q. $T>T_e$, and since $q_s \geq q_e$ the terms in the square brackets will be positive and while the entrainment factor $(1/M)(dM/dz)$ is positive the equivalent potential temperature of the cloud air must decrease with height. In cumulus clouds $T-T_e \approx$ 1°C such that the first, evaporative cooling term in equation is the dominating factor in lowering the equivalent potential temperature [*Rogers and Yau*, 1989]. *Brown and Zhang* [1997] showed that the entrainment of dry air above the boundary layer could even discourage the growth of deep convective clouds by depleting parcel buoyancy. However, in case of mesoscale clusters of cumulonimbus clouds present in the ITCZ the central core updrafts are protected from entrainment by the surrounding cloud air so that they can penetrate nearly to the tropopause without dilution by environmental air [*Holton*, 1979]. Nevertheless, comparing the low tropospheric ozone values in the MBL with the about a factor 1.5-2 higher values in the upper part inside the MCC (See also Figures 6.5 and 6.6) it is obvious that the strength of entrainment must be comparatively large.

Although, all of the vertical profiles of ozone measured in the equatorial trough zone (Figure 6.6) show the effect of entrainment by the increasing mixing ratio of ozone above an altitude of about 9 km, there is only one profile, obtained at 5°N (Figure 6.6-E) that shows a fairly constant mixing ratio of ozone throughout the entire troposphere which indicates that almost no mixing, i.e. entrainment had taken place. This can also be concluded from the slope of the moist static energy which shows only a very weak minimum in the lower troposphere and which is thus a further indication of very little entrainment in this part of the ITCZ. Further, the sudden drop of the air temperature near the surface (Figure 6.9) from 299 down to 295.5 K between 5°15' N and 6°N in coincidence with relative humidity increases up to saturation were caused by evaporation of rain droplets during the heavy rains occurring at that time [*Behr et al*, 1989] indicates that this ozone sounding was made just after the ship had passed an active deep convective event. Deep convective towers at the end of their life cycle are at a dissipating stage that is characterized by precipitation with strong cooling effects through evaporation of hydrometeors and associated downdrafts.

The contours of the MCC presented as the 40 ppbv isoline in the ozone cross section in the equatorial region show that, above the region of convergence the 40 ppbv ozone contour line of the MCC also maps the divergent outflow regime of deep convection. This is seen in the upper troposphere between 9 and 14 km altitude where the lateral broadening of the MCC marks the divergent outflow due to detrainment of deep convection in these altitudes. As figure 6.8 shows that the divergent part of the MCC has its maximum width at an altitude between 10 and 12 km. This suggests that the detrainment is most effective at this altitude

level. Assuming that the detrainment flow is initially saturated, there must also be significant subsiding motion to both sides of the high humidity core as can be inferred from low relative humidities to both sides of the central core.
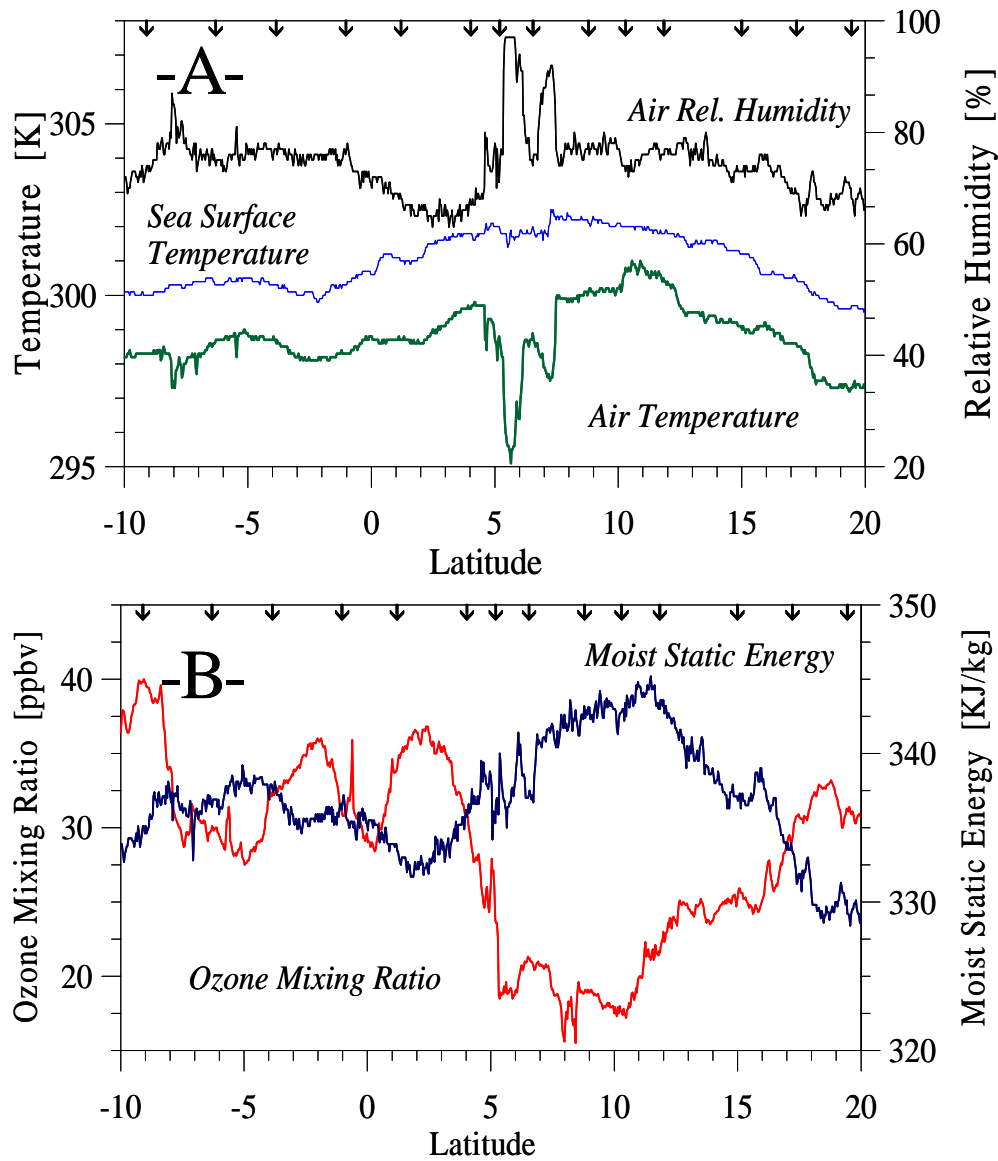
Figure 6.9: *Latitudinal variation of sea surface temperature, surface air temperature and relative humidity obtained during ANT-VII/1 cruise in September/October 1988. Arrows at the top of the panel mark individual ozone/humidity soundings*

Assuming that no mixing of the air parcels occurs this agrees very well with the theoretical findings of *Mapes et al.* [2001] who showed by using a radiative transfer model that radiative driven subsidence can dry the upper troposphere very rapidly from 100% RH down to 50% RH within one day (See also Figure 2.9).

6.3.5 Mean Vertical Profile of Ozone and Humidity in Convective Areas

The means of the ozone, relative humidity, temperature and moist static energy vertical profiles in the convective equatorial trough between $0^{o}N$ and $12^{o}N$ during ANT-VII/1 are displayed in the left panel o f Figure 6.10.

Figure 6.10: *Mean vertical profile of ozone (thick solid line), temperature (dotted line), relative humidity (thin solid line) and moist static energy (thick broken line) derived from the soundings made in the convective equatorial trough between $0^{o}N$ and $12^{o}N$ (left diagram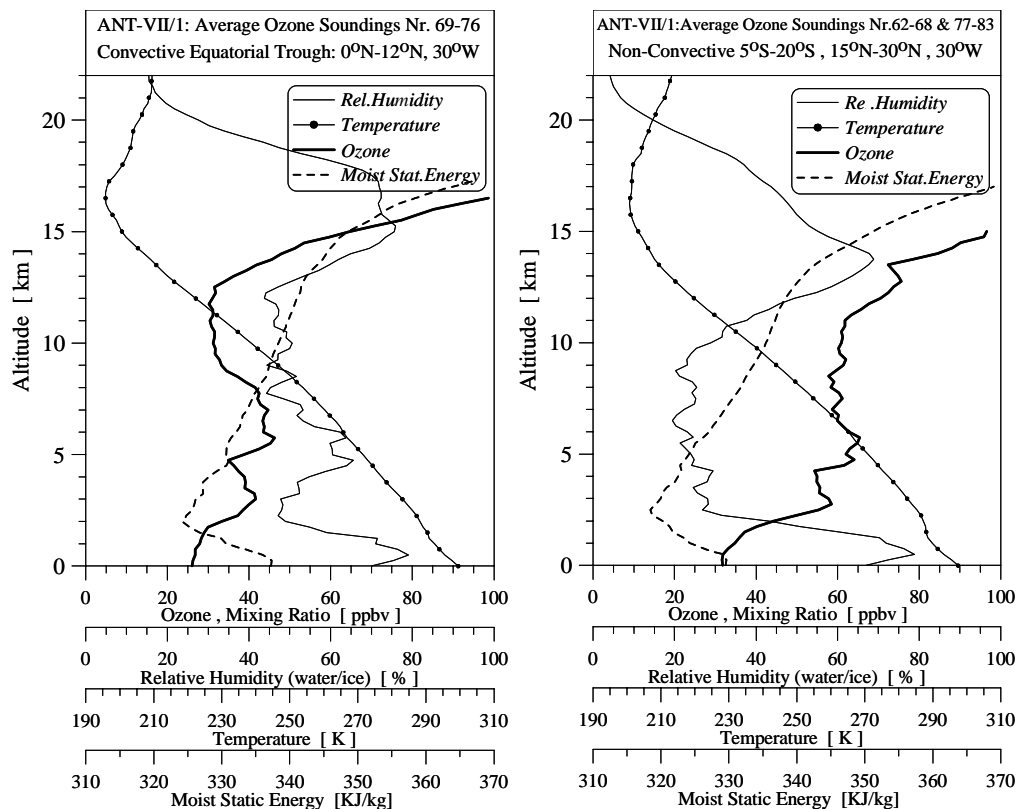) and in the non-convective (c.q. subsidence) regions $20^{o}S$-$5^{o}S$ & $15^{o}N$-$30^{o}N$ (right diagram) during ANT-VII/1.*

Characteristic for the mean ozone profile are low mixing ratios near the surface, enhanced values in the middle troposphere and low values in the upper troposphere at 8-13 km altitude while further above a steep increase with altitude in the transition layer (TTL) is observed. This shows that the convection reaches an altitude of about 13-14 km and bypasses the middle troposphere. The relatively low mixing ratios of about 40-45 ppbv at 8-12 km altitude are in good agreement with ozone climatologies measured from aboard passenger aircraft at the edge of convective outflow at about 10-11 km altitude in this tropical region ($0^{o}N$-$10^{o}N$) over the Central Atlantic [*Nawrath, 2002*].

An interesting feature is the dip in the ozone profile at about 5 km altitude which might indicate that convection has detrained ozone deficient air from the surface at his altitude level. This could be explained by the fact that the level is centered at around $0^{o}C$ temperature level which is often associated with temperature inversions caused by the melting of falling hydrometeors [*Johnson et al., 1996*]. The inversion can cause detrainment of uplifted air with cloud material and most likely explain the local increase of relative humidity and moist static

energy observed at this level (See left diagram Figure 6.10). This detrainment effect of low ozone associated with a temperature inversion at about 0°C and almost saturated relative humidities at about 5 km altitude is very pronounced present in the ozone soundings No. 75 and 76 shown in Figure 6.5 in diagram G and H respectively.

Despite of the fact that moisture is driving deep convection, the mean relative humidity profile in this active convective region is far from saturation, which implies efficient drying of air parcels after they have been saturated during uplifting, particularly in the upper troposphere. The increasing RH above 14 km altitude in the TTL is most likely caused by the slow uplifting of air due to the weak radiative heating in the TTL [e.g. *Sherwood and Dessler,* 2000, *Mapes et al.,* 2001]. This finally can form thin cirrus clouds which are typically observed at the tropopause and, although speculative, could influence stratospheric humidity. However, it is to be noted that the RH-measurements obtained in the UT/LS region during ANTVII/1 are suffering a strong broadening effect on the vertical profiling due to the very slow response time of the Humicap-A RH-sensor of the RS80 radiosonde at the extreme low temperatures of -60°C to -80°C in the tropical tropopause region (See also Section 3.3.3).

6.4   Large Scale Subsidence Exterior to the Equatorial Trough Zone

Figure 6.11 shows the mean vertical profiles of ozone, relative humidity, temperature and moist static energy in the non-convective regions in the tropics in the SH: 20°S-5°S (left diagram) and in the NH: 15°N-30°N (right diagram) during ANT-VII/1. Non-convective tropical regions are characterized by large scale subsidence. In accordance with that the lower/middle troposphere was relatively dry (RH < 20-30%). However, above 8-10 km altitude RH is increased with altitude with values of 60-80% in the TTL region, very similar to the observations made in the trough region (see previous section).

In section 5.3.5 it is shown that in the SH the enhanced ozone values observed in the troposphere have a photochemical origin associated with biomass burning emissions. Above 8 km the air masses were been transported by westerlies which advected air from the South American biomass burning regions while in the lower/middle troposphere the air masses originated from the east where African biomass burning regions are located. In both cases ozone rich air was transported to the free troposphere by convective processes over both continents followed by large scale quasi-horizontal transport. In the NH the ozone profile above 5 km altitude is rather constant up to 12-13 km, while above ozone fits more to stratospheric values.

The right panel of Figure 6.10 represents the mean vertical profile of ozone, relative humidity, temperature and moist static energy from the non-convective regions in the SH and NH. The virtually constant mixing ratio above 2-3 km altitude and up to 12-13 km implies that no significant photochemical changes (production or destruction) occur during large scale subsidence of air masses in the middle/upper troposphere This in contrast to the low troposphere where, due to efficient net photochemical destruction, ozone decreases very quickly to almost half of the ozone levels observed in the middle/upper troposphere.
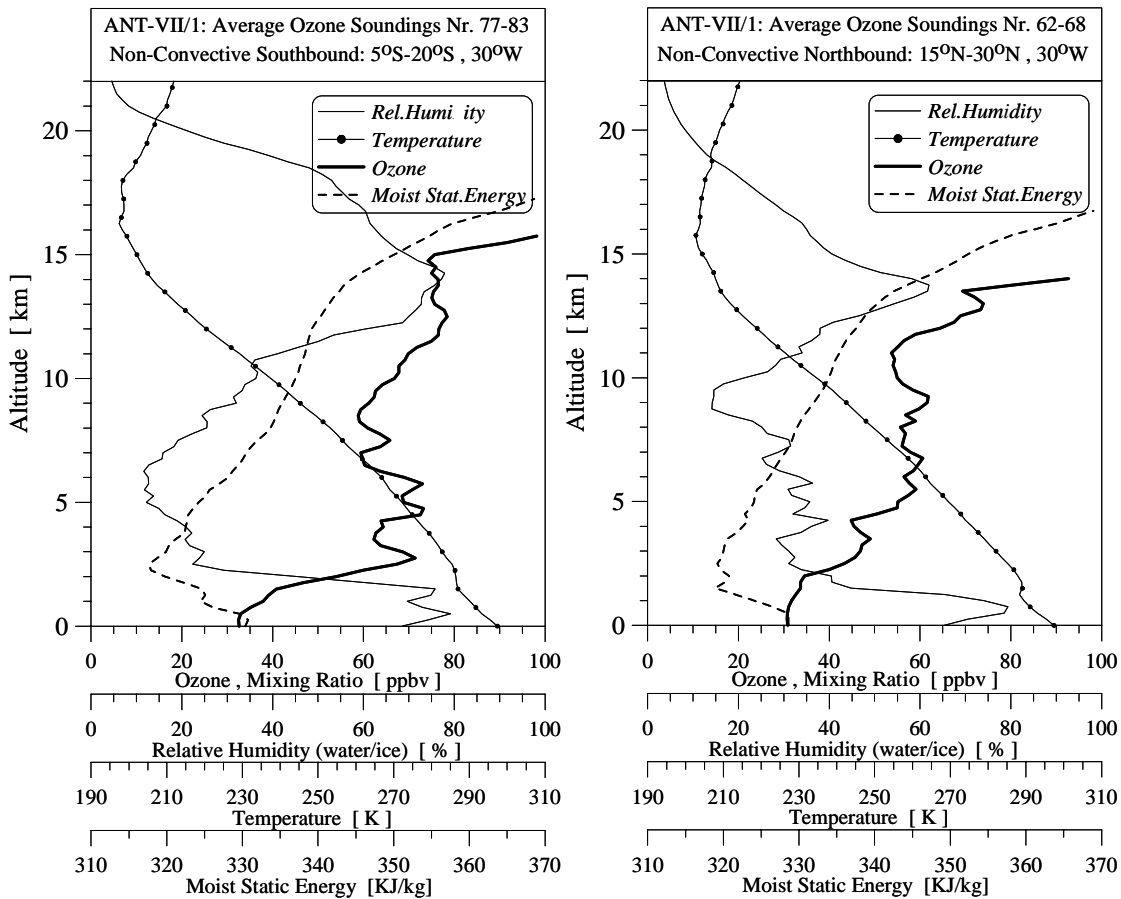
Figure 6.11: *Mean vertical profile of ozone (thick solid line), temperature (dotted line), relative humidity (thin solid line) and moist static energy (thick broken line) derived from the ozone/humidity soundings made in the non-convective (c.q. subsidence) regions $20^o S$-$5^o S$ (left diagram) and $15^o N$-$30^o N$ (right diagram) during ANT-VII/1*

6.5   Large Variability of Relative Humidity

From the cross-sections of the latitude/altitude distribution of relative humidity (See Figure 4.11 or 6.8) it is seen that the relative humidity in the tropics can vary from extremely low values of less than 10% RHI in the middle troposphere to saturated values. This large variability of RHI is demonstrated in more detail in Figure 6.12 showing histograms of relative humidity over ice for the convective region in the equatorial trough ($0^o N$-$12^o N$) and the non-convective regions in the SH ($5^o S$-$20^o S$) and NH ($15^o N$-$30^o N$) in the lower/middle troposphere (Z=2-8 km) and middle/upper troposphere (Z=8-14 km), respectively. In non-convective regions, characterized by large scale subsidence, the distributions show only dry branches with mean values for RHI of about 30±20 % in the NH (Z=2-14 km) and 18±16 % in the SH at Z=2-8 km. However, in the SH at higher levels the air is more variable, namely from dry to almost saturated. This is probably due to the fact that relatively wet air was transported by fast strong westerly winds in the upper troposphere (See Figure 5.13) which had traversed convective outflow regions located over South America (See lower panel in Figure 6.4). At horizontal wind speeds of more than 100 km per hour the initially saturated air masses from the convective outflow regions of South America reach the Central Atlantic within less than one day such that during this transported the air masses remain relatively wet.
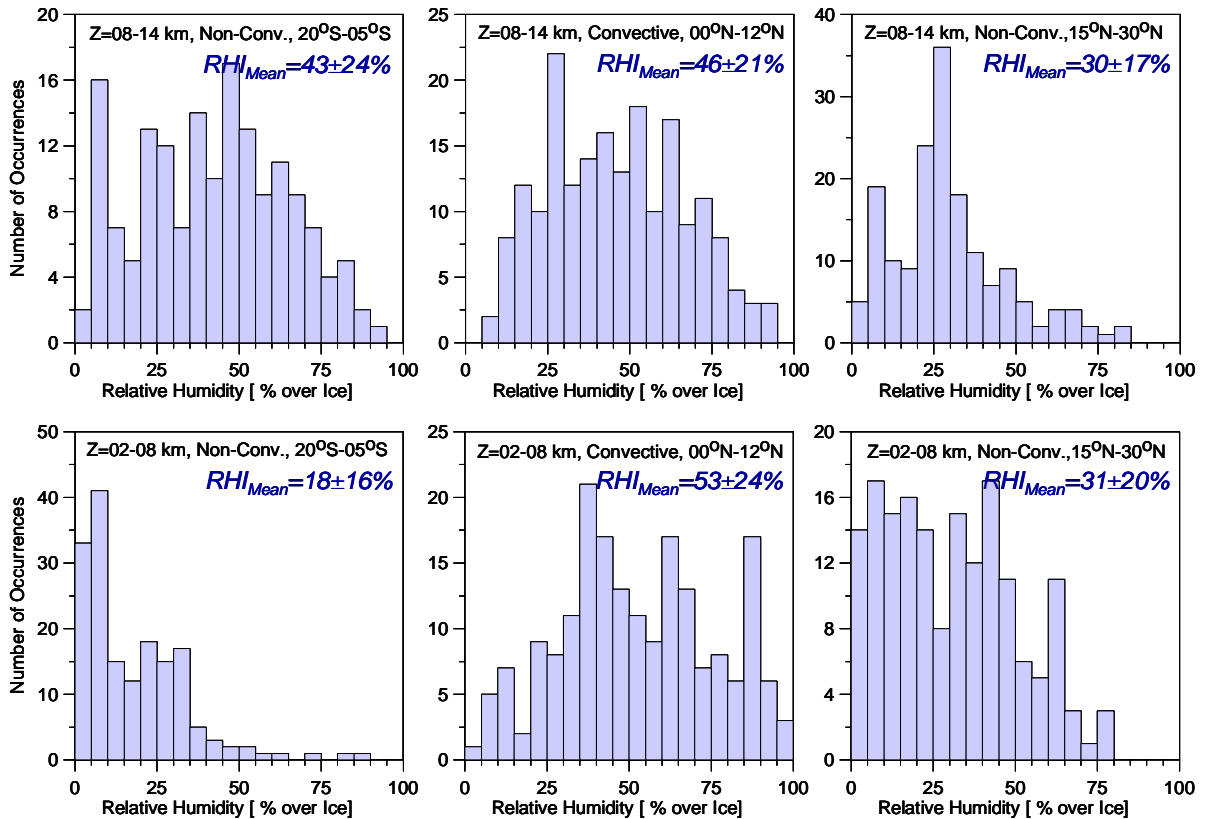
Figure 6.12: Histogram of relative humidity (over ice) in tropospheric tropics in the convective area (middle panels; equatorial trough: 0^oN-12^oN) and the non-convective areas in SH (left panels; 5^oS-20^oS) and NH (right panels; 15^oN-30^oN) at two altitude regions: Z=2-8 km (lower panels) and Z=8-14 km (upper panels) derived from humidity soundings made during ANT-VII/1. The mean values are given with ± one standard deviation.

Although, the RHI-histogram in the SH at Z=8-14 km was measured in a non-convective region it shows large similarities with the RHI-histograms derived for the convective region in the equatorial trough, particularly in the Z=8-12 km altitude region. The convective RHI-histograms in the divergent part of the MCC (Z=8-14 km) shows a broad distribution and tends to have a bi-modal character with a dry and wet branch. This bi-modality implies sharp gradients between dry and moist regimes in the divergent part of the MCC and that a substantial part of the detrained air dries rather fast.

The typical bi- modality of RHI-distribution in the tropics is qualitatively also found in radiosondes [*Brown and Zhang*, 1997], satellite [*Soden and Bretherton,* 1993] and aircraft [*Nawrath,* 2002] observations. The bi-modality suggests that the radiative drying time after an injection of moisture by convection is short compared to a homogenizing time, whether physical (mixing) or mathematical (averaging). This has been quantitatively demonstrated in a recent experimental study about the evolution of the relative humidity in the outflow region of cumulonimbus clouds [*Nawrath,* 2002]. The study showed that under clear sky conditions the relative humidity in an air parcel in the outflow of a Cb-convection declines very quickly from saturated values at the outflow edge of the anvil cloud down to about 50% RHI within less than 1 day.

Climate models have difficulties to reproduce the observed bi-modality. This also means that there is a strong potential significance of the bi-modality in water vapor feedback to climate variation [*Zhang et al.,* 2003]. However, the origin of the bi-modality of UTH in the tropics is not understood at all and at the present subject of a controversy debate about climate change and the role of convective processes.

6.6   Mid-Tropospheric Ozone

A characteristic feature of the vertical ozone profile observed in the convective region of the equatorial trough as had been shown in the right diagram of Figure 6.10 is a shape with low values near the surface, a relative maximum in the middle troposphere at around 6-7 km altitude, a relative minimum in the upper troposphere at about 12-14 km altitude and subsequent increase towards the tropopause. In regions of active deep convection such as in the equatorial trough zone during ANT-VII/1 this is the direct result of Cb convection lifting ozone poor air from the MBL into the upper troposphere and thereby bypassing the middle troposphere. From the results presented in the previous chapter (See section 5.3.5) it could be concluded that the enhanced ozone values might have either a photochemical continental or a stratospheric origin.
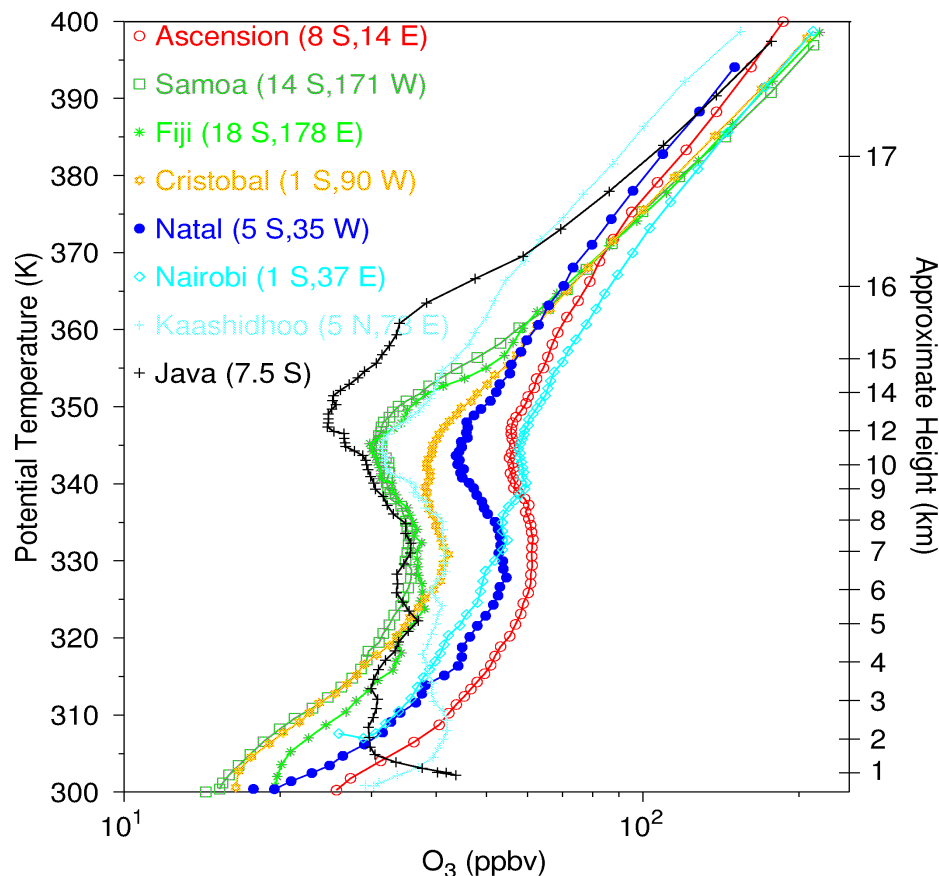

Figure 6.13:   *Mean annual vertical ozone profile for different SHADOZ-stations [Source: Folkins et al. 2003]*

However, interesting in this context is a recent publication by *Folkins* et al. [2003] who studied the mean annual vertical ozone profiles at different locations in the tropics as obtained from the SHADOZ ozone sounding network (see Figure 6.11) which reveal a more or less S-shape. *Folkins* was able to reproduce the main features of the observed S-shaped vertical ozone profiles by employing a 1D-chemical model of the tropics in which the mass fluxes were derived from clear sky radiative heating rates while any mass flux divergence was assumed to be balanced by convective detrainment The only free parameter in their model is the mean ozone mixing ratio of air which detrains from deep convective clouds at 12-14 km altitude. They found good agreement (on a logarithmic scale) of modeled with observed profiles. The model calculates a steady state situation in which the profile is adjusted from detrained air with a given ozone mixing ratio (free parameter), which is subsiding from 12-14 km altitude down to the surface. During this subsidence there is a net ozone production (1-2 ppbv per day) in the upper part (Z=6-14 km) and a net destruction (1-2 ppbv per day) in the lower part (Z=0-6 km). Above 14 km towards the tropopause vertical exchange is slow and the residence times of air parcels with respect to a vertical displacement become larger than 100 days at an altitude of about 16-17 km. It is concluded that the calculated ozone profile is entirely determined by in-situ photochemistry. By a proper choice of the mean ozone mixing ratio of detraining air at 12-14 km altitude the modeled vertical ozone profile could be adjusted to the observed profiles.

The Folkins model neglects the fact that the locations of convection and subsidence in conjunction with the locations of major photochemical ozone sources and sinks are geographically separated by large distances. Ozone is predominantly formed photochemically in the PBL over the continents while photochemical destruction occurs mainly, after long range transport with subsidence, in the oceanic MBL whereby the large scale Walker circulation plays an important role (See also Section 2.2.6). Folkins model neglects the influence of large scale horizontal transport of ozone and its photochemical precursors. In doing so, the model fully neglects the lateral mass transport between the tropics and extra-tropics, which is necessary to equalize the pole-equator radiative energy imbalance (see Section 2.1.1).

In order to see that the Folkins model is non tenable consider Figure 6.14: This figure shows a 2 years (1999-2000) evolution of the vertical ozone distribution at two SHADOZ sounding sites, Natal 5°S, 35°W and Ascension (8°S, 14°E), respectively. Both stations are also included in Figure 6.11. Both distributions clearly demonstrate that the vertical distribution is influenced by either convective events with low ozone values (30-40 ppbv) in the upper troposphere and enhanced ozone values in the middle troposphere or by subsidence with high ozone values (60-80 ppbv) throughout the entire free troposphere. However, in case of subsidence the ozone concentration is more or less constant or increasing with altitude throughout the entire troposphere, which indicates that during subsidence local formation of ozone, cannot be significant. These observations are in agreement with the observations made during ANT-VII/1: (i) As shown in Figures 6.6 and 6.10 (left panel) vertical ozone profiles under the influence of recent deep convection show a profile which is entirely the result of fast vertical dynamics which redistribute low ozone from the surface into the upper troposphere while bypassing the middle troposphere (See Section 6.3.4). (ii) The vertical ozone distribution under large scale subsidence (See Figures 6.10 and 6.11) shows a rather constant vertical profile and thus no evidence for any significant influence of in-situ photochemical ozone formation (See section 6.4).

The annual mean profiles shown in Figure 6.13 are actually derived from the individual soundings composing the distributions presented in Figure 6.14 and are thus the resulting in a net profile obtained from convective and non-convective profiles. Only the convective profiles have a typical S-shape and can thus contribute to the S-shape of the annual mean profile. In other words it is indicated that the more convective profiles are encountered, the more pronounced the annual S-shape would be. This effect indeed can be derived from Figure 6.13 and 6.14 where the Natal station shows more convective activity and thus a stronger S-shaped ozone profile than the Ascension station which is more often under the influence of large scale subsidence.
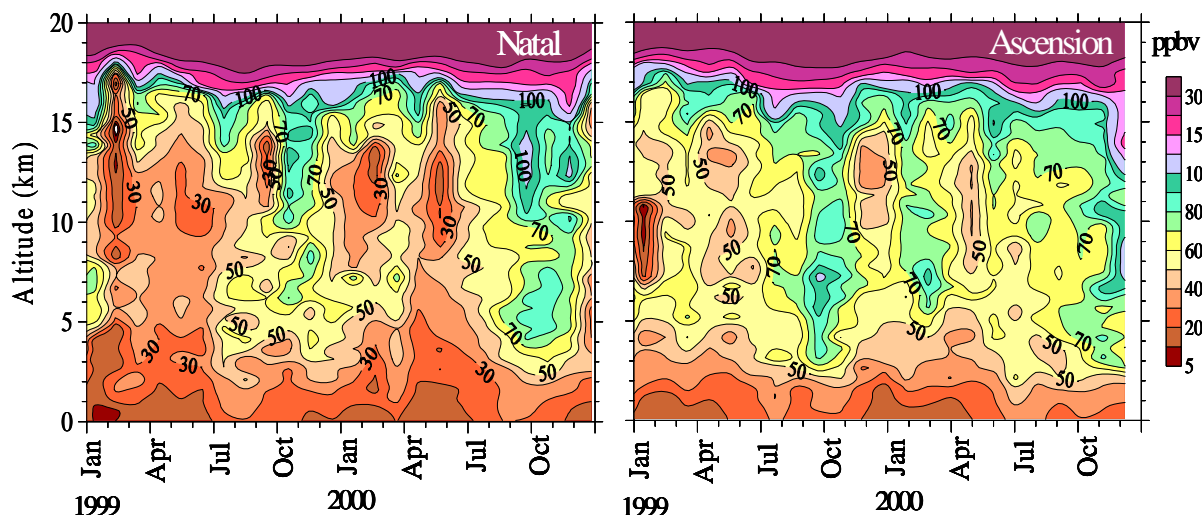

Figure 6.14: *Evolution of the evolution of the vertical ozone distribution at two SHADOZ sounding sites, Natal (5^oS, 35^oW) and Ascension (8^oS, 14^oE) over the period 1999-2000 obtained from regular ozone soundings of about one per week [Source: Thompson et al., 2003].*

It is concluded that the S-shape ozone profile can be an indication for deep convection as the result that convection lifts ozone deficient air from the lower troposphere, bypassing the middle troposphere, and is expelled over the height range that the convection reaches. However, there is no vidence that the enhanced ozone values in the mid-troposphere are caused by local photo chemical production as *Folkins et al.* [2003] is suggest, but most likely have a photochemical continental or a stratospheric origin as be shown previously in section 5.3.7 [*Roelofs et al.*, 1997-b].

The general nature of exchanges of tropospheric air between the Tropics and midlatitudes is becoming well known [e.g. *Newell et al.,* 1992, *Pierrehumbert and Yang,* 1993, *Yang and Pierrehumbert,* 1994]. It is most likely that the subsiding outflows of anti-cyclonic systems which are typically centered at about 30[o]N at 30[o]S in the NH and SH respectively [*e.g. Hastenrath,* 1995], provide upper tropospheric air with relatively high ozone and low humidity from the sub-tropics towards the equatorial trough [e.g. *Yang and Pierrehumbert,* 1994]. During this subsiding lateral transport, which occurs on a time scale of less than one week, photochemical formation of ozone (1-2% ozone per day) is too slowand thus only has a minor impact on the ozone content of the transported air masses.

Mass Fluxes in Cb-Convection in the Equatorial Trough Zone

In this section the ozone distribution obtained during the ANT-VII/1 cruise is used to quantify the individual contributions to the net upward mass fluxes originating from a) the convective boundary layer and b) from entrainment. This is done in a heuristic model approach that is displayed in Figure 6.15.
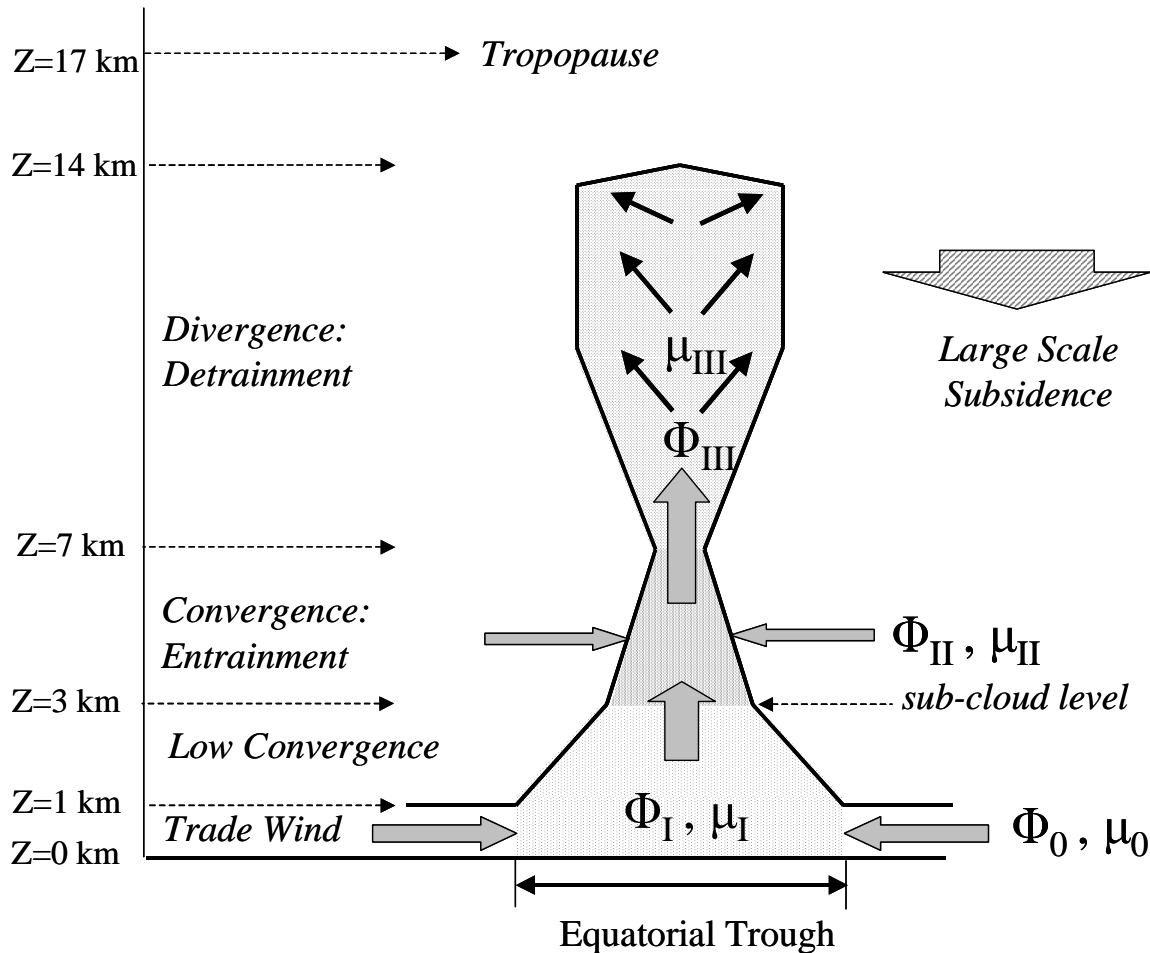
Figure 6.15: *Heuristic model of the mesoscale convective cell (MCC) in the equatorial trough*

The deep convective cell is divided in 3 compartments: The first (lower) one ($0 < Z < 3$ km) comprises the regime of the trade wind inflow[13]. The second part ($4 < Z < 7$ km) describes the entrainment (confluence) of free tropospheric air into the deep convective cell with a mass flow contribution Φ_{II}. The third part, Φ_{III}, ($7 < Z < 14$ km), the divergence zone, describes the outflow part which is also referred to as the detrainment part. Mass balance requires that $\Phi_{III}=\Phi_{I}+\Phi_{II}$

---

[13] Φ_1 = Total inflow towards the ITCZ within in the convective boundary layer. Mass balance requires that the horizontally converging Φ_1 flow results in an overall vertical directed mass flow of equal magnitude.

In the lower part between 5°N and 18°N ozone mixing ratios are about 20 ppbv, down from 30 ppbv, just outside the confluence region (Figures 6.5 and 6.10). This part of the equatorial trough zone is characterized by cumulus clouds. The air masses are well mixed in the sub-cloud layer as indicated by the constant ozone mixing ratio of 20-25 ppbv. The lower ozone mixing ratio in the sub-cloud layer is caused by photochemical losses at an increased residence time. Air from this lower part will be "pumped" in the upper parts of the deep convective cell. Only at locations with active deep convection the net result of these convective events is the upward flux Φ_1, which now can be determined by using the drop of ozone within this region compared to the region exterior. Therefore using a mass balance for ozone over the control volume in the lower part of the MCC marked by the latitude belt between 5 °N and 12°N and an altitude of 3 km. Thereby the losses of ozone will be equal to the difference of the input mass flow of ozone by the horizontal trades and the vertical output mass flow of ozone. The air and ozone mass balance equations for the lower compartment are respectively:

$$\Phi_O = \Phi_I \qquad\qquad [6.1]$$

$$\Phi_O \bullet \mu_O = \Phi_I \bullet \mu_I + \frac{\partial \mu_I}{\partial t} \bullet \rho_I \bullet V_I \qquad\qquad [6.2]$$

where Φ and μ indicate mass flow and ozone mixing ratio, respectively, ρ_1 is the average mass density of the air in the lower compartment of the MCC with a volume V_I and $\partial \mu_{I'}/\partial t =$ the net total photochemical loss rate of ozone.

The net upward flux from lower compartment is then expressed as:

$$\Phi_I = \frac{\frac{\partial \mu_I}{\partial t}}{(\mu_O - \mu_I)} \bullet \rho_I \bullet V_I \qquad\qquad [6.3]$$

This means that the inverse of the ratio of the net total relative photochemical ozone loss rate and the difference of the incoming and outgoing ozone mixing ratio can be seen as the evacuation time of the lower compartment of the MCC. With $\mu_0 = 30$ ppbv and $\mu_1 = 25$ ppbv, and a net total photochemical ozone loss rate of 2 ppbv/day this means an evacuation time of about 2-3 days for the convective boundary layer (lower 3 km) in the ITCZ. *Riehl and Simpson* [1979] derived a similar number from an estimate of the number of active hot towers and the vertical mass flux per hot tower.

To estimate the amount of entrainment the following air- and ozone mass balance equations for the compartments I & II are respectively:

$$\Phi_{III} = \Phi_I + \Phi_{II} \qquad\qquad [6.4$$

$$\Phi_{III} \bullet \mu_{III} = \Phi_I \bullet \mu_I + \Phi_{II} \bullet \mu_{II} \qquad\qquad [6.5]$$

The ratio of the trade wind flow and entrainment flow is thus given by:

$$\frac{\Phi_{II}}{\Phi_I} = \frac{(\mu_{III} - \mu_I)}{(\mu_{II} - \mu_{III})} \qquad\qquad [6.6]$$

With $\mu_I = \approx 25$ ppb, $\mu_{II} = \approx 60$ ppb and $\mu_{III} = \approx 35$ ppb, the ratio of entrainment flow to that of trade wind flow is estimated to be $\Phi_{II} / \Phi_I = 0.40$. The numerical value of this ratio is strongly dependent on the proper knowledge of differences of ozone mixing ratios ($\mu_{III} - \mu_I$) and ($\mu_{II} - \mu_{III}$). It cannot be expected that a single cruise can yield representative numbers, however it shows that, in mesoscale clusters of cumulonimbus convection as treated here, the entrainment flow above the sub cloud layer is large and almost of the same order of magnitude as the uplifted flow from below the sub cloud layer. This means that large amounts of air are entrained into the mesoscale clusters of deep convective cells. In other words a MCC as was encountered in the equatorial trough during ANTVII/1 was "pumping" substantial amounts of mid-tropospheric air to the upper troposphere.

The analysis also shows that convergence is not limited to low level frictional inflow in the planetary boundary layer, but extends up to nearly 400 hPa, which is the height where the hot towers achieve their maximum buoyancy [*Holton*, 1979]. Because the mid-tropospheric air is dry, this entrainment will require evaporation of liquid water in order to keep the mixture of cloud and environment air at saturation. It will thus reduce the buoyancy of the uprising air, and may in fact produce negatively buoyant convective downdrafts if there is sufficient evaporative cooling.

As a consequence that the flow of entrained mid-tropospheric air is comparably large to the upward flow from the low level convergence of the trade winds, the turnover time of air masses in the middle troposphere will be of the same order of magnitude as the 2-3 days of evacuation time of air masses below the subcloud layer (Z=3 km). This means that the enhanced ozone values observed in the middle troposphere in the convective equatorial trough can only be sustained at this level by an effective horizontal inflow from regions with enhanced ozone mixing ratios (e.g. upper troposphere or stratosphere).

6.8   Regulation of Deep Convection through Entrainment of Dry Air?

In the previous section it was shown that substantial amounts of dry air are entrained in mesoscale clusters of Cb convective cells. Particularly at the edge of the clusters of Cb-convective cells the entrainment of relatively dry air could have an attenuating effect on the strength of the convection and finally on its penetrating power to the upper troposphere. Therefore, the question arises in how far this entrainment of dry air can also have a regulating effect on deep convection. In other words, in how far the interaction of tropical deep convection with large scale dynamics can account for the possibility of a "dry air valve" on deep convection resulting not only from subsidence, but also from the lateral advection of dry midlevel air.

In mesoscale convective systems, it is known that once convection is initiated, dry mid-level air can be entrained into the system and enhance the strength of surface cool outflows that in turn enhance or disrupt the formation of new convective cells [e.g. *Zipser*, 1977, *Houze and Betts*, 1981, *Rotunno et al.*, 1988]. However, radar analysis indicates that dry layers and deep convective precipitation are negatively correlated over the convectively active warm pool [*Rickenbach and Rutledge*, 1998]. Satellite data also reinforce that deep convection is reduced during dry events [*Brown and Zhang*, 1997]. *Parsons et al.* [1994] noted that dry events tend to be associated with strong inversion near the top of the boundary layer, significantly inhibiting deep convection [*Kloesel and Albrecht*, 1989].

6.8.1   Impact of Large Scale Mid-Tropospheric Minimum of Moist Static Energy

In this context, one of the striking and largely unexplained characteristics of the low latitude troposphere is the mid-troposphere minimum in the moist static energy (Q_{MS}). The minimum of Q_{MS} and the existence of an apparently stable Q_{MS} gradient within the middle and upper troposphere create a situation that requires the concept of penetrative deep convection to explain the ubiquitous deep convective cloud systems of the tropics [*Riehl and Malkus*, 1958 and *Riehl and Simpson*, 1979]. The vertical transfer takes place in protected cores of cumulonimbus ascents whereby the moist static energy of the ascending parcel is conserved such that the ascending air "bypasses" the mid tropospheric in small "chimneys" and the Q_{MS}-minimum (see Section 2.1.2). Since deep convection from the sea surface to the upper troposphere occurs on a time scale of less than one hour, diabatic processes can be neglected and, consequently, Q_{MS} of a convective parcel should be conserved in the vertical at its surface value. However, this is only true for most recently deep convective events. The distribution of Q_{MS} shown in Figure 6.3 shows a large scale view and in case of older convective events diabatic processes can change Q_{MS}. Under clear sky conditions radiative cooling generally tends to decrease Q_{MS} by about 1.5 KJ kg^{-1} day^{-1} [*Mapes and Zuidema*, 1996].

Not considering the possibility of overshooting the neutral buoyancy level the equilibrium height of the ascending parcel can be obtained by considering it's surface values, $Q_{MS, Surf} \approx$ 345 kJ kg^{-1} in (see Figure 6.9) for ANT-VII-cruise) against Q_{MS} of the upper troposphere at a given altitude. The minimum in the vertical profile of the moist static energy ($Q_{MS, min} \approx$ 325-330 kJ kg^{-1}) is found around 600-700 hPa (see Figure 6.3) and above the minimum a steady increase of Q_{MS} with altitude is observed. Surface values of moist static energy ($Q_{MS,surf}$) are again reached in the upper troposphere, usually around 200 hPa (see Section 2.1.2).

Using tropospheric ozone as a quasi-conservative tracer of large scale transport, results from the Central Equatorial Pacific Experiment (CEPEX) indicated that dry, ozone rich, air from the upper troposphere is entrained into rising convection around the 700 hPa level (Θ = 320-330K) (*Kley et al.,* 1996, 1997). The CEPEX results, obtained in a zonal plane at 2°S, revealed that mixing of dry air of upper tropospheric origin with convective, high humidity, air occurs whereby the moist static energy (Q_{MS}) for convective elements is lowered, reducing their neutral buoyancy levels. The CEPEX ozone/humidity measurements did not pinpoint the origin of the dry, ozone rich, air.

Using the cross section of the latitude/altitude distribution of moist static energy (Q_{MS} in KJ/kg) in the equatorial region during ANT-VII/1 (September/October 1988) as shown in Figure 6.16 suggests that the minimum of Q_{MS} in the tropics can be explained by a lateral transport from the extra-tropics. This is supported from the corresponding enhanced ozone mixing ratios observed north and south of the equatorial trough (See Figure 6.4) which have most likely an upper tropospheric origin in the sub-tropics as previously was shown in sections 5.3.5 and 6.6. As a necessary mechanism to equalize the pole-equator radiative energy imbalance (see Section 2.1.1) the general nature of mass exchanges of tropospheric air between the Tropics and midlatitudes is well known [e.g. *Newell et al.,* 1992, *Pierrehumbert and Yang,* 1993, *Yang and Pierrehumbert,* 1994]. During the lateral transport towards the equatorial trough upper level extra-tropical air is subsiding to the lower-middle tropical troposphere. It is obvious that: the minimum of Q_{MS} around 600-700 hPa in the central maritime tropics is the result of advection and mixing of dry sub-tropical upper tropospheric air with humid low level tropical air.

However, the application of the ozone tracer to deep convection clearly reveals a remarkable fact, namely that a considerable large scale quasi-horizontal mass flow takes place above the MBL which supplies dry air to the convective cell. An equivalent estimate as above but for moist static energy can also be made with the result that the minimum of Q_{MS} is brought about by convergence and confluence of low Q_{MS} air from outside the MCC with high Q_{MS} air from the subcloud layer from within the MCC.

The results from the Atlantic cruise are analog to the CEPEX-results [*Kley et al.*, 1997] that high ozone/low humidity layers in the low troposphere in deep convective regimes are a common occurrence. The shape of the ozone isolines suggests that upper tropospheric air with relatively high ozone and low water vapor content had been transported from the sub-tropics to equatorial latitudes.
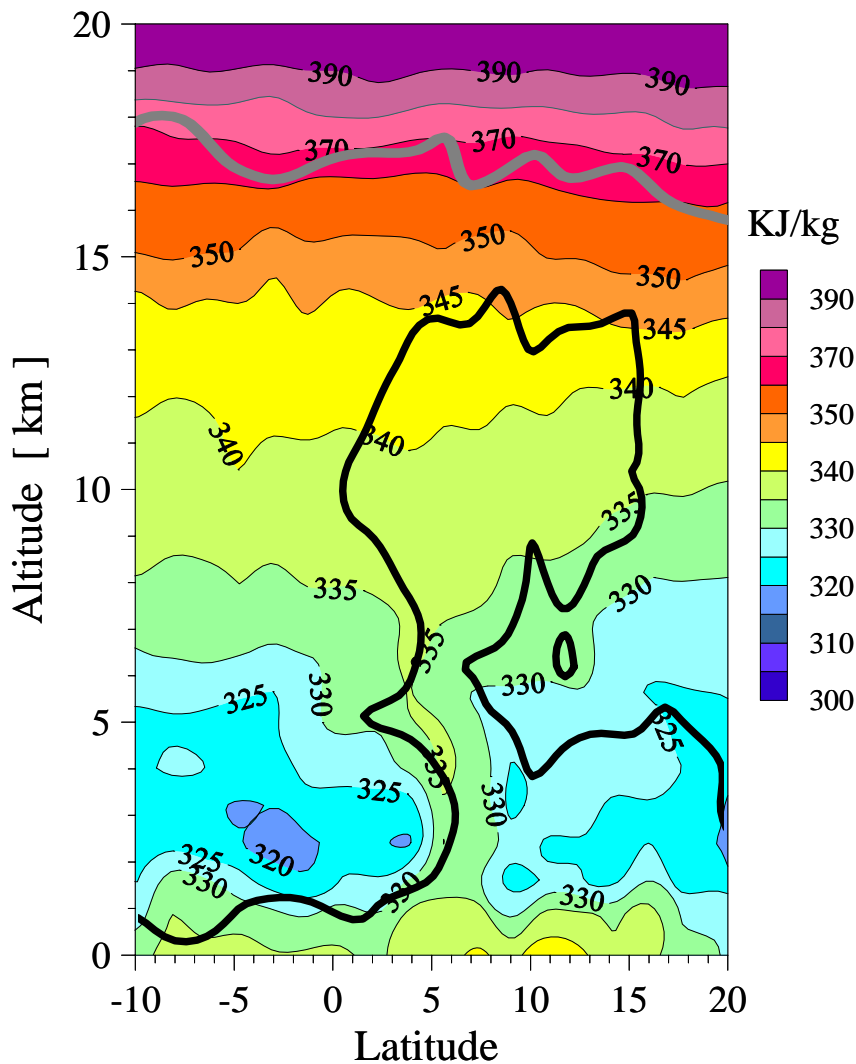
Figure 6.16: *Cross section of the latitude/altitude distribution of moist static energy (Q_{MS} in KJ/kg) over the Central Atlantic derived from ozone/humidity-soundings made during ANT-VII/ (September/October 1988) in the tropical region along the 30^oW meridian. The fat grey line is the tropopause and the fat black line the 40 ppbv ozone contour line of the MCC (Mesoscale Convective Cell)*

Pierrehumbert [1995] showed the significance of this lateral inflow of dry extra-tropical air for the climate of the Tropics, arguing that dry air exchanges might regulate the tropical climate to an even larger degree than cloudiness.

6.8.2 Influence of Intrusions of Dry Air Tongues

An intriguing feature are the sharp relative humidity minimums together with enhanced ozone mixing ratios observed in the lower troposphere during deep convective activity. This characteristic is very pronounced in the ozone/humidity sounding made under deep convective conditions at 4°N (Fig. 6.6, Panel F, Sounding No.74) at the southern edge of the convective equatorial trough during ANT-VII/1. A very similar observation has been made during CEPEX [*Kley et al.,* 1997], shown in Figure 6.17.
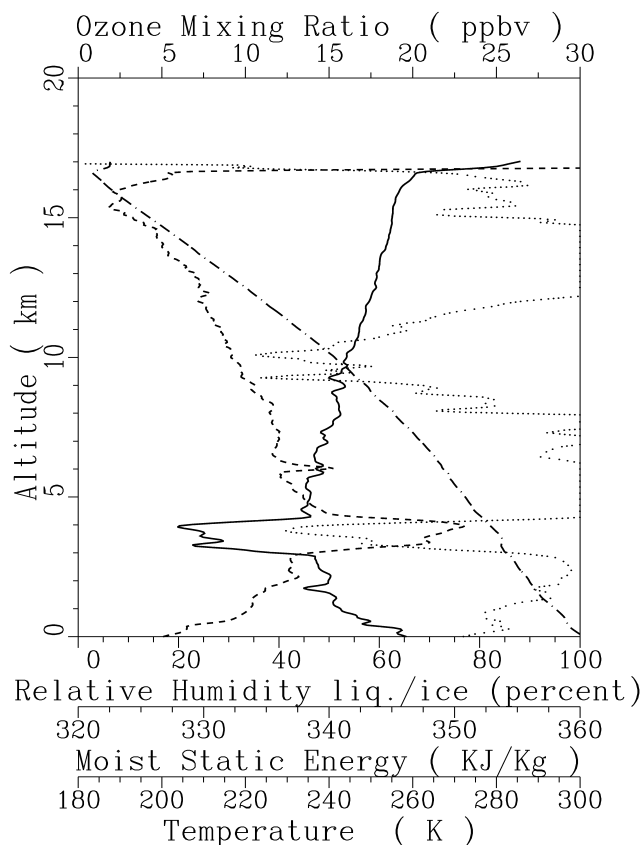

Figure 6.17: *Vertical profile of relative humidity (dotted line), moist static energy (solid line), temperature (dashed-dotted line), and ozone mixing ratio (dashed line) of a CEPEX sounding made at 7. March 1993 (9°S, 160°E)*

The dry layer corresponds with a sharp decrease of the moist static energy. Since clear sky radiation tends to decrease Q_{MS} by about 1.5 KJ/kg/day, the very dry air mass near 850 hPa, with a Q_{MS} deficiency of about 15 KJ kg^{-1} relative to the surface value, has undergone something like 10 days of radiative cooling since it was last in contact with a low latitude sea surface. This is in contrast to mean mid tropospheric air, with a deficiency of less than 5-10 KJ kg^{-1}, i.e. a similarly defined "radiative age" of just a few days. The corresponding sharp ozone peaks with mixing ratios of 60-80 ppbv clearly indicate that an upper tropospheric origin is most likely. Even for a lifetime of 10 days of a dry tongue any photochemical production of ozone can only give a minor contribution to the observed ozone peak values. These filaments or tongues of dry air are anomalously virtually warm near bases with a slight cool layer below; that is they sit atop sharp layers of inversions (See Figures 6.6-F and 6.17).

From TOGA COARE[14] sounding data *Parsons et al.* [1994], *Numaguti et al.* [1995], *Yoneyama and Fujitana* [1995], *Sheu and Liu* [1995], *Mapes and Zuidema* [1996], *Johnson et al.* [1996] and *Yoneyama and Parsons* [1999] have shown that the dry air was advected from higher (subtropical) latitudes. *Numaguti et al.* [1995] showed that dry layers at about 3 km altitude level in the Tropics are caused by intrusions of dry subtropical air associated with westward-propagating tropical disturbances on a typical time period of 4-5 days. Using backward trajectories *Yoneyama and Parsons* [1999] traced the origin of these dry events to processes in midlatitudes. They proposed that meridional circulations in the deep Tropics are coupled with dry air from the higher latitude westerlies being injected into the Tropics from breaking Rossby waves associated with the lifecycle of baroclinic waves. In a statistical way *Waugh and Polavani* [2000] came to same conclusions by analyzing a climatology of dry air intrusions from 20 years of meteorological analyses. Although the superimposition of the subtropical and midlatitude circulations appears chaotic, the dry air events can have a characteristic timescale of 1-2 weeks.

Low-level dry tongues can prevent deep convection outright [*Parsons et al.*, 1994], while the stable layers associated with dry tongues at higher altitudes may cause convection to detrain mass [*Bretherton and Smolarkiewicz,* 1989, *Johnson et al.,* 1996]. This detrainment of convective air is clearly depicted from the relatively low ozone values at about 5 km altitude level as observed in the successive ozone/humidity soundings made at 1°N and 1°S, respectively (See Fig. 6.6, Panel G & H, Sounding No.75 & 76, respectively). The layer of ozone deficient air is most likely uplifted air from the surface and detrained at about 550 hPa level corresponding to a temperature inversion at 0°C, probably a direct result from melting of falling hydrometeors in precipitating systems [*Johnson et al.,* 1996]. The layer is wet with humidities close to saturation indicating a "detrainment shelf" of cloud material [*Parson et al.,* 1994]. *Brown and Zhang* [1997] demonstrated that the stable and dry layers could lower the buoyancy of a rising air parcel substantially and even inhibit the convection.

From a statistical analysis of more than 2400 radiosoundings from the TOGA-COARE field program *Mapes and Zuidema* [1996] showed that, despite of the relatively small horizontal scale of each realization, dry tongues are frequent enough to be climatologically important. Mapes and Zuidema also showed that, under non convective conditions, dry tongues could sustain for 3-4 days or even longer because radiative heating stabilizes the dry tongue base. This means that dry tongues can be transported over long distances. Since convection is the source of moisture in the troposphere, dry tongues and their radiatively maintained stable layers may organize the persistence of the absence of convection.

Thus, the well known minimum of moist static energy at ~600-700 hPa, which the presented results suggests, is associated with dry layers might be the result of a linkage between tropical and extra-tropical dynamics. If this would be so, then a negative feedback to deep convection seems to operate in the sense that advection and entrainment of dry air acts like a controlling valve (low moist static energy), which would regulate Cb-convection. At any rate, the ANT-VII/1 results suggest long-range, inclined, transport of low humidity air into the convective region. A similar result has previously been found during CEPEX (*Kley et al,* 1997).

The role of deep convection in driving the large scale circulation (through latent heat release) is well known. What is not known, however, is the possibility that dry air transported by the large scale circulation might an important aspect in the regulation of deep convection. These

---

[14] TOGA-COARE = Tropical Ocean and Global Atmosphere- Coupled Ocean Atmosphere Response Experiment, [*Webster and Lukas*, 1993]

unique observations, as displayed in Figure 6.4-F and Figure 6.9, were made at the edge of a mesoscale cluster of Cb-convective cells. The sequence of the ozone soundings displayed in Figure 6.4 shows that this low ozone/high humidity signature, due to entrainment, becomes weaker towards the centre of the mesoscale convective area and this suggests in turn that the inner core is protected by those surrounding it.

The interaction of tropical deep convection with large scale dynamics might account for the possibility of a dry air valve on deep convection resulting not only from subsidence, but also from the lateral advection of dry mid level air. If dry air entrainment is indeed a viable mechanism limiting the growth of deep convective clouds, then a particularly intriguing question can be asked: Does tropical deep convection regulate itself on large scales by inducing a circulation that would advect dry air into the Tropics from higher latitudes? *Pierrehumbert* [1995] showed the significance of this exchange for the climate of the Tropics, arguing that dry air exchanges can regulate the tropical climate to a larger degree than cloudiness. *Yoneyama and Parsons* [1999] suggested that these exchanges can commonly produce extreme drying events in the Tropics, perhaps even more efficiently than subsidence of tropical air. At present these streamers of dry events are poorly represented by global weather and climate models and thus may have significant error on the prediction of weather prediction and climate [*Yoneyama and Parsons*, 1999].

Chapter 7

Summary with General Conclusions and Outlook

In this thesis the chemical and dynamical aspects governing the tropospheric ozone distribution in the tropics over remote warm oceans are investigated. The analysis is focused on the question in how far ozone can be used as a quantitative proxy to study deep convection and large scale subsidence in relation to the influence on the vertical distribution of humidity. This is investigated in an experimental approach using measured cross sections of latitudinal/altitude distribution of ozone and humidity which were simultaneously measured over the Central Atlantic Ocean between 36°S and 52°N, mostly along the 30°W meridian. The cross-sections were obtained from vertical ozone/humidity balloon soundings made from board the research vessel „Polarstern" during two cruises in March/April 1987 (ANT-V/5) and September/October 1988 (ANT-VII/1).

In a number of laboratory and field experiments the ozone/humidity sonde performance in the troposphere and lower stratosphere was investigated and evaluated, particularly with regard to the low ozone concentrations and extremely low temperatures in the tropics. Based on these studies new correctional methods to process the sounding data were developed which significantly improved the accuracy of the ozone and humidity measurements in the middle and upper troposphere.

One of the prominent large scales features observed in the meridional distributions of ozone, obtained during ANT-V/5 and ANT-VII/1, is the latitudinal decrease of ozone in the tropical regions towards the equator. This was very pronounced in the MBL with minimum values of about 10-20 ppbv in the vicinity of the equator. In this region the low mixing ratios in the MBL occur in coincidence with enhanced values in the middle troposphere (Z=3-7 km), decreasing values towards the upper troposphere (Z=7-14 km) and a subsequent increase towards the tropopause (Z=17 km) and above. The free troposphere exterior the equatorial region ozone is mostly characterized by a sharp increase of ozone just above the MBL with almost no vertical gradient towards about 12-14 km altitude, while above the ozone increases rapidly to stratospheric values. To understand whether the observed features are caused by photochemistry or dynamics the in-situ photochemical changes of ozone are estimated as a function of latitude and altitude through the use of a photochemical box model and compared to the characteristic time scales of horizontal and vertical transport of the tropical Hadley circulation.

The analysis shows that in the tropical MBL high water vapor content, high UV-flux and low (<10 pptv) mixing ratios of NO_X act together to cause a strong local photochemical ozone destruction with ozone life times of less than 5-7 days that dominates the photochemical formation of ozone by far. The photochemistry provides an effective loss mechanism of ozone. Air masses during their transport with the trade winds steadily loose ozone through photolytic destruction which is responsible for the low ozone values in the MBL and the latitudinal decrease of ozone towards the ITCZ. Due to the much lower water vapor concentrations and lower temperature in the free troposphere the photochemical conversion rates of ozone are much slower by a factor 10 or more compared to the photochemistry of ozone in the MBL In the lower free troposphere there is a net destruction of ozone declining with altitude from about -4% per day at 2 km to less than -1% per day at 6 km. In the

middle/upper troposphere photochemical ozone formation dominates with a net production rate of about 1-3% per day.

During a deep convective event, which carries ozone deficient air to the upper troposphere, the ozone content of the vertically transported air cannot be significantly influenced by chemical processes, because photochemical changes are rather slow compared to the time scale of fast upward transport of only 1-2 hours. Further, in the free troposphere the typical times of local photochemical changes of ozone are weeks to months, depending on the altitude, and are thus even significantly slower than the time scales (1-2 weeks) of large scale subsidence in the non convective regions of the tropics. Using a coupled chemistry general circulation model (ECHAM-4) it was further shown [*Roelofs et al.*, 1997-b] that during the ANT-VII/1 cruise most of the enhanced ozone values observed in non-convective (c.q. subsidence) regions originated from the stratosphere or from photochemistry. However, if a photochemical origin is assumed, then, most of this ozone would have already been produced in the vicinity of the source regions over the continents before it was transported to the Central Atlantic region. Only minor amounts of ozone could have been produced in the middle/upper troposphere during long range horizontal transport while the major ozone destruction proceeded in the MBL over the Central Atlantic.

It is concluded that in the absence of significant sources of NO from surface emissions and from lightning in the remote tropical marine troposphere the in-situ photochemistry in the free troposphere is too slow compared to the tropical motion systems involving deep convection and large scale subsidence. Approximately on a time scale of 1 week the impact of in-situ photochemistry of ozone is estimated to be less than 10% with regard to the observed morphology of ozone in the middle/upper troposphere up to about 14 km altitude. It is obvious that the morphology of ozone observed during both cruises is governed by dynamics. Therefore, a concept was developed that within tropical motion systems in remote oceanic environments with characteristic time scales of the order of one week ozone can be used as a quasi-inert chemical tracer to describe the dynamics of deep convection associated with entrainment and detrainment processes in conjunction with large scale subsidence.

The concept of using ozone as a quasi-conservative tracer was applied on the mesoscale convective system encountered in the equatorial trough region during ANT-VII/1 to study deep convection and its influence on the humidity distribution. Active or recent deep convection marks its appearance in the upper tropical troposphere by the relative low ozone mixing ratios whereby inside cumulonimbus convective clouds, so called "hot towers", ozone deficient surface air surface is lifted to the upper troposphere where it detrains and displaces air with higher mixing ratios. This is clearly identified in the equatorial region during ANTVII/1 where the morphology of the deep convective middle/upper troposphere is mapped approximately by the 40 ppbv ozone mixing ratio contour line which envelopes the spatial extension of a mesoscale convective cell (MCC) consisting of a cluster of individual deep convective cells. From the upper boundary of the MCC it is clearly depicted that deep convection did not penetrate above 14 km altitude.

Inside the MCC above the subcloud layer the relative humidity reveals a large variability from dry to saturated values, particularly in the divergent part where MCC has its maximum width at an altitude between 10 and 12 km. This suggests that the detrainment is most effective at this altitude level. Assuming that the detrainment flow is initially saturated, there must be also strong subsiding motion to both sides of the high humidity core as can be inferred from the low relative humidities to both sides of the central core. The humidity distribution shows a large variability and tends to have a bi-modal character with a dry and wet branch that

indicates that the radiative drying time after detrainment of moisture by convection is short compared to mixing. Outside the MCC, in the non-convective regions of large scale subsidence, the mid/upper tropospheric air is rather dry (10-40% RH) and shows enhanced ozone mixing ratios (60-80 ppbv).

Based on the ozone distribution inside the MCC three compartments were identified. The first (lower) one (0 < Z < 3 km) comprises the regime of low level convergence of the trade wind inflow with low MBL ozone ($\approx$20-25 ppbv) and high humidities. The convergence of moisture provided by the trade wind inflow actually drives deep convection. The second part (4 < Z < 7 km) describes the entrainment (confluence) of dry mid tropospheric air with enhanced ozone mixing ratios ($\approx$60-70 ppbv) into the deep convective cell. The enhanced ozone values show that this fast vertical transport virtually bypasses this part of the troposphere. The third part (7 < Z < 14 km), the divergence zone, which is also referred to as the detrainment part. The ozone mixing ratios in this part ($\approx$30-40 ppbv) are low, but significantly higher compared to the values in the low level convergence part, which implies a consoiderable strength of entrainment.

From air and ozone mass balance over the three compartments inside the MCC the evacuation or flushing time for the convective boundary layer (lower 3 km) in the equatorial trough region was estimated to be about 2-3 days. Further, the ratio of the trade wind inflow (low level convergence of moist air) and entrainment flow (upper level convergence of dry air) was estimated to be about 0.40, which means that the flow of entrained air is comparable large to the upward flow from the low level convergence of trade winds. It is concluded that within a MCC the turn over time of mid-tropospheric air is approximately of the same magnitude as the 2-3 days of evacuation time of air masses below the sub cloud layer (Z=3km). As a consequence this implies that the observed enhanced ozone content c.q. minimum values of moist static energy in the mid-troposphere can only be sustained at this level through an substantial large scale inflow from regions with enhanced ozone mixing ratios and low moist static energy (Q_{MS}) contents, presumably from the subtropics. Because the mid-tropospheric air from higher latitudes is rather dry and contains low Q_{MS}, this mid level entrainment will decrease Q_{MS} of the rising air parcel substantially and reduce the buoyancy of the lifted air through evaporation of hydrometeors in order to keep the air parcel saturated. This means that substantial large amounts of dry, low Q_{MS} air that is entrained in the updrafts of the mesocale cluster of deep convective cells can have a significant influence on the rising and penetrating power of the deep convection.

An intriguing aspect also is the existence of dry air tongues with enhanced ozone mixing ratios and low Q_{MS} in the lower/middle troposphere between 2 and 6 km altitude. These filaments of dry air sit atop sharp layers of temperature inversions. Under non-convective conditions the filaments are radiatively stable such that they can be transported over long distance and presumably got their origin at higher latitudes in the subtropics or midlatitudes. This could occur through a coupling of the meridional circulation in the Tropics with intrusions of dry and ozone rich air originating from breaking Rossby waves associated with the life cycle of baroclinic waves. Low level dry tongues can prevent the onset of deep convection. At higher altitudes dry tongues can initiate that convection starts to detrain cloud mass together with ozone deficient air from the boundary layer below and thus finally moistening the air at these altitudes. The signature of these tongues were most pronounced at the edge of the MCC but gets weaker towards the center which means that the central core updrafts were protected from entrainment by the surrounding cloud air and thus they can penetrate upto about 14 km without dilution by environmental air.

Although the role of deep convection in driving the large scale circulation (through latent heat release) is well known, the presented results suggest also that deep convection is "pumping" mid-/upper-tropospheric air from the subtropics and thus indicating a linkage between tropical and extra-tropical dynamics. If this is so, then, a negative feedback to deep convection seems to operate in the sense that advection and entrainment of dry air acts like a controlling valve (low moist static energy), which regulates the Cb-convection. Particularly the role of the dry tongues as a result from the interaction between the dynamics in the tropics and extra-tropics is intruiging but still poorly understood.

From the results obtained in this thesis it is demonstrated that the use of ozone as a suitable tracer to map deep convection in remote areas over the tropical oceans is a very promising concept with a wide perspective to investigate tropical dynamics and their interactions with higher latitudes. Firstly, the study of dry tongues in conjunction with the enhanced ozone mixing ratios to trace the origin should be extended in a more climatological approach to investigate the statistical significance and impact of these dry tongues on deep convection and its regulation. Secondly, ozone can be used as a quantitative tracer to investigate in how far the humidity distribution in the outflow of deep convection is influenced by mixing processes. A further interesting study could be that total tropospheric ozone columns can be used to map the morphology of the MJO (Madden-Julian Oscillation) in order to investigate the influence of the MJO on the large scale humidity distribution in conjunction with the influence of sea surface temperature. The synergetic use of observational data from different observation platforms like balloon sondes (e.g. SHADOZ), aircraft (e.g. MOZAIC) and satellites (e.g. ENVISAT, SAGE III) could thereby be a big advantage.

Annex-A:

Sonde Validation Studies

Annex A-1

Simulation Experiments Under Quasi Flight Conditions

A-1.1 Introduction

In order to address questions about the performance of the ECC-ozone sensor under tropical as well as extra-tropical conditions the environmental simulation chamber (ESC) of the ozone sounding simulation facility at Jülich (See Figure A-1.1) , has been used to simulate vertical ozone soundings under quasi realistic atmospheric flight conditions [*Smit et al.*, 1994-A, 2000]. The chamber is computer controlled whereby vertical profiles of pressure, temperature and ozone concentration up to an altitude of about 30 km can be simulated while an ozone UV-photometer serves as reference.

After a brief description of the ozone sounding simulation facility the results of simulation experiments under mid-latitudinal as well as tropical conditions are reported. The results are discussed in terms of sensitivity, precision and accuracy of the ECC-ozone sensor and recommendations for processing ECC-sonde data are reported.

Figure A-1.1: *Environmental Simulation Chamber (ESC) at Research Centre Jülich*

A-1.2 Set Up of Ozone Sounding Simulation Facility

The ozone sounding simulation facility and its performance is described in detail in a technical report [*Smit et al.,* 2000]. The experimental set up of the facility shown in Figure A-1.2 consists of the following major components:

1.) Environmental simulation chamber, shown in Figure A-1.1, is a temperature controlled vacuum chamber of stainless steel with a test room volume of about 500 liter (80x80x80 cm) whereby pressure as well as temperature can be regulated dynamically between 5 and 1000 hPa and between 200 and 300 K ($-2K/min \leq rate \leq +2K/min$) respectively.

2.) Fast response dual beam UV-photometer, developed by *Proffitt et al.* [1983] for the use on stratospheric balloons, serves as ozone reference. The precision of the UV-photometer is estimated to be better than ±0.025 mPa of O_3 ($\cong 0.6 \times 10^{10}$ O_3 molecules/cm^3) [*Smit et al.*, 2000]. *Proffitt et al.* [1983] estimated the overall accuracy of the UV-Photometer to be better than $\pm2\%$ for simulated altitudes up to 25 km while it declines to $\pm3.5\%$ at 35 km altitude. Response time is better than 5 seconds.

3.) Ozone profile simulator to simulate vertical profiles of ozone in time and to achieve reproducible ozone concentrations. The simulator consist of a separate gas flowing system installed inside the chamber and can provide 4 ozone sondes plus UV-photometer with regulated ozone concentrations.

4.) Computer controlled data processing system for automatic control of the simulation process as well as the data acquisition.
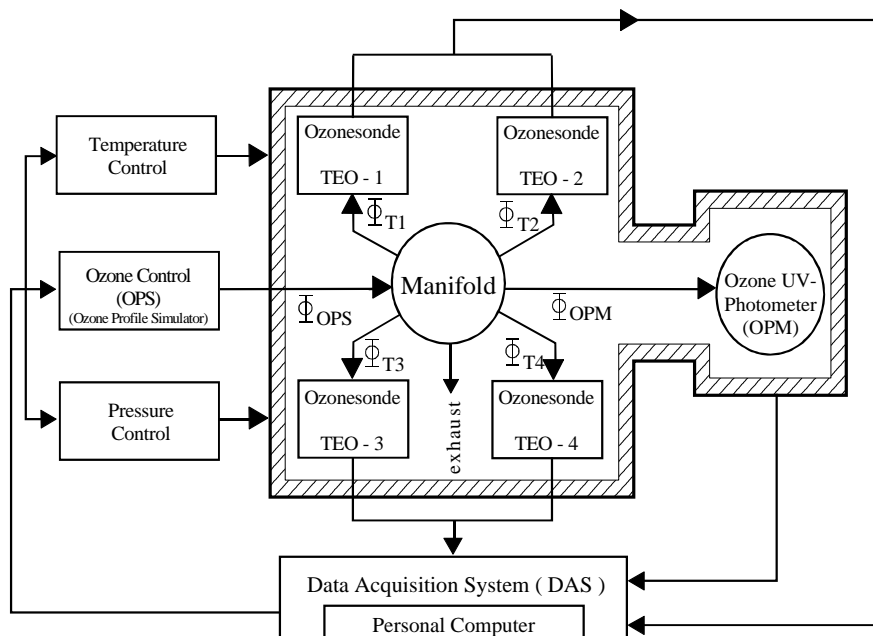

Figure A-1.2: *Scheme of the set up of the ozone sounding simulation experiment*

Four ECC-ozone sondes can be „flown" simultaneously and compared to the UV-Photometer whereby different types of vertical profiles of pressure, temperature and ozone concentrations versus time according vertical soundings with ascent velocities of about 5 m/s can be simulated.

A-1.3   Simulations of Vertical Ozone Soundings

A-1.3.1.   Experimental Design

In several simulation experiments 4 ozone sondes of the ECC-type SPC-5A (Science Pump Corporation, USA) were "flown" simultaneously and compared to the UV-photometer. The major objective of the experiments was to characterize and to determine precision and accuracy of the ECC-ozone sensor as a function of altitude and ozone level. Particularly the question, in how far the data analysis is affected by procedures like background signal correction and total ozone column normalization, was addressed. As shown in Section 3.4.2.3 the accuracy of the ECC-sensor in the upper troposphere is very sensitive to the background signal, particularly in the tropics.

Two different types of vertical profiles of pressure, temperature and ozone concentrations were simulated. The first type of profile was a typical mid-latitude profile taken from the *US-Standard Atmosphere* [1976] for 40-50°N with a tropopause height of 12 km. The second type of profile relates to typical tropical conditions of high convective activity, high tropopause at 18 km and low tropopause temperature which means extremely low ozone values in the middle and upper troposphere [*Kley et al.,* 1996]. Both profiles reflect typical vertical profiles of pressure, temperature and ozone concentrations as encountered during the two ship cruises across the Central Atlantic.

A-1.3.2   Results

Figure A-1.3 shows the vertical ozone profiles measured by the individual ozone sondes and the UV-photometer which were obtained during two different simulation experiments made under typical mid-latitudinal (Diagram A) and tropical (Diagram B) conditions respectively.
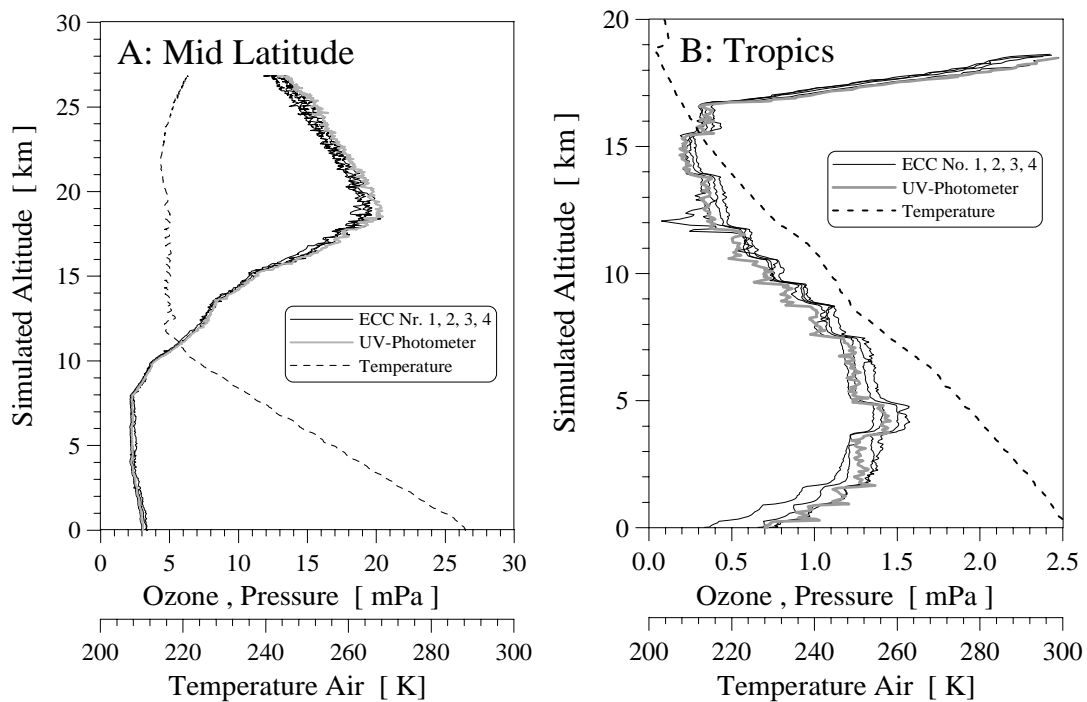

Figure A-1.3: *Vertical ozone profiles measured by 4 ECC-ozone sondes (thin-lines) and UV-photometer (fat line) during two different simulation runs with mid-latitudinal and tropical conditions respectively. Broken line is the actual temperature in the chamber.*

The results of both experiments show that the vertical profiles of ozone measured by the individual sondes are generally in rather good agreement with each other as well as with the UV-photometer. The „flown" sondes track the simulated ozone profile very well. Even in the tropical case in the middle/upper troposphere under extreme low ozone pressures between 0.2 and 1 mPa the sondes respond fast and reliable to the small, fast variations of the simulated vertical ozone profile. The precision of the ozone sonde is determined by the standard deviation of the mean of the ozone readings of the four simultaneously „flown" sondes, while the accuracy of the ECC-sonde is determined as the sum of sonde precision and the absolute value of its deviation (=bias) with the UV-photometer.

A-1.3.3   Precision

Figure A-1.4 shows the mean ozone pressure (incl. absolute and relative standard deviation) measured by the four simultaneously tested ECC-sensors as a function of the simulated height obtained from the mid-latitudinal (Diagram A) and tropical (Diagram B) type of simulation run, respectively.
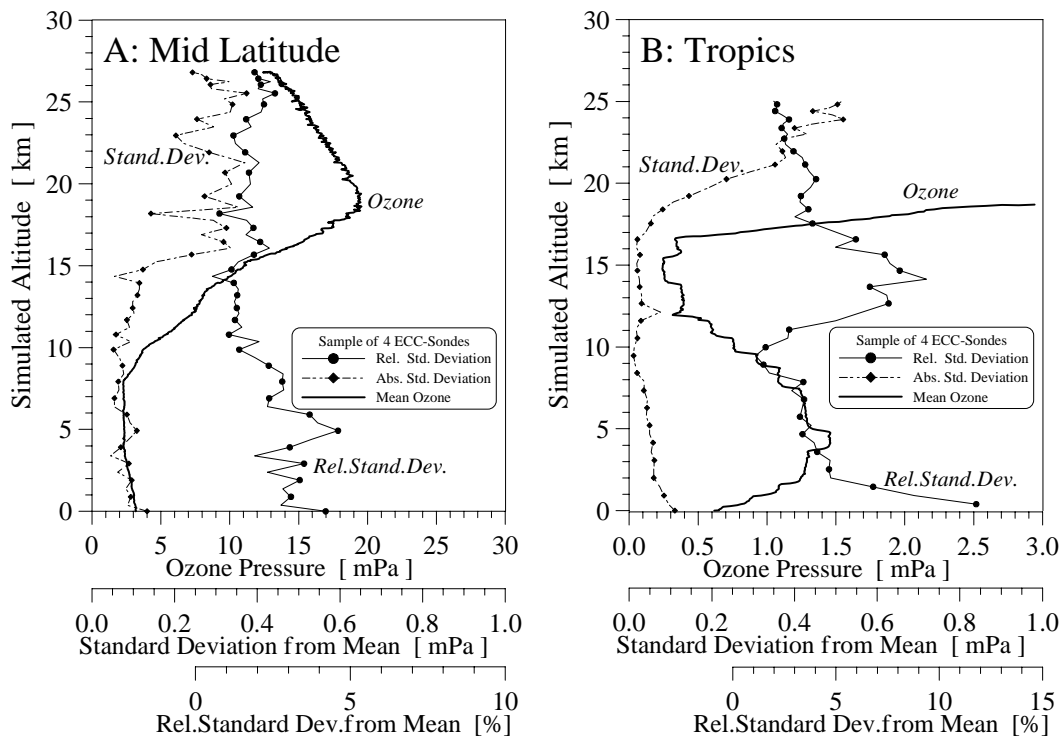

Figure A-1.4: *Mean partial pressure (fat line), absolute standard deviation (broken line) and relative standard deviation (thin line) of the mean of 4 ECC-sondes simultaneously „flown" in the case of mid-latitudinal (Diagram A) and tropical (Diagram B) conditions, respectively.*

From Figure A-1.4 it is depicted that in the stratosphere, up to an altitude of 25-28 km, the relative precision of the ECC-sonde is better than 2-3 %. In the troposphere the relative precision of the ECC-sonde showed to be better than 2-3 % for the mid-latitude profiles, while for the tropical profiles the relative precision was better than 5 % in the lower/middle and 10 % in the upper part of the troposphere.

A-1.3.4. Accuracy and Background Current

The results of the comparison of the ECC-sonde with the UV-photometer for both types of simulated profiles are shown in Figure A-1.5. Relative deviations of the mean partial pressure of ozone measured by the ECC-sonde are compared to the UV-photometer in relation to two different ways of correcting for the contribution of the background current . In the first stage the background current used is determined before first exposure to ozone in the preparation procedure prior to the simulation.
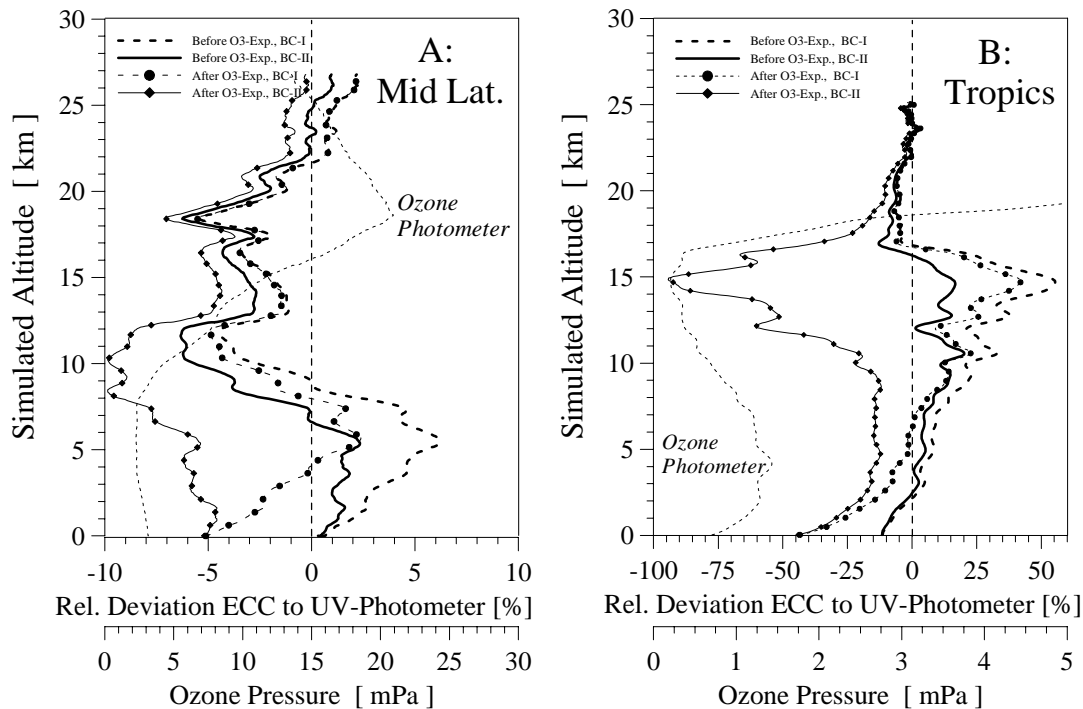

Figure A-1.5: *Relative deviation of ozone measured by ECC-sonde compared to UV-photometer in relation to four different ways of background current correction: background determined before and after exposure with ozone (see text) whereby the oxygen (BC-method I) and the non-oxygen (BC-method II) dependent background current correction for the mid-latitudinal (Diagram A) and the tropical (Diagram B) case, respectively. The results are obtained over a sample of 4-sondes tested simultaneously in the simulation facility (see text).*

In the first method (BC-method I) which is the conventional method of background correction, prescribed by *Komhyr* [1986] and applied world wide, it is assumed that the background current depends on the oxygen partial pressure. This means that the background current becomes smaller in the middle/upper troposphere and stratosphere. However, our laboratory studies and those of other investigators [*Thornton et al.*, 1982], do not show any oxygen dependence of the background current. Therefore, the second method (BC-method II) of background current correction which does not include any oxygen dependence of the background current requires a full subtraction of the background current from the measured cell current.

In the troposphere using the conventional method of background correction, BC-Method I, it is seen from Figure A-1.5 that the ECC-sonde can overestimate the ozone up to 10 percent for the mid-latitudinal case (Diagram A) and even up to 50 percent for the tropical case (Diagram B). Much better results are achieved by applying the full background current correction, BC-Method II. Now the overestimate of ozone compared to the UV-photometer has decreased to 2-3 percent for the mid-latitude case and to approximately 10 percent for the tropical case. Compared to the UV-photometer, the ECC shows a different behavior in the stratosphere than in the troposphere for both methods. Above 10 km all ECC sondes show lower values of about 5-6 % up to an altitude of 20 km, while the deviations become as small as 2 % at 27 km.

During the preparation of the ECC-sondes it was observed that the background current increased from values of 0.04±0.02µA before exposure of ozone to values of 0.08±0.03 µA after exposure of ozone. Similar observations were made during JOSIE (=Jülich Ozone Sonde Intercomparison Experiment) conducted in the simulation facility at Jülich [*Smit et al.,* 1998-A, 1998-B]. ECC-sondes exhibit a residual signal after ozone was temporarily set to zero during some simulation runs. The „rest" signal was significant larger than the background observed before exposure to ozone during the preparation. The origin of the background current and its change during the sounding is not understood. Recent laboratory studies of ECC-sondes have indicated that the background signal of ECC-sondes can be positively correlated with past exposure to ozone [*Johnson et al.,* 2002]. From the simulation experiments, however, it turned out that the best accuracy was achieved when the background current is measured before the first exposure to ozone in the preparation procedure. This is clearly demonstrated in Figure A-1-5 by comparison of the present results using the background current before exposure to ozone with results using the background current after exposure to ozone. Our findings were confirmed in a field study by *Reid et al.* [1996].

The reported results are representative for the ECC as a type. In other words: repeated simultaneous "flights" always yielded identical results. An overview of the ECC-sonde precision, bias and accuracy obtained from the simulation experiments are summarized in Table A-1.1 in altitude bins of 5 km for mid-latitude as well as tropical conditions and applying full background current correction (BC-Method II).

	Region	0-5 km	5-10 km	10 km-TP	TP-20 km	20-25 km
Precision	Mid Latitude	±3%	±3%	±3%	±2%	±2%
	Tropics	±5%	±3%	±7%	±4%	±3%
Bias	Mid Latitude	+1%	-4%	-3%	-2%	-1%
	Tropics	-5%	+7%	+12%	-5%	-2%
Accuracy	Mid Latitude	±4%	±7%	±6%	±4%	±3%
	Tropics	±10%	±10%	±19%	±9%	±5%

Table A-1.1: *Overview of the ECC-sonde precision, bias and accuracy obtained from the simulation experiments splitted in altitude bins of 5 km for mid-latitude as well as tropical conditions and applying full background current correction (BC-Method II). TP = Tropopause*

A-1.3.5 Conclusions and Recommendations

If the BC-Method II is applied, the accuracy of ECC-sondes for tropospheric measurements of ozone is better than ±(4-7) % for the mid-latitude profiles and approximately ±(10-19) % for the tropical profiles. The ECC-sonde slightly overestimates the ozone concentration in the lower and middle troposphere. On the other hand, in the stratosphere the ECC underestimates ozone by approximately 0-4 %, depending on altitude. Therefore, a height dependent correction and not the standard correction factor, based on the local measurement of total ozone by a Dobson spectrophotometer, should be applied. However, this standard correction, based on total ozone column measurements, should not be applied to the tropospheric ozone profile because this would lead to a significant overestimate of the ozone mixing ratio. To achieve the best accuracy, particularly in the troposphere, it is important that the measured ozone sensor current is corrected for the background current which is determined before first exposure of ozone.

The results of these simulation experiments and the disagreement with the conventional methods of data processing may have large implications for the comparison of vertical profiles obtained from different sounding stations, but also for the results obtained from investigations of ozone trends in the stratosphere as well as in the troposphere. Therefore, the following recommendations for processing ECC-sonde data are given:

- Background current determined before first ozone exposure.

- Full background current correction throughout the entire vertical profile.

- No total ozone correction for the vertical ozone profile in the troposphere.

- A height dependent correction factor for the stratospheric part needs to be applied.

The first three recommendations like background current before ozone exposure, full background correction and no total ozone normalization in the troposphere were applied in the post flight processing of the ozone sounding data obtained from the two Atlantic cruises in 1987 and 1988 reported in this thesis. However, the altitude dependent total ozone normalization is at the present not characterized sufficiently and more research is required.

A-1.4 Pressure and Temperature Sensors of RS80-Radiosonde

At discrete levels of pressure (5-1000 hPa) and temperature (200-300 K) the precision and accuracy of the pressure (Barocap) and temperature (Thermocap) transducers of the RS80-radiosonde were investigated in the simulation chamber. Under realistic atmospheric conditions pressure and temperature sensors of 8 different RS80-radiosondes (4 RS80-radiosondes simultaneously per run) were compared to accurate pressure and temperature instrumentation. As pressure reference served two capacitive manometers covering the ranges of 10-1000 hPa (MKS-Baratron, type 122 AX, accuracy better than ±0.5% of readings) and 1 to 12.5 hPa (MKS-Baratron, type 220 BA, accuracy better than ±0.5 % of readings). A Pt-100 sensor was used as temperature reference with an accuracy better than ±0.2 K

Temperature comparison was only reliable at pressure levels above 100 hPa because at lower levels temperature fluctuations inside the testroom of the chamber become larger than ±1 K due to inefficient air ventilation [*Smit et al,* 2000]. Differences of pressure and temperature readings of each of the sondes and coresponding references are shown as a function of pressure in Figure A-1.6, Diagram A and B respectively. All tested radiosondes show a good reproducibility in the pressure and temperature ranges 4-1000 hPa and 190-300 K, respectively. The observed differences of the individual sondes with the references are small

and show little fluctuation. From the plotted standard deviations of the mean of the differences of pressure and temperature obtained over the ensemble of 8 sondes the precision of the pressure and temperature sensor of the RS80-sonde is determined as ± (0.4-0.6) hPa and ±(0.2-0.4 K), respectively.
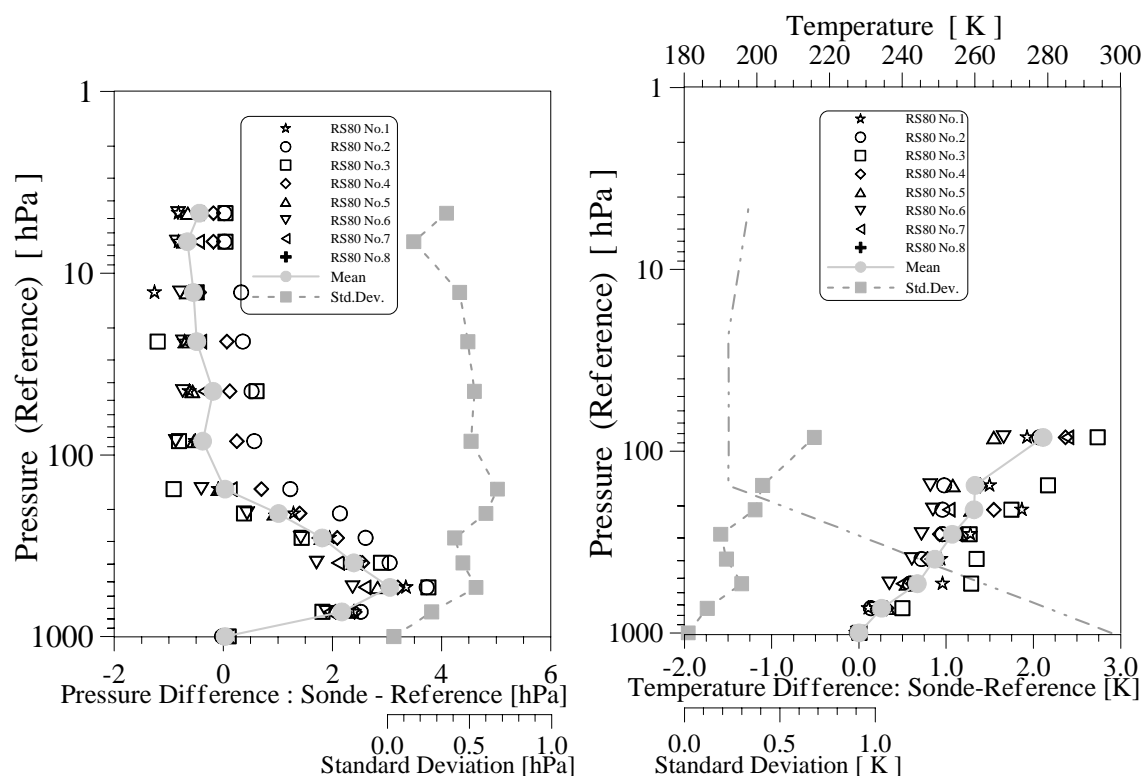

Figure A-1.6: *RS80-radiosonde comparison experiment in simulation chamber: Differences of pressures (left diagram) and temperatures (right diagram) from the Barocap- and Thermocap- sensors of the RS80-radiosonde to their references (pressure: MKS-Baratron, type 122 AX and 220 BA, temperature: Pt100) as a function of pressure. Means over 8 radiosondes and their standard deviations are presented by the solid and dashed lines respectively. The course of the temperature inside the testroom of the simulation chamber is shown in right diagram by the dash-dotted line.*

In the tropospheric part of the pressure profile between 1000 and 200 hPa the Barocap-sensors show a positive bias to the reference with maximum values of about 3 hPa at about 500 hPa. Below 200 hPa the Barocap show a rather constant small negative bias of about -(0.3-0.5) hPa. It is obvious that at pressures between 200 and 1000 hPa the accuracy (= precision + absolute value of bias) of the Barocap-sensor of the RS80-radiosonde is better than ± 2.5 hPa while below 200 hPa down to 5 hPa, the absolute accuracy is better than about ±1 hPa.

In the observed pressure range of 1000-100 hPa the Thermocap-sensors of the RS80 are measuring slightly enhanced temperatures (+(0.3-1.0)K) compared with the Pt100-reference. At tropospheric conditions the accuracy of the Thermocap-sensor of the RS80-sonde is estimated to be better than ±1 K and at lower stratospheric conditions better than ±1.5 K.

An overview of the precision, bias and accuracy of the pressure and temperature sensors of the RS80-radiosonde at different altitude regions is given in Table A-1.2.

Pressure [hPa]	Region	0-5 km	5-10 km	10 km-TP	TP-20 km	20-25 km
Precision (ESC)	Mid Latitude	±0.4 hPa	±0.5 hPa	±0.6 hPa	±0.5 hPa	±0.4 hPa
Bias (ESC)	Mid Latitude	+2 hPa	+2 hPa	+0.5 hPa	-0.3 hPa	-0.5 hPa
Accuracy (ESC)	Mid Latitude	±2.4 hPa	±2.5 hPa	±1.1 hPa	±0.8 hPa	±0.9 hPa
Temperature [K]	Region	0-5 km	5-10 km	10 km-TP	TP-20 km	20-25 km
Precision (ESC)	Mid Latitude	±0.2 K	±0.3 K	±0.4 K	---	---
Bias (ESC)	Mid Latitude	+0.3 K	+0.5 K	+1.0 K	---	---
Accuracy (ESC)	Mid Latitude	±0.5 K	±0.8 K	±1.4 K	---	---

Table A-1.2: *An overview of the precision, bias and accuracy of the pressure and temperature sensors of the RS80-radiosonde at different altitude regions obtained from simulation experiments.*

Annex-A-2

Twin Sounding Comparisons

A-2.1   Introduction

In two field experiments the in-flight precision of the different sensors of the ozone sonde and the radiosonde measuring ozone, pressure, temperature and relative humidity were investigated from twin soundings. For this purpose two complete sondes were prepared and simultaneously flown on the same gondola such that each sonde encountered the same air masses. Each ozone sonde had its own radiosonde. Six twin soundings were made on two different locations. The first set of three twin flights was made over the Atlantic Ocean between 27 ^{o}N, 30 ^{o}W and 47 ^{o}N, 13 ^{o}W during the ANT-V/5 cruise of the RV-"Polarstern" in April 1987. Further three twin soundings were made at Helsinki, Finland (60 ^{o}N, 25 ^{o}E) in collaboration with the division of research and development of Vaisala Ltd. during a comparison campaign at the terrain of the Vaisala factory in November 1987.

A-2.2   Experimental Details

For all twin soundings ECC-ozone sondes of the type ECC-5A (Science Pump Corporation, USA) and radiosondes of the type RS80-15 (Vaisala, Finland) [1] were used. The set up of the gondola of the twin sondes flown from aboard the Polarstern (twin sounding type A) was slightly different from the set up flown at Helsinki (twin sounding type B) as shown in Figure A-2.1. In both configurations the two sondes were separated sufficiently far to avoid that the sondes may affect each others performance during flight. The 403-MHz carrier frequency of one radiosonde was slightly detuned to the other and reception of the sonde data was achieved with a dual equipped ground station.
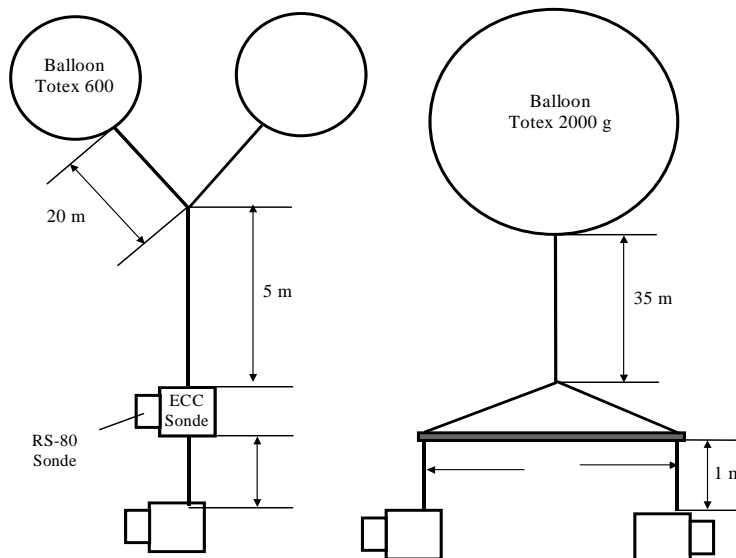

Figure A-2.1:   *Scheme of the set ups of the gondolas of the twin sondes flown at the RV-"Polarstern" (left diagram) and at Helsinki (right diagram), respectively.*

---

[1] PTU-sensor of RS80-15 radiosonde :: Pressure sensor : BAROCAP (capacitive aneroid) ; Temperature sensor : THERMOCAP (capacitive bead) ; Relative humidity sensor : HUMICAP-A (thin film capacitor).

The flight dates, launch times, geographical positions of the individual twin flights are listed in Table A-2.1

	Polarstern Cruise ANT-V/5			Helsinki , Finland		
Twin Sounding	TWS-I	TWS-II	TWS-III	TWS-IV	TWS-V	TWS-VI
Date	08-04-1987	10-04-1987	14-04-1987	17-11-1987	17-11-1987	18-11-1987
Time (UTC)	15:35	15:10	14:20	10:00	13:40	10:00
Latitude	27° 8' N	33° 30' N	47° 00' N	60° 16' N	60° 16' N	60° 16' N
Longitude	30° 00' W	27° 12' W	13° 42' W	24° 52' E	24° 52' E	24° 52' E
Altitude (m)	10	10	10	25	25	25
Flight Code Sonde A	FLH019	FLH022	FLH030	FLH041	FLH042	FLH043
Flight Code Sonde B	FLH020	FLH023	FLH029	FLH047	FLH048	FLH049
Twin Sounding Type	A	A	A	B	B	B

Table A-2.1: *Twin ozone/radio-soundings made at the RV „Polarstern" in April 1987 and at Helsinki in November 1987.*

Only flight data obtained during the ascent of the twin sondes were used for comparison. The flight time is used as the independent and common parameter for coupling and comparison of the simultaneously measured vertical profiles of ozone, pressure, temperature and relative humidity.

A-2.3   Individual Vertical Profiles

The individual vertical profiles of ozone pressure, temperature and relative humidity obtained from each twin sounding are presented in the Figure A-2.2 for the twin flights made at the Polarstern (TWS-I, TWS-II and TWS-III) and at Helsinki (TWS-IV, TWS-V and TWS-VI) respectively. The vertical profiles are presented as a function of altitude which was computed step by step as the cumulative sum of the height difference between two successive pressure levels using the hydrostatic equation. For the sake of clarity the altitude was always determined from the set of pressure (P), temperature (T) and relative humidity (U) measured by sonde A, while the presented profiles measured by sonde B are coupled to this altitude scale of sonde A via the common flight time. The absolute differences between the altitudes determined from the PTU-data sets measured by Sonde-A and Sonde-B respectively are only 30-50 m in the troposphere and around 50-100 m in the lower/middle stratosphere (See Figure A-2.3).

For temperatures below 0 °C the relative humidity was determined with respect to ice instead of liquid water. For the twin sounding TWS-III above 12 km altitude no data are available for sonde B due to the failing of the reception of the telemetry signal.
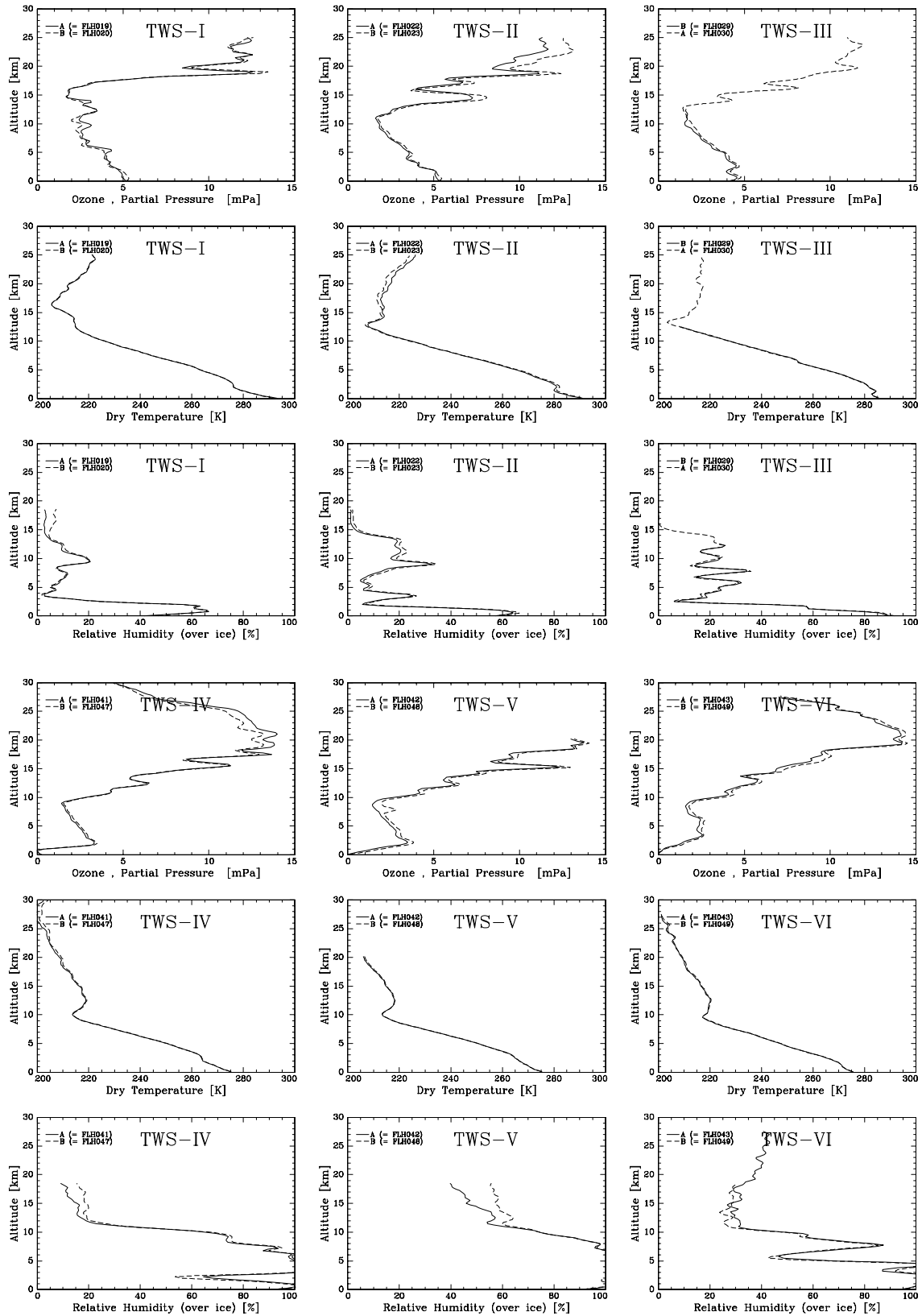
Figure A-2.2: *Vertical profiles of ozone pressure, temperature and relative humidity of the individual twin soundings made at the RV „Polarstern" in April 1987 during ANT-V/5 (TWS-I, TWS-II and TWS-III) and at Helsinki, Finland in November 1987 (TWS-IV, TWS-V and TWS-VI).*
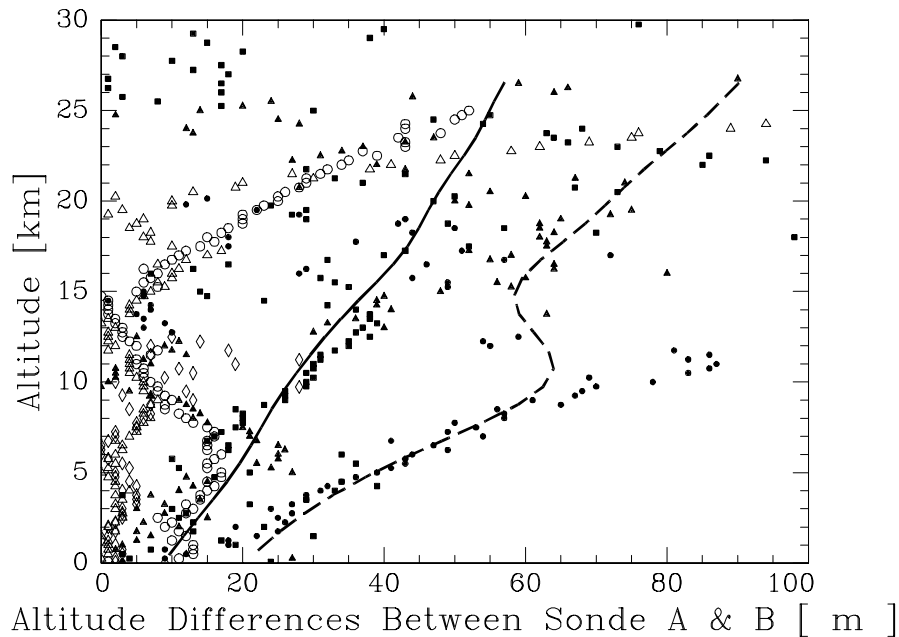
Figure A-2.3: *Twin soundings at RV „Polarstern" and Helsinki: Vertical distribution of the absolute differences between the altitudes determined from the sets of pressure, temperature and relative humidity measured by the simultaneously flown radiosondes A and B respectively.* o = TWS-I , Δ = TWS-II , ⊘ = TWS-III , v = TWS-IV , λ = TWS-V , σ = TWS-VI , *whereby the statistical 0.7- and 0.95-quantiles are represented by the fat solid and broken line respectively.*

The twin soundings at the two sounding sites were made under rather different meteorological conditions. The sonde comparisons from aboard the RV „Polarstern" were made during a strong anti-cyclonic situation with clear sky and relatively dry air conditions in the troposphere. This in contrast with the twin flights made at Helsinki, which were performed under cyclonic weather conditions with a strong and thick coverage of clouds in the lower and middle troposphere and hazy conditions near the surface.

During the three twin soundings carried out at Helsinki the ozone measured within the planetary boundary layer (PBL) was almost zero near the surface and increased to about 3.5 mPa at the top of the PBL at about 2 km altitude. This is probably affected by local air pollution which may have caused instrumental interferences by SO_2 (negative O_3), atmospheric removal of O_3 due to titration with NO into NO_2 or a combination of both. Above the PBL the recovery of both ozone sensors is fast and almost simultaneous. However, the ozone data obtained between the surface and the top of the PBL are discarded from further comparison.

The vertical profiles of the relative humidity obtained at Helsinki show large values above the tropopause which are unrealistic high for the relatively dry stratosphere [*Harries,* 1976, *Elsaesser et al.,* 1980]. The enhanced values measured in the stratosphere are of instrumental origin caused by icing of undercooled water droplets or condensation of water vapor flying through saturated clouds [*Antikainen and Paukkunen,* 1994]. The performance of the Humicap-A sensor above the tropopause is not reliable (see also Annex A-3, Section A-3.3) and therefore stratospheric humidity data were discarded from further comparison.

From the individual vertical profiles of ozone, temperature and relative humidity shown in Figure A-2.2 it is seen that the simultaneously flown sondes agree very well. Each sensor tracks atmospheric structures of length scales larger than 200 m very well.

A-2.4　Comparison Dual Flown Sondes

The vertical distributions of the absolute differences of pressure, temperature, relative humidity and ozone obtained from the simultaneous flown sondes are shown as scatter plots in figure A-2.4 which includes the results of the six twin soundings.
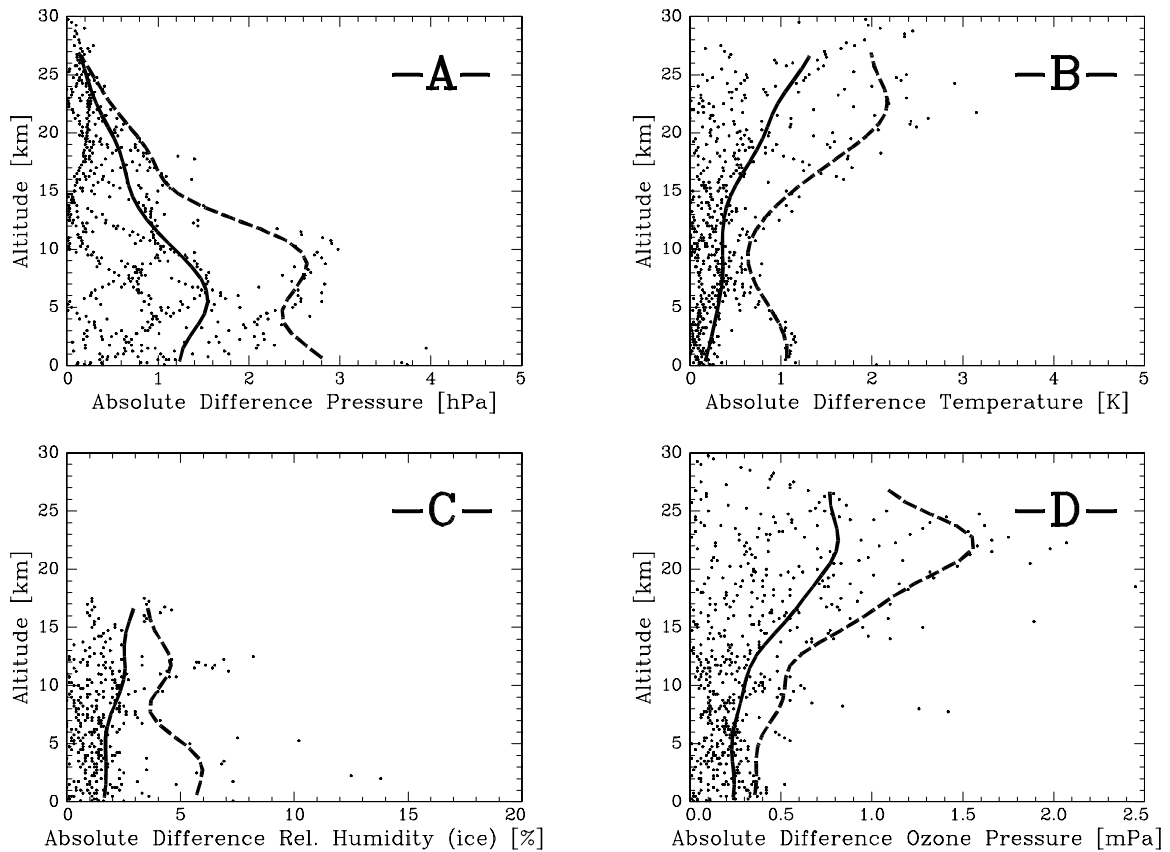

Figure A-2.4: *Twin soundings at RV „Polarstern" and at Helsinki: Vertical distribution of the absolute differences of pressure, temperature, relative humidity and ozone pressure between the two simultaneously flown sondes whereby the 0.7- and 0.95-quantiles are represented by the fat solid and broken line respectively.*

The distributions were obtained by first making the individual profiles for each twin sounding equidistant in flight time with an interval step of 50 s which corresponds to a height interval of around 250 m and then calculating the absolute differences between the two profiles for each quantity measured by the twin sonde.

From Figure A-2.4 it is seen that the pressure differences are relatively small: about 1-2 hPa in the lower troposphere and above 10 km altitude the differences are about 0.3-0.5 hPa.

The observed temperature differences, as shown in Figure A-2.4, are rather small. Near the surface the differences are between 0.2 an 0.4 K. The temperature differences are increasing

with altitude to about 0.5 K at 10 km and more pronounced to 1-2 K in the stratospheric regions. The upper limit of 2 K is exclusively determined by twin sounding TWS-II.

The increase of scattering of the data in the stratosphere is probably caused by a different sensitivity (heating) of the temperature sensors due to solar radiation. For solar radiation effects a standard empirical temperature correction, prescribed by the manufacturer, was applied [*Vaisala* , 1988] which is a function of the sun elevation angle, air density and ascent velocity (ventilation) and based on experimental investigations. However, the radiation correction is „rough", not very accurate[*Nash and Schmidlin,* 1987, *Nash,* Private Communication].

Differences of the relative humidity, shown in Figure A-2.4, are in general below 2-3 %. The incidental high values of around 5-15 % observed in the lower troposphere are exclusively obtained from the twin soundings made at Helsinki and may be caused by differences between the time responses of the two sensors entering the air masses with the strong vertical humidity gradients at 2 km altitude (See Figure A-2.2).

From Figure A-2.5 (left diagram) it is obvious that the observed differences between the simultaneously flown humidity sensors are rather constant over the entire range of the relative humidity. Neither show the observed differences a significant temperature dependence (see right diagram figure A-2.5).
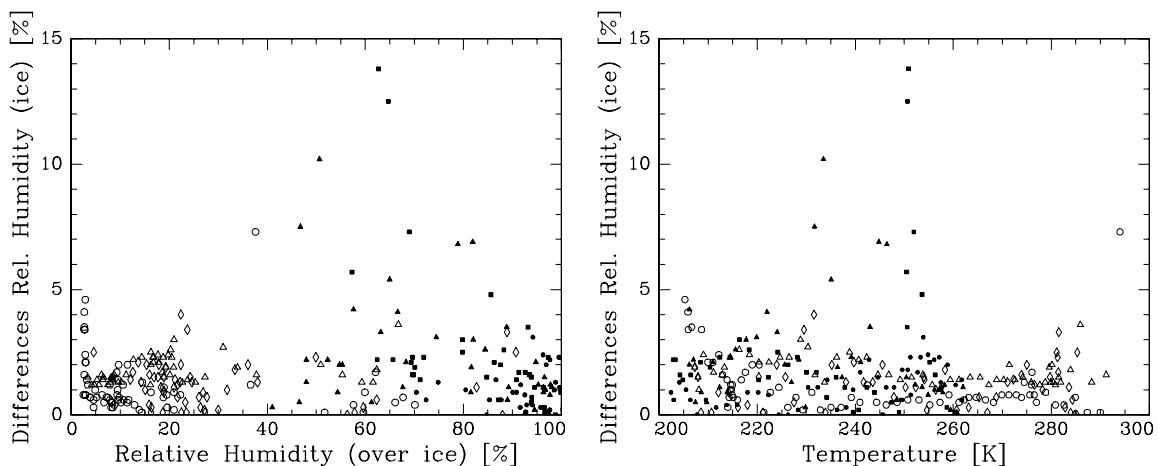

Figure A-2.5: *Twin soundings at RV „Polarstern" and Helsinki: Differences of the relative humidity between simultaneous flown ozone sondes as a function of the measured relative humidity itself (Figure-A: left diagram) and the air temperature (Figure-B: right diagram) respectively, whereby o = TWS-I , Δ = TWS-II , ⊘ = TWS-III , v = TWS-IV , λ = TWS-V , σ = TWS-VI.*

The absolute differences of the ozone pressure, shown in figure F-A-2-3, are about 0.2-0.3 mPa in the lower/middle troposphere and above 10 km the differences are increasing with altitude to about 0.4-0.6 mPa at 15 km and up to 0.5-1.0 mPa at 25 km.

The relative differences of ozone as a function of altitude are shown in Figure A-2.6. Different twin soundings represented by different symbols plus the 0.7- and 0.9-quantile are shown by the fat solid and dashed line respectively. It is depicted that the relative differences of ozone observed in the lower troposphere (0-5 km) are between 5-10 %. In the middle/upper

troposphere the differences are increasing up to about 10-15 %, while the scattering of the data is also increasing due to the low ozone pressures in the middle/upper troposphere. In the stratosphere the relative differences of ozone were about 5-10 %.
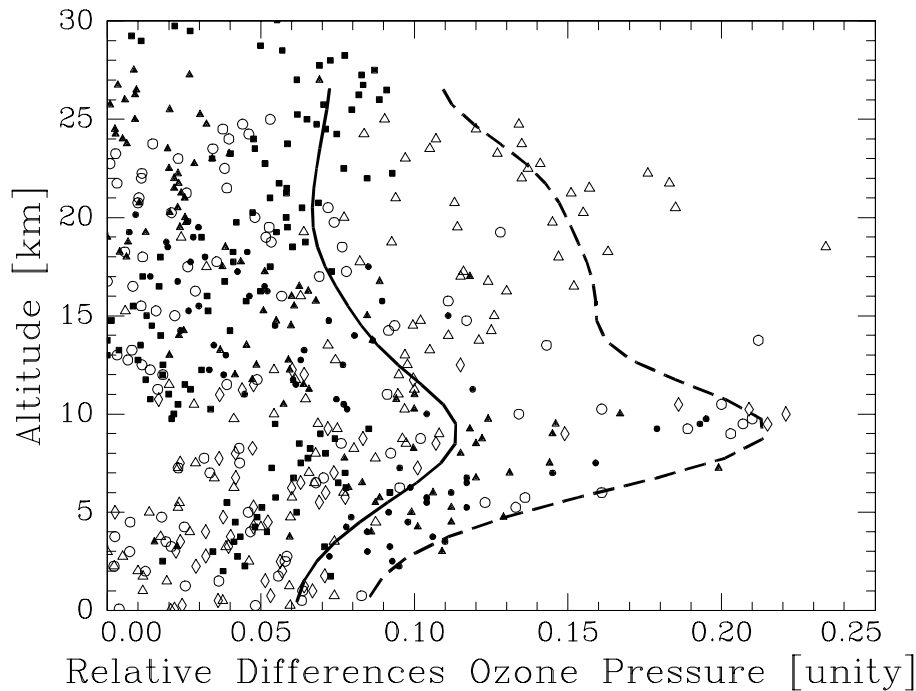

Figure A-2.6: *Twin soundings at RV „Polarstern" and Helsinki: Vertical distribution of the relative differences of the ozone pressure between simultaneously flown ozone sondes, whereby o = TWS-I , Δ = TWS-II , ⊘ = TWS-III , v = TWS-IV , λ = TWS-V , σ = TWS-VI , 0.7- and 0.95-quantiles are represented by the fat solid and broken line respectively.*

A-2.5   In-Flight Precision

The twin soundings have shown that each sensor of the ozone sonde as well as of the radiosonde tracks vertical structures in the atmosphere very well for length scales > 200 m. Good agreement between the individual profiles of ozone, pressure, temperature and relative humidity measured by the two simultaneously flown sondes has been observed.

The observed absolute differences of the different sensors can be directly interpreted in terms of reproducibility or precision of the sensors, namely half of the statistical width of about 0.7-quantile of the presented absolute differences corresponds to 1σ-precision of the different sensors. An overview of the precision of the different sensors of the sonde obtained from the twin soundings are summarized in Table A-2.2

It is concluded that the relative precision of the pressure sensor of the RS80 is good and only slightly decreasing with altitude. The precision of the temperature sensor of the sonde is good and slightly increasing with altitude which is probably due to solar radiation and its heating effect on the performance of the temperature sensor. The precision of the humidity sensor is better than ±(1-2) % of relative humidity over water/ice throughout the entire troposphere and independent of the relative humidity level itself. Further, the precision of the humidity sensor does not show any significant temperature dependence. Based on the precision of the P-, T-

and U-sensors the precision of the determination of altitude is ±10 m at 0-5 km, ±20 m at 5-10 km, ±30m at 10-15 km, ±40 m at 15-20 km , ±50 m at 20-25 km using the hydrostatic altitude equation [*Lenhard,* 1970, *Rieker,* 1976*, Parsons et al.*, 1984].

| | Ozone sonde 5A-ECC | | Radiosonde RS80 | | | | |
| | Ozone Pressure | | Pressure | | Tempera-ture | Relative Humidity | Altitude |
Altitude [km]	Absolute Precision [mPa]	Relative Precision [%]	Absolute Precision [hPa]	Relative Precision [%]	Absolute Precision [K]	Absolute Precision [%]	Uncertainty [m]
20-25	0.4	3	0.3	0.5	0.5	---	50
15-20	0.3	4	0.3	0.4	0.3	---	40
10-15	0.2	5	0.5	0.3	0.2	1-2	30
5-10	0.13	4	0.7	0.2	0.2	1-2	20
0-5	0.1	3	0.7	0.1	0.2	1-2	10
0	0.1	3	0.6	0.06	0.1	1-2	5

Table-A-2.2:   *Overview of the in-flight precision of the different sensors of the ECC-5A/RS80-sonde at different altitude levels obtained from twin soundings made at the RV-"Polarstern" and at Helsinki*

Annex-A-3

Performance of Humicap-A (RS80) at Low Temperatures

A-3.1   Introduction

At temperatures below 250 K little is known about the performance of the Humicap-A humidity sensor of the RS80-radiosonde. At the factory each Humicap-A sensor is calibrated only at temperatures well above 250 K. [*Antikainen,* private communication]. In other words, humidity measurements made with a Humicap-A sensor at temperatures below 250 K are in fact obtained from an extrapolation of the sensor's calibration curve determined at temperatures well above 250 K. To investigate the vertical water vapor distribution measured by the Humicap-A sensors during the two Atlantic cruises, it is important to know the thermal behavior of the sensor and to quantify its precision and accuracy, particularly under middle/upper tropospheric temperature conditions. In this section results of laboratory and field investigations about the performance of the Humicap-A sensor at low temperature are reported. Based on these investigations a correctional scheme for the dry bias observed at low temperatures has been derived.

A-3-2 Humicap-A Sensor at Zero and Saturated Humidities

The performance of the Humicap-A sensors of three RS80-radiosondes was tested in the simulation chamber at zero and saturated humidity conditions. The temperature was varied between 210 and 300 K. Zero and saturated relative humidity conditions were achieved by putting the sensor boom of the RS80 in a small closed aluminium box containing either a bed of molecular sieve as desiccant or a bed of water, respectively. At zero humidity conditions the sondes show zero drifts smaller than 1 % relative humidity over the entire temperature range of 210 - 300 K. The results of the experiments made at saturated conditions are shown in Figure A-3.1 and are presented in terms of relative humidity with respect to liquid water.
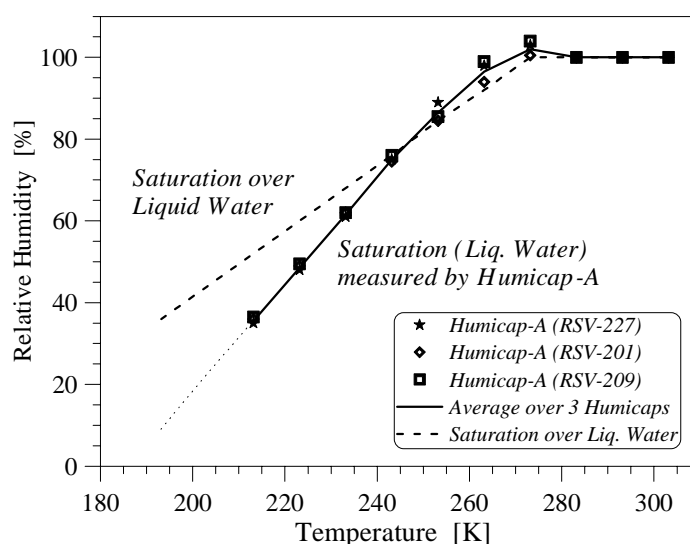

Figure A-3.1: *Simulation chamber experiment of Humicap-A sensor at saturated humidity conditions as a function of temperature (solid thick line). The thin dotted line is a hypothetical linear extrapolation to temperatures below 215 K. The theoretical curve of saturation with respect to liquid water is presented by a dashed line.*

Each humidity sensor showed similar results with a good reproducibility and a precision better than ±(1-2) %. At temperatures above 275 K the sensors agreed within ±1% at saturation. At lower temperatures comparing the results with the theoretical curve of saturation with respect to liquid water it is seen that in the temperature range of 250-275 K the sensors were slightly overestimating saturation. Below 250 K the opposite was the case: a dry bias was observed which was strongly increasing with decreasing temperatures.

Although only an ensemble of three sensors were measured the experiments have shown that the reproducibility i.e. precision of the Humicap-A sensors is good and in agreement with the results obtained from the twin sounding (see overview in Table A-2.2 in Annex A-2). However, below 250 K the Humicap-A sensors are suffering a dry bias such that a recalibration of the sensor at lower temperatures is required. Down to 190 K the dynamic range of the sensor is getting smaller but the sensitivity is still sufficient to enable a calibration or at least a correctional procedure to eliminate the dry bias at low temperatures.

A-3.3   Humicap-A Sensor Versus Frost Point Hygrometer

In collaboration with NOAA/CMDL, Boulder-CO, USA, and MPI, Mainz, Germany a field intercomparison of the Humicap-A sensor and the newer Humicap-H sensor of the RS80 radiosonde against a frost point hygrometer (FPH) was made as part of the CEPEX (=Central Equatorial Pacific Experiment) program in March 1993 [*Kley et al.*, 1997]. Reference humidity profiles obtained by balloon borne frost point hygrometers were used to validate simultaneously measured profiles by the Humicap-A sensors (see this section) or the Humicap-H sensors which were flown regularly (every 6 hours) in the same campaign period and launch platform (see Section A-3.4). The intercomparison was part of an extensive water vapor sounding program using different types of water vapor sensors to investigate the role of deep convection on the water vapor distribution in the central equatorial Pacific. The results are reported in detail by *Kley et al.* [1997].

A total of 12 balloon soundings of frost point hygrometers (FPH) with attached RS80-radiosondes, flown during CEPEX in March 1993, were used to validate and calibrate the Humicap-A sensor at temperatures below 275 K. The soundings were made in the central equatorial Pacific between 160 ^{o}W and 160 ^{o}E under typical tropical conditions: extreme low upper tropospheric temperatures (minimum 183 K), high tropopause at 17 km and high humidities up to the tropopause. The frost point hygrometer used as reference instrumentation is of the type developed by *Mastenbrook* [1966] and modified by *Mastenbrook and Oltmans* [1983]. The instrument measures the temperature of a chilled mirror at which frost starts to form. During the intercomparison the accuracy of the Frost Point Hygrometer was estimated ±2 ^{o}C [*Kley et al,* 1997], slightly higher than the usual accuracy of ± 1 ^{o}C due to radio interferences [*Vömel et al.,* 1995]. The Frost Point Hygrometer is only operational at temperatures below 273 K, no FPH results are given at higher temperatures.

Examples of simultaneously measured vertical profiles of temperature and relative humidity from Humicap-A and frost point hygrometer are shown in Figure A-3.2. From both soundings it is seen that below 10 km altitude the Humicap-A is in good agreement with the frost point hygrometer and tracks very well structures of length scales larger than 500 m. Above that altitude the Humicap-A readings are too low. This effect is observed in all soundings which is clearly seen by the differences of frost point temperatures derived from Humicap-A to frost point hygrometer of all relevant combined soundings plotted as function of temperature as shown in Figure A-3.3.
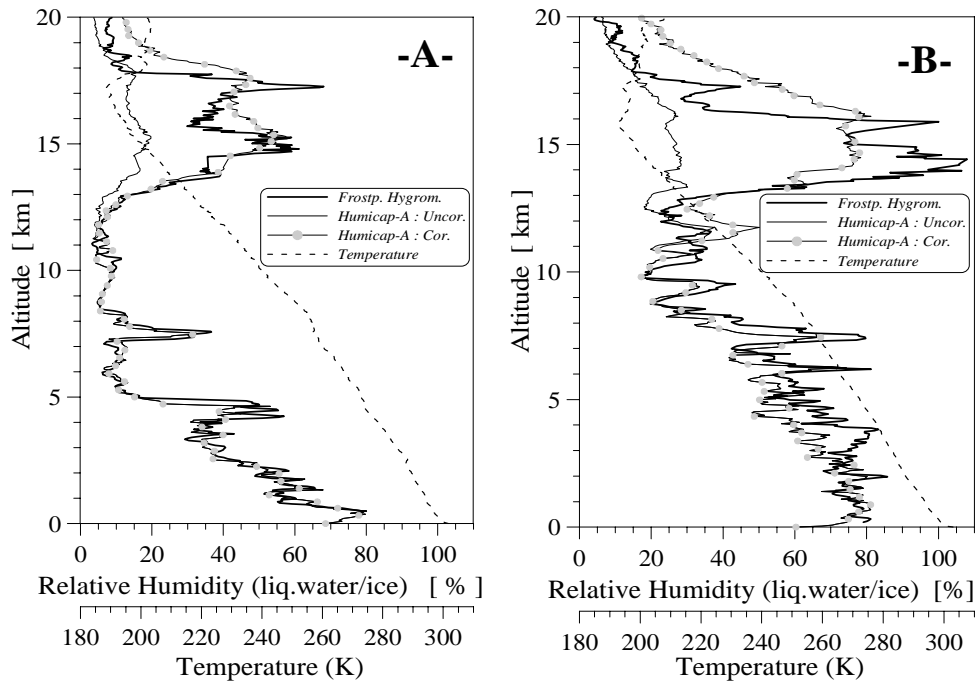
Figure A-3.2: *Vertical humidity profiles by Humicap-A (thin solid line) and Frost Point Hygrometer (thick solid line) and Temperature (dashed line) obtained from combined soundings at 1 °S, 159 °W at 17 March 1993 (Diagram A) and at 1 °N, 157 °W at 24 March 1993 (Diagram B) made during CEPEX. Thin line plus dotted symbol is temperature corrected Humicap-A reading after use of the scheme listed in Table A-3.1.*
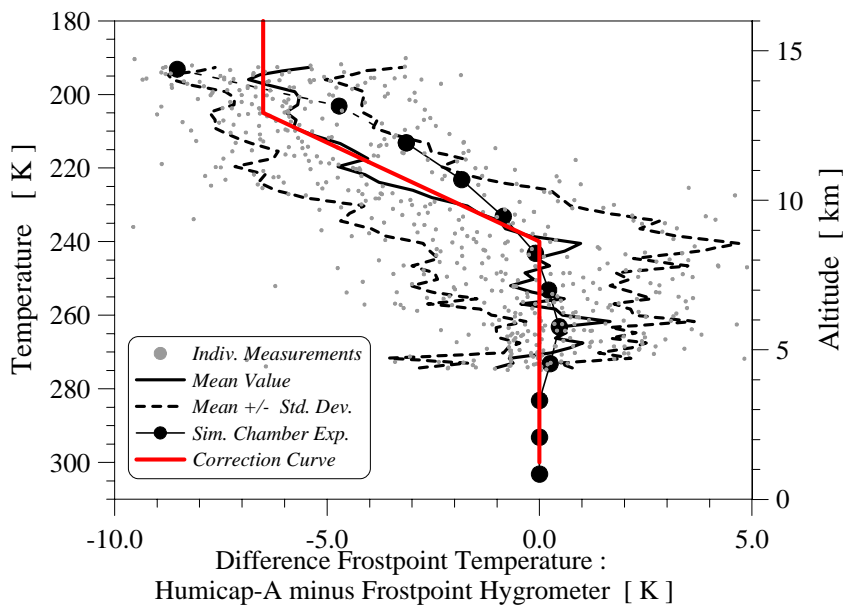

Figure A-3.3: *Differences of Humicap-A derived frost point temperatures to frost point temperatures measured by the Frost Point Hygrometer obtained from 12 combined soundings made during CEPEX. Data points (gray dots) are averages over 250 m intervals. Mean (solid line) plus/minus 1σ-standard deviation (broken lines). Gray line functional fit of mean used to correct for dry bias of Humicap-A at low temperatures. Thin solid line with fat dots is the dry bias observed from simulation chamber experiments (see Section A-3.3)*

The scatter plot reveals a very small positive bias of the Humicap-A at temperatures between 250 K and 275 K and below 240 K a trend to a negative bias of -6.5 K at 200 K. The standard deviation from the mean is rather constant at ±3 K and is dominated by the contributions of the uncertainties of the Frost Point Hygrometer (± 1-2 K), Humicap-A (±1 K) and the temperature sensor (±1 K) of the RS80. Since the sensors were flown on the same balloon both were exposed to identical humidities. Therefore, Figure A-3.3 represents a true evaluation of the Humicap A sensor under the flight conditions.

The thermal behavior of the Humicap-A derived from the results of the simulation chamber experiments carried out at saturated conditions (see Figure A-3.3: thick line with the fat dotted symbols) shows also a negative bias between 240 K and 200 K. However, the slope of the bias is not steep and assuming the hypothetical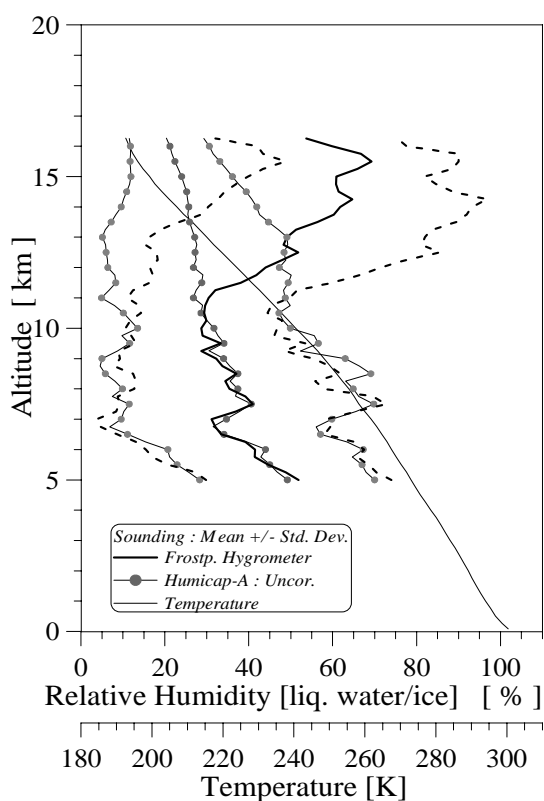 extrapolation of the curve from 215 K to lower temperatures the bias may even exceed -6.5 K below 200 K. Although the thermal behavior of the Humicap-A is similar to the observed differences and may explain that the statistical comparison of the differences of the Humicap-A to FPH shown in Figure A-3.3 have an inherent response time problem. At an ascent rate of 5 m/s the response time (height resolution) of the Humicap is strongly increasing at lower temperatures: at 293 K ≈1 s (5 m), at 230 K ≈ 1 min (300 m) and at 200 K ≈10 min (3 km) [*Antikainen and Paukkunen,* 1994] [1] . This causes a humidity lag (phase shift) between Humicap-A and FPH and an integration effect which reduces the amplitude of the humidity changes observed by the Humicap-A and will spread out the actual humidity structures measured by the FPH. Both effects are clearly seen in the two combined soundings shown in Figure A-3.2. With regard to the statistical comparison shown in Figure A-3.3 the humidity lag and the integration effect of the Humicap-A will cause an overestimation of the difference of Humicap-A to FPH at increasing parts of the individual relative humidity profiles and an underestimation at decreasing relative humidities.

Figure A-3.4: *Mean relative humidity vertical profile (solid line) plus/minus 1σ-standard deviation (dashed lines) over 12 combined soundings of Frost Point Hygrometer (fat lines) plus attached Humicap-A (thin lines plus circle-symbol) made during CEPEX. Temperature represented by thin solid line.*

From the mean profiles plus/minus their standard deviations of all relevant relative humidity profiles obtained from the Frost Point Hygrometer shown in Figure A-3.4 it is clearly seen that during ascent at temperatures from

---

[1] Dominating factors determining the time response of the sensor are the porosity of the surface electrode and the diffusivity of the polymer layer with respect to water vapor. Both factors are strongly decaying with decreasing temperature such that at lower temperatures the response times are increasing drastically.

230 K down to 200 K trends of increasing relative humidities are more favorable. It indicates that in this part of the profile the mean difference of Humicap-A to FPH (see Figure A-3.3) has been overestimated and may explain the enhanced values compared with the results obtained from the simulation chamber experiments. It is obvious that the statistical comparison may reflect not only the Humicap-A sensor sensitivity to relative humidity at different temperatures but contains also contributions originating from the time response behavior of the sensor.

A-3.4   Correctional Scheme for Dry Bias of Humicap-A Below 240 K

The results of the comparison (See Figure A-3.3) are used to derive a revised algorithm to correct the Humicap-A sensor readings for the dry bias at temperatures below 240 K by a straight line fit to the mean of the differences of Humicap-A to FPH (See Figure A-3.3: gray thick line). The scheme to correct the frost point temperature derived Humicap-A readings are listed in Table A-3.1. The uncertainty of the corrected Humicap-A derived frost point temperature is assumed to ± 3 K according to the standard deviation of the differences between Humicap-A and FPH. Correspondingly corrected relative humidity readings of the Humicap-A have an uncertainty factor of about ± 0.3 of the corrected values.

Temperature Range	Correction Frost Point Temperature: $\Delta T_{F,C}$
$T > 240$ K	$\Delta T_{F,C} = 0$ K
205 K $\leq T \leq 240$ K	$\Delta T_{F,C} = -0.186 \cdot T + 44.6$ K
$T < 205$ K	$\Delta T_{F,C} = +6.5$ K

Table A-3.1: *Correctional scheme of frost point temperature derived Humicap-A sensor reading at low temperatures obtained from comparison with frost point hygrometer.*

According to the scheme in Table A-3.1 the vertical humidity profiles of the Humicap-A from the two soundings are corrected and shown in Figure A-3.2. Both Humicap-A profiles show a much better agreement and deviations are within the uncertainty factor of ± 0.3 of the corrected value. However, this shows also very clearly the limits of the sensor at temperature below about 200 K: the humidity lag exceeding 3 km due to the large response times at low temperatures and a strong spread out of the humidity structures is seen. It is obvious that the performance at these lower temperatures is not limited by sensitivity of the sensor but by the large response times. The large humidity lag may cause that the humidity values observed above the tropopause, in the lower stratosphere, being too large. In general, the performance of the Humicap-A sensor is not reliable above the tropopause and Humicap-A measurements made in the stratospheric region have been excluded from further investigation. All relative humidity measurements made with the Humicap-A sensor of RS80-radiosounding during the two Atlantic cruises have been revised according the scheme shown in Table A-3.1.

A-3.5   Condensation/Icing on the Surface of the Humicap Sensor

Water condensation or icing on the surface of the sensor or surfaces nearby can have a dramatic influence on the performance of the Humicap-A. This is illustrated in Figure A-3.5 which shows this unfavorable effect from a sounding made at 20. March 1993 during CEPEX by comparing the vertical humidity profiles measured by FPH and Humicap-A
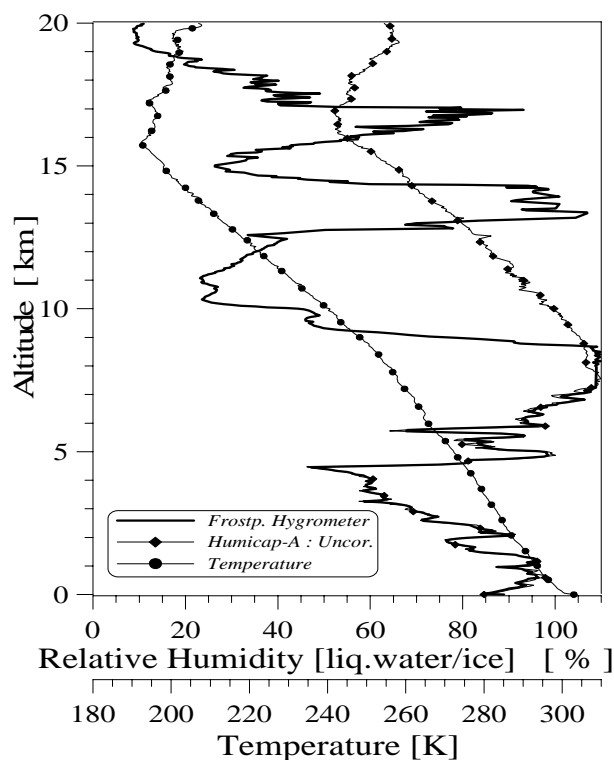
The FPH-derived humidity profile shows saturation between 5 and 9 km followed by a drop to 25 % between 10 and 12 km and an almost saturated layer at 13-14 km. The Humicap-A never recovers after entering the saturated, perhaps precipitating, layer above 5 km. Since the temperatures inside this saturated layer were near freezing it is likely that the sensor was coated with ice and that evaporation was too slow during the remainder of the sounding to recover the sensor.

Ice on the sensor may form when super cooled water droplets hit the sensor or when water vapor condenses on the surface. Condensation of ice is a minor phenomenon [*Antikainen and Hyvonen, 1985, Antikainen and Paukkunen, 1994*]. In general erroneous Humicap-A readings caused by ice coating of the sensor can clearly be identified by the erroneous large humidity readings in the stratosphere and may serve as quality screening criterion to check the performance of the sensor in the troposphere (see also Annex A-2).

Figure A-3.5: *Vertical relative humidity profiles measured by Humicap-A (thin solid line) and Frost Point Hygrometer (thick solid line) plus temperature (dashed line) obtained from combined sounding made at 1 °N, 157 °W at 20 March 1993 during CEPEX..*

References

Andrews, D.G., J.R. Holton, C.B. Leovy, Middle atmosphere dynamics, *Academic Press Inc., London,* **1987**.

Anderson, P.S., Mechanism for the behavior of hydroactive materials used in humidity sensors, *J. Atmos. Oceanic. Tech., 12*, 662-667, **1995**.

Antikainen, V., and V. Hyvonen, The accuracy of Vaisala RS80 radiosonde, *Proc. Fifth Symposium on Meteorological Observations and Instrumentation 1983, Amer. Meteor. Soc.*, Washington DC, 134-140, **1983.**

Antikainen, V., and V. Hyvonen, Radiosonde performance in rain and clouds, WMO/TD-No.50, Geneva , **1985.**

Antikainen, V., and Paukkunen, A., Studies on improving humidity measurements in radiosondes. In: Instruments and observing methods, *Report No. 57, WMO-TD-No. 588,* 137-141, **1994**.

Arlander, D.W., D. Brüning, U. Schmidt, and D.H. Ehhalt, The tropospheric distribution of formaldehyde during TROPOZ II, *J. Atmos. Chem., 22,* 251-268, **1995**.

Attmannspacher, W. and H. Dütsch , International Ozone Sonde Intercomparaison at the Observatory of Hohenpeissenberg, *Berichte des Deutschen Wetterdienstes, 120*, **1970**.

Attmannspacher, W. and H. Dütsch, 2nd International Ozone Sonde Intercomparaison at the Observatory of Hohenpeissenberg, *Berichte des Deutschen Wetterdienstes, 157,* **1981**.

Balsley, B.B., W.L. Ecklund, D.A. Carter, A.C. Riddle, and K.S. Gage, Average vertical motions in the tropical atmosphere observed by a radar wind profiler on Pohnpei (7°N Latitude, 157°E Longitude, *J. Atmos. Sci., 45*, 396-405, **1988**.

Beekmann, M., G. Ancellet, G. Megie, H.G.J. Smit, and D. Kley, Intercomparison campaign for vertical ozone profiles including electrochemical sondes of ECC and Brewer-Mast type and a ground based UV-differential absorption lidar, *J. Atmos. Chem., 19,* 259-288, **1994.**

Beekmann, M., G. Ancellet, D. Martin, C. Abonnel, G. Duverneuil, F. Eidelimen, P. Bessemoulin, N. Fritz, and E. Gizard, Intercomparison of tropospheric ozone profiles obtained by electrochemical sondes, a ground based lidar and airborne UV-photometer, *Atm. Env., 29,* 1027-1042, **1995**.

Behr, H.D., H. Köhler, R. Schmidt, and D. Winterkemper, Weather conditions during the expedition ANT-VII/1, in I. Hempel (ed.), *Reports on polar research vol. 62, 9-15, Alfred Wegener Institut für Polar -und Meeresforschung, Bremerhaven, FRG,* **1989**.

Behr, H. D., and G. Gravenhorst, Synoptic situation in the Atlantic Ocean region during ANT-V/5, *J. Geophys. Res., 95,* 20569-20581, **1990**.

Betts, A.K., Greenhouse warming and the tropical water budget, *Bull. Amer. Meteor. Soc., 71*, 1464-1465, **1990.**

Bevington, P.R, and D.K. Robinson, Data reduction and error analysis for the physical sciences, *MacGraw-Hill Inc, New York*, **1992**.

Brauers, T., and A. Hofzumahaus, Latitudinal variation of measured NO_2 photolysis frequencies over the Atlantic Ocean between 50°N and 30°S, *J. Atmos. Chem., 15,* 269-282, **1992**.

Bretherton, C.S., and P.K. Smolarkiewicz, Gravity waves, compensating subsidence, and detrainment around cumulus clouds, *J. Atmos. Sci., 46,* 740-759, **1989**.

Brewer, A.W., Evidence for a world circulation provided by the measurements of helium and water vapor distribution in the stratosphere, *Q.J.R. Meteorol. Soc., 76,* 351-363, **1949.**

Brewer, A. and J. Milford, The Oxford Kew ozone sonde, *Proc. Roy. Soc.London, Ser. A, 256,* 470, 1960.

Brown, R.G., and C. Zhang, Variability of mid-tropospheric moisture and its effect on cloud top height distribution during TOGA-COARE, *J. Atmos. Sci., 54,* 2760-2774, **1997.**

Carroll, M.A. and A.M. Thompson, NO_X in the non-urban troposphere, In: Progress and problems in atmospheric chemistry (Ed. J.R. Barker), *Advanced Series in Physical Chemistry-Vo.3, World Scientific Publ., Singapore,* 198-255, **1995**.

Cess, R.D., M.H. Zhang, P. Minnis, L. Corsetti, E.G. Dutton,B.W. Forgan, D.P., Garber, W.L. Gates, J.J. Hack, E.F. Harrison, X. Jing, J.T. Kiehl, C.N. Long, J.J. Morcrette, G.L. Potter, V. Ramanathan, B. Subasilar, C.H. Whitlock,D.F. ,Young, and Y. Zhou, Absorption of solar radiation by clouds: observation versus model, *Science, 267,* 496-499, **1995**.

Chameides, W., and J.C.G. Walker, A photochemical theory of tropospheric ozone, *J. Geophys. Res., 78,* 8751-8760, **1973**.

Chatfield, R.B., and P.J. Crutzen, Sulfur dioxide in remote oceanic air: cloud transport of reactive precursors, *J. Geophys. Res., 89,* 7111-7132, **1984**.

Cohan, D.S., M.G. Schultz, and D.J. Jacob, Convective injection and photochemical decay of peroxides in the tropical upper troposphere: Methyl iodide as a tracer of marine convection, *J. Geophys. Res. 104,* 5717-5724, **1999**.

Cotton, W. R., R.A. Anthes, Storm and Cloud Dynamics, *Academic Press, New York,* **1989.**

Crawford, J., D. Davis, J. Olsen, G. Chen, S. Liu, G. Gregory, J. Barrick, G. Sachse, S. Sandholm, B. Heikes, H. Singh, and D. Blake, Assessment of upper tropospheric HO_X sources over the tropical Pacific based on NASA GTE/PEM data: Net effect on HO_X and other photochemical parameters, *J. Geophys. Res., 104,* 16,225-16,273, **1999**.

Crutzen, P.J., A discussion of the chemistry of some minor constituents in the stratosphere and troposphere, *Pure Appl. Geophys., 106-108,* 1385-1399, **1973**.

Crutzen, P.J., Photochemical reactions initiated by and influencing ozone in unpolluted tropospheric air, *Tellus, 26,* 47-57, **1974**.

Crutzen, P.J., The role of NO and NO_2 in the chemistry of the troposphere and stratosphere, *Ann. Rev. Earth Planet. Sci., 7,* 443-472, **1979**.

Crutzen, P.J., Tropospheric Ozone: An overview, *in Tropospheric Ozone, edited by I.S.A. Isaksen, D. Reidel, Dordrecht*, 3-32*,* **1988**.

Crutzen, P.J., and M.O. Andreae, Biomass burning in the tropics: Impact on atmospheric chemistry and biochemical cycles, *Science, 250,* 1669-178, **1990**.

Curry, J.A., and P.J. Webster, Thermodynamics of Atmospheres & Oceans, *Int. Geophys. Ser. Vol. 65, Academic Pres, New York,* **1999**.

Daniels, F. and R.A. Alberty, Physical Chemistry, Fifth Edition, *Wiley and Sons, New York*, **1979.**

Danielsen, E. F., Stratosphere-troposphere exchange based on radioactivity, ozone, and potential vorticity, *J. Atmos. Sci., 25,* 502-518, **1968**.

Danielsen, E.F., and V.A. Mohnen, Project Duststorm report: Ozone transport, in situ measurements and meteorological analyses of tropopause folding, *J. Geophys. Res., 82,* 5867-5877, **1977**.

Danielsen, E.F., In situ evidence of rapid, vertical, irreversible transport of lower tropospheric air into the lower tropical stratosphere by convective cloud turrets and by large scale upwelling in tropical cyclones, *J. Geophys. Res., 98,* 8665-8681, **1993.**

Denton, D.D., J.B. Camou, and S.D. Senturia, Efects of moisture take up on the dielectric permttivity of polymide films, *Proc. of Int. Symp. on Moisture and Humidty 1985: Measurement and Control in Science and Industry, Washington DC*, **1985**.

Donahue, N.H. and R.G. Prinn, In situ nonmethane measurements on SAGA 3, *J. Geophys. Res., 98,* 16,915-16,932, **1993**.

Dopplick, T.G., Radiative heating of the global atmosphere, *J. Atmos. Sci., 29,* 1278-1294, **1972**.

Drummond, J.W., D.H. Ehhalt, and, A. Volz, Measurements of nitric oxide between 0-12 km altitude and 67^ON - 60^OS latitude obtained during Stratoz III., *J. Geophys. Res., 93,* 15831-15849, **1988**.

Ehhalt, D.H., F.Rohrer, and A. Wahner, Sources and distribution of NO_X in the upper troposphere at northern mid-latitudes, *J. Geophys. Res., 97,* 3725-3738, **1992**.

Elliott, W.P. and D.J. Gaffen, On the utility of radiosonde humidity archives for climate studies, *Bull. Am. Met. Soc., 72,* 1507-1520, **1991**

Elsaesser, H.W., J.E. Harris, D. Kley, and R. Penndorf, Stratospheric H_2O, Planet. *Space Sci., 28,* 827-835, **1980**.

Emmons, L.K., et al., Climatologies of NO_X and NO_Y: A comparison of data and models, *Atmos. Environ., 31,* 1851-1903, **1997**.

Fabian, P., and P.G. Pruchniewicz, Meridional distribution of ozone in the troposphere and its seasonal variations, *J. Geophys. Res., 82,* 2063-2073, **1977**.

Finlayson-Pitts, B.J., and J.N. Pitts, Jr., Tropospheric air pollution: Ozone, airborne toxics, polycyclic aromatic hydrocarbons, and particles, *Science, 276,* 1045-1052, **1997.**

Fishman, J.,and P. J. Crutzen, The origin of ozone in the troposphere, *Nature, 274,* 855-858, **1978**.

Fishman, J., S. Solomon, and P. J. Crutzen, Observational and theoretical evidence in support of a significant in-situ photochemical source of tropospheric ozone, *Tellus, 31,* 432-446, **1979**.

Fishman, J., C.E. Watson, J.C. Larsen, and J.A. Logan, Distribution of tropospheric ozone determined from Satellite data, *J. Geophys. Res., 95,* 3599-3617, **1990**.

Folkins et al., OH , HO_2 , and NO in biomass burning plumes: Sources of HO_X and implications for ozone production, *Geophys.Res.:Lett., 24,* 3185-3188, **1997.**

Folkins, I., R. Chatfield, H. Singh, Y. Chen, and B. Heikes, Ozone production efficiences of acetone and peroxides in the upper troposphere, *Geophys. Res. Letters, 25,* 1305-1308, **1998.**

Folkins, I., M. Loewenstein, J. Podolske, S. Oltmans, and M. Proffitt, A barrier to vertical mixing at 14 km in the tropics: Evidence from ozonesondes and aircraft measurements, *J. Geophy. Res., 104,* 22095-22101, **1999**.

Folkins, I., C. Baum, A.M. Thompson, and J.C. Witte, Tropical ozone as an indicator of deep convection, *J. Geophys. Res.*, *107,* 10.1029/2001JD001178, **2003**.

Fujiwara, M., K. Kita, and T. Ogawa, Stratosphere-troposphere exchange of ozone associated with the equatorial Kelvin waves as observed with ozone sondes and rawind-sondes, *J. Geophys. Res., 103*, 19173-19182, **1998.**

Gaffen, D.J., Historical changes in radiosonde instruments and practices, -Final Report.- Instr. And Obs. Methods Rep. No. 50, *WMO/TD-No.541*, 123 p., Geneva, **1993**.

Gage, K.S., J.R. McAfee, D.A. Carter, W.L. Ecklund, A.C. Riddle, G.C. Reid, B.B. Balsley, Long term mean vertical motion over the tropical Pacific: Wind profiling Doppler radar measurements, *Science, 254,* 1771-1773, **1991**.

Galbally, I. E.,and C. R. Roy, Destruction of ozone at the earth's surface. *Quart. J. Roy. Met. Soc.*, *106*, 599-620, **1980**.

Gidel, L.T., Cumulus cloud transport of transient tracers, *J. Geophys. Res., 88,* 6587-6599, **1983**.

Goff, J.A., and Gratch, S., Low-pressure properties of water from -160 to 212 F, *Trans. Amer. Soc. Heat. Vent. Eng., 52,* 95-122, **1946.**

Graedel, T.E., and P.J. Crutzen, Atmospheric change, *Freeman and Company, New York,* **1993**.

Graham, N.E., and T.P. Barnett, Sea surface temperature, surface wind divergence, and convection over tropical oceans, *Science, 238,* 657-659, **1987**.

Haagen-Smit, A.J., Chemistry and physiology of Los Angeles smog, *Indust. Eng. Chem., 44*, 1342-1346, **1952**.

Haagen-Smit, A.J., C.E. Bradley, and M.M. Fox, Ozone formation in photochemical oxidation of organic substances, *Indust. Eng. Chem., 45*, 2086-2089, **1953**.

Harries, J.E., The distribution of water vapor in the stratosphere, *Rev. Geophys. Space Phys., 14,* 565-575, **1976**.

Harries, J.E., The greenhouse effect: A view from space, *Q.J.R. Meteorol. Soc., 122,* 799-818, **1996**.

Harries, J.E., Atmospheric radiation and atmospheric humidity, *Q.J.R. Meteorol. Soc., 123*, 2173-2186, **1997**.

Harris, G.W., D. Klemp, T. Zenker, J.P. Burrows, and B. Mathieu, Tunable diode laser measurements of trace grases during 1988 Polarstern cruise and intercomparisons with other methods, *J. Atmos. Chem.,* 15, 315-326, **1992**.

Harrison, E.F., P. Minnis, B.R. Barkstrom, V. Ramanathan, R.D. Cess, and G.G. Gibson, Seasonal variation of cloud radiative forcing derived from the Earth Radiation Budeget Experiment, *J. Geophys. Res., 95,* 18,687-18,703, **1990.**

Hartmann, D.L., Global physical climatology, *Academic Press, London*, **1994**

Hastenrath, S., Climate dynamics of the tropics, *Kluwer Academic Publishers, Dordrecht*, **1995.**

Held, I.M., and B.J. Soden, Water vapor feedback and global warming, *Ann. Rev. Energy Environ., 25,* 441-475, **2000.**

Highwood, E.J., and, B.J. Hoskins, The tropical tropopause, Q. J. R. Meteorol. Soc., 124, 1579-1604, **1998**.

Hilsenrath, E., W. Attmannspacher, A. Bass, W. Evans, R. Hagemeyer, R.A. Barnes,W.Komhyr, K. Mauersberger, J. Mentall, M. Profitt, D. Robbins, S. Taylor, A. Torres and E. Weinstock, Results from the Balloon Ozone Intercomparison Campaign (BOIC), *J. Geophys. Res. 91,* 13137-13152, **1986**.

Hofzumahaus, A., T. Brauers, U. Platt, and J. Callies, Latitudinal variation of measured O_3 photolysis frequencies J(O1D) and primary OH production rates over the Atlantic Ocean between 50^ON and 30^OS, *J. Atmos. Chem., 15,* 283-298, *1992*.

Holten, J.R., An introduction to dynamic meteorology, Second Edition, *Academic Press Inc., London,* **1979**.

Holton, J.R., P.H. Haynes, M.E. McIntyre, A.R. Douglass, R.B. Rood, and L. Pfister, Stratosphere-troposphere exchange, *Rev. Geophys., 33,* 403-439, 1995.

Horowitz, L.W., and D.J. Jacob, Global impact of fossil fuel combustion on atmospheric NO_X, *J. Geophys. Res., 104,* 23,823-23,840, **1999**.

Houze, R.A., and A.K. Betts, Convection in GATE, *Rev. Geophys. Space Phys., 19*, 541-765, **1981.**

IGAC, Atmospheric Chemistry in a Changing World, An integration and synthesis of a decade of tropospheric Chemistry Research, Eds. G.P. Brasseur, R.G. Prinn, A.A.P. Pszenny, *Springer Verlag, Berlin,* **2003**.

Inamdar, A.K., and V. Ramanathan, Physics of greenhouse effect and convection in warm oceans, *J. Clim., 5*, 715-731, **1994**.

Inamdar, A.K., and V. Ramanathan, Tropical and global scale interactions among water vapor, atmospheric greenhouse effect, and surface temperature, J. Geophys. Res., 103, 32,177-32,194, **1998**.

IPCC (=Intergovernmental Panel on Climate Change), Climate Change 1995, The Science of Climate Change, Intergovernmental Panel on Climate Change, *Cambridge University Press, Cambridge, UK,* **1996.**

IPCC, Third Assessment Report, Intergovernmental Panel on Climate Change, Cambridge University Press, Cambridge, UK, 2001.IPCC, Climate Change 1995, The Science of Climate Change, Intergovernmental Panel on Climate Change, *Cambridge University Press, Cambridge, UK*, **2001**.

Jacob, D.J., J.A. Logan, G.M. Gardner, R.M. Yevich, C.M. Spivakovsky, and S.C. Wofsy, Factors regulating ozone over the United States and its export to the global atmosphere, *J. Geophys. Res. 98,* 14817-14826, 1993.

Jacob, P., and D. Klockow, Hydrogen peroxide measurements in the marine atmosphere, *J. Atmos. Chem., 15,* 353-360, **1992**.

Jacob, D.J., B.G. Heikes, S.M. Fan, J.A. Logan, D.L. Mauzerall, J.D. Bradshaw, H.B. Singh, G.L. Gregory, R.W. Talbot, D.R. Blake, and G.W. Sachse, Origin of ozone and NO_X in the tropical troposphere: A photochemical analysis of aircraft observations over the South Atlantic basin, *J. Geophys. Res., 101*, 24,235-24,250, **1996.**

Jaeglé, L., D.J. Jacob, P.O. Wennberg, C.M. Spivakovsky, T.F. Hanisco, E.J. Lanzendorf, E.J. Hintsa, D.W. Fahey, E.R. Keim, M.H. Proffitt, E.L. Atlas, F. Flocke, S. Schauffler, C.T. McElroy, C. Midwinter, L. Pfister, and J.C. Wilson, Observed OH and HO$_2$ in the upper troposphere suggest a major source from convective injection of peroxides *Geophys. Res. Letters, 24*, 3181-3184, **1997.**

Jaeglé, L., D.J. Jacob, W.H. Brune, D. Tan, I.C. Faloona, A.J. Weinheimer, B.A. Ridley, T.L. Campos, and G.W. Sachse, Sources of HO$_X$ and production of ozone in the upper troposphere over the United States, *Geophys. Res. Letters, 25*, 1709-1712, **1998.**

Jet Propulsion Laboratory-JPL Evaluation Number 14, National Aeronautics and Space Administration (NASA), Chemical kinetics and photochemical data for use in atmospheric studies, Evaluation 14, *JPL Publication 02-25*, **2003**.

Johnson, J.E. , R.H. Gammon, J. Larsen, T.S. Bates, S.J. Oltmans, and J.C. Farmer, Ozone in the marine boundary layer over the Pacific and Indian Oceans: Latitudinal gradients and diurnal cycles, *J. Geophys. Res., 95,* 11847-11856, **1990**.

Johnson, R.H., P.E. Ciesielski, and K.A. Hart, Tropical inversions near the 0oC level, *J. Atmos. Sci, 53,* 1838-1855, **1996.**

Johnson, B.J., S.J. Oltmans, H. Vömel, H.G.J. Smit, T. Deshler, C. Kröger, Electrochemical concentration cell (ECC) ozonesonde pump efficiency measurements and tests on the sensitivity to ozone of buffered and unbuffered ECC sensor cathode solutions, *J. Geophys. Res., 107,* 10.1029/2001JD000557, **2002**.

Junge, C.E., Air Chemistry and Radioactivity, *Academic Press, New York,* **1963**.

Kerr, J.B., H.Fast, C.T. McElroy, S.J. Oltmans, J.A. Lathrop, E. Kyro, A. Paukkunen, H. Claude, U. Köhler, C.R. Sreedharan, T. Takao, and Y.,Tsukagoshi, The 1991 WMO International Ozonesonde Intercomparison at Vanscoy, Canada, *Atm. Ocean, 32,* 685-716, **1994**.

Kiehl, J.T., and K.E. Trenberth, Earth's annual global mean energy budget, *Bull. Am.. Meteorol. Soc., 78,* 197-208, **1997**.

Kim, J.H., R,D. Hudson, and A.M. Thompson, A new method of deriving time averaged tropospheric column ozone over the tropics using total ozone mapping spectrometer (TOMS) radiances: Intercomparison and analysis using TRACE-A data, *J. Geophys. Res., 101*, 24,317-24,330, **1996**.

Kley, D., A.L. Schmeltekopf, K. Kelly, R.H. Winkler, T.L. Thompson, and M. McFarland, Transport of water vapor through the tropical tropopause, Geophys. *Res. Lett., 9,* 617-620, **1982.**

Kley, D., P.J. Crutzen, H.G.J. Smit, H. Vömel, S.J. Oltmans, H. Grassl, and V. Ramanathan, Observations of near-zero ozone levels over the convective Pacific: Effects on air chemistry, *Science, 274,* 230-233, **1996**.

Kley, D., H.G.J. Smit, H. Vömel, H. Grassl, V. Ramanathan, P.J. Crutzen, S. Williams, J. Meywerk and S.J. Oltmans, Tropospheric water vapour and ozone cross sections in a zonal plane over the central equatorial Pacific, *Q. J. R. Meteorol. Soc., 123,* 2009-2040, **1997**.

Kloesel, K.A., and B.A. Albrecht, Low-level inversions over the tropical Pacific-thermodynamic structure of thze boundary layer and the above inversion moisture structure, *Mon. Wea. Rev., 117*, 81-101, **1989**.

Komhyr, W.D., Nonreactive gas sampling pump, *Rev. Sci. Inst., 38,* 981-983, **1967**.

Komhyr, W.D., Electrochemical concentration cells for gas analysis, *Ann.Geoph., 25,* 203-210, **1969**.

Komhyr, W.D., Development of an ECC-Ozonesonde, *NOAA Techn. Rep. ERL 200-APCL 18ARL-149,* **1971**.

Komhyr, W.D., Operations handbook - Ozone measurements to 40 km altitude with model 4A-ECC-ozone sondes, *NOAA Techn. Memorandum ERL-ARL-149,* **1986**.

Komhyr, W.D., R.A. Barnes, G.B. Brothers, J.A. Lathrop, and D.P. Oppermann, ECC ozonesonde performance evaluation during STOIC 1989, *J. Geophys. Res., 100,* 9231-9244, **1995**.

Koppmann, R., R. Bauer, F.J. Johnen, C. Plass, and J. Rudolph, The distribution of light nonmethane hydrocarbons over the Mid-Atlantic: Results of the Polarstern cruise ANT VII/1, *J. Atmos. Chem., 15,* 215-234, **1992**.

Krisnamurti, T.N., M.C. Sinha, M. Kanamitsu, D. Oosterhof, E.L. Bensman, and V.B. Kumar, The meteorological environment of the tropospheric ozone maximum over the tropical South Atlantic Ocean*, J. Geophys. Res., 98,* 10,621-10,641, **1993**.

Lelieveld, J., and P.J. Crutzen, The role of clouds in tropospheric photochemistry*, J. Atmos. Chem., 12,* 229-267, **1991**.

Lelieveld, J., and F.J. Dentener, What controls tropospheric ozone?, *J. Geophys. Res., 105*, 3531-3551, **2000.**

Lenhard, R.W., Accuracy of radiosonde temperature and pressure height determination*, Bull. Am. Meteorol. Soc., 51,* 842-846, **1970**.

Lenschow, D. H., R. Pearson, Jr, and B. B. Stankov, Measurements of ozone vertical flux to ocean and forest, *J. Geophys. Res., 88,* 1360-1368, **1982.**

Levy, H.II, Normal atmosphere: Large radical and formaldehyde concentrations predicted, *Science, 173,* 141-143, **1971**.

Levy, H.II, J.D. Mahlman, and W.J. Moxim, Tropospheric ozone: The role of transport, *J. Geophys. Res., 90,* 3753-3772, **1985.**

Levy II, H., P.S. Kasibhatla, W.A. Moxim, A.A. Klonecki, A.I. Hirsch, S.J. Oltmans and W.L. Chameides, The global impact of human activity on tropospheric ozone, *Geophys. Res. Lett.,* 24, 791-794, **1997**.

Lindzen, R.S., Some coolness concerning global warming, *Bull. Am.. Meteorol. Soc., 71,* 288-299, **1990**.

Lindzen, R.S., The importance and nature of the water vapor budget in nature and models. *Climate Sensistivity to Radiative Perturbations: Physical Mechanisms and their Validation, H. Le Trevt, Ed., NATO ASI Series I: Global Environmental Change, Vol. 34, Springer Verlag,* 51-66, **1995**.

Liu, S.C., D. Kley, M. McFarland, J.D. Mahlman, and H. Levy, II, On the origin of tropospheric ozone*, J. Geophys. Res., 85,* 7546-7552, **1980**.

Liu, S. C., M. McFarland, D. Kley, O. Zafiriou, and B. Huebert, Tropospheric NO_X and O_3 budgets in the equatorial Pacific, *J. Geophys. Res., 88,* 1360-1368, **1983**.

Logan, J.A., M.J. Prather, S.C. Wofsy, and M.B. McElroy, Tropospheric chemistry: A global perspective, *J. Geophys. Res., 86,* 7210-7254, **1981**.

Ludlum, F.H, Clouds and storms: The behavior and effect of water in the atmosphere, *Pennsylvania State University Press*, **1980**.

Madden, R.A., and P.R. Julian, Detection of a 40-50 day oscillation in the zonal wind in the tropical Pacific, *J. Atmos. Sci.,* 28, 702-708, **1971**.

Madden, R.A., and P.R. Julian, Observation of the 40-50 day tropical oscillation- a review, *Mon. Wea. Rev.,* 122, 814-837, **1994**.

Manabe, S., and R.T. Wetherald, Thermal equilibrium of the atmsopherewith a given distribution of relative humidity, *J. Atmos. Sci*, 24, 241-259, **1967.**

Mapes, B.E., and P. Zuidema, Radiative-dynamical consequences of dry tongues in the tropical troposphere, *J. Atmos. Sci., 53,* 620-638, **1996.**

Mapes, B.E., Water's two height scales: The moist adiabat and the radiative troposphere, *Q. J. R. Meteorol. Soc., 127,* 2353-2366, **2001.**

Marenco, A., M. Macaigne and S. Prieur, Meridional and vertical CO and CH_4 distributions in the background troposphere (70^oN-60^oS; 0-12 km altitude) from scientific aircraft measurements during the STRATOZ III experiment (June 1984), *Atmos. Environ., 23*, 185-200, **1989**.

Mastenbrook, H.J., Water vapor observations at low, middle and high latitudes, *NRL Report 6447, Naval Research Laboratory, Washington, DC*, **1966**.

Mastenbrook, H.J., and S.J. Oltmans, Stratospheric water vapor variability fro Washington, DC / Boulder, CO: 1964-82, *J. Atmos. Sci., 40,* 2157-2165, **1983**.

Matsuguchi, M., S. Umeda, Y. Dadaoka, and Y. Sakai, Characterization of polymers for a capacitive type humidity sensor based on water sorption behavior, *Sensors and Actuators, 49,* 179-185, **1998**.

McFarland, M., D. Kley, J.W. Drummond, A.L. Schmeltekopf, and R.J. Winkler, Nitric oxide measurements in the Equatorial Pacific region, *Geophys. Res. Lett., 6*, 605-608, **1979**.

Miloshevich, L.M., H. Vömel, A. Paukkunen, A.J. Heymsfield, and S.J. Oltmans, Characterization and correction of relative humidity measurements from Vaisala RS80-A radiosondes at cold temperatures, *J. Atmos. Oceanic. Tech., 18*, 135-156, **2001**.

Müller, J.F., and G. Brasseur, Images: A three-dimensional chemical transport model of the global troposphere., *J. Geophys. Res., 100,* 16,445-16,490, **1995**.

Müller, K.P., and J. Rudolph, Measurements of peroxyacetylnitrate in the marine boundary layer over the Atlantic, *J. Atmos. Chem. 15,* 361-368, **1992**.

Nash, J., and F.J. Schmidlin, WMO international radiosonde comparison (UK 1984, USA 1985): *Final report, WMO Instruments and Observing Methods Report No. 30, WMO/TD-No. 195*, **1987**

Nawrath, S., Water Vapor in the Tropical Upper Troposphere: On the Influence of Deep Convection, PhD-Thesis Report, Universität Köln, May 2002.

Newell, R.E., J.W. Kidson, D.G. Vincent, and G.J. Boer, The general circulation of the tropical atmosphere and its interactions with extratropical latitudes, *MIT Press, Cambridge, Massachusetts,* **1974**.

Newell, R.E., and S. Gould-Stewart, A stratospheric fountain?, *J. Atmos. Sci., 38,* 2789-2796, **1981**.

Newell, R.E., Y. Zhu, and C. Scott, Tropospheric rivers?- A pilot study, *Geophys. Res. Lett., 19,* 2401-2404, **1992.**

Numaguti, A.R., K. Oki, K. Nakamura, K. Tsuboki, N. Misawa, T. Asai, and Y.M. Kodma, 4-5 day period variation and low level dry air observed in the equatorial western Pacific during TOGA COARE, *J. Meteorol. Soc. Japan, 73,* 267-290, **1995**

O'Sullivan, D.W., B.G. Heikes, M. Lee, W. Chang, G.L. Gregory, D.R. Blake, and G.W. Sachse, Distribution of hydrogen peroxide and methylhydroperoxide over the Pacific and South Atlantic Oceans, *J. Geophys. Res., 104,* 5,635-5,646, **1999**.

Papenbrock, Th., F. Stuhl, K.P. Müller, and J. Rudolph, Measurement of gaseous HNO_3 over the Atlantic Ocean, *J. Atmos. Chem., 15,* 369-379, **1992**.

Parsons, C.L., G.A. Norcross, and R.L. Brooks, Radiosonde pressure sensor performance: Evaluation using tracking radars, *J. Atmos. and Oceanic Tech., 1,* 321-327, **1984**.

Parsons, D., W. Dabberdt, H. Cole, T. Hock, C. Martin, A.L. Barrett, E. Miller, M. Spowart, M. Howard, W. Ecklund, D. Carter, K. Gage, and J. Wilson, The integrated sounding system: Description and preliminary observations from TOGA-COARE, *Bull. Amer. Meteor. Soc., 75*, 553-569, **1994.**

Peixoto, J.P., and A.H. Oort, Physics of Climate, *American Institute of Physics,* New York, **1991.**

Philander, S.G., El Nino, La Nina, and the Southern Oscillation, *Academic Press, San Diego*, **1990**.

Pickering, K.E., A.M. Thompson, Y. Wang, W.K. Tao, D.P. McNamara, V.W.J.H. Kirchhoff, B.G. Heikes, G.W. Sachse, J.F. Bradshaw, G.L. Gregory, and D.R. Blake, Convective transport of biomass burning emissions over Brazil during TRACE-A, *J. Geophys. Res., 101,* 23,993-24,012, **1996**.

Pierrehumbert, R.T., and H. Yang, Global chaotic mixing on isentropic surfaces, *J. Atmos. Sci., 50,* 2462-2480, **1993**.

Pierrehumbert, R.T., Thermostats, radiator fins, and the local runaway greenhouse, *J. Atmos. Sci., 52,* 1784-1806, **1995.**

Piotrowicz, S. R., D. A. Boran, and C. J. Fischer, Ozone in the boundary layer of the equatorial Pacific Ocean, *J. Geophys. Res., 91,* 13113-13119, **1986.**

Piotrowicz, S.R., R.A. Rasmussen, K.J. Hanson, and C.J. Fischer, Ozone in the boundary layer of the equatorial Atlantic Ocean, *Tellus, 41B,* 314-322, **1989**.

Piotrowicz, S.R., C.J. Fischer, and R.S. Artz, Ozone and Carbon monoxide over the North Atlantic during a boreal summer, *Global Biogeochem. Cycles, 4,* 215-224, **1990**.

Piotrowicz, S.R., H.F. Bezdek, G.R. Harvey, and M. Springer-Young, On the ozone minimum over the equatorial Pacific Ocean, *J. Geophys. Res., 96,* 18679-18687, **1991**.

Platt, U., J. Rudolph, T. Brauers, and G.W. Harris, Atmospheric measurements during Polarstern cruise ANT-VII/1, 54 [O]N to 32 [O]S: An overview, *J. Atmos. Chem., 15,* 203-214, **1992**.

Prather, M.J., and D.J. Jacob, A persistent imbalance in HO_X and NO_X photochemistry of the upper troposphere driven by deep tropical convection, *Geophys. Res. Lett., 24,* 3189-3192, **1997**.

Proffitt, M.H., and R.J. McLaughlin, Fast response dual-beam UV-absorption photometer suitable for use on stratospheric balloons, *Rev. Sci. Instrum., 54,* 1719-1728, **1983**.

Ramanthan, V., L. Callis, R. Cess, J. Hansen. I. Isaksen, W. Kuhn, A. Lacis, F. Luther, J. Mahlman, R. Reck, and M. Schlesinger, Climate-chemical interactions and effects of changing atmospheric trace gases, *Rev. Geophys., 25,* 1441-1482, **1987**.

Ramanathan, V., R.D. Cess, E.F. Harrison, P. Minnis, B.R. Barkstrom, E. Ahamed, and D. Hartmann, Cloud radiative forcing and climate: results from the Earth Radiation Budget Experiment, *Science, 243,* 57-63, **1989**.

Ramanathan, V., and W. Collins, Thermodynamic regulation of ocean warming by cirrus clouds deduced from observations of the 1987 El Nino, *Nature 351,* 27-32, **1991**.

Ramanathan, V., B. Subasilar, G.J. Zhang, W. Conant, R.D. Cess, J.T. Kiehl, H. Grassl, and I. Shi, Warm pool heat budget and short wave cloud forcing: a missing physics?, *Science, 267,* 499-503, **1995**.

Ravishankara, A.R., Heterogeneous and multiphase chemistry in the troposphere, *Science, 276,* 1058-1065, **1997**.

Regener, E., Ozonschicht und atmosphärische Turbulenz, Ber. Deutsche Wetterdienstes US-Zone 11, 45-??, 1949.

Reid, G.C., , and K.S. Gage, On the annual variation in the height of the tropical tropopause, *J. Atmos. Sci., 38*, 1928-1938, **1981.**

Reid, S.J., G. Vaughan, A.R. Marsh, and H.G.J. Smit, Intercomparison of ozone measurements by ECC sondes and BENDIX chemiluminescent analyser, *J. Atm. Chem., 25,* 215-226, **1996**.

Rhoads, K.P., P. Kelley, R.R. Dickerson, T.P. Carsey, M. Farmer, D.L. Savoie, and J. Prospero, The composition of the troposphere over the Indian Ocean during the monsoonal transition, *J. Geophys. Res., 102,* 18,981-18,995, **1997**.

Rickenbach, T.M, and S.A. Rutledge, Convection in TOGA COARE: Horizontal scale, morphology, and rainfall production, *J. Atmos. Sci., 55,* 27152729, **1998.**

Ridley, B.A., M.A. Carroll and G.L. Gregory, Measurements of nitric oxide in the boundary layer and free troposphere over the Pacific Ocean, *J. Geophys. Res., 92,* 2025-2047, **1987**.

Ridley, B.A., S. Madronich, R.B. Chatfield, J.G. Walega, R.E. Shetter, M.A. Carroll, and D.D. Montzka, Measurements and model simulations of the photostationary state during the MaunaLoa Observatory Phochemistry Experiment: Implications for radical concentrations and ozone production and loss rates, *J. Geophys. Res., 97,* 10,375-10,388, **1992.**

Riehl, H., and J. Malkus, On the heat balance in the equatorial zone, *Geophysica (Helsinki), 6,* 503-538, **1958.**

Riehl, H., Climate and weather in the tropics, *Academic Press, London,* **1979**.

Riehl, H., and J. Simpson, The heat balance of the equatorial trough zone, revisited, *Contr. Atm. Physics, 52,* 287-305, **1979.**

Rieker, J., Influences of temperature and pressure errors on the determination of the geopotential between two constant pressure levels and on the height of a spatial body in the atmosphere, *Brit. Lib. Lending Div., Boston Spa , Engl., Transl. into english from Schweiz. Met. Zentralen. Arbeitsber. No. 65*, **1976**.

Roelofs, G.J., J. Lelieveld, and R. Dorland, A three-dimensional chemistry general circulation model simulation of anthropogenically derived ozone in the troposphere and ist radiative climate forcing, *J. Geophys. Res., 102,* 23,389-23,401, **1997-a**.

Roelofs, G.J., J. Lelieveld, H.G.J. Smit, and D. Kley, Ozone production and transports in the tropical Atlantic region during the biomass burning season, *J. Geophys. Res., 102,* 10,637-10,651, **1997-b**.

Röth, E.P., Fast algorithm to calculate the photon flux in optically dense media for use in photochemical models, *Ber. Bunsenges. Phys. Chem., 96,* 417-420, **1992**.

Rogers, R.R., and M.K. Yau, A short course in cloud physics, Third Edition, *Pergamon Press, Oxford,* **1989**.

Rohrer, F., and D. Brüning, Surface NO and NO_2 mixing ratios measured between 30^ON and 30^OS in the Atlantic region, *J. Atmos. Chem., 15,* 253-268, **1992**.

Rohrer, F., D. Brüning, and D. Ehhalt, Tropospheric mixing ratios of NO obtained during TROPOZ II in the latitude region 67^ON-56^OS, *J. Geophys. Res., 102,* 25,429-25,449, **1997**.

Rotunno,R., J.B. Klemp, and M.L. Weisman, A theory for strong, long-lived squall lines, *J. Atmos. Sci.,* 45, 463-485, **1988.**

Routhier, F. R., R. Dennet, P. D. Davis, A. Wartburg, P.Haagenson, and A. C. Delany, Free tropospheric and boundary layer airborne measurements of ozone over the latitude range of 58^OS to 70^ON, *J. Geophys. Res.,* 85, 7307-7321, **1980**.

Rudolph, J., B. Vierkorn-Rudolph, and F.X. Meixner, Large-scale distribution of peroxyacetylnitrate results from STRATOZ III flights, *J. Geophys. Res., 92,* 6653-6661, **1987**.

Rudolph, J., Two-dimensional distribution of light hydrocarbons: Results from the Stratoz III experiment, *J. Geophys. Res., 93,* 8367-8377, **1988**.

Rudolph, J., and F. J. Johnen, Measurements of light atmospheric hydrocarbons over the Atlantic in the regions of low biological activity, *J. Geophys. Res., 95,* 20583-20591, **1990**.

Salasmaa, E., and P. Kostamo, New thin film humidity sensor, *Proc. of Third Symposium on Meteorological Observations and Instrumentation, Amer. Meteor. Soc., Washington DC*, 33-38, **1975**.

Schenkel, A. and Broder B., Interference of some trace gases with ozone measurements by the KI-method, *Atmos. Environ. 16,* 2187-2190, **1982**.

Schmidlin, F.J., Can the standard radiosonde system meet special atmospheric research needs?, *Geophys. Res. Lett., 9,* 1109-1112, **1982.**

Schultz, M.G., D.J. Jacob, Y. Wang, J.A. Logan, E.L. Atlas, D.R. Blake, N.J. Blake, J.D. Bradshaw, E.V. Browell,M.A. Fenn, F. Flocke, G.L. Gregory, B.G. Heikes, G.W. Sachse, S.T. Sandholm, R.E. Shetter, H.B. Singh, and R.W. Talbot, On the origin of tropospheric ozone and NO_X over the tropical South Pacific, *J. Geophys. Res., 104,* 5829-5843, **1999**.

Sherwood, S.C., and A.E. Dessler, On the control of stratospheric humidity, *Geophys. Res. Lett., 27,* 2513-2516, **2000**.

Sheu, R.S., and G. Liu, Atmospheric humidity variations associated with westerly wind bursts during Tropical Ocean Global Atmsophere (TOGA) Coupled Ocean Atmsophere Response Experiment (COARE), *J. Geophys. Res., 100*, 25,759-25,768, **1995.**

Singh, H.B., D.O'Hara, D. Herlth, W.Sachse, D.R.Blake, J.D. Bradshaw, M.Kanakidou, P.J. Crutzen, Acetone in the Atmosphere: Distribution, sources, and sinks. *J. Geophys.Res., 99,* 1805-1819, **1994.**

Singh, H.B. M. Kanakidou, P.J. Crutzen, and D.J. Jacobs, High concentrations and photochemical fate of oxygenated hydrocarbons in the global troposphere, *Nature, 378,* 50-54, **1995.**

Slemr, F., and H.G. Tremmel, Hydroperoxides in the marine troposphere over the Atlantic Ocean, *J. Atmos. Chem., 19,* 371-404, **1994**.

Smit, H.G.J., D. Kley, S. McKeen, A. Volz, and S. Gilge, The latitudinal and vertical distribution of tropospheric ozone over the Atlantic Ocean in the southern and northern hemispheres, *in: R.D. Bojkov, P. Fabian (eds), Ozone in the Atmosphere, 419-422, Deepak Publ.,* **1989-A**.

Smit, H.G.J., W. Sträter, H. Loup, and D. Kley, Ozone profiles at Jülich, FRG during 1988 and 1989, *Jül Berichte Nr 2337, Forschungszentrum Jülich,* **1989-B**.

Smit, H.G.J., S. Gilge, and D. Kley, The meridional distribution of ozone and water vapor over the Atlantic Ocean between 30°S and 52°N in September/October 1988, *in G. Restelli, G. Angeletti (eds.), Physico-chemical behaviour of atmospheric pollutants, CEC., Air Pollution Report 23, Kluwer Acad. Publ.,* 630-637, **1990**.

Smit, H.G.J., S. Gilge, and D. Kley, Ozone profiles over the Atlantic Ocean between 36 ^{O}S and 52 ^{O}N in March/April 1987 and September/October 1988, *Jül Berichte Nr 2567, Forschungszentrum Jülich,* **1991**.

Smit, H.G.J., W. Sträter, D. Kley, and M.H. Profitt, The evaluation of ECC-ozone sondes under quasi flight conditions in the environmental simulation chamber at Jülich, *in P.M. Borell et al. (eds.), Proceedings of Eurotrac symposium 1994, SPB Academic Publishing bv, The Hague, The Netherlands,* 349-353, **1994-A**.

Smit, H.G.J. and D. Kley, A Description of TOR Ozone Sounding Station Jülich, FRG, *In: The TOR Network, T. Cvitas and D. Kley (eds.), International Scientific Secretariat, Garmisch-Partenkirchen,* 160-168, **1994-B**.

Smit H.G.J and D. Kley, JOSIE: The 1996 WMO International intercomparison of ozonesondes under quasi flight conditions in the environmental simulation chamber at Jülich, *WMO/IGAC-Report, WMO Global Atmosphere Watch report series, No. 130 (Technical Document No. 926). World Meteorological Organization, Geneva,* **1998**.

Smit H.G.J., W. Sträter, M. Helten, and D. Kley, Environmental simulation facility to calibrate airborne ozone and humidity sensors. *Jül Berichte Nr 3796, Forschungszentrum Jülich,* **2000**.

Smit, H.G.J., Ozone sondes, *In: "Encyclopedia of Atmospheric Sciences", J. Holton, J. Pyle, and J. Curry (Eds.), Academic Press, London*, **2002**.

Soden, B.J., and F.P. Bretherton, Upper tropospheric humidity from the GOES 6.7 µm channel: Method and climatology for July 1987, *J. Geophys. Res., 98,* 16,669-16,688, **1993.**

Sonntag, D., Advancements in the field of hygrometry, *Meteorol. Zeitschrift, N.F. 3,* 51-66, **1994**.

SPARC-IOC-GAW Assessment of Trends in the Vertical Distribution of Ozone, *SPARC report No.1, WMO Global Ozone Research and Monitoring Project Report No. 43,* **1998**.

SPARC Assessment of Upper Tropospheric and Stratospheric Water Vapour, Eds. D. Kley, D., J.M. Russell III, C. Phillips, , *SPARC Report No. 2, World Climate Research Programme Report No. 113, WMO/TD-Report-No. 1043*, **2000**.

Spencer, R.W., and W.D. Braswell, How dry is the tropical free troposphere? Implications for global warming theory, *Bull. Am. Meteorol. Soc., 78,* 1097-1106, **1997**.

Stallard, R. F., J. M. Edmond, and R. E. Newell, Surface Ozone in the south east Atlantic between Dakar and Walvis Bay, *Geophys. Res. Letters, 2,* 289-292, **1975**.

Sun, D.Z., and R.S. Lindzen, Distribution of tropical tropospheric water vapour, *J. Atmos. Sci., 50,* 1643-1660, **1993**.

Thompson, A.M., The oxidizing capacity of the earth's atmosphere: Probably past and future changes, *Science, 256,* 1157-1165, **1992**.

Thompson, A.M., J.E. Johnson, A.L. Torres, T.S. Bates, K.C. Kelly, E. Atlas, J.P. Greenberg, N.M. Donahue, S. A. Yvon, E.S. Saltzman, B.G. Heikes, B.W. Mosher, A.A. Shaskov and V.I., Yegorov, Ozone observations and a model of marine boundary layer photochemistry during SAGA-3, *J. Geophys. Res., 98,* 16,955-16,968, **1993**.

Thompson, A.M., K.E. Pickering, D.P. McNamara, M.R. Schoeberl, R.D. Hudson, J.H. Kim, E.V. Browell, V.W.J.H. Kirchhoff, and D. Nganga, Where did tropospheric ozone over southern Africa and the tropical Atlantic come from in October 1992? Insights from TOMS, GTE TRACE A and SAFARI 1992, *J. Geophys. Res., 101,* 24,251-24,278, **1996**.

Thompson A.M., B.G. Doddridge, J.C. Witte, R.D. Hudson, W.T. Luke, J.E. Johnston, B.J. Johnson, S.J. Oltmans, R. Weller, A tropical Atlantic paradox: Shipboard and satellite views of a tropospheric ozone maximum and wave-one in January-February 1999.*Geophys. Res. Lett., 27 ,*3317-3320, **2000.**

Thompson, A.M., J.C. Witte, R.D. McPeters, S.J. Oltmans, F.J. Schmidlin, J.A. Logan, M.Fujiwara, V.W.J.H. Kirchhoff, F. Posny, G.J.R. Coetzee, B. Hoegger, S. Kawakami, T. Ogawa, B.J. Johnson, H. Vömel and G. Labow, Southern Hemisphere Additional Ozonesondes (SHADOZ) 1998-2000 tropical ozone climatology 1. Comparison with Total Ozone Mapping Spectrometer (TOMS) and ground-based measurements, *J. Geophys. Res.*, Vol. 108 No. D2, 8238, doi: 10.1029/2001JD000967, **2003**

Thornton, D.C., and N. Niazy, Sources of background current in the ECC-ozone sonde: Implication for total ozone measurements, *J. Geophys. Res., 87,* 8943-8950, **1982**.

Thornton, D.C. and N. Niazy, Effects of solution mass transport on the ECC ozonesonde background current, *Geophys.Res.Lett. 10,* 148-151, **1983**.

Torres, A.L., ECC ozonesonde performance at high altitude: pump efficiency, *NASA Technical Memorandum 73290, 10 pp., NASA Wallops Flight Center, Wallops Island, VA.,* **1981**.

Torres, A.L. and A.M. Thompson, Nitric oxide in the equatorial Pacific boundary layer: SAGA-3 measurements, *J. Geophys. Res., 98,* 16,949-16,954, **1993**.

US Standard Atmosphere, *NOAA, NASA, USAF, U.S. Government Printing Office, Washington, D.C.*, **1976**.

Vaïsala, Instruction manual for radiosonde RS 80 and windsonde WS 80 operation, *Edition: RS80-O0036-2.2,* **1988**.

Vaïsala, Instruction manual for ground check set GC 22, *Edition: GC22-T0199-1.3*, **1985**.

Vömel, H., Oltmans S.J., Kley, D., Crutzen, P.J., New evidence for the stratospheric dehydration mechanism in the equatorial Pacific, *Geophys. Res. Lett.,* 22, 3235-3238, **1995**

Waliser, D.E., and N.E. Graham, Comparison of the high reflective cloud and outgoing longwave radiation data sets for use in estimating tropical deep convection, *J. Climate, 6,* 331-353, **1993**.

Wang, Y.H., D.J. Jacob and J.A. Logan, Global simulation of tropospheric O_3-NO_x-hydrocarbon chemistry: 3, Origin of tropospheric ozone and effects of non-methane hydrocarbons, *J. Geophys. Res.*, 103, 10757-10768, **1998**.

Warneck, P., Chemistry of the natural atmosphere, *Academic Press, London,* **1988**.

Waugh, D.W., and L.M. Polvani, Climatology of intrusions into the tropical upper troposphere, *Geophys. Res. Lett., 27*, 3857-3860, **2000**.

Webster, P.J., The large scale structure of the tropical atmosphere, in: B.J. Hoskins and R.P. Pearce (eds.), Large dynamical processes in the atmosphere, *Academic Press, London,* **1983**.

Webster, P.J., The variable and interactive monsoon, in Monsoons, J.S. Fein and P.L. Stephens, eds., *John Wiley, New York,* 269-330, **1987**.

Webster, P.J., and R. Lukas, TOGA-COARE: The Coupled Ocean Atmosphere Response Experiment, *Bull. Am. Meteor. Soc., 73,* 1377-1416, **1993.**

Webster, P.J., The role of hydrological processes in ocean-atmosphere interactions, *Rev. Geophys., 32,* 427-476, **1994**.

Weller, R., R. Lilischkis, O. Schrems, R. Neuber, and S. Wessel, Vertical ozone distribution in the marine atmosphere over the central Atlantic Ocean (56^oS-50^oN), *J. Geophys. Res., 101,* 1387-1399, **1996**.

Wennberg P.O. et al., Hydrogen radicals, nitrogen radicals, and the production of O_3 in the upper troposphere, *Science, 279,* 49-53, **1998**.

Wielicki, B.A., and R.N. Green, Cloud identification for ERBE radiative flux retrieval, *J. Appl. Meteorol., 28,* 1131-1146, **1989.**

Winkler, P., Surface Ozone over the Atlantic Ocean, *J. Atmos. Chem., 7,* 73-91, **1988**.

WMO-Report No.8, Measurement of atmospheric humidity, Guide to meteorological instruments and methods of observation., 5th ed., *World Meteorological Organization, Geneva,* 5.1-5.19, **1983**

WMO (=World Meteorological Organization) , Scientific Assessment of Ozone Depletion: 1994, *Global Ozone Research and Monitoring Project - Report No. 37, World Meteorological Organization, Geneva ,* **1995**.

WMO (=World Meteorological Organization) , Scientific Assessment of Ozone Depletion: 1998, *Global Ozone Research and Monitoring Project - Report No. 44, World Meteorological Organization, Geneva ,* **1999**.

WMO (=World Meteorological Organization) , Scientific Assessment of Ozone Depletion: 2002, *Global Ozone Research and Monitoring Project - Report No. 57, World Meteorological Organization, Geneva ,* **2003**.

Yang, H., and R.T. Pierrehumbert, Production of dry air by isentropic mixing, *J. Atmos. Sci., 51,* 3437-3454, **1994.**

Yoneyama, K., and T. Fujitani, The behavior of the dry wersterly air associated with convection observed during the TOGA/COARE R/V Natsushima Cruise, *J. Meteor. Soc. Japan, 73,* 291-304, **1995.**

Yoneyama, K., and D.B. Parsons, A proposed mechanism fro the intrusion of dry air into the tropical western Pacific region, *J. Atm. Sci., 56,* 1524-1546, **1999**

Zhang, Y.C., and W.B. Rossow, Estimating meridional energy transports by the atmospheric and oceanic general circulations using boundary fluxes, *J. Clim., 10*, 2358-2373, **1997**.

Zhang, C., B.E. Mapes, and B.J. Soden, Bimodality in tropical water vapour, *Q. J. R. Meteorol. Soc., 129,* 2847-2866, **2003.**

Zipser, E.J., Mesoscale and convective scale downdrafts as distinct components of squall-line structure, *Mon. Weath. Rev., 105*, 1568-1589, **1977.**

Acknowledgements

Lebenslauf

Persönliche Daten

Name:	Herman Gerrit Jan Smit
Geburtsdatum:	4. Mai 1955
Geburtsort:	Hengelo (Ov), die Niederlande (NL)
Eltern:	Engelbert Smit
	Gerda Smit-Hobbelink

Schulausbildung

1961-1967	Grundschule (Wilbertschool & Opleidingschool, Hengelo (O), NL)
1967-1972	Gymnasium (Bataafsche Kamp, Hengelo (O), NL)
Jun.1972	Abitur

Hochschulstudium

Aug.1972 - Jan.1981	Studium der Technische Physik an der Technische Universität Twente, Enschede, NL
Jun.1978	Bachelor
Jan.1981	Diplom
	Diplomarbeit: „Experimentelle und numerische Untersuchungen an rotierende Strömungen", angefertigt in der Fachgruppe Wärme-und Strömungslehre (Prof. Dr. Ir. L. van Wijngaarden) an der Technische Universität Twente, Enschede, NL

Berufliche Tätigkeiten

seit Feb.1981	wissenschaftlicher Angestellter am Forschungszentrum Jülich im Bereich der Atmosphärenforschung
Apr.1981-Mär.1985	Institut für Chemie der Atmosphäre (Prof. Dr. D.E. Ehhalt)
Apr.1985-Feb.2002	Institut für Chemie der belasteten Atmosphäre (Prof. Dr. D. Kley)
Seit Mär.2002	Institut für Chemie und Dynamik der Geosphäre: Troposphäre (Prof. Dr. A. Wahner)

Persönliche Erklärung der Dissertation

Ich versichere, dass ich die von mir vorgelegte Dissertation selbständig angefertigt, die benutzten Quellen und Hilfsmittel vollständig angegeben und die Stellen der Arbeit – einschließlich Tabellen, Karten und Abbildungen -, die anderen Werken im Wortlaut oder dem Sinn nach entnommen sind, in jedem Einzelfall als Entlehnung kenntlich gemacht habe; dass diese Dissertation noch keiner anderen Fakultät oder Universität zur Prüfung vorgelegt hat; das sie – abgesehen von unten angegebenen Teilpublikationen – noch nicht veröffentlicht worden ist sowie, dass ich eine solche Veröffentlichung vor Abschluss des Promotionsverfahrens nicht vornehmen werde. Die Bestimmungen dieser Promotionsordnung sind mir bekannt. Die von mir vorgelegte Dissertation ist von Prof. em. Dr. Dieter Kley betreut worden.

Aachen, 25. Mai 2004

Herman G.J. Smit

Keine Teilpublikationen